D. A. Harmsen

Design of a Partial Discharge Test Platform

Partial discharge artificial defects, characterization, clustering, analysis and pattern recognition.

TU Delft

Design of a Partial Discharge Test Platform

Partial discharge artificial defects, characterization, clustering, analysis and pattern recognition.

By

Daniel Antonio Harmsen

in partial fulfilment of the requirements for the degree of

Master of Science
in Electrical Engineering

at the Delft University of Technology,
Faculty of Electrical Engineering, Mathematics and Computer Science,
Electrical Sustainable Energy Department,
DC Systems and Storage Group,
The Netherlands,
to be defended publicly on Tuesday May 13, 2016 at 09:30 AM.

Supervisor:	Prof. dr. ir. P. (Pavol) Bauer	TU Delft
Daily Supervisor:	Dr. A. (Armando) Rodrigo Mor	TU Delft

This thesis is confidential and cannot be made public until May 13, 2018.

An electronic version of this thesis is available at http://repository.tudelft.nl/.

Thesis committee:

Dr. M. (Marjan) Popov

Dr. A. (Armando) Rodrigo Mor

Dr. L.M. (Laura) Ramirez Elizondo

Delft University of Technology
Faculty of Electrical Engineering, Mathematics and Computer Science
Electrical Sustainable Energy Department
DC Systems and Storage Group
The Netherlands

Abstract

Partial discharge (PD) measurements are an effective tool for insulation diagnostics and assessment. Therefore, a good understanding of these PD measurements is an essential part of an electrical engineer's background knowledge. During this research project a PD test platform was designed and build for electrical PD detection. The setup included artificially created defects for six different types of PDs, with origins in positive and negative corona, internal discharge, floating electrodes, free-moving particles and surface discharge. These defects were designed to have a partial discharge inception voltage (PDIV) of around 10kV, and could easily be connected or disconnected from the setup. Therefore, it was possible to measure individual defects or a combination of them. This PD test platform was used during this research project to characterize the different PD types (single and multiple), and as a check for testing new clustering and pattern recognition techniques. In addition, the platform could also be used as a test platform for educational purposes and to train people and test equipment.

In this thesis research project, the "initial step" towards PD defect origin recognition for AC voltage without any phase dependency was conducted with the use of time-resolved partial discharge (TRPD) analysis. This thesis shows that it is possible to conduct the time analysis and recognition for AC voltage for the artificially created defects. From the analysis in this thesis, it can be concluded that the TRPD analysis for PD recognition under AC voltage is as good as, or even better than, phase-resolved partial discharge (PRPD) analysis. For most of the data analysed, the TRPD analysis provides the same results compared to the PRPD analysis. However, further checking is needed, such as validating the findings with mathematical models.

The thesis goals are to build a setup suitable for the research, determining the optimal combination of hardware/software to discriminate among different types of defects, and to realize experiments to validate the design.

Acknowledgments

I am very grateful to have had many people by my side who have contributed directly and indirectly to the completion of this thesis/research project. I am grateful for their contribution to my enrichment through new knowledge and experiences.

I would like to thank and show my enormous gratitude for my supervisor, Dr. ir. Armando Rodrigo Mor, for guiding me through this whole project and steering me in the right direction whenever needed. I am very grateful that the door to your office was always open whenever I got stuck or had a question about the research. I am truly thankful to have constantly received such unique support.

Special thanks goes to the staff of the High Voltage Laboratory, Wim Termorshuizen, Remko Koornneef and Paul van Nes, for their all their support and contributions to this research project, and of course for the 3 o'clock tea times.

I would also like to thank the experts who were involved in the validation of this thesis research project, Dr. ir. Marjan Popov and Dr. ir. Laura M. Ramirez Elizondo. Without their passionate participation and input, the validation survey could not have been successfully conducted.

Finally, I would like to thank my family and close friends for always supporting and encouraging me. This accomplishment would not have been possible without them.

Delft, March 2016

Daniel Antonio Harmsen

Table of Contents

Abstract III
Acknowledgments IV
Table of Contents V
List of Figures VII
List of Tables XIII
Nomenclature, Acronyms and Abbreviations with Notation XV
1. Introduction 1
1.1. Objectives and Goals 1
1.2. Contributions 2
1.3. Thesis Overview 3
2. The Origins of Partial Discharges 4
2.1. PD Types and Sources 5
2.2. PD Pulses 10
3. PD Analysis 12
3.1. Testing and Measuring PDs 12
3.2. Phase-Resolved Partial Discharge (PRPD) 15
3.3. Time-Resolved Partial Discharge (TRPD) 16
3.4. Clusters 17
3.5. Calibration 19
4. Experimental Setup 21
4.1. Electrodes 21
4.2. Noise, Disturbance, Interference & Attenuation 22
4.3. Final Setup 25
5. Artificial Defects 31
5.1. Initial Setup PD Measurement 31
5.2. The Final Samples 31
5.3. Selecting the Samples 37
5.4. Aging & Deterioration 43
5.5. PRPD Characterization 49
6. Characterization, Analysis and Recognition of PD patterns 52
6.1. PD Defect Characterization 52
6.2. Influence of Time (Number of Discharges) 74
6.3. Restrictions in Defect Analysis 78

6.4. Discussion of Defect Characterization, Analysis and Recognition 83
7. Multiple Sample Combinations Analysis 85
7.1. Defect Combinations 1-12 85
7.2. Cluster Detection Comparison 113
7.3. Summary of PRPD Analysis 114
7.4. Summary of TRPD Analysis 115
7.5. Summary of Energy Per Charge vs. Charge 116
7.6. Renewed Internal Discharge Sample (Aging) 117
7.7. Results and Evaluation of Multiple Sample Analysis 127
8. PD Pattern Recognition 130
8.1. Edge Detection 130
8.2. Shape Characterization 131
8.3. Consistency of Characterized Shapes 136
8.4. Summary and Discussion of Shape Consistency 147
8.5. PD Shape Recognition 150
9. Conclusions and Future Work 152
9.1. Conclusions 152
9.2. Recommendations for Future Research 154
Appendix 155
A. Dimensions Electrodes 155
B. PD graphs of final individually measured samples 156
C. Partial Discharge Inception Voltage of Internal Discharge Sample 161
D. Influence of time in PRPD & TRPD 165
E. Experimental Setup Schematic 183
F. Multiple Defect combinations Figures 184
G. Multiple defect combinations figures of renewed internal discharge 200
H. Shapes for PD Recognition 205
J. Graphs 2nd Internal Discharge & Floating Electrode Samples 206
Bibliography / References 208

List of Figures

Figure 1: Proposed schematic test setup. 2
Figure 2: Proposed schematic coaxial test setup. 2
Figure 3: Internal discharge, abc model [12]. 5
Figure 4: Internal discharge, abc model graphs [11]. 6
Figure 5: (a) Surface discharge schematic [12]; (b) Examples of bushings [45]; (c) Schematic bushing [11]; (d) Surface discharge inception voltage graph [12]. 6
Figure 6: Surface discharge, abc model [12]. 7
Figure 7: (a, b) Negative corona and (c, d) positive corona [11]. 8
Figure 8: (a) Negative corona, abc model; (b) PD occurrence with corona [12]. 8
Figure 9: (a) Cable joint; (b) Field control element (stress-cone) [47]. 9
Figure 10: PD pulse of streamer-like discharge [36]. 11
Figure 11: PD pulse of Townsend-like discharge [36]. 11
Figure 12: Schematic of PD measurement circuits possibilities: (a) Coupling device in series with the coupling capacitor; (b) Coupling device in series with the test object; (c) Balanced circuit arrangement. 14
Figure 13: PRPD graph explanation; 50 Hz sine-wave representation (phase-signal) with positive and negative PD current pulses. 16
Figure 14: TRPD figure explanation, positive and negative PD current pulses. 17
Figure 15: Calibration, 50 pulses of 10pC. 20
Figure 16: Calibration, 50 pulses of 100pC. 20
Figure 17: Calibration, 50 pulses of 1000pC. 20
Figure 18: (a) Field line between half u=π and full line u=0; (b) Rogowski gap [11]. 21
Figure 19: Internal noise with trigger at ±0mV PRPD. 23
Figure 20: Internal noise with trigger at ±3mV PRPD. 23
Figure 21: Internal noise, pulse 1340. 24
Figure 22: Internal noise, pulse 1340 PRPD. 24
Figure 23: Internal noise, pulse 31923. 24
Figure 24: Internal noise, pulse 31923 PRPD. 24
Figure 25: Blocking inductor: 6 turn coil (left) and isolated 6 turn coil (right). 25
Figure 26: PRPD of surface discharge with disturbance (ungrounded metal near sample); (a) Clusters 1 and 2; (b) Cluster 1: floating particle; (c) Cluster 2: surface discharge. 25
Figure 29: Experimental setup block diagram. 26
Figure 30: Experimental setup (coloured sections from block diagram). 27
Figure 31: Complete experimental setup. 27
Figure 32: The "box" in a faraday cage and an oscilloscope with protection. 28
Figure 33: Schematic, MI circuit: (a) Simplified schematic; (b) Realistic schematic. 29
Figure 34: Synchronization of saw tooth with the "box". 29
Figure 35: The "box" 30
Figure 36: PD measurement circuit. 31
Figure 37: Coaxial setup with samples. 32
Figure 38: Final internal discharge defect schematic. 32
Figure 39: Final internal discharge defect. 32
Figure 40: Final positive corona defect schematic. 33
Figure 41: Final positive corona defect. 33
Figure 42: Final negative corona defect schematic. 34
Figure 43: Final negative corona defect. 34

Figure 44: Final floating electrode defect schematic. 34
Figure 45: Final floating electrode defect. 34
Figure 46: Final surface discharge defect schematic. 35
Figure 47: Final surface discharge defect. 35
Figure 48: Final free-moving particle defect schematic. 35
Figure 49: Final free-moving particle defect. 35
Figure 50: Schematic of the second artificially created defect, consisting of a glass jar filled with oil, using the cavity on the bottom of the jar as a void. 36
Figure 51: Second floating electrode sample; (a) The “dialev”; (b) Floating graphite disc, 1mm away from four neodymium magnets; (c) Arrangement of the four neodymium magnets [60]. 37
Figure 52: The DIV as a function of flatness [22]. 38
Figure 53: Flatness of void [22]. 38
Figure 54: Final individually measured internal discharge sample: (a) Schematic cross-section; (b) Schematic top-view; (c) Picture sample. 41
Figure 55: Final individually measured positive corona sample. 41
Figure 56: Final individually measured negative corona sample. 42
Figure 57: Final individually measured floating electrode: (a) Schematic sample with dimensions; (b) Picture of sample, with a as the “spacer” hole length, b as the gap length between the floating electrode and grounded electrode, and c as the “spacer” diameter. 42
Figure 58: Final individually measured surface discharge: (a) Schematic cross-section; (b) Picture. . 43
Figure 59: Floating electrode with Plexiglas. 43
Figure 60: Experimental electrode in bowl shape. 43
Figure 61: Simplified schematic of the process leading to breakdown [36]. 44
Figure 62: (a) Top-view void location, depth location void; (b) Void in middle of sample; (c) Void near positive electrode; (d) Void near negative electrode. 45
Figure 63: Void in electrode. 45
Figure 64: Aging of internal discharge sample: time evolution and clusters. 47
Figure 65: Aging, internal discharge 0-200 seconds. 48
Figure 66: Aging, internal discharge 200-400 seconds. 48
Figure 67: Aging, internal discharge 400-600 seconds. 48
Figure 68: Aging, internal discharge 600-800 seconds. 48
Figure 69: Aging, internal discharge 800-1000 seconds. 48
Figure 70: Negative corona PRPD. 49
Figure 71: Positive corona PRPD. 50
Figure 72: Surface discharge PRPD. 50
Figure 73: Free-moving particle PRPD. 50
Figure 74: Floating electrode PRPD. 51
Figure 75: Internal discharge PRPD. 51
Figure 76: Negative corona time evolution and clusters. 53
Figure 77: Negatively pulsed corona, pulse 34970. 53
Figure 78: Positive corona time evolution and clusters. 54
Figure 79: Positively pulsed corona, pulse 32497. 54
Figure 80: Surface discharge time evolution and clusters. 55
Figure 81: Negatively pulsed surface discharge, pulse 10110. 55
Figure 82: Positively pulsed surface discharge, pulse 6981. 56
Figure 83: Free-moving particle time evolution and clusters. 56
Figure 84: Negatively pulsed free-moving particle, pulse 27173. 57
Figure 85: Positively pulsed free-moving particle, pulse 27173. 57

Figure 86: Floating electrode time evolution and clusters. 58
Figure 87: Negatively pulsed floating electrode, pulse 47485. 58
Figure 88: Positively pulsed floating electrode, pulse 10741. 59
Figure 89: Internal discharge time evolution and clusters. 59
Figure 90: Negatively pulsed internal discharge, pulse 37715. 60
Figure 91: Positively pulsed internal discharge, pulse 36567 60
Figure 92: Negative corona - Energy per charge vs. charge. 61
Figure 93: Positive corona - Energy per charge vs. charge. 61
Figure 94: Surface discharge - Energy per charge vs. charge. 61
Figure 95: Free-moving particle - Energy per charge vs. charge. 61
Figure 96: Floating electrode - Energy per charge vs. charge. 61
Figure 97: Internal discharge - Energy per charge vs. charge. 61
Figure 98: Negative corona – Pulse fall-time vs. rise-time. 63
Figure 99: Positive corona – Pulse fall-time vs. rise-time. 63
Figure 100: Surface discharge – Pulse fall-time vs. rise-time. 63
Figure 101: Free-moving particle – Pulse fall-time vs. rise-time. 64
Figure 102: Floating electrode – Pulse fall-time vs. rise-time. 64
Figure 103: Internal discharge – Pulse fall-time vs. rise-time. 64
Figure 104: Negative corona TRPD – Positively charged pulses. 66
Figure 105: Positive corona TRPD – Negatively charged pulses. 66
Figure 106: Surface discharge TRPD. 66
Figure 107: Surface discharge TRPD – Negatively charged pulses. 67
Figure 108: Surface Discharge TRPD – Positively charged pulses. 67
Figure 109: Free-moving particle TRPD. 68
Figure 110: Free-moving particle TRPD – Negatively charged pulses. 68
Figure 111: Free-moving particle TRPD – Positively charged pulses. 68
Figure 112: Floating electrode TRPD. 69
Figure 113: Floating electrode TRPD – Negatively charged pulses. 69
Figure 114: Floating electrode TRPD – Positively charged pulses. 69
Figure 115: Internal discharge TRPD. 70
Figure 116: Internal discharge TRPD – Negatively charged pulses. 70
Figure 117: Internal discharge TRPD – Positively charged pulses. 70
Figure 118: Summary of TRPD analysis – Positive and negative charges separated. 73
Figure 119: Defect combination 1: Clusters green and red. 86
Figure 120: Defect combination 1: Red cluster. 86
Figure 121: Defect combination 1: Green cluster. 86
Figure 122: Defect combination 2: Negatively charged pulses TRPD. 88
Figure 123: Defect combination 2: Positively charged pulses TRPD. 88
Figure 124: Defect combination 3: Red cluster pulse. 89
Figure 125: Defect combination 3: Clusters, green and red. 90
Figure 126: Defect combination 3: Green cluster TRPD. 90
Figure 127: Defect combination 3: Red cluster TRPD. 90
Figure 128: Defect combination 3: Green negatively charged cluster TRPD. 91
Figure 129: Defect combination 3: Green positively charged cluster TRPD. 91
Figure 130: Defect combination 3: Red negatively charged cluster TRPD. 92
Figure 131: Defect combination 3: Red positively charged cluster TRPD. 92
Figure 132: Defect combination 4: Clusters. 93
Figure 133: Defect combination 4, pulse 24379. 93

Figure 134: Defect combination 4: Green clusters PRPD. 94
Figure 135: Defect combination 4: Red clusters PRPD. 94
Figure 136: Defect combination 4: TRPD green cluster. 95
Figure 137: Defect combination 4: TRPD red cluster. 95
Figure 138: Defect combination 5: Clusters, green and red. 96
Figure 139: Defect combination 5: TRPD red cluster. 96
Figure 140: Defect combination 5: TRPD green cluster. 96
Figure 141: Defect combination 5: TRPD red cluster negatively charged pulses. 98
Figure 142: Defect combination 5: TRPD red cluster positively charged pulses. 98
Figure 143: Defect combination 5: TRPD green cluster negatively charged. 99
Figure 144: Defect combination 5: TRPD green cluster positively charged. 99
Figure 145: Defect combination 6: Clusters. 100
Figure 146: Defect combination 6, left part: Clusters, green and red. 100
Figure 147: Defect combination 6: TRPD red cluster negatively charged. 101
Figure 148: Defect combination 6: TRPD green cluster negatively charged. 101
Figure 149: Defect combination 7: Clusters. 102
Figure 150: Defect combination 7: PRPD green cluster. 102
Figure 151: Defect combination 7: PRPD red cluster. 102
Figure 152: Defect combination 7: TRPD green cluster. 103
Figure 153: Defect combination 7: TRPD red cluster. 103
Figure 154: Defect combination 9: TRPD green and red clusters. 105
Figure 155: Defect combination 9: TRPD green cluster. 105
Figure 156: Defect combination 9: TRPD red cluster. 105
Figure 157: Defect combination 9: TRPD red cluster negatively charged pulses. 106
Figure 158: Defect combination 9: TRPD red cluster positively charged pulses. 106
Figure 159: Defect combination 9: TRPD green cluster negatively charged pulses. 107
Figure 160: Defect combination 9: TRPD green cluster positively charged pulses. 107
Figure 161: Defect combination 10: TRPD green and red clusters. 108
Figure 162: Defect combination 10: TRPD green cluster. 109
Figure 163: Defect combination 10: TRPD red cluster. 109
Figure 164: Defect combination 10: TRPD red cluster negatively charged pulses. 110
Figure 165: Defect combination 10: TRPD red cluster positively charged pulses. 110
Figure 166: Defect combination 10: TRPD green cluster negatively charged pulses. 110
Figure 167: Defect combination 10: TRPD green cluster positively charged pulses. 110
Figure 168: Defect combination 11: Negatively and positively charged pulses. 112
Figure 169: Defect combination 11: Negatively charged pulses. 112
Figure 170: Defect combination 11: Positively charged pulses. 112
Figure 171: (a) Cable represented as a series of inductors and capacitors; (b) PD pulse attenuation time-domain; (c) PD pulse attenuation frequency-domain. 114
Figure 172: Defect combination 2; energy per charge. 117
Figure 173: Cluster A (green), pulse 116. 117
Figure 174: Cluster B, pulse 3922. 118
Figure 175: Defect combination 2 (renewed internal discharge sample); Left: Energy versus charge cluster; Right: Frequency-equivalent versus time-equivalent cluster. 119
Figure 176: Defect combination 2 with renewed internal discharge sample: TRPD red cluster negatively charged pulses. 120
Figure 177: Defect combination 2 with renewed internal discharge sample: TRPD red cluster positively charged pulses. 120

Figure 178: Defect combination 2 with renewed internal discharge sample: TRPD green cluster negatively charged pulses. 120
Figure 179: Defect combination 2 with renewed internal discharge sample: TRPD green cluster positively charged pulses. 120
Figure 180: Defect combination 6 (renewed internal discharge sample); Left: Energy versus charge cluster; Right: Frequency-equivalent versus time-equivalent cluster..... 121
Figure 181: Defect combination 6: PRPD red cluster. 121
Figure 182: Defect combination 6: PRPD green cluster..... 121
Figure 183: Defect combination 6: TRPD red cluster..... 122
Figure 184: Defect combination 6: TRPD green cluster..... 122
Figure 185: Defect combination 6: TRPD green cluster negatively charged pulses. 122
Figure 186: Defect Combination 6: TRPD green cluster positively charged pulses..... 122
Figure 187: Defect combination 6: TRPD red cluster negatively charged pulses. 123
Figure 188: Defect Combination 6: TRPD red cluster positively charged pulses..... 123
Figure 189: Defect combination 7 with renewed internal discharge; Left: Energy versus charge cluster; Right: Frequency-equivalent versus time-equivalent cluster. 123
Figure 190: Defect combination 7 with renewed internal discharge sample: TRPD reen cluster negatively charged pulses. 124
Figure 191: Defect combination 7 with renewed internal discharge sample: TRPD green cluster positively charged pulses. 124
Figure 192: Defect combination 7 with renewed internal discharge sample: TRPD red cluster negatively charged pulses. 125
Figure 193: Defect combination 7 with renewed internal discharge sample: TRPD red cluster positively charged pulses. 125
Figure 194: Defect combination 8 with renewed internal discharge; Left: Energy versus charge cluster; Right: Frequency-equivalent versus time-equivalent cluster. 125
Figure 195: Defect combination 8 with renewed internal discharge sample: PRPD green cluster.... 126
Figure 196: Defect combination 8 with renewed internal discharge sample: PRPD red cluster..... 126
Figure 197: Defect combination 8 with renewed internal discharge sample: TRPD green cluster negatively charged pulses. 126
Figure 198: Defect combination 8 with renewed internal discharge sample: TRPD green cluster positively charged pulses. 126
Figure 199: Defect combination 8 with renewed internal discharge sample: TRPD red cluster negatively charged pulses. 127
Figure 200: Defect combination 8 with renewed internal discharge sample: TRPD red cluster positively charged pulses. 127
Figure 201: Positive corona, shapes of negatively charged pulses. 131
Figure 202: Surface discharge, shapes of negatively charged pulses. 132
Figure 203: Free-moving particle, shapes of negatively charged pulses. 132
Figure 204: Floating electrode, shapes of negatively charged pulses. 132
Figure 205: Internal discharge, shapes of negatively charged pulses. 133
Figure 206: Negative corona, shapes of positively charged pulses. 133
Figure 207: Surface discharge, shapes of positively charged pulses. 133
Figure 208: Free-moving particle, shapes of positively charged pulses. 134
Figure 209: Floating electrode, shapes of positively charged pulses. 134
Figure 210: Internal discharge, shapes of positively charged pulses. 134
Figure 211: Negatively charged pulses: Positive corona, consistency check 1. 136
Figure 212: Negatively charged pulses: Positive corona, consistency check 2. 136

Figure 213: Negatively charged pulses: Positive corona, consistency check 3. 137
Figure 214: Negatively charged pulses: Positive corona, consistency check 4. 137
Figure 215: Negatively charged pulses: Internal discharge sample 1, consistency check 1. 137
Figure 216: Negatively charged pulses: Internal discharge sample 1, consistency check 2. 137
Figure 217: Negatively charged pulses: Internal discharge sample 1, consistency check 3. 138
Figure 218: Negatively charged pulses: Internal discharge sample 1, consistency check 4. 138
Figure 219: Negatively charged pulses: Internal discharge sample 2, consistency check 1. 138
Figure 220: Negatively charged pulses: Internal discharge sample 2, consistency check 2. 138
Figure 221: Negatively charged pulses: Internal discharge sample 2, consistency check 3. 138
Figure 222: Negatively charged pulses: Free-moving particle, consistency check 1. 139
Figure 223: Negatively charged pulses: Free-moving particle, consistency check 2. 139
Figure 224: Negatively charged pulses: Free-moving particle, consistency check 3. 139
Figure 225: Negatively charged pulses: Floating electrode sample 1, consistency check 1. 140
Figure 226: Negatively charged pulses: Floating electrode sample 1, consistency check 2. 140
Figure 227: Negatively charged pulses: Floating electrode sample 1, consistency check 3. 140
Figure 228: Negatively charged pulses: Floating electrode sample 2, consistency check. 140
Figure 229: Negatively charged pulses: Surface discharge, consistency check 1. 141
Figure 230: Negatively charged pulses: Surface discharge, consistency check 2. 141
Figure 231: Negatively charged pulses: Surface discharge, consistency check 3. 141
Figure 232: Positively charged pulses: Negative corona, consistency check 1. 142
Figure 233: Positively charged pulses: Negative corona, consistency check 2. 142
Figure 234: Positively charged pulses: Negative corona, consistency check 3. 142
Figure 235: Positively charged pulses: Negative corona, consistency check 4. 142
Figure 234: Positively charged pulses: Internal discharge sample 1, consistency check 1. 143
Figure 235: Positively charged pulses: Internal discharge sample 1, consistency check 2. 143
Figure 236: Positively charged pulses: Internal discharge sample 1, consistency check 3. 143
Figure 237: Positively charged pulses: Internal discharge sample 1, consistency check 4. 143
Figure 238: Positively charged pulses: Internal discharge sample 2, consistency check 1. 144
Figure 239: Positively charged pulses: Internal discharge sample 2, consistency check 2. 144
Figure 240: Positively charged pulses: Internal discharge sample 2, consistency check 3. 144
Figure 241: Positively charged pulses: Free-moving particle, consistency check 1. 145
Figure 242: Positively charged pulses: Free-moving particle, consistency check 2. 145
Figure 243: Positively charged pulses: Free-moving particle, consistency check 3. 145
Figure 244: Positively charged pulses: Floating electrode, consistency check 1. 146
Figure 245: Positively charged pulses: Floating electrode, consistency check 2. 146
Figure 246: Positively charged pulses: Floating electrode, consistency check 3. 146
Figure 247: Positively charged pulses: Floating electrode sample 2, consistency check. 146
Figure 248: Positively charged pulses: Surface discharge, consistency check 1. 147
Figure 249: Positively charged pulses: Surface discharge, consistency check 2. 147
Figure 250: Positively charged pulses: Surface discharge, consistency check 3. 147
Figure 251: Edge detection and shape matching. 130
Figure 252: Shape matching (resizing, centring, rotating, flipping, reflecting and cropping). 131
Figure 253: Example TRPD defect recognition flowchart. 150

List of Tables

Table 1: Calibration, 50 pulses of 10, 100 and 1000pC. 20
Table 2: Voltage and current peaks of noise and PDs. 24
Table 3: Final internal discharge specifications. 33
Table 4: Final positive corona specifications. 33
Table 5: Final negative corona specifications. 34
Table 6: Final floating electrode specifications. 34
Table 7: Final surface discharge specifications. 35
Table 8: Final free-moving particle specifications. 36
Table 9: Summary: selecting internal discharge sample. 40
Table 10: Summary, slopes of energy per charge vs. charge 62
Table 11: Summary of PRPD analysis. 65
Table 12: Summary of TRPD analysis – Charge successor vs. charge. 71
Table 13: Summary of TRPD analysis – Number of discharges vs. charge. 72
Table 14: Summary of TRPD analysis – Time presessor and successor vs. charge. 72
Table 15: Summary of TRPD analysis – Positive and negative charges separated. 73
Table 16: Pulses per cycle. 73
Table 17: Pulses per cycle – Positively and negatively charged pulses. 74
Table 18: Calculation deviation of time vs. recorded pulses. 75
Table 19: Average deviation, direct proportionality of time and pulses. 75
Table 20: Minimum running time or number of discharges (pulses) needed. 78
Table 21: PD pulse restrictions. 79
Table 22: Energy vs. charge cluster restrictions. 79
Table 23: Energy vs. charge cluster in logarithmic scale restrictions. 79
Table 24: PRPD analysis restrictions. 80
Table 25: TRPD analysis restrictions. 82
Table 26: Energy per charge vs. charge cluster restrictions. 83
Table 27: Discharges per cycle analysis restrictions. 83
Table 28: Measured defect combinations. 85
Table 29: Defect combination 2, negatively charged: Summary of TRPD analysis. 88
Table 30: Defect combination 3, green cluster: Summary of TRPD analysis. 91
Table 31: Defect combination 5, red cluster negatively charged: Summary of TRPD analysis. 97
Table 32: Defect combination 5, red cluster positively charged: Summary of TRPD analysis. 97
Table 33: Defect combination 5, green cluster negatively charged: Summary of TRPD analysis. 98
Table 34: Defect combination 5, green cluster positively charged: Summary of TRPD analysis. 98
Table 35: Defect combination 9, red cluster negatively charged: Summary of TRPD analysis. 106
Table 36: Defect combination 9, red cluster positively charged: Summary of TRPD analysis. 106
Table 37: Defect combination 9, green cluster negatively charged: Summary of TRPD analysis. 106
Table 38: Defect combination 9, green cluster positively charged: Summary of TRPD analysis. 107
Table 39: Defect combination 10, red cluster negatively charged: Summary of TRPD analysis. 109
Table 40: Defect combination 10, red cluster positively charged: Summary of TRPD analysis. 109
Table 41: Defect combination 10, green cluster negatively charged: Summary of TRPD analysis. 110
Table 42: Defect combination 10, green cluster positively charged: Summary of TRPD analysis. 110
Table 43: Summary cluster analysis of multiple defects. 113
Table 44: Summary of PRPD analysis of multiple defects. 115
Table 45: Summary of TRPD analysis of multiple defects. 116
Table 46: Slope relations of energy per charge versus charge. 117

Table 47: Shapes for recognition of negatively charged artificially created defects..... 135
Table 48: Shapes for recognition of positively charged artificially created defects..... 135
Table 49: Corona discharge shapes for TRPD pattern recognition. 148
Table 50: Internal discharge shapes for TRPD pattern recognition. 148
Table 51: Free-moving particle shapes for TRPD pattern recognition. 149
Table 52: Floating electrode shapes for TRPD pattern recognition. 149
Table 53: Surface discharge shapes for TRPD pattern recognition. 150
Table 54: PDIV for Void Depth 1mm 164
Table 55: PDIV for Void Depth 3mm 164
Table 56: PDIV for Void Depth 2mm 164
Table 57: All paring sample combinations 184
Table 58: Summary shapes for recognition artificially created defects..... 205

Nomenclature, Acronyms and Abbreviations with Notation

A	Atom
A^*	Atom at a higher energy level (excited atom)
AC	Alternating current
AC-PD	PDs occurring under AC voltage
A^m	Atom in a metastable state
B	A second atom
Ca	Test object/sample
CC	Connecting cables
C_c	Coupling capacitor [Farad]
CD	Coupling device
CIV	Corona inception voltage
Ck	Coupling capacitor
C_k	Coupling capacitor [Farad]
CT	Current transformer
DC	Direct current
DC-PD	PDs occurring under DC voltage
DIV	Discharge inception voltage
e	Charge or electron [Coulomb]
eV	Electron volt; unit of energy equal to $\pm 1.6 \cdot 10^{-19}$J [Joule]
EV	Extinction voltage
eV_i	Ionization energy [$1eV=1.602 \cdot 10^{-19}$J]
eV^m	Atom energy level when in metastable state
GIS	Gas insulated systems
h	Planck's constant (equal to $6.626 \cdot 10^{-34}$ m^2kgs^{-1}) $[m^2kgs^{-1}]$
HFCT	High-frequency current transformer
HV	High voltage
HVAC	High voltage alternating current
IEC	International Electrotechnical Commission
IEEE	Institute of Electrical and Electronics Engineering
IV	Inception voltage

LV	Low voltage
Mi	Partial discharge measuring instrument
MV	Medium voltage
n	PD number of pulses
NV	Not valid
p	Gas pressure [bar]
PD	Partial discharges
PDIV	Partial discharge inception voltage
PRPD	Phase-resolved partial discharge
q	PD charge magnitude [Coulomb]
RI	Radio influence
TO	Test object
TRPD	Time-resolved partial discharge
U_t	Test voltage [volts]
v	Radiated frequency [Hz]
W	Kinetic energy [Joule]
Z_m	Measuring impedance as part of the coupling device
Z_{mi}	Input impedance of measuring circuit
Z_n	Noise-blocking filter
α	Ionization factor
α_{eff}	Mean value of the effective ionization factor
ε_r	Relative permeability
λ	The path length (free path) [meters]
τ_s	Average time lag of the occurrence of an initiatory electron [seconds]
φ	Phase angle

1. Introduction

In daily life, it is nearly impossible to function without electricity. We need it for everything, from watches to working, cooking, and more. Nearly all consumers want (and expect) an uninterrupted electricity supply. The cost associated with the failure to deliver continuous power can be great not only for the consumer, but also for the distributor. Therefore, it is even more important to do proper maintenance and efficiently operate the electricity grid. With preventive maintenance, for instance with partial discharge measurements, maintenance costs and time can be reduced. PD detection is one of the most promising methods for determining the condition of power systems and for monitoring and detecting possible insulation defects in components of power systems before a fault occurs. The current on-line partial discharge monitoring systems are too expensive and complex. Because of this, they cannot be implemented on a large scale for online monitoring of MV cables.

Partial discharge is an electrical discharge that occurs without completely bridging the gap/insulation between two conducting materials/electrodes. According to the International Standard IEC60270 [1], partial discharges are defined as localized electrical discharges that only partially bridge the insulation between conductors and that can or cannot occur adjacent to a conductor. PDs are, in general, a consequence of local electrical stress concentrations in the insulation. Generally, such discharges appear as pulses with a duration of much less than 1µs. There are many types of PDs, each with their own cause for occurrence.

During this research project a PD test platform was designed and build for electrical PD detection. The setup included artificially created defects for six different types of PDs, with origins in positive and negative corona, internal discharge, floating electrodes, free-moving particles and surface discharge. These defects were designed to have a partial discharge inception voltage (PDIV) of around 10kV, and could easily be connected or disconnected from the setup. Therefore, it was possible to measure individual defects or a combination of them. This PD test platform was used during this research project to characterize the different PD types (single and multiple), and as a check for testing new clustering and pattern recognition techniques. In addition, the platform could also be used as a test platform for educational purposes and to train people and test equipment. The thesis goals are to build a setup suitable for the research, determining the optimal combination of hardware/software to discriminate among different types of defects, and to realize experiments to validate the design.

Thesis Statement: ***Design of a Partial Discharge Test Platform.***

1.1. Objectives and Goals

The final goals of this project are to:

- Design and build a workbench for education, training and research purposes
- Study pattern recognition under AC conditions

In order to validate the proposed design, a circuit with multiple PD sources (artificial defects), such as those that can be encountered in real MV cable circuits, is designed and built. The purpose of this circuit is to test the hardware/software design to recognize multiple defects. The circuit consists of a collection of different samples with artificial defects. The inception voltage is around ±10kVrms. The samples are placed in parallel, as shown in Figure 1. A coaxial setup is used to achieve an equal inductance and equal path length, and therefore equal attenuation. The coaxial setup will also help in ease of measurement. As shown in Figure 2, there is the possibility of 1 or multiple connections.

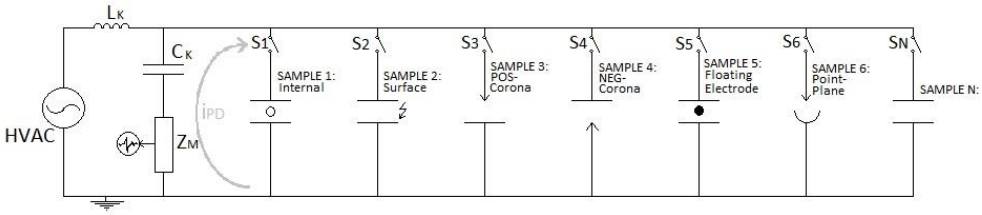

Figure 1: Proposed schematic test setup.

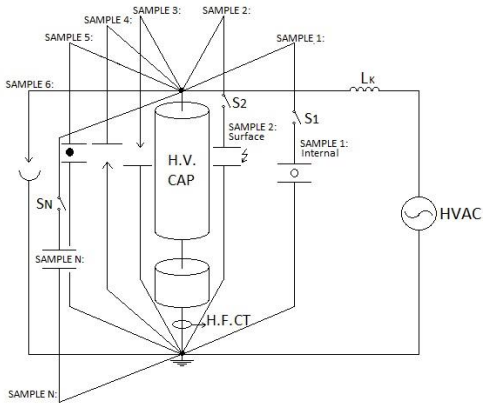

Figure 2: Proposed schematic coaxial test setup.

The thesis goals are to build a setup suitable for the research, determining the optimal combination of hardware/software to discriminate among different types of defects, and to realize experiments to validate the design.

1.2. Contributions

In general, this thesis has two contributions to the literature and to practice:

I. Partial discharge (PD) measurements are an effective tool for insulation diagnostics and assessment, and a good understanding of these PD measurements is essential background knowledge for an electrical engineer. During this research project a PD test platform was designed and made for electrical PD detection with e.g. the following benefits:
   - coaxial arrangement including six different types of artificially created PD defects
   - equal attenuation, distortion and path length
   - low (inception) voltage
   - time domain pulse comparison
   - pattern recognition platform

II. In conventional PD measurements, phase-resolved partial discharge (PRPD) analysis is used for origin recognition for partial discharge under AC voltage. This research project attempts to find new PD origin recognition tools (for AC voltage) that do not depend on the phase of the voltage, so with e.g. the use of time-resolved partial discharge (TRPD) analysis. Through this attempt various conclusion are drawn, and in the end a good solution is found to replace PRPD analysis for AC voltage. This provides simpler, cheaper and more compact PD measurement equipment. Due to the fact that the phase does not need to be measured, no phase measurements will be needed when applying TRPD analysis.

1.3. Thesis Overview

The thesis consists of nine chapters. The first chapter explains the thesis statement along with the motivation, objectives, goals and a general overview of the thesis.

Chapters 2 and 3 are a literature review describing, among other things, PD pulses, their origins, PD measuring techniques, their representation and their aging. In chapter 3 analysis methods and clustering techniques used during this thesis will be elaborated. Chapter 4 presents the designed partial discharge test platform with its associated components. The artificial defects created for the PD test platform are explained in chapter 5, including the steps taken to achieve these results. In addition, the influence of aging is analysed to understand how it affects each type of defect. Chapter 6 characterizes and analyses all the different artificially created defects. Different cluster techniques are investigated with their possibilities, along with PRPD and TRPD analysis. In this chapter, restrictions are also set for the PD type recognition. In chapter 7 data from multiple artificial defects are analysed, looking at different cluster detection methods for PD type/origin separation and selection by using PRPD and TRPD analysis tools. The analysis methods and clustering techniques, as described in chapter 4, are investigated and confirmed in what extend each finding is possible. These findings of TRPD analysis for ACPD are further explored and characterized in chapter 8, where PD shape pattern recognition is proposed with the final shapes for each artificially created defect. Finally, in chapter 9, the findings and conclusions drawn in the previous chapters are summarized, and the thesis goals and objectives are clearly reviewed. After this, recommendations are made for future research.

2. The Origins of Partial Discharges

The modern world relies heavily on electricity, to the point that we cannot go a day without it. Because of this, we have very high standards for the continuity of the electric grid: outages and blackouts are simply unacceptable. In order to achieve an uninterrupted service for a long period of time, some circumstances that cause breakdowns must be prevented [10, 11]:

- **Overheating that is caused by dielectric losses**
  In new equipment there is little overheating, because most of the time this equipment has low dielectric losses. As a consequence, there is no danger to the insulation. However, due to aging, dielectric losses increase gradually over time. The process of aging is accelerated by a combination of operating at high temperatures and heating by dielectric losses. Therefore, limits are set to the tan δ.
- **PDs**
  PDs that occur in the technical insulation decrease the object lifetime. Therefore, there are some limits in the test specifications in the areas of:
  1. Inception voltages, PDIV.
  2. Discharge magnitudes, q.
- **Treeing**
  The electrical treeing phenomena can be divided into three stages: initiation, propagation and breakdown. The initiation stage determines whether an electrical tree will grow in the insulation or not. There are different types of defects in a material that can cause treeing, such as:
  - protrusions (at the electrode)
  - inclusions (in the dielectric)
  - cavities (containing PDs)
  - interstices (containing PDs)

  The progress rate of treeing depends on the applied electric field. If the field is low it can take years before breakdown occurs, but at an elevated field, the growth rate increases rapidly and breakdown can occur within minutes [11, 41].

Therefore, to achieve an uninterrupted electricity supply it is best to conduct (preventive) maintenance on the grid. With PD analysis we can accurately assess the reliability of the electrical insulation [8]. On-line diagnosis is the only feasible solution to investigate insulation systems of the state of the electrical apparatus and plan effective maintenance actions, looking at the advantages in terms of cost, time and real operating conditions [10]. The demand for non-destructive diagnostic tests on electrical devices is constantly increasing, because we want quality control and reliability assessments for electrical systems [14]. While PDs occur in AC and DC voltage, PDs in DC voltage will not be considered in this thesis; the focus will be on AC voltage.

A partial discharge is an electrical discharge that occurs without completely bridging the gap/insulation between two conducting materials/electrodes. According to the International Standard IEC60270 [1], partial discharges are defined as localized electrical discharges that only partially bridge the insulation between conductors and that can or cannot occur adjacent to a conductor. PDs are in general a consequence of local electrical stress concentrations in the insulation. Generally, such discharges appear as pulses with a duration of much less than 1µs. These pulses will be explained in more detail in section 2.2. There are many types of PDs, each of which occur in real-life situations. This topic is elaborated in more detail in section 2.1.

PDs occur at voids, gaps, or other defects in MV and HV cable systems (apparatus). These inevitable minor flaws lead to partial discharges; all these defects/dielectric imperfections (weak points) are the vulnerable sites of PD occurrence. PDs dissipate energy continuously and therefore cause gradual damage to these weak points, bringing about premature failure of the apparatus. [21] This aging and deterioration of the material will be supported in section 5.4. The “imperfections” cause local field enhancement, which might exceed the intrinsic field strength. Therefore, PDs develop in these areas of the insulation system where the localized electric field strength exceeds its dielectric strength. Because of these high local fields, self-sustaining electron avalanches can be ignited [6].

As mentioned above, PDs can originate from various local defects, and in order to ensure the reliable operation of HV equipment it is important to know as much as possible about these PDs, from their statistical characteristics to their individual properties such as their type and origin [17]. The different types of PD’s will be explained below.

2.1. PD Types and Sources

In general, there are three types of PDs, namely, internal discharges (including those in electrical treeing), surface discharges and corona discharges [12]. However, in our experimental setup we will distinguish between more types of defects (PD types): internal discharge, surface discharge, positive and negative corona, floating electrode and free-moving particle. Not all insulation systems for electrical apparatus have similar PD types. The PD types are material-dependent, whether it is a solid material, e.g. cables and condenser bushings; a liquid material, e.g. oil-filled cables; or a gaseous material, e.g. gas insulated systems (GIS). The different types of defects are explained in more detail below.

2.1.1. Internal Discharge

This type of discharge occurs in gas-filled voids/cavities within solid dielectrics. This type of discharge can also be initiated due to electrical treeing, because electrical treeing creates cavities in a dielectric. In these cavities the (internal) discharges take place. For example, modern power cables cannot avoid the formation of voids, cavities and cracks or the inclusion of dust particles or small metallic turnings, and therefore they always have these defects [21]. The dielectric strength of the gas is represented by the Paschen curve; the PDIV (ignition field strength) can be determined from this curve, but it can also be calculated. Internal discharges within a dielectric can be represented by the equivalent circuit shown in Figure 3. This circuit is known as the abc-circuit. It is actually a representation of the actual behaviour of the electrical fields in a dielectric.

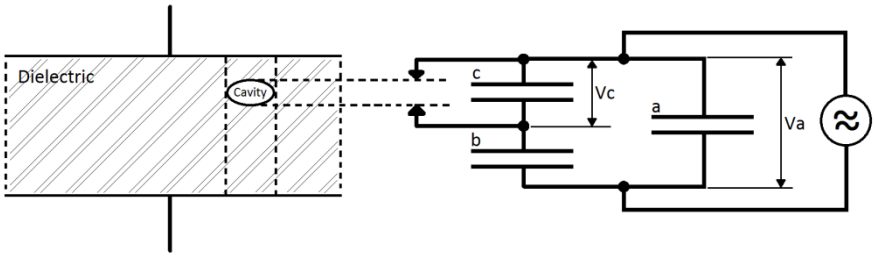

Figure 3: Internal discharge, abc model [12].

On the left is the dielectric with the cavity. The size of the cavity determines the breakdown voltage of the cavity and is illustrated by a spark-gap in the schematic. Capacitor ‘c’ represents the capacitance of the cavity with Vc the synchronous voltage at the cavity (‘c’ is the part of the configuration that breaks down). ‘B’ is the capacitance of the dielectric in series with the cavity, and the capacitance ‘a’ is the capacity of the rest of the dielectric with Va the voltage over the sample, and

is the unaffected part of the dielectric. Therefore, if an AC voltage (Va) is applied over the sample, a synchronous voltage (Vc) results at the cavity:

$$V_c = \frac{b}{b+c} \cdot V_a$$

In the cavity, discharges occur when this voltage Vc reaches the breakdown voltage ±U; the voltage over the cavity drops down to the voltage level ±V. This recurrent discharge pattern is the result of the process happening several times per period, an example of which can be seen in Figure 4. The voltage level ±U can be derived from the Paschen curve [11, 12, 21].

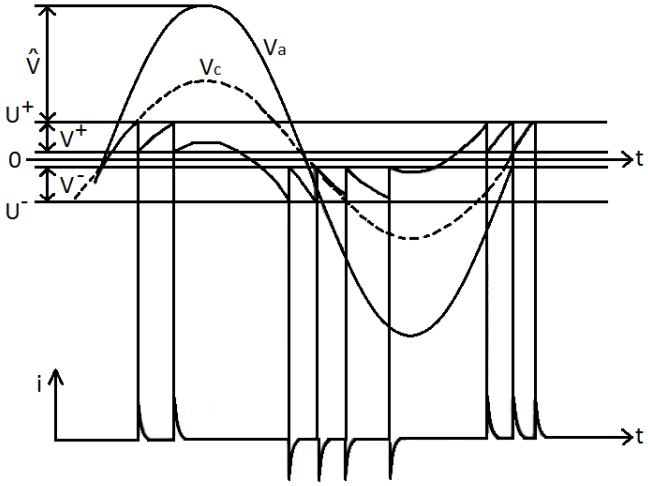

Figure 4: Internal discharge, abc model graphs [11].

Even if there are defects in a dielectric, it does not necessarily mean that there are PDs when voltage is applied. Sometimes it takes time; for instance, in very small voids, when no initiating electron(s) are present there can be no ignition, and the partial discharges do not occur. This ignition can be initiated by creating initiating electron(s) by subjecting the sample to X-rays [12].

2.1.2. Surface Discharge

In cases in which a tangential field is present, surface discharges occur along gas- or liquid-bounded dielectric interfaces. Below, Figure 5(a) presents an example of a schematic representation of surface discharges.

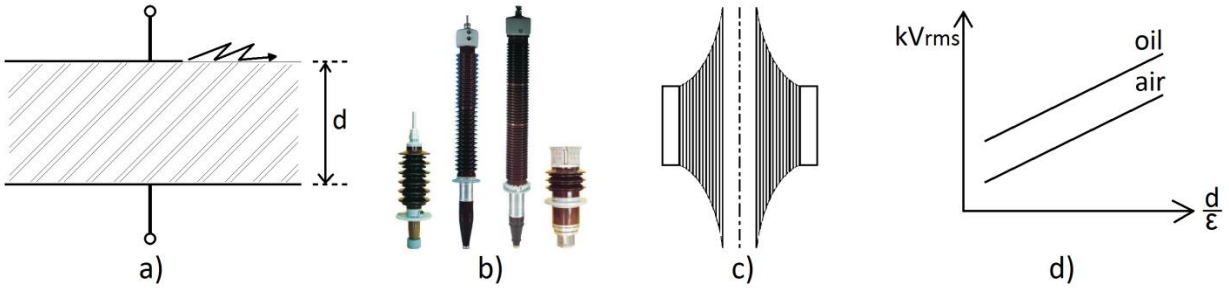

Figure 5: (a) Surface discharge schematic [12]; (b) Examples of bushings [45]; (c) Schematic bushing [11]; (d) Surface discharge inception voltage graph [12].

The surface discharge schematic is a representation of discharges occurring at the edges of metallic foils within condenser bushings. Examples of these condenser bushings can be seen in Figure 5(b), and Figure 5(c) shows a schematic representation of these foils, where they are inserted in the insulation. The field strength in a dielectric is relatively low because of these surface

discharges, and therefore we have a low inception stress. Figure 5(d) shows a graph with an indication of the inception voltages plotted against the insulation thickness divided by the dielectric permittivity. The surface discharge can also be represented with the abc model, and here the same explanation is valid as for internal discharge. But now, instead of discharges occurring in the void, they occur along the dielectric (the path-length). This abc representation for surface discharge can be seen in Figure 6 [11, 12].

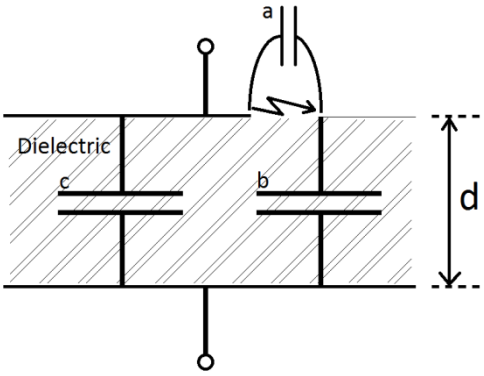

Figure 6: Surface discharge, abc model [12].

2.1.3. Corona Discharge

A corona is a discharge caused by electrical overstress. It is a luminous discharge due to the ionization of the air surrounding a conductor around which exists a voltage gradient exceeding a certain critical value. Corona can occur in liquid or gaseous insulating materials [13]. This type of PD got its name from the crown effect that the luminous discharge has at higher voltages; at lower voltages, just above PDIV, it looks almost like an invisible glow. Corona occur at sharp points and edges in gas insulation between two electrodes, where a high field is present, and they can disturb other discharges during PD measurements. Aside from this, the occurrence of corona is unwanted in the HV apparatus, because it causes losses in HV lines, radio interference and by-products in SF6 (this by-product attacks the insulation construction), among other issues. One great advantage of corona discharges is that they are efficient producers of ozone in the air (negative more than positive). This partial breakdown phenomenon occurs long before breakdown takes place, and therefore its occurrence is usually associated with the starting phase of electrical failure of the isolation [11, 12].

There are different types of corona, which can be distinguished by the location of the defect. They can occur on the HV side, the earthed side or halfway between electrodes [11, 12]. Between these three locations, two types of corona can be distinguished, namely, positive and negative corona (Figure 7).

Negative Corona:

A negative corona is created by sharp points or edges on or near the cathode. This point at negative voltage in air can be seen in Figure 7(a). Because it is close to the cathode, Townsend discharges can easily be formed in the vicinity of the point. A positive space charge is formed due to a diffusive discharge that occurs around the point that pushes the electrons away. These electrons that are pushed away attach to the oxygen molecules that are a bit further away and therefore form a negative space charge. The discharge stops when the sharp point is screened away from the electric field due to this formed negative space charge. The electric stress recovers when the negative space charge drifts away. In this case, the discharge ignites again and a recurrent phenomenon occurs. This recurrent phenomenon is responsible for radio interference and is the cause of the dielectric losses.

Negative corona discharges are Townsend discharges, and therefore the PDIV can be derived from the Paschen curve. These Townsend discharges can be seen in Figure 7(b).

Positive Corona:

Negative corona appears at lower voltages compared to positive corona, because unlike negative corona, positive corona occur in the regions of high field strength near the anode (no cathode is available). In positive corona the streamer mechanism plays an important role, and the positive space charges are left behind by the streamer discharges occurring in the gas at the point. In this case, it is the same as a negative corona: the positive space charges form a shield, and shield the point from the electric field so that the discharge stops. This can be seen in Figure 7(c). The positive charge will drift away and the discharge will reignite (recurrent discharges). The higher the voltage is, the longer the streamers are, and if the streamers are too long they cannot be extinguished by the space charges. Discharge channels are formed, which can be seen in Figure 7(d).

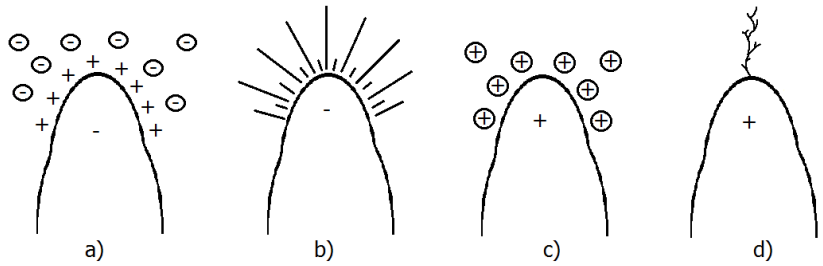

Figure 7: (a, b) Negative corona and (c, d) positive corona [11].

The corona PDIV depends on the radius of the sharp edge: the smaller the radius of the sharp edge, the lower the IV of the corona is in air. The PDIV does not depend on the field strength but on the voltage, because the local field strength is not decreased by the field strength and corona discharges can occur at very low voltages. Therefore, we must prevent our HV apparatus from having any sharp points or edges.

Corona discharges can also be represented with the abc model, just like internal and surface discharges. The model for a negative corona can be seen in Figure 8(a), in which the recurrence of the breakdown in capacitance c is determined by the physical process near the point (the ionization process in this area) and is independent of the voltage wave shape. Corona discharges occur along the phase as long as the applied voltage exceeds the inception voltage ±Ui. This is visualized in Figure 8(b) [11, 12].

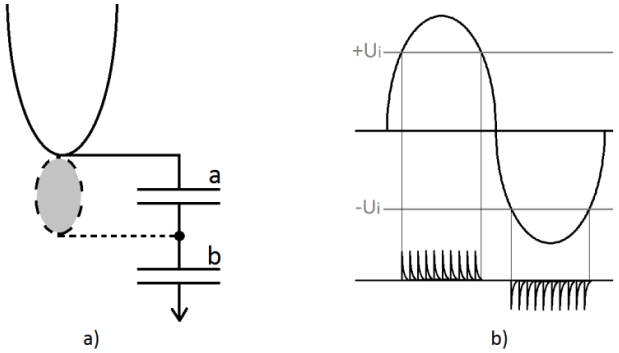

Figure 8: (a) Negative corona, abc model; (b) PD occurrence with corona [12].

2.1.4. (Electrically) Floating Electrodes

This defect can occur when the contacts of a field grading shield become loose from the conductor. Due to electrically floating electrodes, a potential is created, which is determined by the

relationship of the capacitance of the floating electrode and the capacitance of the conductor to the ground. A discharge occurs when, because of the applied voltage and the capacitances, a potential is created that exceeds the insulation strength of the gas. The electrically and acoustically measured PDs in this case are relatively high. These PDs do not immediately lead to breakdown, but the material will be damaged by the PDs and dust particles will be created in the process, and eventually breakdown will occur [46]. An example of a field grading shield (field control element) on a cable joint can be seen in Figure 9(a). The field control element can be seen in Figure 9(b), in which the equipotential lines are evenly spread out between the HV line and the earth (no field concentration), which is due to the shape of the earth electrode.

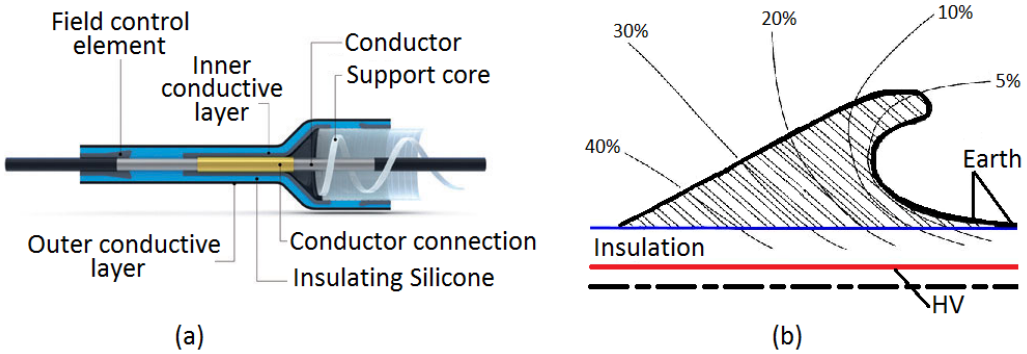

Figure 9: (a) Cable joint; (b) Field control element (stress-cone) [47].

2.1.5. Free-Moving Particles

This PD type, the free-moving particle, occurs mainly in gas insulated systems (GIS). Free-moving particles are responsible for many failures, including:

- The triggering of a flashover, due to a free-moving particle approaching a conductor.
- The carbonization of e.g. a spacer. The free-moving particle is the source of carbonization, and the spacer is carbonized when the free-moving particles lie on the spacer.

The levitation of the free-moving particle is an electric field-driven phenomenon, and it is not influenced by the gas (atmospheric air, CO_2 or SF_6). The particle acquires an induced surface charge when it comes in contact with the enclosure of an energized GIS. This induced surface charge exerts a coulomb force on the particle itself, due to its interaction with the background electric field. The charge distribution is dependent on the size, shape, orientation and location. The charged particle distorts the electric field, and when the exerted coulomb force exceeds the gravitational force, the particle lifts off towards the electrode. This can be visualized by the dynamic equation of the particle motion:

$$F_{Coulomb} + F_{Drag} + F_{Gravity} = m \cdot a$$

Three stages of particle movement exist:

I. Shuffling particle
II. Moving particle
III. Jumping particle

In the first stage the particle moves slowly and causes low PD activity. Afterwards, in the second stage, the particle starts to move and shows higher PD activity. In the last stage the particle starts jumping (one jump can last for more than one voltage cycle) [11, 12, 46].

2.1.6. Inception and Extinction Voltage

The voltage at which PDs start to occur is the PDIV. However, if afterwards the voltage is decreased, the PDs disappear at a different voltage level compared to the IV. This voltage level is the extinction voltage EV. The extinction voltage is lower than the IV, and it could be as low as 50% below the IV (in practice it is around 10-35%) [12].

2.2. PD Pulses

As explained above, dielectric imperfections cause a local field enhancement. If these field enhancements are greater than the intrinsic field strength, self-sustaining electron avalanches can be ignited. Because of the formation of the electron avalanches within the nanosecond range, we can associate each individual PD event with a very fast current pulse. These current pulses are caused by the moving charge carriers [6].

The defect origins are within the technical insulation of the test object (TO). Because of this, the defect origin is inaccessible with a physical measurement device. However, at the terminals (electrodes) of the TO, fast transient current pulses can be measured, which are associated with the movement of the charge carriers inside the defect origin. These pulses must travel through the technical insulation of the TO, so the pulse will be attenuated. Therefore, the true shape of the PD current pulse cannot be measured. A disadvantage of this method is that the frequency content of the PD signal is dramatically reduced. This reduction is due to the attenuation and dispersion of the PD pulse when it propagates through the insulation, from the source of the PD to the terminals/electrodes of the TO (propagation path of the pulse) [6].

The shape of the PD pulse is influenced by the mechanism and the discharge magnitude. Therefore, we can distinguish between three types of PD pulses when looking at the PD evolution in voids:

I. The pulse shape of a streamer-like discharge
II. The pulse shape of a Townsend-like discharge
III. The pulse shape of a pitting discharge

The difference between these discharges is the running time; the first stage can be seen as a virgin pulse, the second as a more mature pulse, and the third stage is the one just before breakdown. Aside from this, the sensor used for PD detection and the source/location of the PD also affect the PD shape. This will be elaborated further in section 7.2.1 [36, 37].

2.2.1. Pulse Shape of a Streamer-like Discharge

Normally, the pulses have a very steep front and a short duration (on the order of 1ns). The magnitudes of the discharges depend on the sample/defect. The repetition rate of PDs in streamer-like discharges is very high, with a time between the PD pulses in the ns range, or sometimes even a fraction of an ns. This pulse is shown graphically in Figure 10.

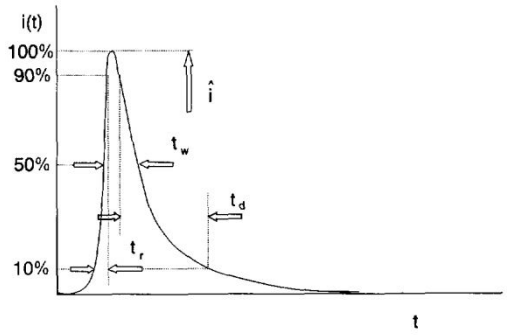

Figure 10: PD pulse of streamer-like discharge [36].

This graph also shows the different parameters that characterize a PD pulse [36]:

- Pulse amplitude (100%)
- Pulse rise time t_r [ns]
- Pulse width t_w [ns]
- Pulse decay time t_d [ns]

2.2.2. Pulse Shape of a Townsend-like Discharge

A Townsend-like discharge has a different discharge mechanism from a Streamer-like discharge, and, compared to a Streamer-like discharge, it is a slower process. In this pulse, this difference can be seen in the “slower” front (on the order of 10ns) and longer pulse duration (on the order of 100ns). Unlike the sharp pulses from the streamer-like discharges, here in the Townsend-like discharge pulses the peaks are flatter (widely scattered). This pulse is seen graphically in Figure 11. For this pulse the same characteristic parameters as pulses from Streamer-like discharges are valid and include one extra parameter for the pulse width, namely, a pulse width at 20% of its amplitude $t_{w,20\%}$ [ns] [36].

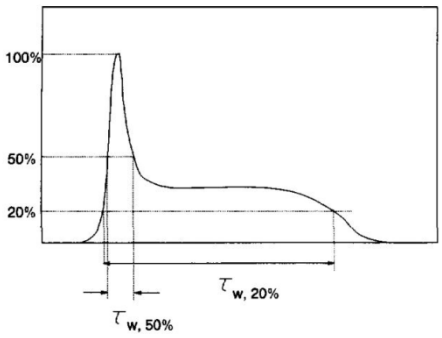

Figure 11: PD pulse of Townsend-like discharge [36].

2.2.3. Pulse Shape of a Pitting Discharge

In the case of a pitting discharge, the pulse height is smaller and has a repetition rate of several discharges per microsecond. The steep front of this pulse is similar to the fast pulses of streamer-like discharges, but the decay time is longer, in the order of 10ns. This discharge type received its name because these discharges cause severe pitting of the dielectric (e.g. void surfaces). This is because the pitting discharges are a very localized event, and are therefore more damaging. This pulse has the same characteristic parameters as streamer-like discharge pulses, and can be seen graphically in Figure 10 [36].

3. PD Analysis

As explained above, the movement of the charge carriers is associated with fast transient current pulses that are detectable at the electrodes of the test object (TO). These measured pulses are used to recognize the PDs [6]. By interpreting the PD patterns, the PD source and the reason of occurrence can be revealed. Therefore, this method is used for condition monitoring and quality control. For many years this interpretation of patterns was done by (human) experts, but lately, due to the great advances in pattern recognition tools/techniques and in processing hardware, this is no longer necessary. The PD pattern interpretation process and recognition has been improved and automated because of these recent advancements; due to these computer-aided processes the interpretation and recognition of PD measurements has become more efficient and reliable [9, 11, 16]. When identifying the source of the PD, we want to know its [18]:

- geometrical configuration
- size
- location

With these, we can differentiate the PD pulse pattern from outside interference (if there is any present). Important PD pulse attributes for achieving this and the interpretation of PD patterns are [18]:

- discharge pattern
- discharge amplitude
- rise time
- recurrence rate
- discharge epochs (phase relationship of occurrence with respect to the applied voltage)
- time interval to the preceding and successive pulses

When analysing PDs, we are interested in the dielectric materials used. The insulation may consist of gaseous, liquid or solid materials, or even a combination of them. These different sources of PDs each have different effects on the performance of the insulation. This is why it is important to classify the PDs in order to evaluate the harmfulness of the discharge [16].

At the moment there are three categories of PD pulse data patterns that are used for the analysis and evaluation of PDs: phase-resolved data (PRPD), time-resolved data (TRPD) and data without phase/time information [18]. PRPD is commonly used for recognizing and identifying AC-PDs (PDs occurring under AC voltage) and TRPD for DC-PDs (PDs occurring under DC voltage). In this thesis, all three types will be used. The main goal for representing the PDs is to recognize and identify the typical PD sources by means of oscilloscopes or a computerized PD measuring system [6].

In this chapter testing/measuring systems with phase-resolved (PRPD) and time-resolved (TRPD) partial discharge analysis methods will be explained, followed by the different clusters used with explanations of the calculations and calibration.

3.1. Testing and Measuring PDs

PD analysis has been used as a condition monitoring and quality control tool, because by interpreting PD patterns, their origin/source and reason for occurrence can be revealed. For a long time this interpretation was done by human experts. Lately, however, PD analysis has become automated and pattern interpretation and recognition has become much easier due to advancements in electronics and pattern recognition tools [9]. PD tests are a non-destructive predictive qualitative analysis tool, with which we can:

- Detect insulation defects (from the cable manufacturing process or from cable system operation), e.g. terminations producing corona, damaged cable insulation, dirty contaminated terminations, defective terminations and splices
- Detect insulation deterioration (from normal system operating conditions)
- Locate problem areas in a cable system (cable/splices/terminations)

When performing PD tests we evaluate the level of PDs present. By compiling and trending the measurements we can determine to what extend the PDs will increase. With this, we can determine when and where to take action before failure occurs, which is why we can warn of a potential upcoming system failure with these PD tests.

We want to be able to predict the degradation state of electrical apparatus/cables. This can be achieved by finding the markers that vary as a function of applied stresses and time in such a way that the degradation state can be devised and/or predicted [10].

3.1.1. Measuring Instrument

The MI (sensor) is a very important part of the setup in this research project, since the MI must be able to measure/catch the (electrical) signals coming from the PDs. In order to understand this properly it is important to know how a PD presence can be indicated, e.g. by [42]:

- Chemical transformation
- Gas pressure
- Light
- Heat
- Sound
- Electrical signals

Not all of these indicators can be used for PD detection. Light, heat, sound and electrical signals have a practical importance for PD detection in cable systems. We can differentiate between different types of methods for determining the PD severity in HV apparatus, e.g. [6, 42]:

- **Chemical measuring methods:**
  Heat originating from PDs can be detected with heat cameras. Because small discharges generate only a small amount of heat, they cannot be detected with this method.
- **Optical measuring methods:**
  Light originating from PDs can be detected with optical sensors. This method detects only external or corona discharges, due to limited visibility. With corona, just above the inception voltage there is an almost invisible glow, while at higher voltages a crown of light (corona) can be seen that occurs at the regions of electrical overstress. This light (radiation) comes principally from the recombination of positive ions with free electrons [6, 13, 42].
- **Acoustical measuring methods:**
  With ultrasonic sensors, sounds originating from PDs can be detected. This method works well with corona and surface discharges but not with internal discharges.
- **Electrical measuring methods:**
  According to [7], these non-electrical methods are not suitable for quantitative measurement of PDs, but are primary used to detect and locate PDs. In our experimental setup we will be using an electrical detection method with a CT, N32 Coil. This will be explained in more detail in section 4.5.3.

There are different PD technologies available on the market for both on-line and off-line PD measurements. Some companies that provide PD measurement equipment and technology are Baur,

SebaKMT, PhenixTECH, HVINC, B2HV, HighVolt and OnSiteHV. Due to our interested in e.g. the pulse shape, length, etc. in our system, a fast oscilloscope will be used since it brings more flexibility for research.

3.1.2. Classical Detection System

There are four basic measuring circuits for alternating voltages. Other test circuits are derived from these basic circuits, according to [4]. Figure 12 presents three of these circuits.

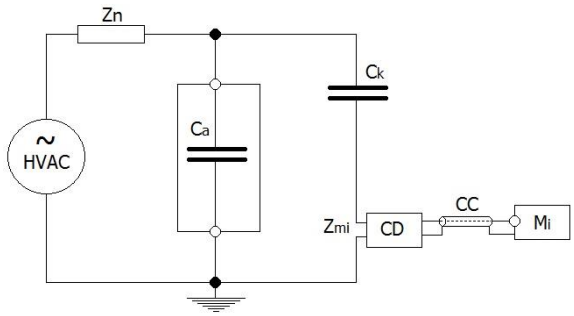

HVAC	High voltage alternating current
Zmi	Input impedance of measuring circuit
CC	Connecting cables
Ca	Test object
Ck	Coupling capacitor
CD	Coupling device
Mi	Measuring instrument
Zn	Filter

Figure 12: Schematic of PD measurement circuits: Coupling device in series with the coupling capacitor.

The PD measuring circuit consists of the following major components:

- Voltage source: high voltage supply
- Filter, Zn: a high voltage inductance used to reject electromagnetic noises coming from the voltage supply. The filter used in the PD test platform will be elaborated in more detail in section 4.2.3.
- Coupling capacitor, C_k: ensures a short duration of the recharging process so there are easily reproducible PD measurements.
- Coupling device, CD: The coupling device has the purpose to separate the PD current pulses from the power frequency test voltage circuit.
- Measuring impedance: converts current impulses into measurable voltage pulses. This voltage pulse has to be proportional to the apparent charge.
- Data acquisition device: must register and evaluate the measurements. In our setup we mainly used the Tektronix DPO7354C Digital Phosphor Oscilloscope with two Transient Voltage Suppressors (TSV) for its protection, but PD detectors from Hubbell and TechImp were also used.
- Signal/data processing: with the post-processing of the data we are able to separate PDs from noise, eliminate as much noise as possible, distinguish between different types of PDs and locate the origin of PDs.

3.1.3. Limitations of PD Measurements

There are many factors that limit proper PD measurements, including measurement/detection sensitivity, noise and interference signals, reliability and structural aspects (physical accessibility).

Measurement/detection Sensitivity

There is no such thing as universal measurement sensitivity, because the sensitivity is dependent on the measurement conditions and circuit. The sensitivity of the measurement also depends on the sensor quality, encountered disturbance levels, the travelled path of the PD and the effectiveness of the signal processing on disturbance removal. The harmfulness of a PD is dependent on its defect type and magnitude, which can range from 1 to 10^4 pC. The sensitivity of the measurement

determines what part of this range can be detected/measured. Therefore, we can say that measurement sensitivity is one of the major limiting factors in partial discharge measurements [42].

Noise and Interference Signals

Noise and interference signals disturb the PD measurements, and the level of noise can vary greatly depending on the day and place. The detection sensitivity is determined by the noise level; therefore, external noise is a fundamental limitation of field testing.

Due to the exponential attenuation nature of the pulse during propagation, sensitivity also decreases exponentially. When most of the higher frequencies are attenuated (long enough propagation), and only lower frequencies remain, then the disturbance will start to play an even more important role, since most of the background noise is distributed over the lower frequencies. Therefore, it will be even more difficult to measure PDs from long MV cables, because the frequency range of the background noise is the same as the measurable frequencies of the PDs [42, 43].

Reliability

The measurement instrument should not hinder the measurement itself; that is, it should not become the reason for a fault by itself.

Structural Aspects (Physical Accessibility)

This type of limitation relates to the physical accessibility of the system, e.g. component structure and the possibility of installing a sensor. Depending on the system accessibility, the length between sensors is limited (PD localization), and therefore the measured frequency of the pulse will be limited.

When our setup (test platform) is finished, it is important to know its limitations. Some of these limitations will be discussed for the designed PD test platform, including its internal noise levels, PDIV, reliability and lifetime of sample(s), in sections 4.2.1, 5.4 and 7.6.

3.2. Phase-Resolved Partial Discharge (PRPD)

For this analysis method we measured not only the PDAC signal (fast transient AC current pulses) but also the corresponding phase. When using the phase-resolved PD (PRPD) analysis we group the PD pulses together by their phase angle with respect to the 50Hz sine-wave (phase signal). Therefore, the voltage cycle is represented in phases, which represent the phase angles from 0^0 to 360^0 [9]. These groups of PD pulses within the 360^0 phase angle form shapes that can be used to determine the source of the PD (PD type).

As shown in Figure 13, the PRPD plots that are used for pattern recognition consists of (red) dots that will form a specific, source-dependent shape. Each dot represents one PD pulse. In PRPD plots the x-axis is the phase angle (location of occurrence), and the y-axis is the charge of the pulse.

By definition we know that the charge of a fast transient current pulse is the area under the pulse, or the integral in time of the pulse:

$$Q = \int_0^\infty i(t) \cdot dt$$

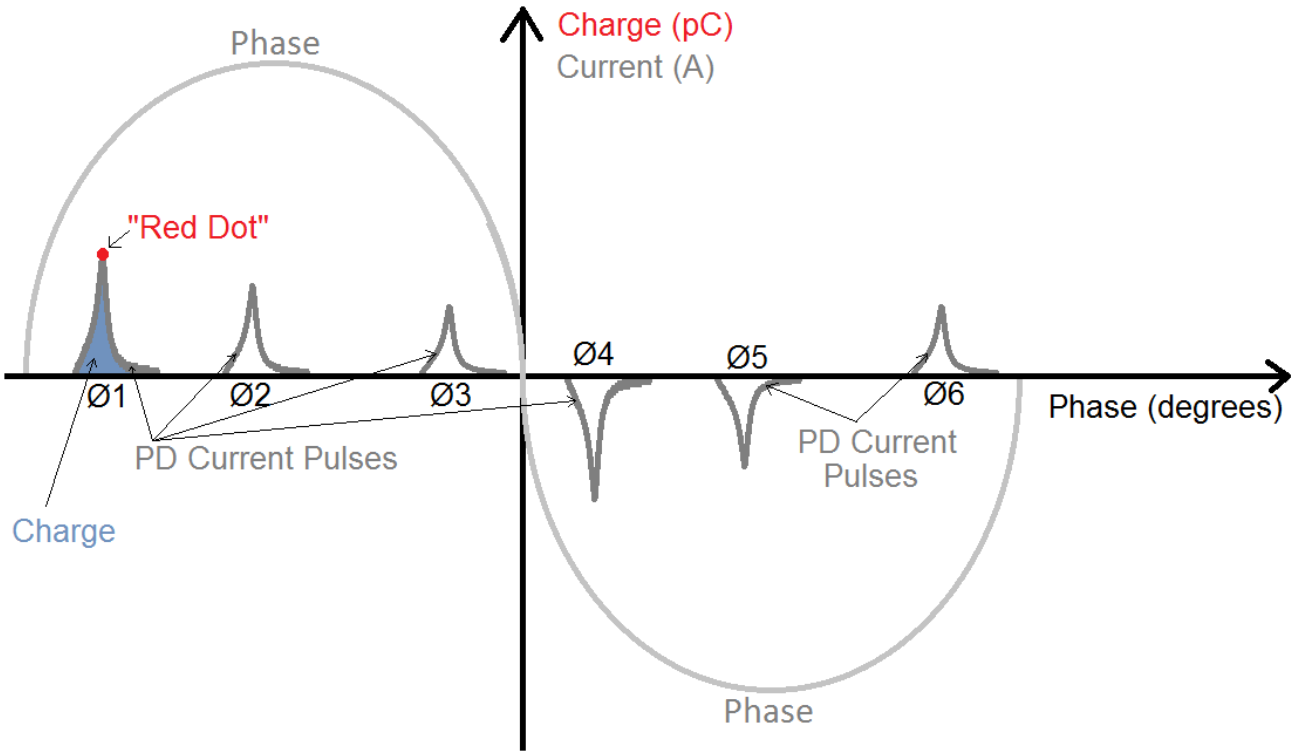

Figure 13: PRPD graph explanation; 50 Hz sine-wave representation (phase-signal) with positive and negative PD current pulses.

3.3. Time-Resolved Partial Discharge (TRPD)

Normally, time-resolved partial discharge (TRPD) analysis is used for PDs occurring under applied DC voltage, because in DC there is no alternation in voltage like there is in AC voltage. In this thesis we will also attempt to use this technique for PD recognition under applied AC voltage.

In the TRPD plots, each PD pulse is also represented by one dot. Multiple dots together will also form shapes that will be used for pattern recognition. During this thesis we will compare four different graphs, with the following representations.

Charge Successor (Qsuc) vs. Charge (Q)

Here the charge of the pulse is plotted on the x-axis, and the charge of the following pulse (successor) is plotted on the y-axis. Examples are shown in Figure 14. Considering the pulse occurring at t1, then the pulse occurring at t2 is its successor, etc. So the charge of this pulse (blue) will be plotted on the x-axis and the charge of the successor (following pulse) is at t2, which will be plotted at the y-axis.

Number of Discharges vs. Charge (Q)

The number of discharges per cycle occurring in one 50Hz cycle is counted and plotted on the y-axis and the charge is plotted on the x-axis.

Time Precessor or time successor vs. Charge (Q)

In this graph the time between the pulses is plotted against the charge. T_{pre} is the time between the pulse and the previous pulse. An example of this is shown in Figure 14. If we take pulse t4, then the time to the precessor pulse is Δ2 and the time to successor is Δ3.

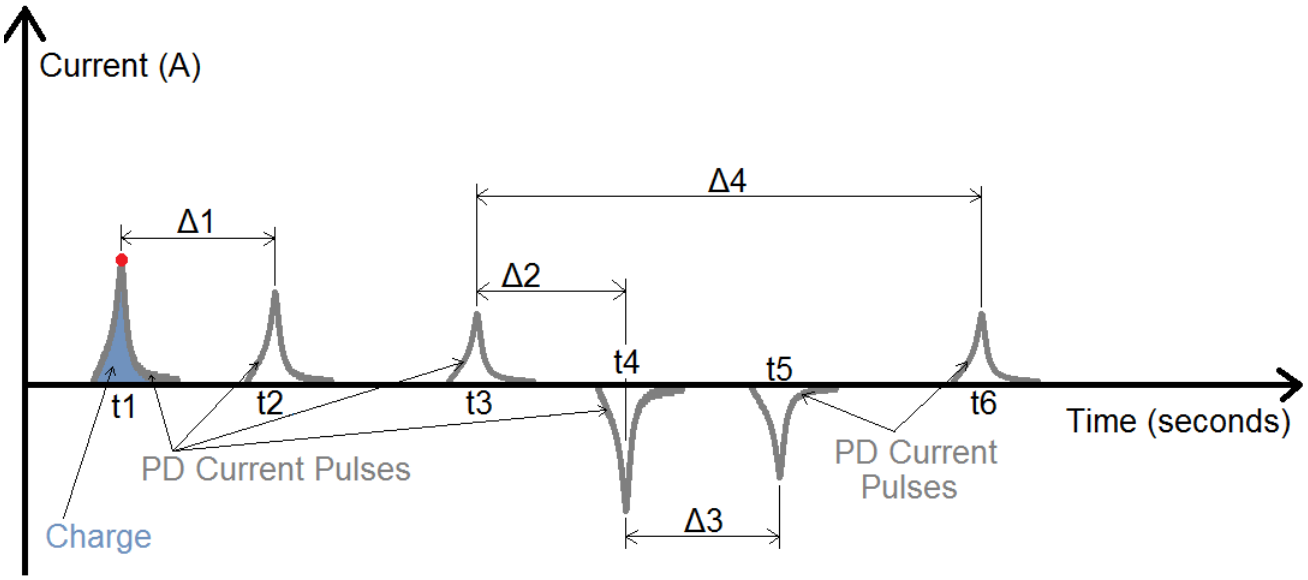

Figure 14: TRPD figure explanation, positive and negative PD current pulses.

Later during the research the charge will be separated into positive and negative charges, so there will be two plots. This will affect the distribution of the discharges (dots) within the TRPD plots. If the charge polarities are separated, the sequence of time will change between the pulses. In this case, for instance, if we take the pulse t3, the time successor will be Δ4, so at t6 the next pulse will occur. Normally this would be the pulse at t4, but this is no longer the case. The same will be done with the TRPD plot of Qsuc vs. charge.

3.4. Clusters

This section presents an explanation of the clusters used in this research. The goal of using these clustering techniques is to distinguish between the different PD types. During the analysis of the PDs we used five types of clustering techniques:

I. Frequency-equivalent vs. time-equivalent
II. Energy vs. charge
III. Energy vs. charge (in logarithmic scale)
IV. Energy per charge vs. charge
V. Rise-time vs. fall-time

3.4.1. Charge Calculation

Charge is one of the representative parameters of a PD. This can be said because the charge represents the damage done to the insulation. In order to calculate (or estimate) the charge, the PD pulse must be measured and processed afterwards [62]. By definition, the charge is the integral of the current, and can therefore be calculated directly by integrating the measured PD current pulse. In practice, this is not exactly the case. A PD measuring system can be described generally as a band-pass filter, where the minimum lower cut-off frequency is dependent on the required attenuation of the

power frequency and the upper cut-off frequency is dependent on the high frequency behaviour of the different components of the measurement system [63]. According to [61] and [62], this integral over the time domain (charge calculation) tends to be zero, due to distortion produced by the measuring system over the PD pulse.

For the PD test platform we will be estimating the charge in the frequency-domain based on [62]. With the Fourier transform, a signal in time domain can be converted into a signal in frequency domain. The Fourier transform for a non-periodic function is by definition:

$$F(w) = \int_{-\infty}^{+\infty} f(t) \cdot e^{-j \cdot w \cdot t} \cdot dt$$

This formula contains implicit information about the area of the function f(t): when w is assumed to be 0 the value of the Fourier transform is equal to the charge of the function f(t). Since the charge is equal to the area of the function f(t), then by definition:

$$Q = \int_{0}^{\infty} i(t) \cdot dt$$

We will be considering short pulses, since PDs are actually short transient current pulses. For example, consider a short rectangular current pulse i(t) with amplitude k and pulse duration d. Therefore:

$$I(w) = \int_{0}^{d} i(t) \cdot e^{-j \cdot w \cdot t} \cdot dt = \int_{0}^{d} k \cdot \cos(wt) \cdot dt - j \int_{0}^{d} k \cdot \sin(wt) \cdot dt$$

Sin(wt) and cos(wt) were checked for different values of frequencies (kHz) and pulse durations (ns) in [62], where it was concluded that the cosine values at low frequencies for short pulses are close to 1 and the sine values are close to 0. Short rectangular pulses can therefore be approached at low frequencies by:

$$I(w) \approx \int_{0}^{d} k \cdot \cos(wt) \cdot dt \approx k \cdot d = \int_{0}^{d} i(t) \cdot dt = Q$$

From this formula we can conclude, according to [62], that under the same conditions, the low frequency components of the Fourier transform approach the charge of the pulse. Therefore it is possible to estimate the pulse charge if the low frequency components of the current pulse are measured (under the defined conditions).

If the lower cut-off frequency of the measuring system is small enough, we can estimate the charge of the pulse in frequency domain. This charge estimation can be done by using spectral analysis and using the low frequency components of the measured pulse.

3.4.2. Energy Calculation

The definition of energy is:

$$e[Joule] = V[Volt] * Q[Coulomb]$$

where V is the applied voltage and Q is the estimated charge. In our case, the voltage is the measured pulse voltage vector and Q is the estimated charge, as explained above in section 3.4.1.

3.4.3. Frequency- and Time-Equivalents

This clustering technique is based on [64], where the classification of the PD pulses is based on the time behaviour and the frequency content of each PD pulse. The classification is carried out using a fuzzy classification (FC) method. The time-equivalent is a parameter related to the time, and is used to get one representation of time for the measured pulse. Assume a PD pulse signal to be sampled in K samples and $s_i(t_i)$ is the sample detected at time t_i (the time of each memory buffer is normalized to a zero reference). The Time-equivalent is: [64]

$$T_{eq} = \sqrt{\frac{\sum_{i=0}^{K}(t_i - t_0)^2 \cdot s_i(t_i)^2}{\sum_{i=0}^{K} s_i(t_i)^2}}$$

where

$$t_0 = \frac{\sum_{i=0}^{K} t_i \cdot s_i(t_i)^2}{\sum_{i=0}^{K} s_i(t_i)^2}$$

with t_0 being the time position of the signal. The frequency-equivalent is calculated in a similar way. It is a parameter related to the frequency, and is used to get one representation of the frequency for the measured pulse. The frequency-equivalent is: [64]

$$W_{eq} = \sqrt{\frac{\sum_{i=0}^{K} {f_i}^2 \cdot |X_i(f_i)|^2}{\sum_{i=0}^{K} |X_i(f_i)|^2}}$$

where $X_i(f_i)$ are the frequency components of the PD signal, obtained via FFT transformation. [64]

3.4.4. Rise- and Fall-Time

For this cluster, the rise-time is taken from 10% to 90% of the pulse peak and the fall-time is taken from 90% down to 10%. This can be visualized in Figure 10.

3.5. Calibration

Irrespective of the method for charge calculation, the calibration used in the program of the PD test platform is based on the calibration described in [62].

According to [3], the capacitance Ca of the test object affects the circuit characteristics. We calibrate the system each time when changing or modifying the sample to ensure that the measuring system is able to measure the PD magnitude correctly.

When measuring with the TechImp or the Hafely PD detector, we calibrated the measuring system by injecting short-duration current pulses of known charge and magnitude into the terminals of the test object. When the PD measurement was conducted with the “BOX” described in section 4.3 below, the calibration was done by measuring the known injected charge of different magnitudes in the final experimental setup. The different measured magnitudes are adjusted with a calibration factor to get the right charges/magnitudes in the Matlab program. The calibration devices used for injecting the pulses are:

- Calibrator Type CAL141 from SEITZ Instruments
- Calibrator from Tettex Instrument

Below, Figure 15, Figure 16 and Figure 17 show the amplitude and charge of the 50 recorded pulses and the different magnitudes for the final experimental setup.

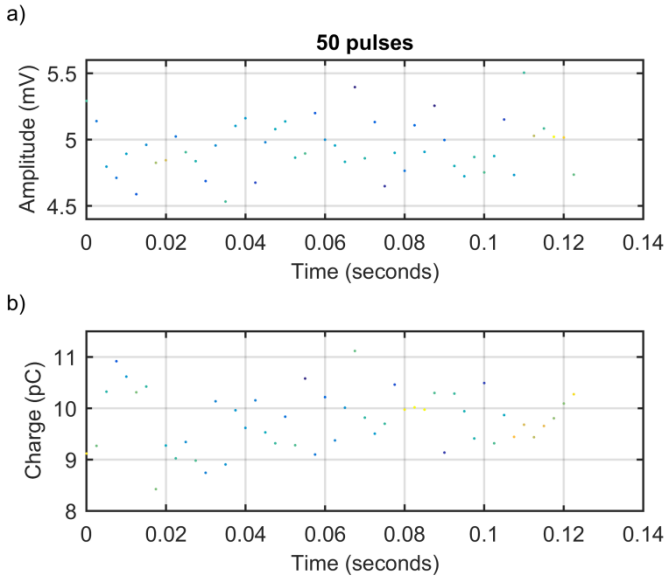

Figure 15: Calibration, 50 pulses of 10pC.

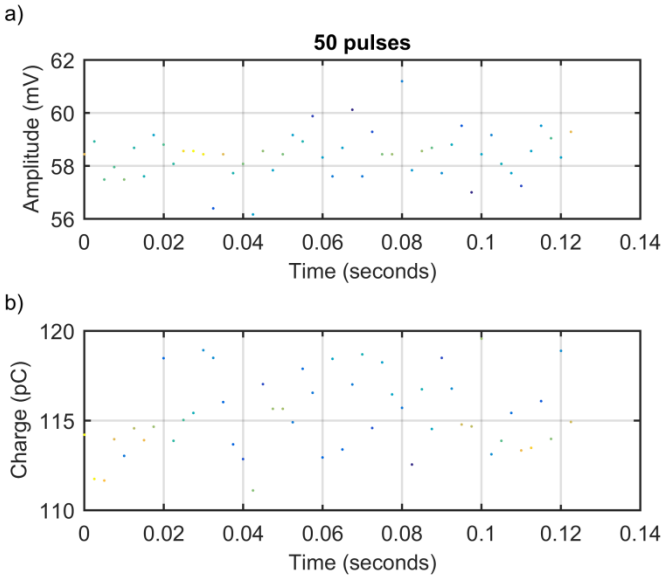

Figure 16: Calibration, 50 pulses of 100pC.

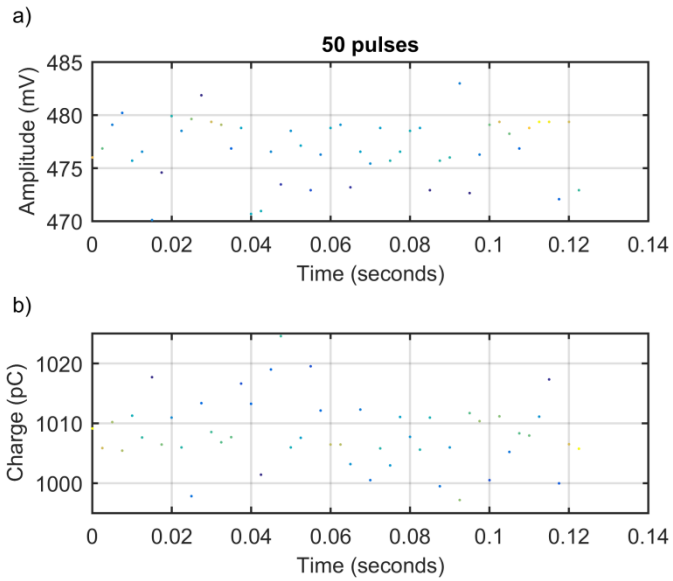

Figure 17: Calibration, 50 pulses of 1000pC.

	10pC pulse			100pC pulse			1000pC pulse		
	Max.	Min.	Avg.	Max.	Min.	Avg.	Max.	Min.	Avg.
Amplitude	5.45	4.57	5	61.11	56.44	58	482.3	470.4	477
Charge	11.12	8.42	10	119.56	111.11	115	1024.54	997.22	1010

Table 1: Calibration, 50 pulses of 10, 100 and 1000pC.

The charges/magnitudes in the matlab program have a relative error of:

$$RE(10pC) = \frac{10-10}{10} \cdot 100\% = 0\%;\ RE(100pC) = \frac{115-100}{100} \cdot 100\% = 15\%;$$

$$RE(1000pC) = \frac{1010-1000}{1000} \cdot 100\% = 1\%$$

The charges measured during the experiments are in the range of 10pC to 10nC, so the error in measuring the charge is minimal. We must keep in mind that the measured charges have a relative maximum error of 15%. The standard accounts for 10%.

4. Experimental Setup

In this chapter the designed PD test platform is explained and presented. We begin by explaining the electrodes used in section 4.1, looking at their shapes, material and distance. Afterwards, some aspects that could influence the measurements are explained in section 4.2. At the end, in section 4.3, the designed PD test platform is presented with its components.

4.1. Electrodes

In the design of the PD test platform, one of the most important aspects is the electrodes that are used. In this section their shape, material and distances will be discussed.

4.1.1. Shapes

The electrodes used have a Rogowski profile uniform-field configuration. The electrodes are made according to the Rogowski profile described in [11]. Here, the field strength at the edge is never larger than that in the centre of the gap. Therefore, there is no breakdown at the edges with an electrode system of this shape. Another advantage of this shape is that there are no concentrated fields on the edges. This shape is derived from the formula:

$$e^{F(Z)} + F(Z) + 1 = Z$$
$$Z = x + jy$$
$$F = v + ju$$
$$\therefore x + jy = e^{v+ju} + v + ju + 1 = e^{v}\cos(u) + e^{v}\sin(u) + v + ju + 1$$
$$\therefore x = e^{v}\cos(u) + v + 1 \; and \; y = e^{v}\sin(u) + u$$

From these equations we can derive the equipotential lines, if we use v as a variable and u as a constant. We will choose the electrodes at u=0 and π:

$$\therefore x - 1 = e^{v} + v \; and \; y = 0$$
$$\therefore x - 1 = v - e^{v} \; and \; y = \pi$$

This can be seen in Figure 18(a). In this figure there are two regions, forming “a” below the line u=0.5π and “b” above. In region “b” the equipotential lines curve back and concentrate at the edges of the top electrode (u=π). In region “a”, on the other hand, no concentration takes place.

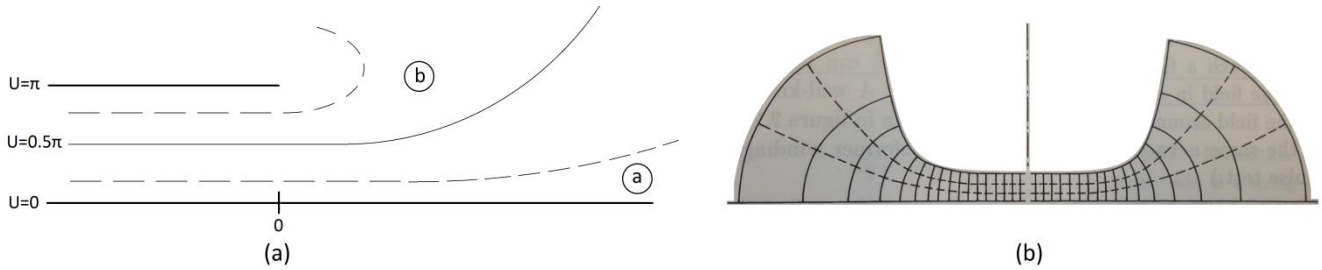

Figure 18: (a) Field line between half u=π and full line u=0; (b) Rogowski gap [11].

As shown in Figure 18(b), due to the shape of the electrode the field lines are evenly distributed. Figure 18(b) further shows that the corners of the electrode are shaped according to the 0.5π line of Figure 18(a). In the middle of the electrode, the field strength is homogeneous and equal to:

$$E = \frac{v}{a} = \frac{Voltage\ over\ electrode}{Electrode\ distance}$$

As shown in Figure 18(b), the field strength is biggest in the middle of the electrode, and therefore the field strength at the edges is everywhere smaller than v/a. The Rogoski profile, therefore, gives us an as evenly possible distributed field, so the electrodes will not affect the measurements.

4.1.2. Material

The electrodes can have different materials with different properties:

- **Stainless steel:** Carbonization does not occur, as it does with brass electrodes.
- **Brass electrode:** According to [20], the brass electrode causes excessive carbonization. This frequently causes PDs to cease, and therefore no complete breakdown will occur. If the sample is placed between brass electrodes, the estimation of life at a certain voltage is less certain, because excessive carbonization frequently inhibits the discharges [20].
- **Platinum:** Carbonization does not occur, as it does with brass electrodes.

In our case, we used good quality stainless steel electrodes.

4.1.3. Distance

The distance between the electrodes at all points should be at least larger than the breakdown voltage of air but not too large, so that there is still enough electric field to create PDs at 10kV. Since we are applying 10kV on the samples/electrodes, the minimum distance needed to create PDs without breakdown is 3⅓mm for air (breakdown voltage of air: 3kV/mm [55]). Depending on the sample, the distance should be even greater to avoid disturbances.

4.2. Noise, Disturbance, Interference & Attenuation

There are different kinds of disturbances, or background noise, present when measuring PDs. The PD measurements are often obscured by interferences caused by these disturbances. According to [56], these disturbances can be classified into two categories:

I. Disturbances occurring without voltage applied to the PD test platform.
   These types of disturbances can be caused by e.g. switching operations of other circuits, other HV tests done in the lab or close by, radio transmissions or communicating machines. In addition, the apparatus used in the measuring circuit can also supply noise, even if no voltage is applied. Therefore, noise originating from the measuring instrument itself is also part of this type of disturbance.

II. Disturbances occurring only with voltage applied to the PD test platform, and that do not occur in the TO:
   This type of disturbance usually increases with increasing voltage, and consists of e.g. PDs in the HV transformer, conductors and bushings. But it can also be caused by spark discharges in the vicinity of HV due to imperfect connections or imperfectly earthed objects. Harmonics of the test voltage within or close to the bandwidth of the measuring system may also be a cause for disturbances. Most of the time, these harmonics are present in the LV supply, and are transferred together with the noise of e.g. sparking contacts from the LV source through the transformer/connections to the rest of the circuit.

There are many methods for disturbance reduction, the most efficient of which are screening and filtering. These methods are, in general, only possible within a laboratory where the (electrical) connections are equipped with filters and the setup is shielded from the outside world (faraday cage). During the design of the PD test platform and the troubleshooting process, different disturbances were encountered, most of which are mentioned, described and elaborated in this section.

There is also attenuation of the PD pulse. As a pulse propagates through e.g. a large cable, the pulse is attenuated, and the shape of the pulses changes slightly. The peak value and the area of the pulse (charge) both attenuate while traveling. The larger the travelled distance, the more the attenuation, so the more data from the “original” pulse is lost. This phenomenon will be explained in more detail in section 7.2.1.

There are many different types of noise, disturbances and interferences. These were considered and taken into account during the design of the PD test platform. There are three steps when dealing with these disturbances: detection, source and reduction. During our measurements we noticed different sources, which are discussed below.

4.2.1. Internal Noise of Circuit & Effect of Trigger

Below, Figure 19 shows the internal noise of the circuit when the trigger is placed at 0mV. When placing the trigger at 1mV, there was no clear difference distinguishable compared to the graph where the trigger was placed at 0mV; thus, the trigger did not have much effect. Therefore, we increased the trigger slightly more, to 3mV. With the trigger placed at 3mV nearly all the noise pulses disappeared, as seen in Figure 20. Here, the number of recorded pulses is only 10 in ±120 seconds, compared to the 50000 pulses in ±23 seconds.

As can be appreciated in Figure 20, the amplitude of the noise seldom goes above 3mV, and nearly never above 4mV. Therefore, we can conclude that when using this setup, the trigger should always be at a minimum of 3mV. To be safe and to ensure no internal noise interference, in our measurements the trigger will never be below 4mV.

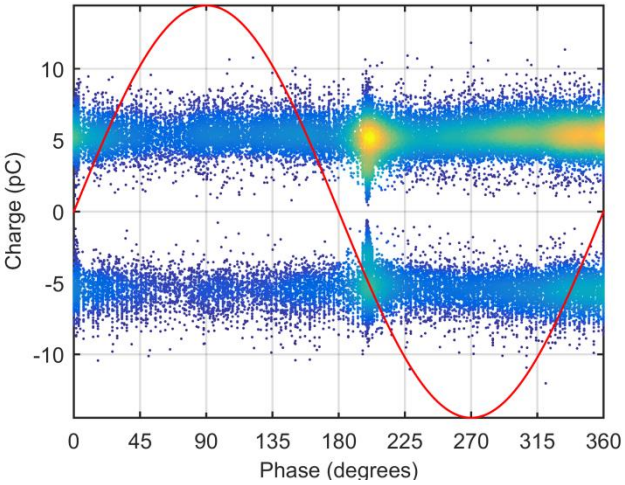

Figure 19: Internal noise with trigger at ±0mV PRPD.

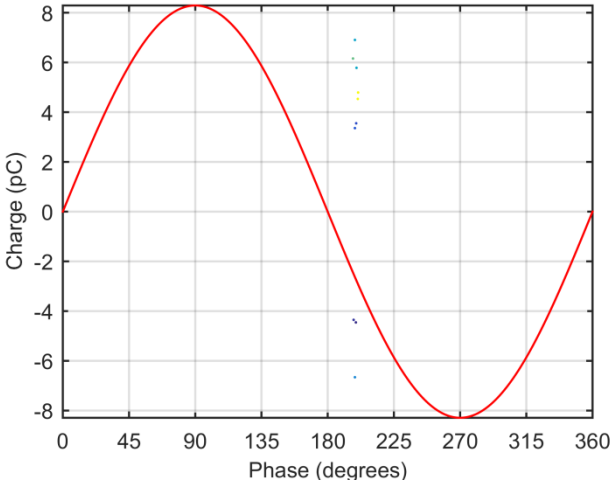

Figure 20: Internal noise with trigger at ±3mV PRPD.

For future analysis it is good to know the shape of a noise pulse, as this will help to distinguish clusters. A typical noise pulse can be seen in Figure 21 and Figure 23. As these figures show, the noise has an amplitude lower than 3mV. The locations of the selected pulses are shown in Figure 22 and Figure 24.

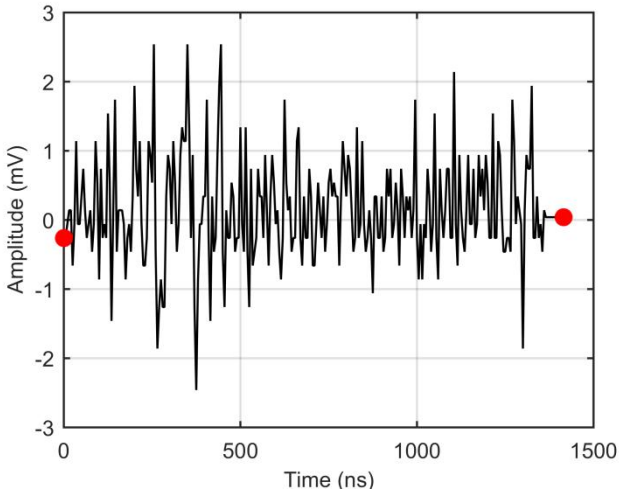

Figure 21: Internal noise, pulse 1340.

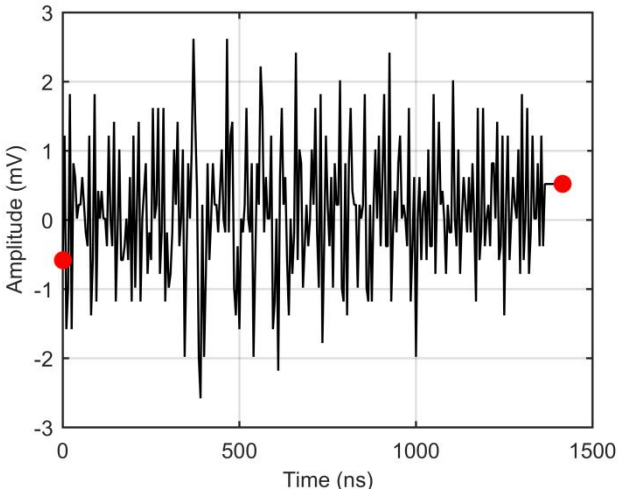

Figure 23: Internal noise, pulse 31923.

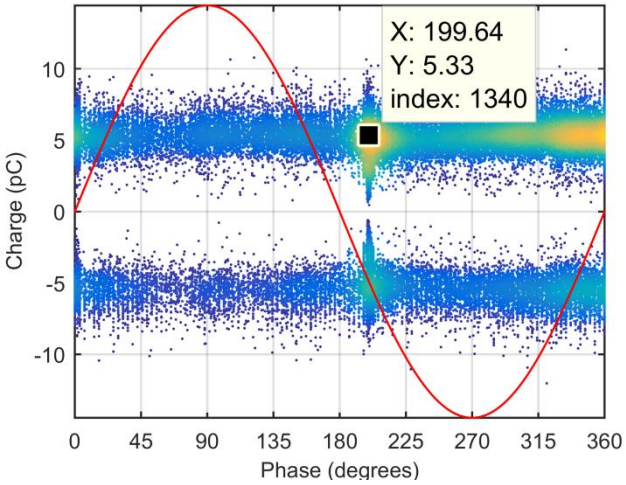

Figure 22: Internal noise, pulse 1340 PRPD.

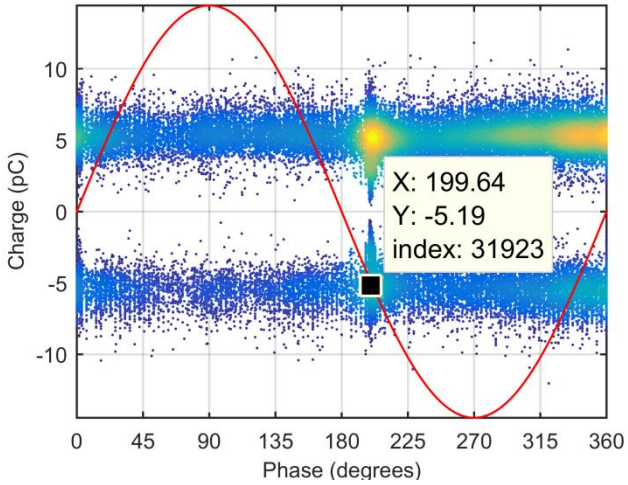

Figure 24: Internal noise, pulse 31923 PRPD.

If we compare the magnitude of the noise pulses to the magnitude of the PD pulses, we can see that the noise does not have much effect on the measurements. The smallest ratio between noise and measured PD pulse (corona) is 0.04. The comparisons are presented in Table 2.

Pulse origin	Voltage peak [mV]
Internal Noise	~3
PD_{Corona}	~70
$PD_{Surface}$	~2000
$PD_{Free\text{-}MovingParticle}$	~100
$PD_{FloatingParticle}$	~5000
$PD_{Internal}$	~1000

Table 2: Voltage and current peaks of noise and PDs.

4.2.2. Variable Autotransformer (Variac)

By adjusting the sliding contact on the variac, it sometimes it gives PDs that are visible on the MI. These are not considered in the PD measurements. The PDs are only recorded when the voltage is steady and changes are no longer made. As a precaution, a net-filter is introduced right after the variac to filter these disturbances. This net-filter can be seen in Figure 361 of appendix E.

4.2.3. Voltage Source

If the noise originating from the power supply is not filtered, the noise will disturb the PD measurement and interfere with our measurements. It will also supply PDs that are visible on the data acquisition device used at that moment. The filter used can be seen in Figure 25, and a schematic between the HV-transformer and the HV-side of the coaxial setup is presented in Figure 28 of section 4.3 and in Figure 361 of appendix E. This is the same type of coil used as the HFCT described in section 3.1 above. Due to the 5 turns, the blocking inductor has an inductance of $8{,}7 \cdot 5^2 \mu H$.

Figure 25: Blocking inductor: 6 turn coil (left) and isolated 6 turn coil (right).

4.2.4. Other On-going Measurements in the Lab

Depending on what other measurements are taking place in the HV-Lab, it is sometimes better to postpone the PD measurements, because of high interference. This interference can be seen on the Mi used at the moment of measurement.

The standard [6] states that an apparent charge of 1pC is attainable by following their guidelines for suppressing the disturbances. During the sample measurements we noticed a disturbance/noise of 0.07pC at 0kV and 0.5-0.6pC at 1.1kV. These minor disturbances are still present from the measurement system itself, from minor imperfections in the screening, grounding or filtering.

4.2.5. Ungrounded Metal Near PD Test Platform

Another disturbance during the measurements was encountered when ungrounded metal near the coaxial setup was present. Figure 26(a) shows a PRPD graph of a surface discharges measurement where an ungrounded metal is present near the coaxial setup. Figure 26(b) shows cluster 1, where the disturbance of the ungrounded metal shows similar patterns to the defect with origins in floating electrode. Figure 26(c) shows the desired surface discharge PRPD pattern.

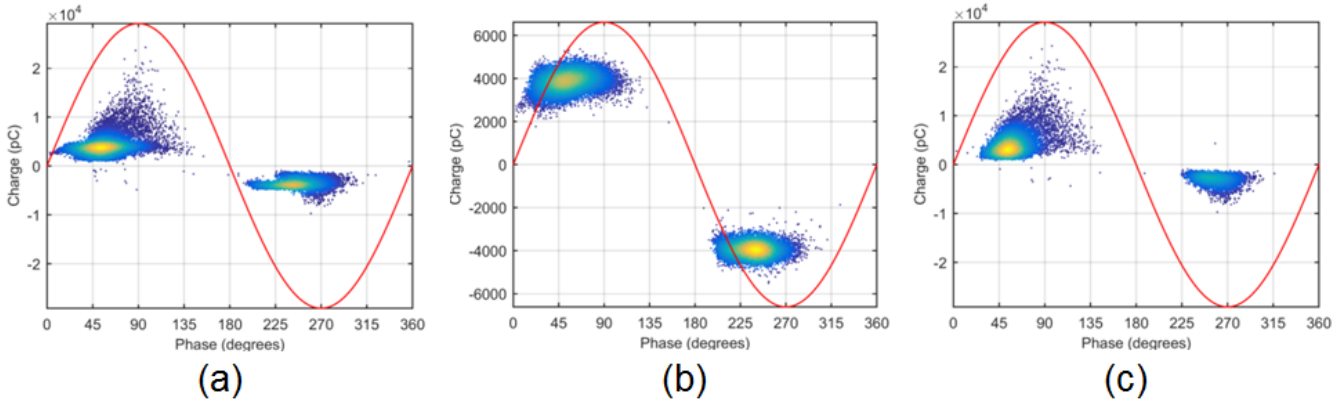

Figure 26: PRPD of surface discharge with disturbance (ungrounded metal near sample); (a) Clusters 1 and 2; (b) Cluster 1: floating particle; (c) Cluster 2: surface discharge.

4.3. Final Setup

When the final setup was assembled, the Tektronix DPO7354C Digital Phosphor Oscilloscope was used to fine-tune the samples again. The fine-tuning was done to remove the last imperfections and disturbances in order to achieve “pure” samples. The data received from the oscilloscope was analysed with a code written by Dr. Armando Rodrigo Mor. During the fine-tuning of the samples, the matlab code was also fine-tuned for minor imperfections.

4.3.1. Schematic of the Complete Setup

The final experimental setup consists of four major parts, as shown in the block diagram below:

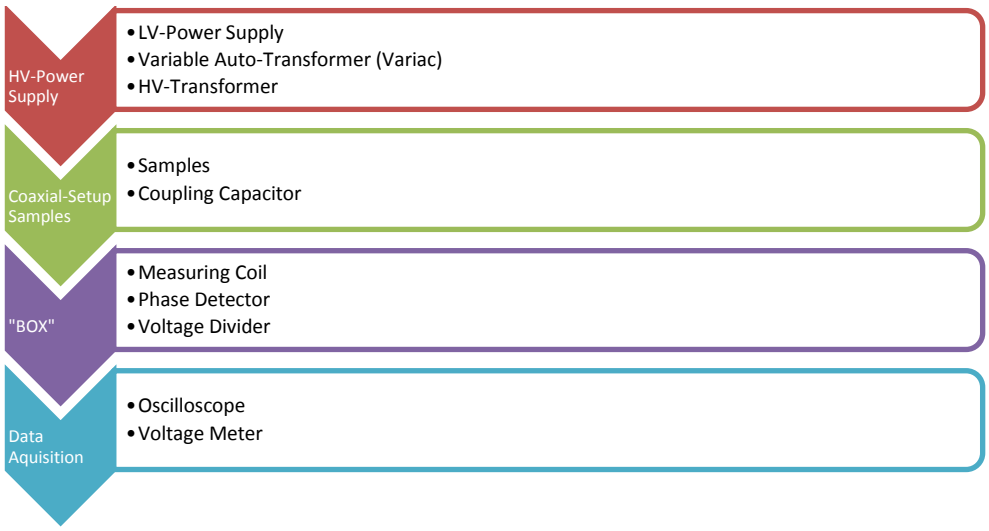

Figure 27: Experimental setup block diagram.

Figure 28 shows the experimental setup with the following sections:

- HV-Power Supply (in **red**):
  The circuit shows the LV power supply, the variable auto-transformer with the net filter and the HV transformer, as described in the previous sections of this chapter.
- Coaxial setup of the samples (in **green**):
  There are three plates in the coaxial setup of the samples. The upper two plates are connected to the HV-transformer through the coil described in section 4.2.3 above; they are thus the HV-side. The bottom plate is connected to the ground and isolated from the connection between the "box" and the upper plates. In the connection between the plates there are two coupling capacitors connected in a series of 2nF each, so a total of 1nF (series connection of capacitors). Each sample can be mounted mechanically with bolts alone or with other samples (up to six samples in total). We chose to have two top plates on the HV side so that the mechanical connections between the plates do not cause any corona or other disturbances when measuring the PD signals. On top of the two upper plates there is a smaller plate, which is there to seal off a mechanical connection from any sharp edges (to avoid disturbances in the measurement). Within the coaxial setup six samples (artificially created defects) can be placed, which will be explained in more detail in chapter 5.
- "Box" (in **purple**):
  This is the box connected to the coupling capacitors. The signal coming from the coupling capacitors goes through a coil to measure the PD signal. The "box" also has the following output signals:
  - Synchronization signal
  - 1/1000 and 1/10000 voltage signal
  - PDDC signal
  - PDAC signal

  These output signals are described in section 4.5.3 below.
- Data acquisition (in **blue**):
  Before the signal goes to the oscilloscope it goes through a coax protector and an overvoltage protector. The signals were recorded with an oscilloscope and the data was processed with a matlab program. The recorded signals are:
  - Channel 1: the PDAC signal; the fast transient current pulses.
  - Channel 2: the phase voltage; the location on the phase that the PD occurred.

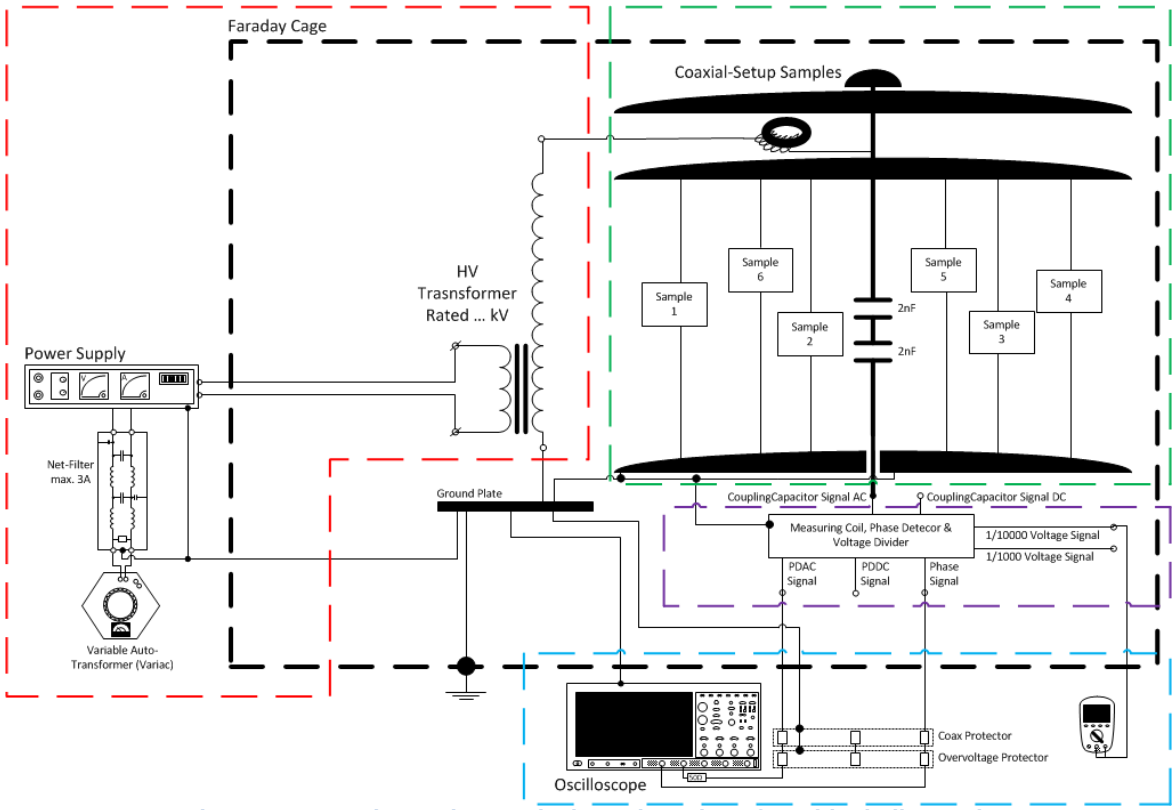

Figure 28: Experimental setup (coloured sections from block diagram).

These four major parts can also be seen in more detail in Figure 361 of appendix E. Figure 29 shows the components (transformer, coaxial setup with samples, oscilloscope, multi-meter, variac, etc.) of the complete setup in the HV-Lab of the TU Delft according to the schematic above. There is also an earth-stick connected to the HV-side of the transformer for safety issues.

Figure 29: Complete experimental setup.

4.5.3. The “Box”

Figure 30 shows a schematic of the box with the two inductive sensors and an oscilloscope with protection.

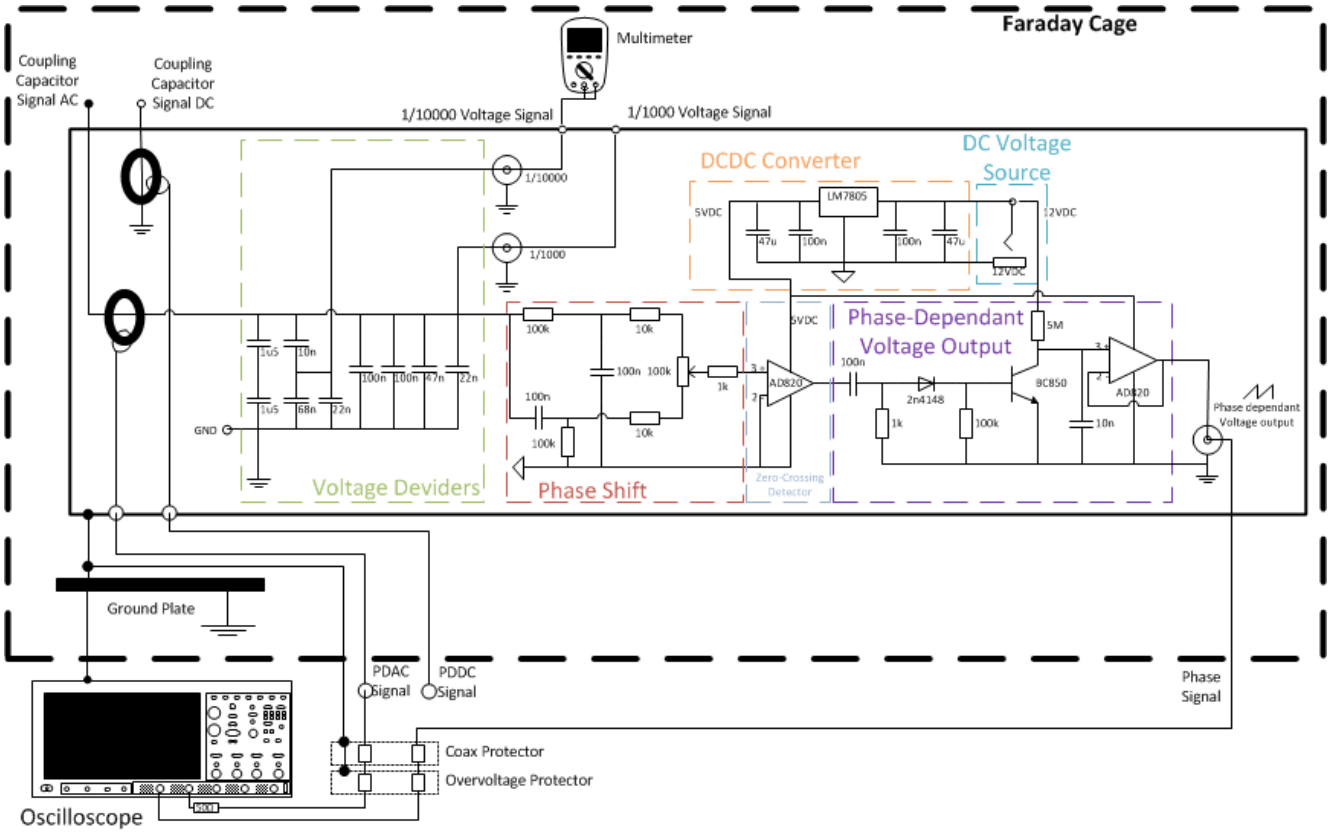

Figure 30: The "box" in a faraday cage and an oscilloscope with protection.

The “box” consists of six main parts:

Inductive Sensors

As explained in section 3.1.1, there are many different kinds of MIs. In our test platform we use two inductive sensors (N32 coil; HFCT) to measure the PDs. One for an applied AC voltage and the other for an applied DC voltage on the samples. The operation of this type of sensor is described in section 3.1 above. Figure 33 and Figure 30 show the coil inside the “box” on the left, which is for PDAC measurements. PDAC cannot be measured directly, as PDs in AC need to be synchronized with the phase in order to know where in the phase the PDs are occurring. Therefore, we measure both the transient current pulses (PDAC signal) and the phase with the oscilloscope. In our case, the N32 coil has one turn, and as a result it has an inductance of 8,7µH. A simplified schematic of a part of the circuit with the MI is shown in Figure 31(a). The schematic part of the MI is indicated in the green block, and there are also the two coupling capacitors of 2nF each and the used sample(s). In Figure 31(b), the MI is drawn in a more elaborate way. The MI is a current transformer with only 1 turn, so the ratio is 1:1. After the MI, the recorded PD signal goes through a coaxial cable to the oscilloscope.

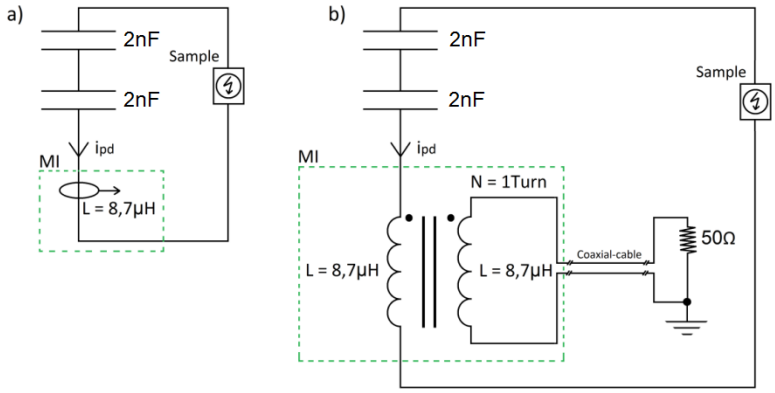

Figure 31: Schematic, MI circuit: (a) Simplified schematic; (b) Realistic schematic.

Voltage Dividers

There are two voltage dividers included with the ratios 1/1000 and 1/10000 in order to be able to measure the applied voltage on the sample(s).

Phase-Dependant Voltage Output

The most important part of the box is the phase signal, which will tell us where the recorded pulse occurs on the phase. With this information we can analyse the data properly. We are using here a ramp, as can be visualized in Figure 32. If a sine was used instead of the ramp, every half cycle there are two equal numbers (incline and decline of sine) which would make things more difficult. Now by using the ramp we know at all times where on the phase the discharges are occurring with just one voltage value.

Phase Shift

There is a possibility that a phase shift occurs. This can be seen at the starting of the phase signal (saw tooth) and the measured voltage signal (voltage over the samples from the voltage divider). This phase shift is due to delays in electronics. The phase shifter rectifies this delay with another delay. With a phase shifter we can make adjustments to the saw tooth signal so that the phase signal can be synchronized properly with the pulses. Figure 32 shows this phase shift; the starting point of the saw tooth is not the same as the starting point of the measured voltage (zero crossing). With the adjustable phase shifter this difference can easily be set to zero.

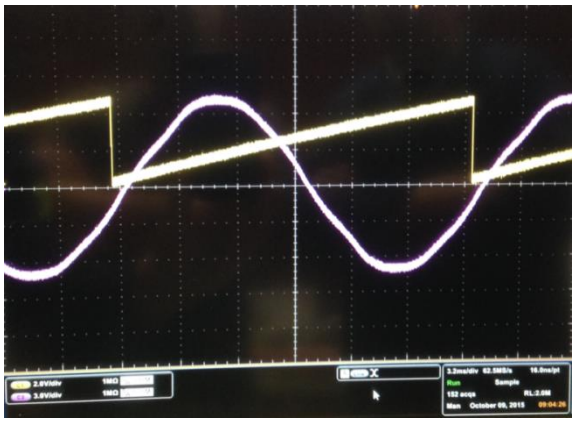

Figure 32: Synchronization of saw tooth with the "box".

DCDC Converter

We use a DCDC converter so that there is always a constant power supply of 5V for the DC input voltage.

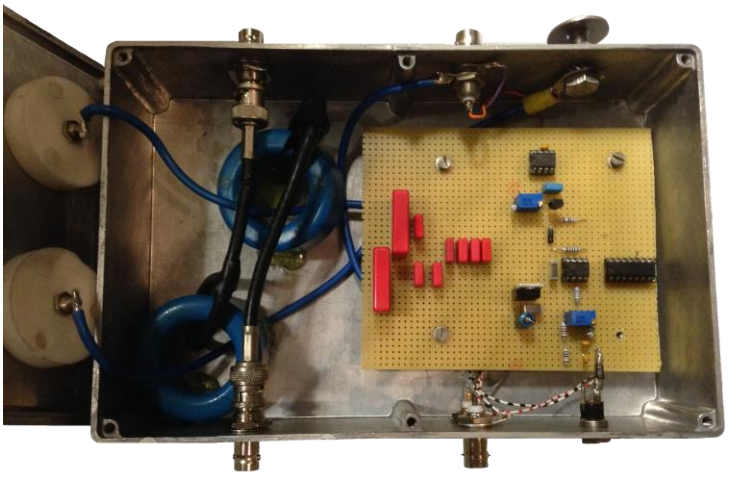

Figure 33: The "box".

5. Artificial Defects

In this chapter the artificially created defects are presented, after which the process of achieving these samples is explained. At the end of this chapter the aging of the samples is discussed and explained, and when possible presented. Before that, the initial setup, the setup that was used to create the artificial defects, is explained.

5.1. Initial Setup PD Measurement

In order to create the "perfect" samples with the different types of PDs, we handled them each separately first. The PDs of each sample were measured in a shielded HV laboratory, using the circuit shown in Figure 34. HVAC was reached by means of a HV transformer rated at 50kV.

The Coupling Capacitor of 1200pF has a low impedance path for high-frequency currents. The voltage divider provides the synchronization to PD pulses in order to obtain conventional PRPD patterns referred to 50Hz sinusoidal voltage waveforms [19].

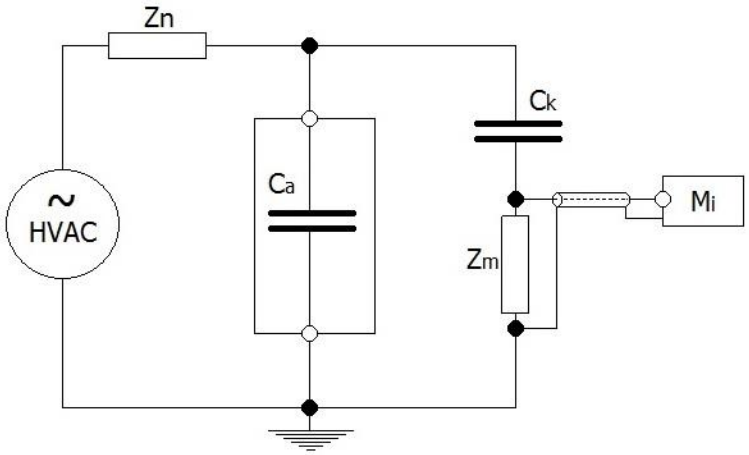

Index:

HVAC	High voltage alternating current
Zn	Noise blocking filter
Ck	Coupling Capacitor
Mi	PD measuring instrument
Zm	Measuring impedance as part of the coupling device
Ca	Test object/sample

Figure 34: PD measurement circuit.

To check the PD activity of the samples we used commercial PD detectors, connected in parallel:

- DDX-9101 PD Detector of Hubbell, Robinson Instruments and Tettex Instruments
- PD Base II from TechImp Systems S.r.l.

The measurements were done in combination with the TechImp HFCT30 & MOXA Ethernet Copper to Fiber Media Converter. Two procedures were followed to get to the final samples:

- **Estimation of PDIV:** By estimating the PDIV we could easily get the PDs at the right voltage. This estimation was done in different ways, depending on each sample.
- **Trial and error:** If we did not have a "pure" sample with PDs at the right voltage with the right IV, we adjusted the sample until it was correct.

In appendix C the two procedures are explained in more detail.

5.2. The Final Samples

The final samples are placed in a coaxial setup, as seen in Figure 35, where each sample can be placed individually or in combinations (up to six in total). The six chosen sample types are described in this section; each dimension, material and shape of the dielectric is chosen and tuned to have PDs at 10 kV. The coaxial setup is compact, easy to construct and easy to handle. On the high voltage side there are two plates, in order to overcome disturbances from the mechanical connections, and on the grounded side there is one plate. The mechanical connections are there to assemble and

disassemble the samples. All the shapes are according to the Rogowski profile described in section 4.1.1 above. All the samples mentioned here in this section represent a real PD defect. Their relationships to the real defects are explained in more detail in section 2.1 above.

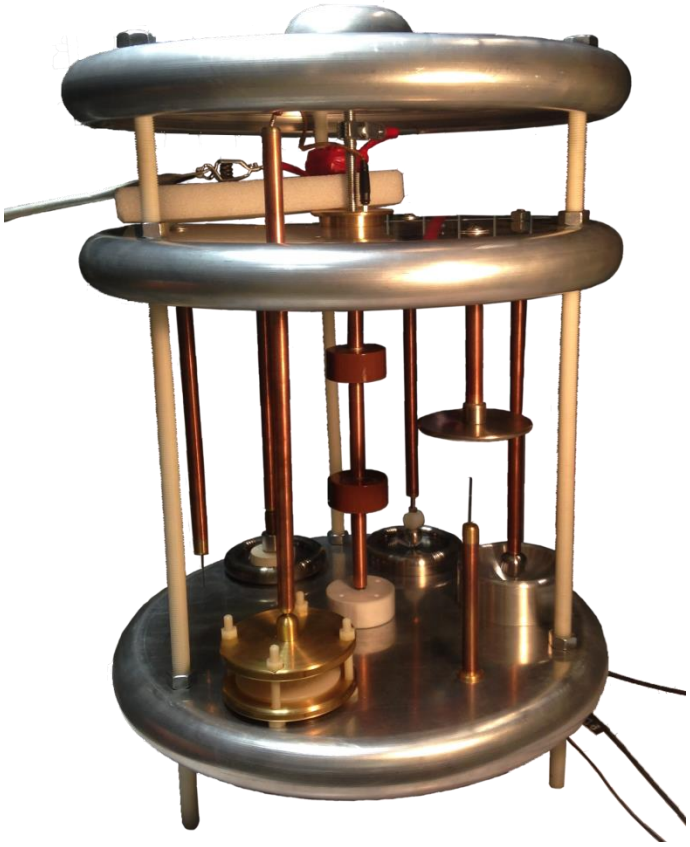

Figure 35: Coaxial setup with samples.

Internal Discharge

Figure 36 and Figure 37 show the final internal discharge sample schematically and in the coaxial setup, respectively.

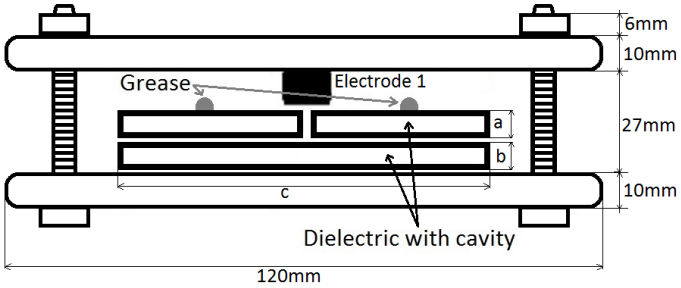

Figure 36: Final internal discharge defect schematic.

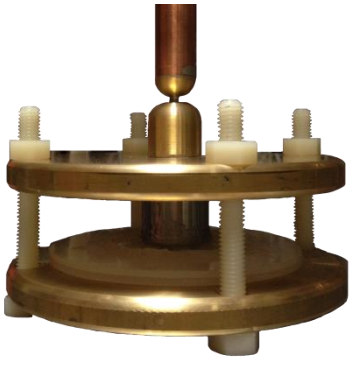

Figure 37: Final internal discharge defect.

The defect has been constructed to have PDs at 10kV with a PDIV at 8.5kV; the sample specifications are listed in Table 3.

Internal Discharge Specifications	
Dielectric	a=2mm
	b=2mm
	c=90mm
Cavity	Surface: round
	Diameter: 1mm
	Depth: 2mm

Table 3: Final internal discharge specifications.

Positive Corona

Figure 38 and Figure 39 show the final positive corona sample schematically and in the coaxial setup, respectively.

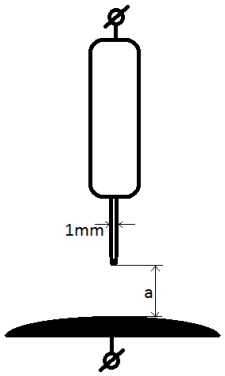

Figure 38: Final positive corona defect schematic.

Figure 39: Final positive corona defect.

The defect has been constructed to have PDs at 10kV with a PDIV at 6kV; the sample specifications are listed in Table 4.

Positive Corona Specifications	
Needle	Thickness: 1mm
	Length: 37mm
	Tip: spherical
Gap	a=45mm

Table 4: Final positive corona specifications.

Negative Corona

Figure 40 and Figure 41 show the final negative corona sample schematically and in the coaxial setup, respectively.

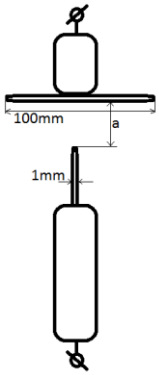

Figure 40: Final negative corona defect schematic.

Figure 41: Final negative corona defect.

The defect has been constructed to have PDs at 10kV with a PDIV at 9kV; the sample specifications are listed in Table 5.

Negative Corona Specifications	
Needle	Thickness: 1mm
	Length: 44.5mm
	Tip: spherical
Gap	a=45mm
Disk	Diameter: 100mm
	Thickness: 5mm

Table 5: Final negative corona specifications.

Floating Electrode

Figure 42 and Figure 43 show the final floating electrode sample schematically and in the coaxial setup, respectively.

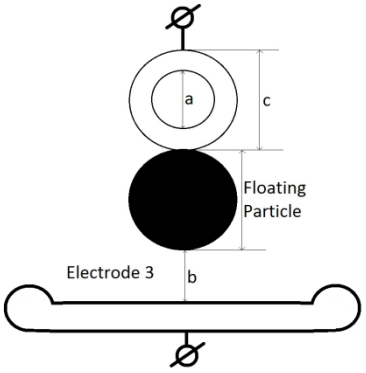

Figure 42: Final floating electrode defect schematic.

Figure 43: Final floating electrode defect.

The defect has been constructed to have PDs at 10kV with a PDIV at 9kV; the sample specifications are listed in Table 6.

Floating electrode Specifications	
Isolation	a=2mm
	c=21mm
Floating electrode	Diameter: 22mm
Gap	b=5mm

Table 6: Final floating electrode specifications.

Surface Charge

Figure 44 and Figure 45 show the final surface discharge sample schematically and in the coaxial setup, respectively.

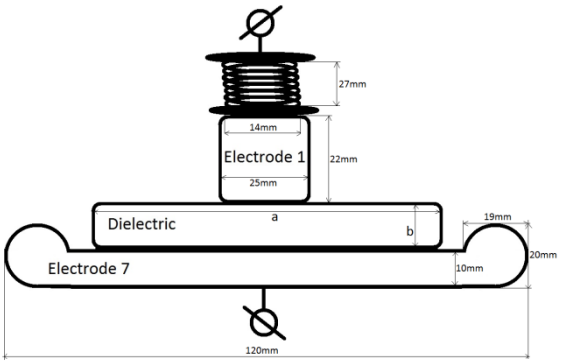

Figure 44: Final surface discharge defect schematic.

Figure 45: Final surface discharge defect.

The defect has been constructed to have PDs at 10kV with a PDIV at 8.5kV; the sample specifications are listed in Table 7.

Surface Discharge Specifications	
Dielectric	a=52mm
	b=12mm
	Material: PVC

Table 7: Final surface discharge specifications.

Free-Moving Particle

Figure 46 and Figure 47 show the final free-moving particle sample schematically and in the coaxial setup, respectively.

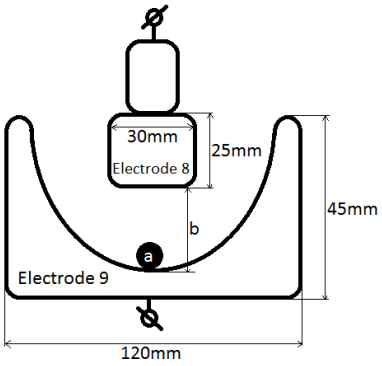

Figure 46: Final free-moving particle defect schematic.

Figure 47: Final free-moving particle defect.

The defect has been constructed to have PDs at 10kV with a PDIV at 8.5kV; the sample specifications are listed in Table 8.

Free-Moving Particle Specifications	
Particle	Diameter: 3mm
	Weight: 0.01g
Gap	Distance: 13mm

Table 8: Final free-moving particle specifications.

5.2.1. Extra Artificially Created Defects

In addition to the additional measurements done with the originally created artificial defects, described above in section 0, data was also gathered from two extra artificially created defects. These two defects were created for PD with origins in internal discharge and floating electrodes. With these extra defects the findings can be even better confirmed.

Internal Discharge Second Sample:

The second artificially created defect for internal discharges was made using a void on the bottom of a glass, as can be seen in Figure 48. Some nice PD patterns for internal discharge were measured with this sample, which are seen in PRPD analysis in Figure 458 to Figure 460 of appendix J. However, this sample was not consistent; once the sample was aged the internal discharge shapes were not recoverable. The idea for this sample was to make a sample where the void was easily accessible, so that once it aged it could easily be cleaned and re-used.

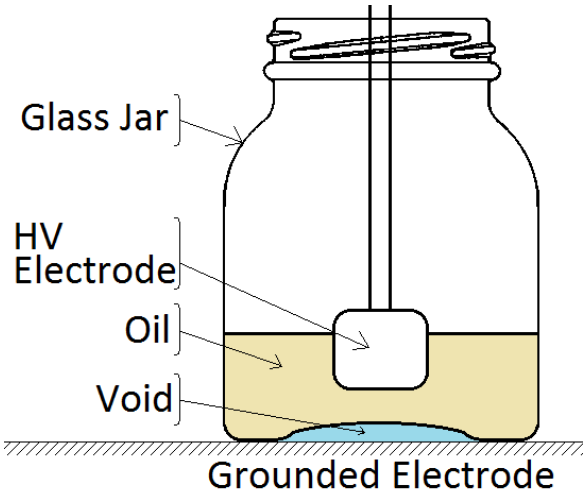

Figure 48: Schematic of the second artificially created defect, consisting of a glass jar filled with oil, using the cavity on the bottom of the jar as a void.

Floating Electrode Second Sample:

The second artificially created defect for floating electrodes was made with the use of four neodymium magnets and a graphite disc. This sample is a so-called “kit” called “dialev” from supermagnete.de (see Figure 49(a)), where a graphite disc levitates approximately 1mm above four strong neodymium magnets (see Figure 49(b)). The magnets are four nickel-plated cube neodymium magnets of 12mm, with a magnetization of N48, and are arranged as shown in Figure 49(c) [60].

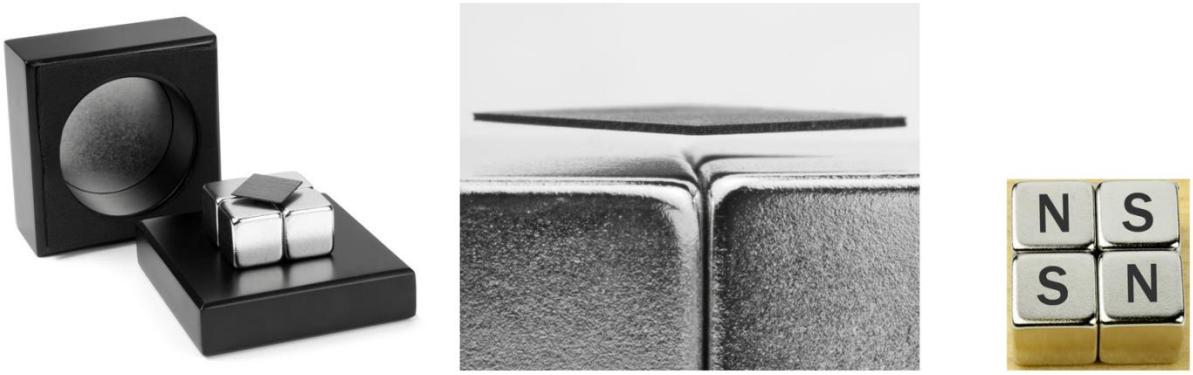

(a) (b) (c)

Figure 49: Second floating electrode sample; (a) The "dialev"; (b) Floating graphite disc, 1mm away from four neodymium magnets; (c) Arrangement of the four neodymium magnets [60].

5.3. Selecting the Samples

In this section the steps for creating the "pure" samples are described. Each sample has been designed such that the PDIV is lower than 10kV, with a defect as "pure" as possible. A defect is considered "pure" when the PRPD shapes are as ideal as possible and represent a real PD defect. Additionally, when possible, the materials were chosen to be more endurable and to have as little degradation as possible, i.e. a long lifetime. Aside from this, the samples must also be easy reproducible.

5.3.1. Internal Discharge (Void in Dielectric)

The idea behind the creation of the internal discharge artificial defect is based on [21]. Here, layered disks are stacked on top of each other, and one of the layers has a hole (void) that will simulate the real-life defect of a void.

The sample was modified in the following aspects:

- **Material of the dielectric:** ε_r (relative permeability) range: $\varepsilon_r = 2 – 10$
  - Epoxy resin (cast): (ε_r=3.6) This sample is unstable; the PDIV keeps changing and carbonization occurs, and the void in epoxy is not easily made. Therefore, it is not suitable for the setup.
  - Glass: (ε_r=3.7 – 10) There is too much surface discharge.
  - Hard/transformer paper (laminated): (ε_r=4.5) The PDIV is very low and needs many layers, which then leads to impurities (unwanted voids), as described in section 2.1.
  - Paper: ($\varepsilon_r = 2.3$)
  - Plexiglas (Perspex/PMMA): ($\varepsilon_r = 3.2 – 3.4$)
  - Polyester resin: ($\varepsilon_r = 2.8 – 4.5$)
  - Polythene: ($\varepsilon_r = 2.2 – 2.4$) Polythene is suitable for this experiment because of its simple mechanical structure, high intrinsic electric strength, low dielectric losses and commercial importance. Polythene is also more resistant to discharges compared to perspex and polytetrafluorethylene [20].
  - Wood (dry): ($\varepsilon_r = 2 – 6$)
- **Shape of the dielectric:**
  The samples are shape like disks. This is to reduce the accumulation of the electric field in the sharp corners (to create an even electric field distribution to reduce surface discharge).
- **Decreasing the surface discharge:**
  - Cleaning: The samples are cleaned with Ethanol (C_2H_5OH); the DIV of the samples becomes higher compared to samples that are not cleaned.

- Sanding: The samples are made coarser with polish. This is to increase the creeping distance, so that the surface discharges are decreased.
- Grease: When possible and when needed, grease was added at the positive electrode to avoid discharges at the three materials point. Grease was also added in circles around the positive electrode to increase the creeping distance.

➢ **Dimensions of the void:**

The voids of the samples were chosen in consideration with the voids found in real cables.

- Depth: The dimensions of voids found in polythene cables are between 0.01 and 0.3 mm. With a larger void the PDs start at a lower voltage, but the damage of the discharge will be bigger [20].
- Surface: The area of the void is directly related to the discharge magnitude. According to [20], if the diameter is larger than 3mm, the PD magnitude becomes very variable and there is no longer a relationship to the area of the void. Cylindrical vs. spherical [23]: Voids in the shape of a sphere have higher IV than cylindrical voids.

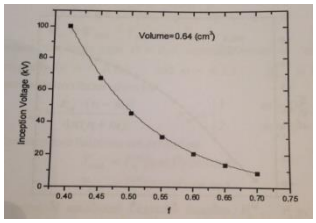

Figure 50: The DIV as a function of flatness [22].

- Volume: The IV decreases with an increasing void size.
- Flatness: Figure 50 shows the discharge inception voltage as a function of flatness.

  $f = 1 - \frac{b}{a}$ for (a > b)

  The larger the value f, the "slimmer" the shape, seen in Figure 51. The void in the example has a constant sample thickness of 4cm with breakdown field strength of 25kV/cm and a fixed void volume of 0.64cm^3. Figure 50 shows that the IV decreases with an increasing value of flatness.

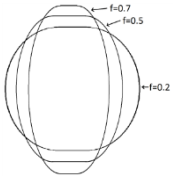

Figure 51: Flatness of void [22].

➢ **Location of the void:**

Depending on whether the PDIV needed to be increased or decreased, the position of the hole was changed. See section 5.4 below for a more detailed explanation.

Estimation of the Internal PDIV

To calculate the PDIV, many parameters must be taken into consideration, including [21]:

- Type of gas in void
- Gas pressure
- Surface properties of the void
- Size and shape of the void
- Location of the void
- Dielectric constant of the surrounding medium

Exact calculation is nearly impossible, which is why we will estimate the PDIV. For our case this is enough, because it will simply be used as a reference to estimate the void and dielectric dimensions.

During this estimation we will use the following limitations [21]:

- Pressure range: 0.00067-1.01333 bar (The standard atmospheric pressure: 1Atm= 1.01325 bar)
- Paschen's Curve: Valid for the whole range
- ε_r (relative permeability) range: 2-10
  The range was chosen from the permittivities of the available materials in the lab. See the section "materials of the dielectric" in section 5.3.1 above for the materials and permittivities.
- t (sample thickness) range: 0.1-0.8cm
  The range was chosen from the thicknesses of the available materials in the lab.

- t' (void depth) range: 0.1-0.5cm
  See the section "dimensions of the void" in section 5.3.1 above for more details.

A technique was developed in [21] to evaluate the PDIV in the case of discharges occurring at the interface as well as in voids in the ambient medium of air. This estimation is based on the analysis of Townsend breakdown criterion. By making a table according to the above-mentioned limitation ranges, we estimated the PDIV. The limitations are used as the variables in the tables and each possible outcome is calculated. With this table, a good estimation of the sample dimensions and materials was made. A part of this table (only the most promising combinations) is in Appendix C3.

With the use of the Townsend breakdown criterion, the capacitive voltage distribution law and with the simplification that we use the breakdown voltages of gas (air) for a wide range of pt' (pressure · gap spacing) instead of the use of the secondary breakdown coefficient for evaluation of sparking potentials for the whole pt' range, we then get, according to [21], the PDIV for discharges occurring in voids:

$$PDIV = V_i = \frac{E_g * [t + t'(\varepsilon_r - 1)]}{\varepsilon_r} = \frac{B * p}{\ln[p * t'] + k} * \frac{[t + t'(\varepsilon_r - 1)]}{\varepsilon_r}$$

where $k = 3.5134 * (p * t')^{0.0599}$, with the parameters:

- E_g Electric strength of the gap at pressure p
- t Thickness of insulation/dielectric sample
- t' Thickness of the discharge gap included within the thickness of t
- ε_r Relative permittivity of dielectric sample
- M Constant
- N Constant

and with the parameter limitations:

- V_i = 10kV
- B = 2737.5V/kPa-cm
- p = 1 bar = 100kPa (atmospheric conditions)
- t (sample thickness = variable): (0.5-0.8) cm = (1-8) mm
- t' (depth of void = variable): (0.2-0.5) cm = (1-5) mm
- ε_r (relative permeability = variable): ε_r = 2 – 10
  Epoxy resin (cast): ε_r = 3.6
  Glass: ε_r= 3.7 – 10
  Hard paper (laminated): ε_r= 4.5
  Paper: ε_r= 2.3
  Plexiglas (Perspex/PMMA): ε_r= 3.2 - 3.4
  Polyester resin: ε_r= 2.8 - 4.5
  Polyethylene: ε_r= 2.2 - 2.4
  Wood (dry): ε_r = 2 - 6

We thus reach the final formula for calculating (estimating) the PDIV:

$$PDIV = V_i = \frac{2737.50 * 100}{\ln[100 * t'] + 3.5134 * (100 * t')^{0.0599}} * \frac{[t + t'(\varepsilon_r - 1)]}{\varepsilon_r}$$

With the aid of this formula, a table with all possible combinations is made in order to choose a proper sample. A part of this table can be seen in appendix C3.

Error in calculation:

The calculated/estimated values from the table in appendix C are, according to [21], higher than the real values under the same conditions. This error becomes bigger as the value of pt' (kPa –cm) increases [21]. Therefore, this estimation is more accurate for small values of pt' (kPa –cm). We will take this into account when selecting the final sample.

Summary: Selecting Internal Discharge Sample

Table 9 shows the summary that was used when making decisions for selecting the sample, e.g. to get the desired PDs at 10kV (fine-tuning the PDIV).

Change	Inception Voltage	Degradation (Damage)	Note
Void			
Depth	Decreases with increasing void depth	Higher	Longer distance for electrons to collide (more avalanches)
Depth	Increases with increasing void depth		
Diameter			If void diameter increases, there is an increase in electric field in void. Fields are perpendicular to the cylindrical void.
Size	Decreases with increasing void size		
Location	Higher in dielectric than in electrode [23]	Slower in dielectric than in electrode [20]	
Shape	Higher with spherical shapes than with cylindrical [23]		
Disk/Sample Dimensions			
Diameter			The surface charge decreases with increasing diameter
Thickness	Increases with increasing thickness		The surface charge decreases with increasing
Disk/Sample Material			
Polythene			Decomposition product found [20]
PVC			
Perspex		Less resistant than polythene	Decomposition product found [20]
Epoxy			
Glass		More resistant than polythene	No decomposition product [20]
Permittivity	Decreases with increasing permittivity		Only valid if void is not completely through sample. t'(sample thickness)≠t(void depth)
Electrode			
Shape			
Diameter	Increases with increasing electrode diameter		Field intensity decreases with increasing electrode diameter
Voltage			
Increase	Unaltered	Higher	Increases discharge frequency
Decrease	Unaltered	Lower	Decreases discharge frequency

Table 9: Summary: selecting internal discharge sample.

Final Individually Measured Internal Discharge Sample

Figure 52 shows the chosen sample. Appendix B3 contains the graphs correlated to this sample.

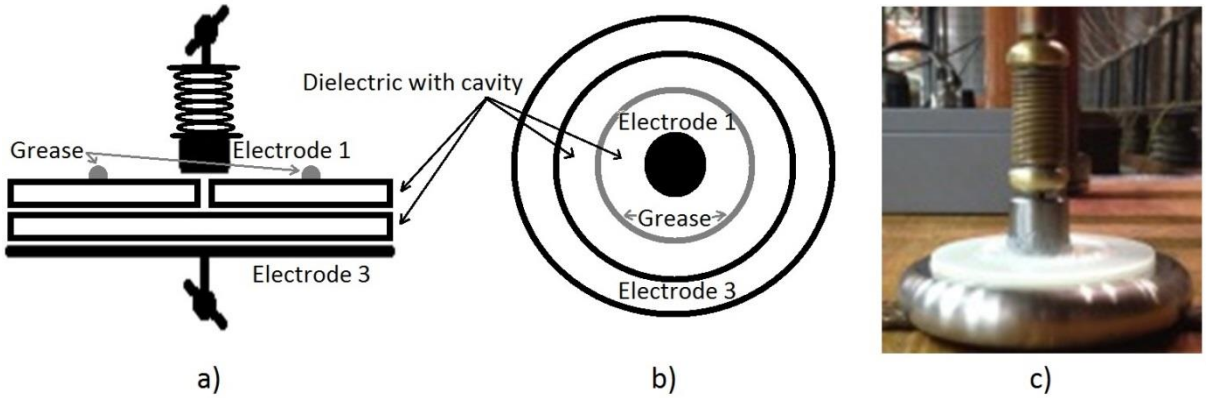

Figure 52: Final individually measured internal discharge sample: (a) Schematic cross-section; (b) Schematic top-view; (c) Picture sample.

5.3.2. Corona

The idea behind the creation of the corona artificial defect is to have a point plane electrode configuration; the electrodes switch (point and plane) depending on whether it is a positive or negative corona. The sample was modified in the following aspects:

- **Electrode tip:**
  When less noble metals are used for the electrodes (noble metals are resistant to corrosion), corona corrosion, uniform or pitting will occur. Therefore, we will use the round electrode (electrode 2) for further measurements. If we use electrode 1 (flat) or 3 (sharp), the sharp points will be rounded off in time and the electrode will eventually become more round, and the measurements will change. With electrode 2 (round) this effect/change will be less. For the electrode, a Weldline WL20 Tungsten+Lanthane2% is used with dimensions Ø1.0x150mm.
- **PDIV:**
  The inception voltage is mainly influenced by changing the tip of the electrode. Changing the distance between the electrodes does not have a great effect on the PDIV, but on the other hand it has a large effect on the breakdown value. The absolute voltage determines the inception voltage in the case of corona. If the voltage is raised slightly above the inception voltage for a dry, clean and smooth conductor, brush discharges will occur (generally limited to the negative half cycle) [13].
- **Air gap size:**
  As explained in section 4.1.3 above, the air gap should be large enough to avoid breakdown and small enough to still cause PDs at 10kV. The gap also must be large enough not to cause any interference with the pure sample, which was explained in section 4.1 above. The air gap size has little effect on the PDIV.

Positive Corona

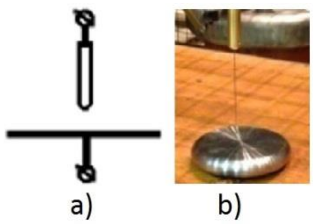

Before making the final sample for the coaxial setup, we chose the sample seen in Figure 53 for positive corona. Appendix B1 contains the graphs correlated to this sample.

Figure 53: Final individually measured positive corona sample.

Negative Corona

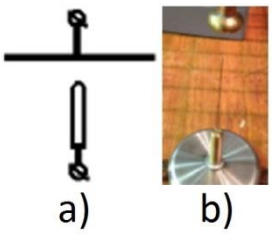

For the negative corona we did the same as for the positive but at the negative electrode. Figure 54 shows the chosen sample before making the final sample for the coaxial setup. Appendix B2 contains the graphs correlated to this sample.

Figure 54: Final individually measured negative corona sample.

5.3.3. Floating Electrodes

The idea behind the creation of the floating electrode artificial defect is based on [38]; here, a metallic bolt was insulated from the HV conductor with an insulating ring. The sample was modified in the following dimensions, which can be seen in Figure 55:

- **"Spacer" hole length:**
  From the modifications done to the spacer, we saw that decreasing the spacer hole decreased the creeping distance and therefore decreased the PDIV.
- **Gap length between floating electrode and grounded electrode:**
  As explained in section 4.1.3 above, the air gap should be large enough to avoid breakdown and small enough to still cause PDs at 10kV.

Figure 55 shows the chosen sample before making the samples for the coaxial setup. Appendix B4 contains the graphs correlated to this sample.

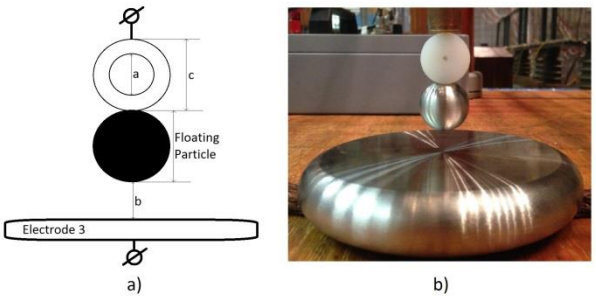

Figure 55: Final individually measured floating electrode: (a) Schematic sample with dimensions; (b) Picture of sample, with a as the "spacer" hole length, b as the gap length between the floating electrode and grounded electrode, and c as the "spacer" diameter.

5.3.4. Surface Charge

The idea behind the creation of the surface discharge artificial defect is based on [29]. Here, the sample is based on a rod-to-plane electrode system; the surface discharge will happen along a pressboard surface from one electrode to the other. We will make use of the different creeping distances when placing the electrodes (positive and negative) at different distances from each other on different materials.

The sample was modified in the following aspects:

- **Shape of the dielectric:**
  We chose a flat disk shape for the sample. This is because the creeping distance is easier to adjust in terms of thickness and diameter to get the right PDIV.
- **Material of the dielectric:**
  While doing the PD measurements we used different types of materials, e.g. plastic, grey PVC, yellow PVC, Perspex, etc.

- **Dimensions:**
  After a few measurements with different materials, we estimated the needed dimensions (diameter and thickness) to get the right PDIV. The estimation was done with simple ratio tables.

Figure 56 shows the chosen sample. The spring was used in order to always have equal and best surface contact. Appendix B5 contains the graphs correlated to this sample.

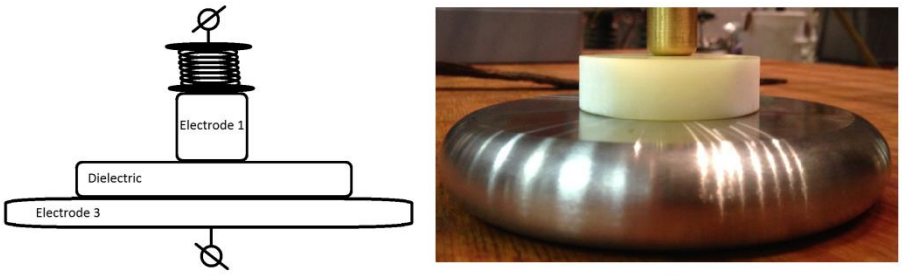

Figure 56: Final individually measured surface discharge: (a) Schematic cross-section; (b) Picture.

5.3.5. Free-Moving Particle

The idea behind this artificial defect is based on [24]. A particle should be light enough to jump/float when charged and stay between the two electrodes (positive and negative).

The sample was modified in the following aspects:

- **Shape of the dielectric:**
  The amount of charge that is accumulated depends on the shape of the sample. According to [30], a curly-shaped particle accumulates more charge than a sphere.
- **Dimensions (mass) of the dielectric:**
  The force caused by the particle needs to exceed the gravitational force. The gravitational force $(F_g = m \cdot g = m \cdot 9.81)$ is dependent of the mass of the particle. Therefore, the material needs to be as light as possible so that it is easier to overcome the gravitational force.
- **Material of the dielectric:**
  The dielectric needs to be an electrically conductive material to accumulate charge. As described above, the particle must be as light as possible, and therefore we chose aluminium (foil) to make the particles.
- **Estimation of PDIV:**
  The shape, size and mass of the (aluminium) particle were chosen by means of a simple ratio table, with some trial and error afterwards. The examples of size and mass of the particle for the ratio table were taken from [24, 25].
- **Shape of the electrode:**
  We made a setup with a “tube” of Plexiglas so that the particle does not “jump out”. After a while the particle kept sticking to the sides of the Plexiglas because of the accumulated charge on the Plexiglas and particle. This sample with Plexiglas is shown in Figure 57. We then made an electrode that is shaped like a bowl so the particle cannot “jump out” and cannot stick to the sides. In Figure 58 shows the electrode with a bowl shape.

Figure 57: Floating electrode with Plexiglas.

Figure 58: Experimental electrode in bowl shape.

5.4. Aging & Deterioration

PDs continuously dissipate energy at vulnerable locations, which causes gradual damage to these locations. Examples of these locations are described in section 2.1 above. PDs adversely affect

the insulation lifetime, and therefore it is important to know the PDIV. With the knowledge of the voltage at which the PDs start, a good design can be made with a reliable operation [21]. To see how PD activity affects the lifetime of the material, we should have some knowledge of how damaging the PD activity is. According to [36], there are different ways to see the damaging effect of PDs:

- **by the chemical reactions:** at the surface of the void, chemical reactions take place between oxygen, ozone and polymer radicals
- **by the bombardment of the surface:** polymer radicals are formed by the bombardment (by high energy ions) of the surface of the void
- **by deterioration of the void surface:** UV radiation causes the void surface to deteriorate

When designing and constructing the artificial defects these effects must be kept in mind in order to have samples that are easy replaceable and fixable when they are damaged and/or aged.

There are many different thoughts and opinions on what is more deleterious. According to [32, 33], streamer-like discharges are more damaging because of their large magnitudes compared to Townsend-like discharges. But according to [34], the opposite is true: the Townsend-like (glow) discharges are more damaging than streamer-like discharges. According to [35, 36], the most extensive degradation takes place with the pitting discharge type. The pitting discharge type is a stage following streamer-like and Townsend-like discharges, as explained in previous sections.

Before breakdown occurs there are several steps that take place. When there is oxygen (O_2) present at the occurrence of PDs, highly oxidative products (O, O_3, O^-) are created, and hydrogen (H_2), methane (CH_4), carbon mono- (CO) and di-oxide (CO_2) are created because of the chemical reactions in the gas phase. Reactions will take place between these created chemicals, and acids will be produced. These acids are conductive and reduce the voltage across the void, which will eventually extinguish the discharge. When all the oxygen (O2) in e.g. the void is used up, then according to [36] the bombardment of nitrogen ions (pitting discharges) causes pitting, and thereafter treeing starts. When the pits reach a critical length, narrow semi-carbonized channels are formed and breakdown follows shortly afterwards. This process, with all its intermediate steps, is shown schematically in Figure 59 [20, 36].

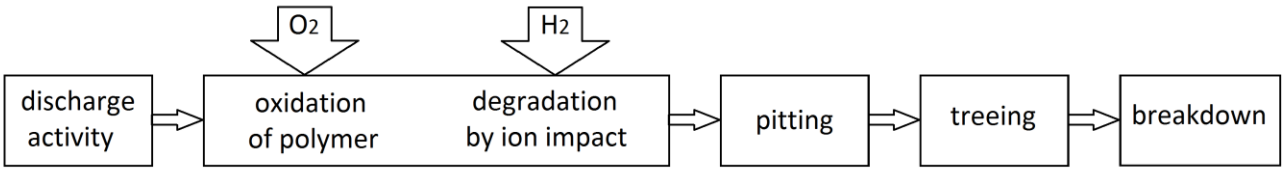

Figure 59: Simplified schematic of the process leading to breakdown [36].

In the end, this process can be summarized in the following stages of deterioration [20]:

- Uniform surface erosion and formation of a transparent resin
- PD concentration near surface/periphery of the void
- Formation of deep pits and formation of a transparent resin at end of each ellipsoidal pit
- Erosion and deposition of resin near the surface/periphery of the void. With increasing pit length the energy released by each discharge increases. Therefore, the erosion increases rapidly. The mechanism of deterioration changes when the pits reach a critical length.
- Carbonization and breakdown

To get an idea and reference about what effect the measured discharges have, we found that according to [20] polythene erodes about $10^{-15}cm^3$ with each discharge of ±10μC. Some materials

degrade faster than others; this must be kept in mind when designing the artificial defects, because in the end this will affect the lifetime of the sample.

Applied Frequency

The number of PDs in a given time frame is roughly proportional to the frequency. If the frequency becomes too high, the deterioration is observable in a short time frame and thermal instability occurs, which in the end leads to failure due to cumulative heating [20]. In our samples we use a frequency of 50Hz in order to simulate e.g. the cables and gas insulated systems in real life as much as possible. According to [20], when the applied voltage has a frequency of 50Hz, the rate of deterioration is unimportant, but the discharge level must then be lower than $2 \cdot 10^{-12}$C (=2pC). This is the “safe“ discharge level.

Location of Defect

The location of the imperfection also makes a difference. The explanation given below uses a void as the imperfection in the material. The samples are mounted between the electrodes, with the cavities in the centre of the disks (see Figure 60(a)). The void can be placed in the centre of the sample, near the positive electrode or the negative, as can be seen in Figure 60(b), (c) and (d).

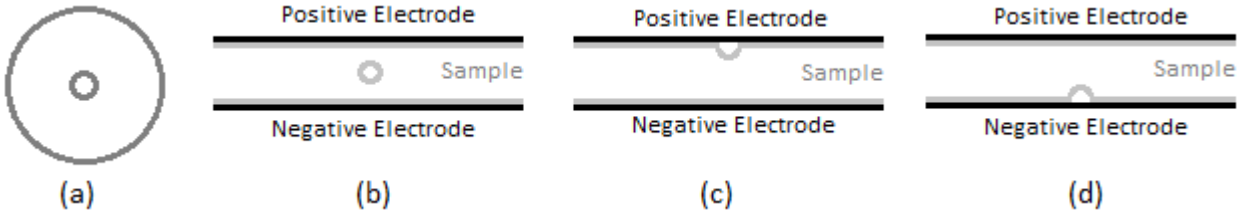

Figure 60: (a) Top-view void location, depth location void; (b) Void in middle of sample; (c) Void near positive electrode; (d) Void near negative electrode.

When the void is adjacent to the electrode (Figure 60(c) and (d)), the deterioration on the void is less compared to when the void is enclosed by the dielectric (Figure 60(b)) [20].

There is also a possibility of the void being in the electrode itself (Figure 61). If the void is a cavity in the electrode, the deterioration of the sample is considerably slower than that occurring under similar conditions (same stress and dimensions) with the void in the sample/dielectric [20]. Additionally, the IV is higher when the void is in the dielectric instead of in the electrode [23].

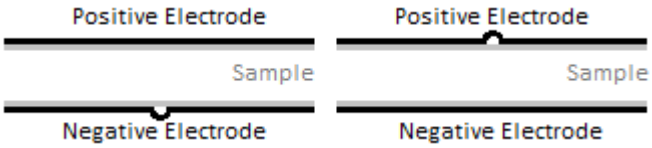

Figure 61: Void in electrode.

Applied Voltage

The applied voltage influences the magnitude of the PDs and therefore the rate of deterioration as well. The PDs increase in magnitude with increasing voltage. According to [20], if the voltage is maintained then the PD magnitude follows a trend (this is true for internal discharges):

- A maximum value is attained
- The PDs stay at this maximum for a while

- The PDs then become irregular and intermittent
- The PDs then become extinct

If the voltage is increased (higher than the inception voltage), then [20]:

- The discharge frequency increases
- The discharge magnitude remains the same
- Deterioration increases

Thus, there is an increased rate of deterioration when the applied voltage is higher than the IV, and the sample lifetime will therefore also decrease. If the voltage is increased to high (more than twice the inception voltage), thermal instability can/will occur. If this temperature rises too much, it can cause local thermal degradation [20].

5.4.1. Aging of Sample

All the build samples have an end of life, some shorter than others. We will likely never know the lifetime of some samples because they age so slowly that we do not see a difference.

Internal discharge is the most vulnerable defect in terms of its lifetime. A newly constructed internal discharge sample has high probability of surface discharge. When all instructions are followed according to the descriptions given in chapter 0 above, there is still a chance that surface discharge occurs. Then we must increase the “ripple” of grease, so that there is a longer creeping distance. When the sample is newly constructed and no surface discharge present, it needs an average aging time of ±25min before internal discharges appear. This initiation of PDs after the aging period can be seen in Figure 62 at the red arrows.

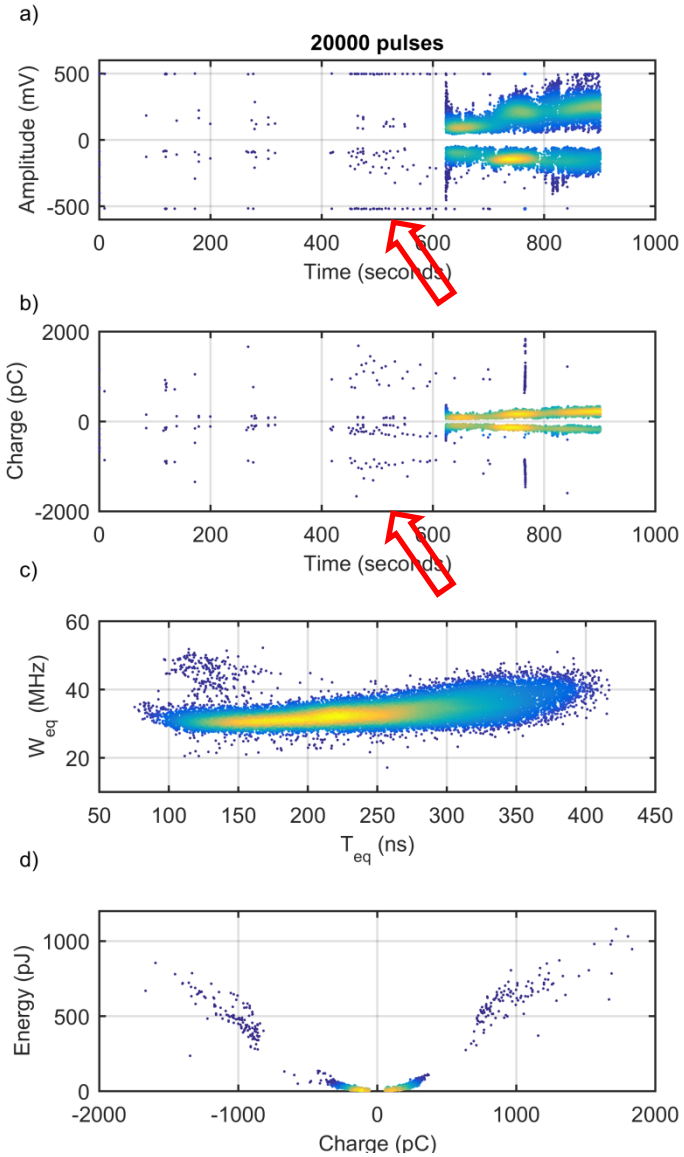

Figure 62: Aging of internal discharge sample: time evolution and clusters.

After the PDs of the internal discharge sample began, there was a change in pattern. This change in pattern is shown in Figure 63 t/m Figure 67; every graph is ±150 seconds of recorded data. Looking at the changes in the patterns of the PRPD analysis, we can see that at 600 seconds the pattern is as described in section 6.1.3 below. Before 600 seconds, Figure 65 shows that the formation of the “arcs” started between 400 and 600 seconds. This can be seen as confirmation that the designed samples are easy to construct (in this case, re-construct).

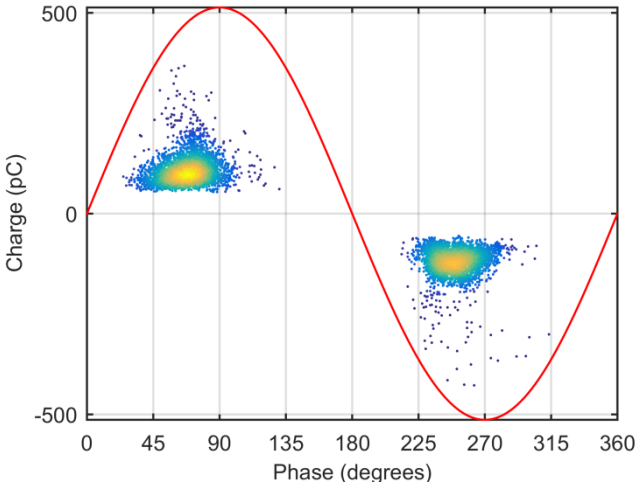

Figure 63: Aging, internal discharge 0-200 seconds.

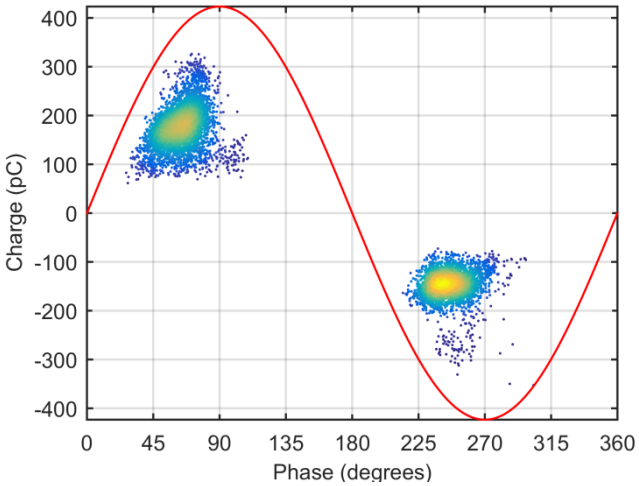

Figure 64: Aging, internal discharge 200-400 seconds.

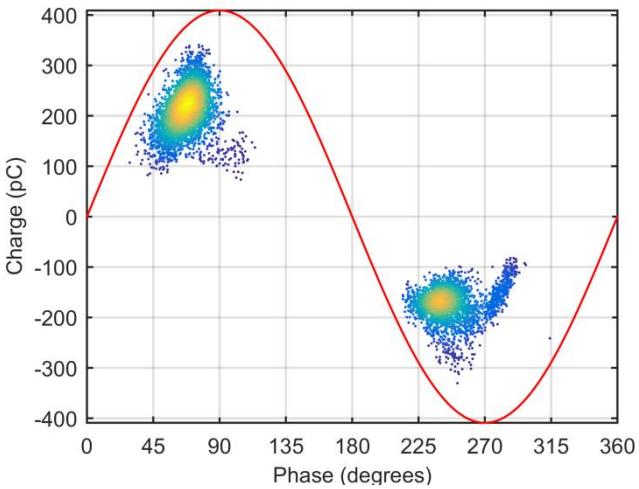

Figure 65: Aging, internal discharge 400-600 seconds.

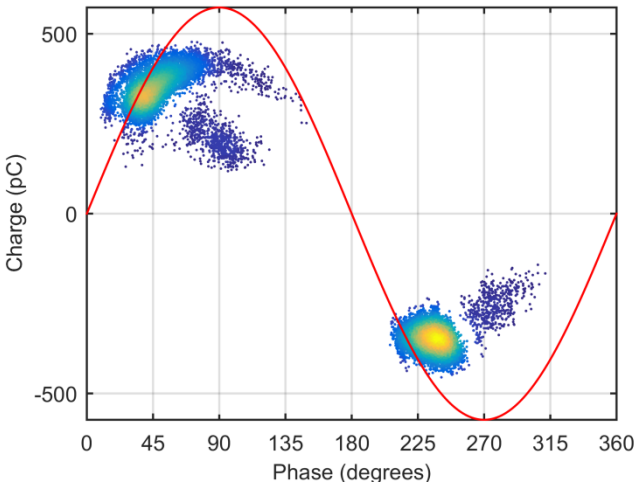

Figure 66: Aging, internal discharge 600-800 seconds.

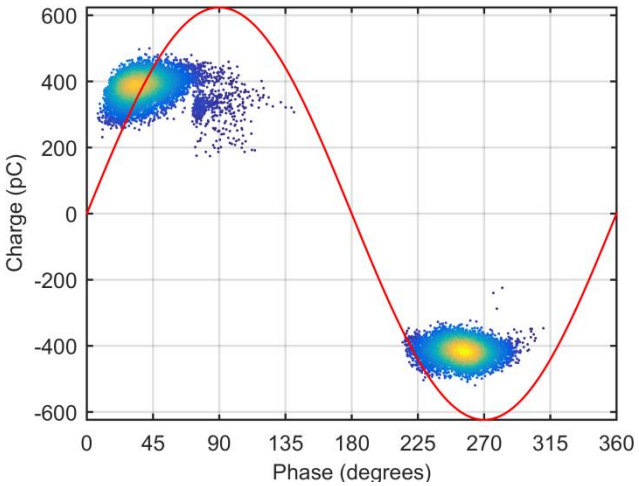

Figure 67: Aging, internal discharge 800-1000 seconds.

5.4.2. Lifetime of Sample

The internal discharge sample is the most unstable of the samples and has the shortest lifetime. This sample is most affected by aging: the higher the applied voltage, the shorter the lifetime of the sample. The internal discharge defect has a lifetime of ±1hour (excluding the aging process before PDs occur) with 10kV AC applied on the sample. When an internal discharge sample is newly constructed and no surface discharge is present, it requires an average aging time of ±25min before internal discharges appear.

In the other artificially created defects (samples), no aging was visible. Therefore, it was not possible to measure or estimate the lifetime of the other artificially created defects (samples).

5.5. PRPD Characterization

When measuring PDs in AC voltage, PRPD analysis was used. Below, Figure 68 t/m Figure 73 show the PRPD graphs in which the charge is plotted against the phase, which is done for all or a selected part of the recorded pulses.

All the clusters were checked to see if they were actually the “pure” form of the defect. This was done according to the manual of the PD Base II of TECHIMP [28] and with information received from the experience of Dr. Armando Rodrigo Mor in this field. Next to this there is a characterization shown below for all the artificially created defects.

PRPD Corona

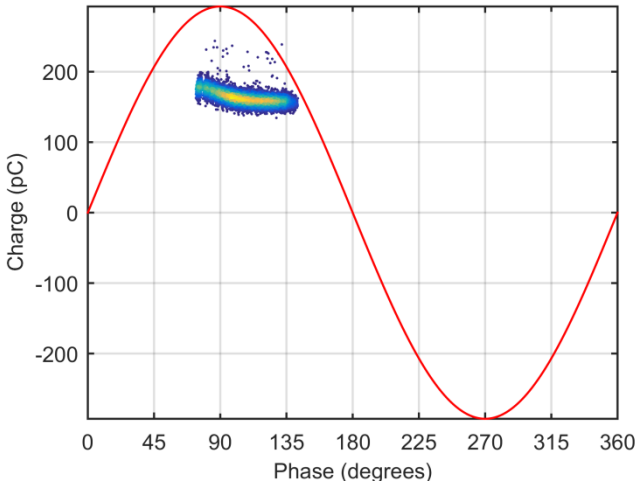

Figure 68: Negative corona PRPD.

Negative corona PRPD:

- **Magnitude order:** 10^2
- **Phase:** PDs occur around 90^0 (maximum of phase signal) with a slight phase shift
- **Concentration:** horizontal line
- **Shape:** horizontal line

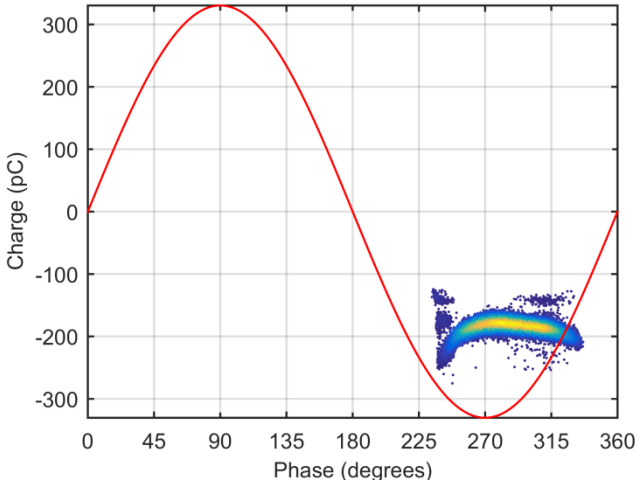

Figure 69: Positive corona PRPD.

Positive corona PRPD:

- **Magnitude order:** 10^2
- **Phase:** PDs occur around 270^0 (minimum of phase signal) with a slight phase shift
- **Concentration:** horizontal line
- **Shape:** horizontal line

PRPD Surface Discharge

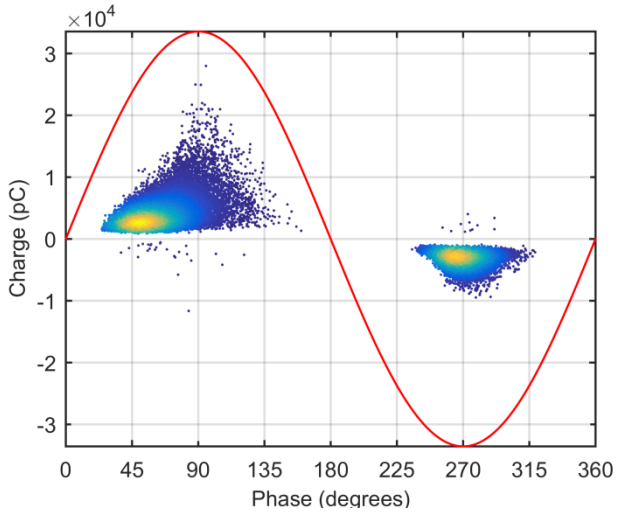

Figure 70: Surface discharge PRPD.

Surface discharge PRPD:

- **Magnitude order:** 10^4
- **Phase:** PDs occur within both the half cycles of the phase "180^0" (it does not cross the zero crossings of the phase) and have centres around 90^0 and 270^0 (maximum and minimum of phase signal)
- **Concentration:** middle, near x-axis
- **Shape:** triangles

PRPD Free-Moving Particle

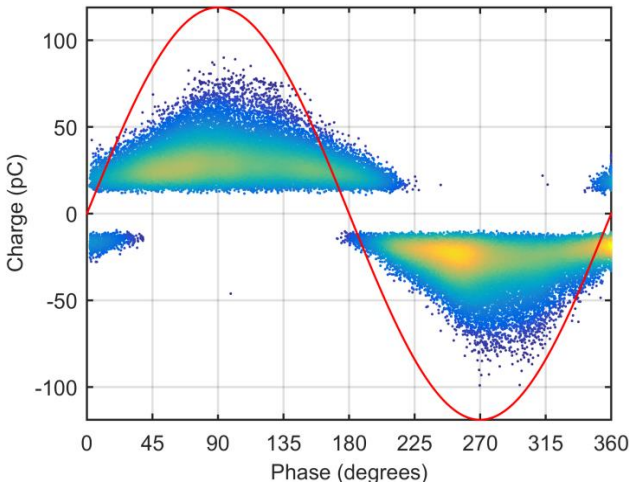

Figure 71: Free-moving particle PRPD.

Free-moving particle PRPD:

- **Magnitude order:** 10^2
- **Phase:** The centres of the triangles are at 90^0 and 270^0 (maximum and minimum of phase signal). The PDs do not stay inside the half cycle of the phase "180^0" (it crosses the zero crossings of the phase). The PDs have a phase length of $\pm 225^0$.
- **Concentration:** along the x-axis, near the x-axis
- **Shape:** triangles

PRPD Floating Electrode

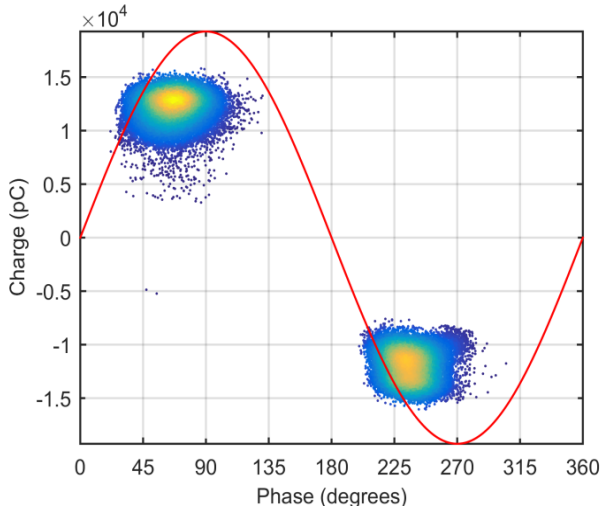

Figure 72: Floating electrode PRPD.

Floating electrode PRPD:

- **Magnitude order:** 10^4
- **Phase:** PDs occur around 67^0 and 247^0
- **Concentration:** in the middle of the squares
- **Shape:** squares

PRPD Internal Discharge

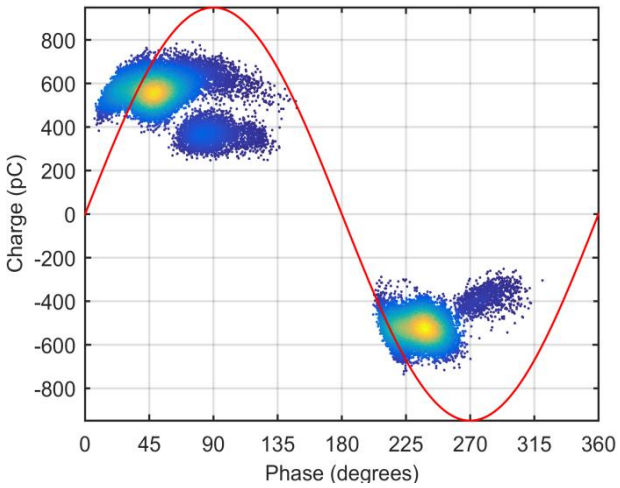

Figure 73: Internal discharge PRPD.

Internal discharge PRPD:

- **Magnitude order:** 10^2
- **Phase:** PDs go along the phase line and start close to zero crossing of phase line
- **Concentration:** in the beginning of the arcs near the phase signal
- **Shape:** arcs

6. Characterization, Analysis and Recognition of PD patterns

The transmission path from the source to the detector is dependent on the equivalent capacitance of the test object (TO) and the wiring. Because of this, even if the defect is the same, the PD pulse shape may change depending on the setup. The PD sensor must have as wide a bandwidth as possible and a technique for source discrimination of the PD. This source discrimination must work even if the TO changes, or when noise is present [19].

It is important to characterize and analyse each type of defect properly before being able to recognize the origins of defects when measuring multiple defects at the same time. In this chapter each created artificial defect will be characterized and analysed, looking at the time evolution of PDs in amplitude and charge and noting e.g. the concentrations and peaks in frequency domain, settling time, signal to noise ratio, oscillations and overshoot in the time domain. Different clustering techniques will also be applied to each defect to look at their differences and the possibilities for defect separation and recognition, including:

- Clustering: W_{eq} vs. T_{eq}
- Clustering: energy vs. charge
- Clustering: energy vs. charge (in logarithmic scale)
- Clustering: energy per charge vs. charge
- Number of discharges per cycle

We will also investigate the patterns for PRPD and TRPD analysis. Here we will be looking at e.g. magnitudes, shapes, concentrations, distribution, PD occurrence locations, slopes and polarity.

The goal here is to characterize each sample as optimally as possible so that we develop a clustering tool that does characterization as well and simple as possible, with a pattern recognition tool (defect origin recognition) that is also as good and simple as possible. Therefore, we will analyse and characterise each defect with different methods to be able to optimize and simplify as much as possible the detection of the origin of the defect. Afterwards, in chapter 7, we will look at the effects and changes in these characterizations when multiple artificial defects are combined.

6.1. PD Defect Characterization

6.1.1. PD Time Evolution and Clusters

Figure 75 t/m Figure 89 show the positive and negative pulses of the samples. In each figure the pulse amplitude is plotted against the time and frequency. In the plots of amplitude vs. time, the pulses have the shapes and slopes that were described in section 2.2 above.

6.1.1.1. Positive and Negative Corona Pulses

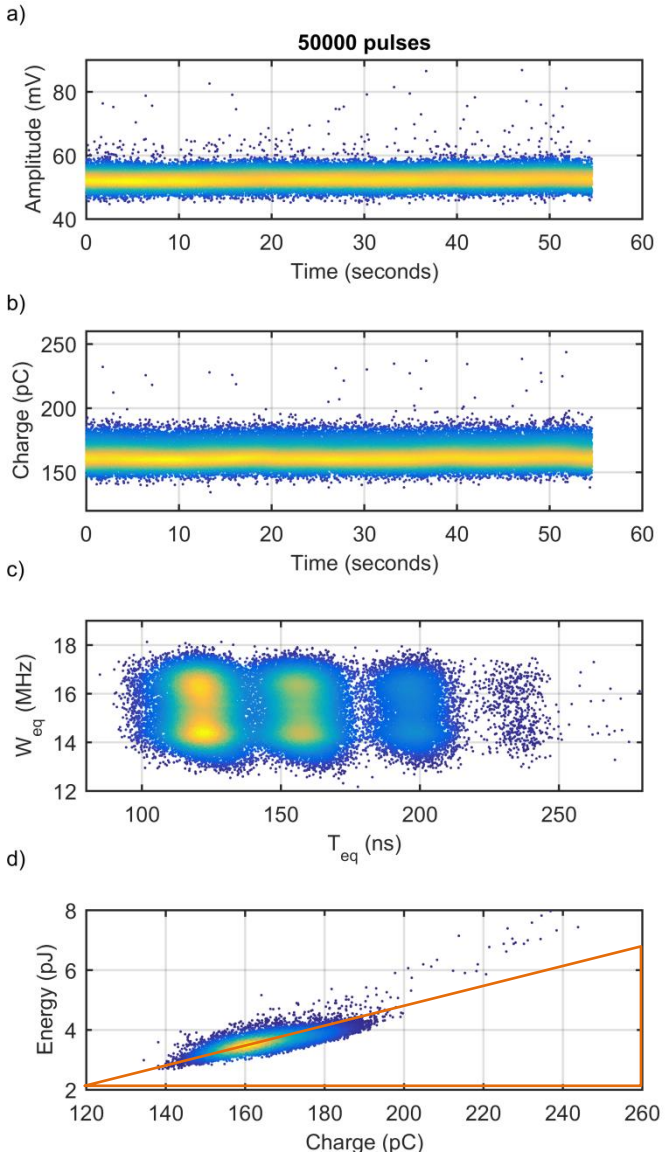

Figure 74: Negative corona time evolution and clusters.

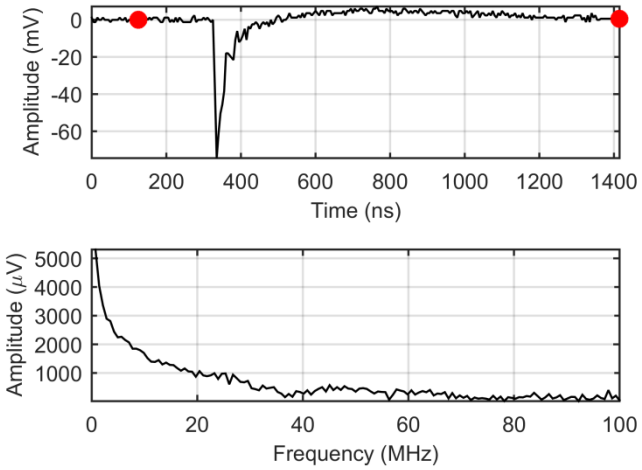

Figure 75: Negatively pulsed corona, pulse 34970.

Magnitude order:

- Voltage: 10^1 mV
- Charge: 10^2 pC

Weq vs. teq cluster negative corona:

- 4 concentrations divided in 2 (horizontally reflected)

Weq vs. teq cluster positive corona:

- 4 concentrations divided in 2 (horizontally reflected)

Energy vs. charge cluster negative corona:

- Single concentration
- Pos. Slope: 0.12 pJ/pC

$$Slope = \frac{\Delta Energy}{\Delta Charge} = \frac{4.8pJ}{40pC} = 0.12\frac{pJ}{pC}$$

Energy vs. charge cluster positive corona:

- Single concentration
- Pos. Slope: 0.06525 pJ/pC

$$\frac{\Delta Energy}{\Delta Charge} = \frac{10.5pJ}{160pC} = 0.06525\frac{pJ}{pC}$$

Figure 75 shows a negatively charged pulse in the time and frequency domain of the corona defect.

Frequency domain:

- **Concentration:** at lower frequencies (f=0), decays exponentially
- **Peaks:** only at beginning (f=0)

Time domain:

- **Settling time:** settles gradually
- **Signal to noise ratio:** large
- **Oscillation:** none
- **Overshoot:** once

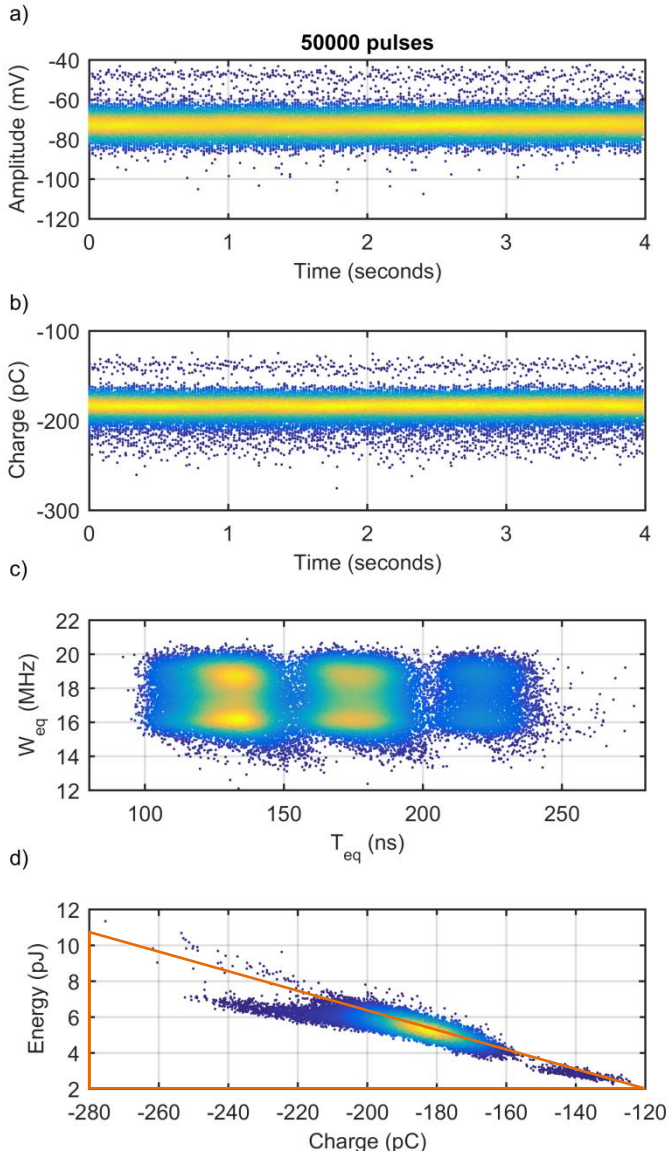

Figure 76: Positive corona time evolution and clusters.

Figure 77 shows a negatively charged pulse in the time and frequency domain of the corona defect.

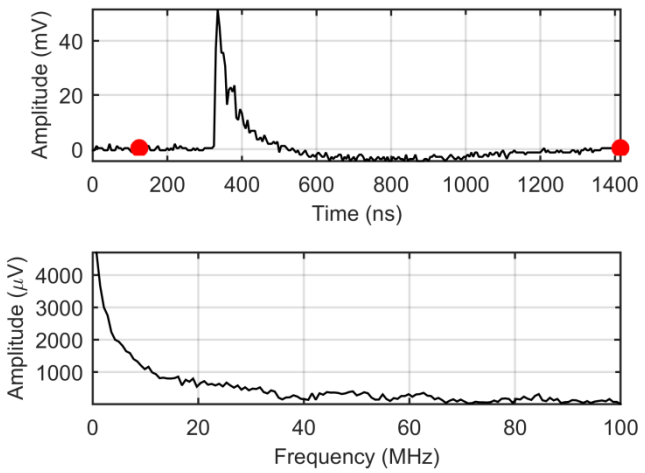

Figure 77: Positively pulsed corona, pulse 32497.

6.1.1.2. Positive and Negative Surface Discharge Pulses

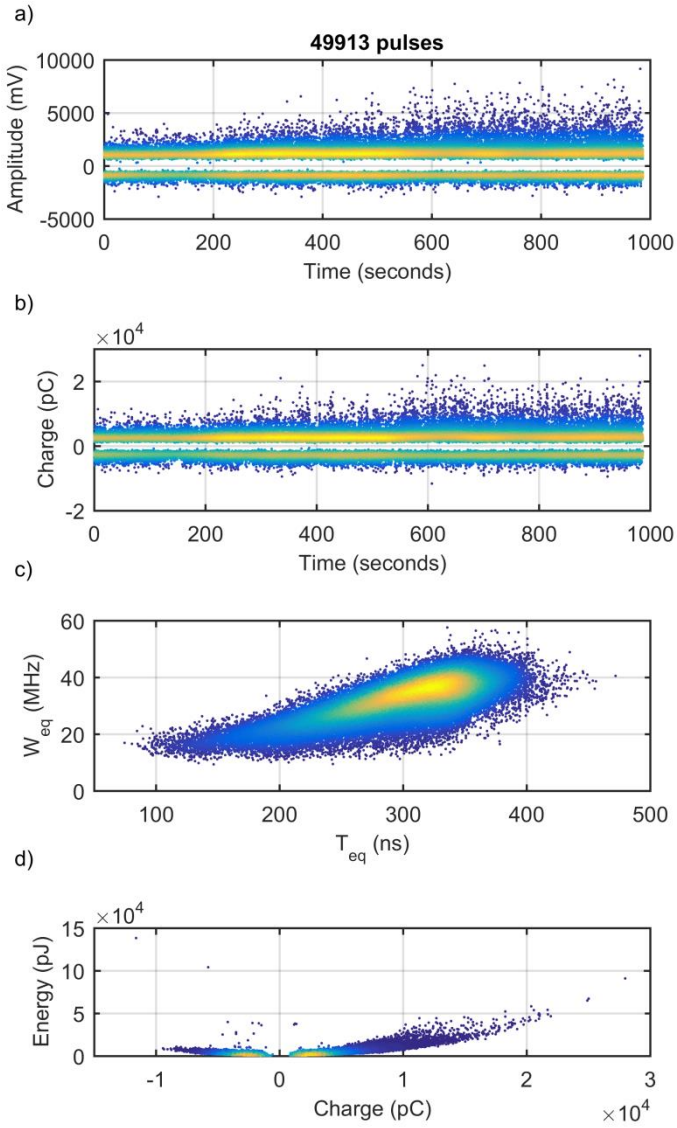

Figure 78: Surface discharge time evolution and clusters.

Magnitude order:

- Voltage: 10^3 mV
- Charge: 10^4 pC

Weq vs. teq cluster surface discharge:

- Single concentration

Energy vs. charge cluster:

- Two concentrations: positive and negative
- Shape: parabolic

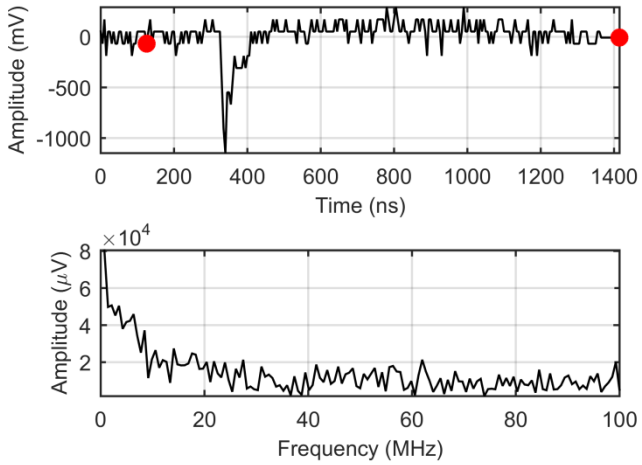

Figure 79: Negatively pulsed surface discharge, pulse 10110.

Figure 79 and Figure 80 show a negatively and positively charged pulse in time and frequency domains of the surface discharge defect.

Frequency domain:

- **Concentration:** at lower frequencies (f=0), decays exponentially
- **Peaks:** only at beginning (f=0)

Time domain:

- **Settling time:** settles gradually
- **Signal to noise ratio:** large
- **Oscillation:** none
- **Overshoot:** once

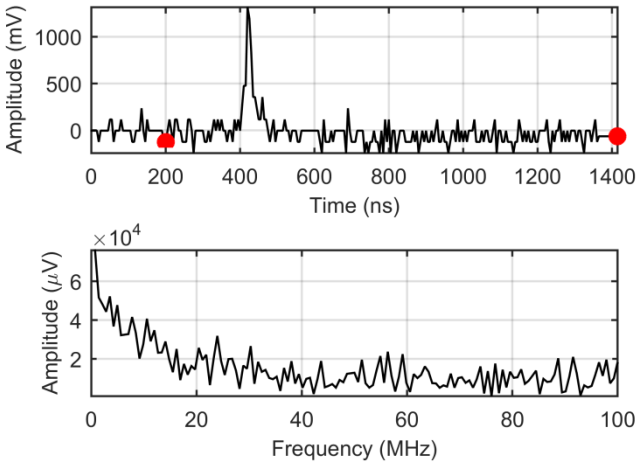

Figure 80: Positively pulsed surface discharge, pulse 6981.

6.1.1.3. Positive and Negative Free-Moving Particle Pulses

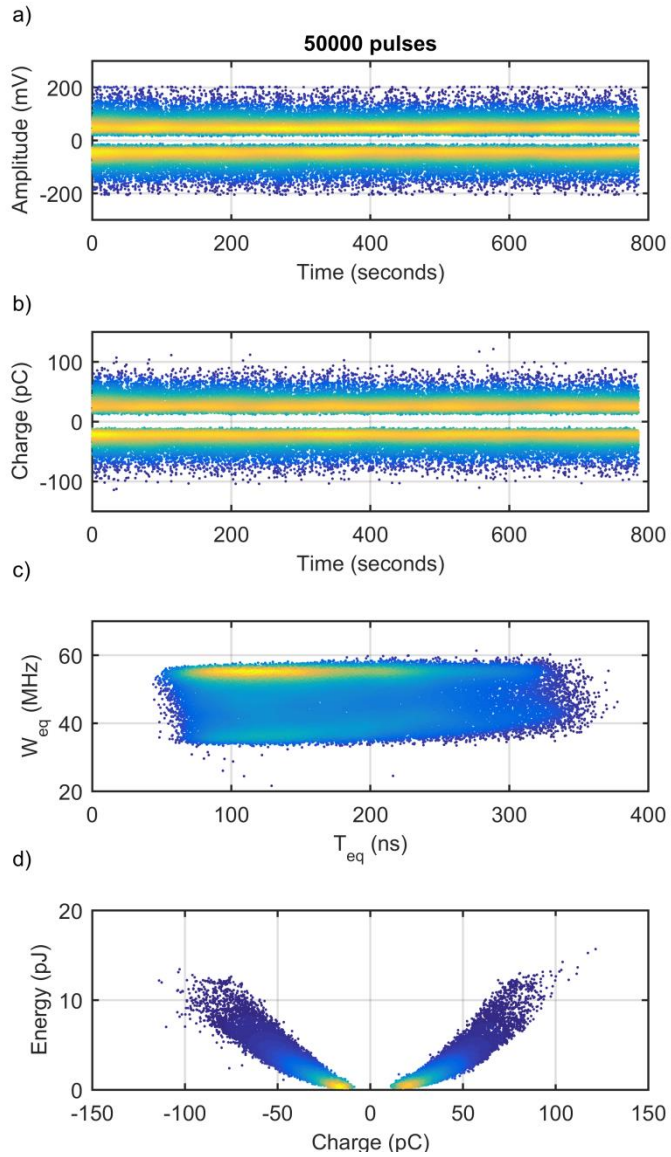

Magnitude order:

- Voltage: 10^2 mV
- Charge: 10^2 pC

Weq vs. teq cluster free-moving particle:

- Single concentration

Energy vs. charge cluster:

- Two concentrations: positive and negative
- Shape: parabolic

Figure 81: Free-moving particle time evolution and clusters.

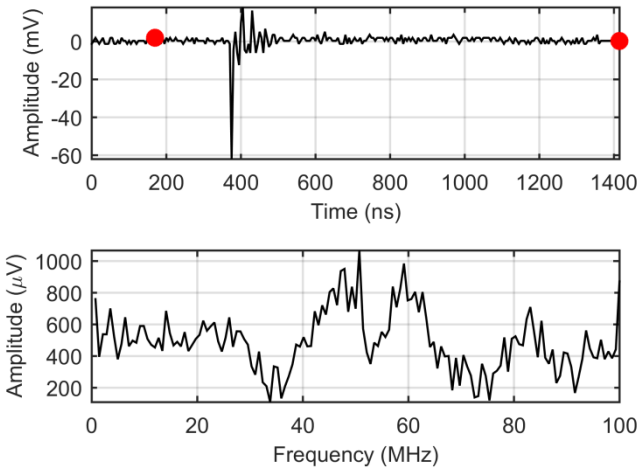

Figure 82: Negatively pulsed free-moving particle, pulse 27173.

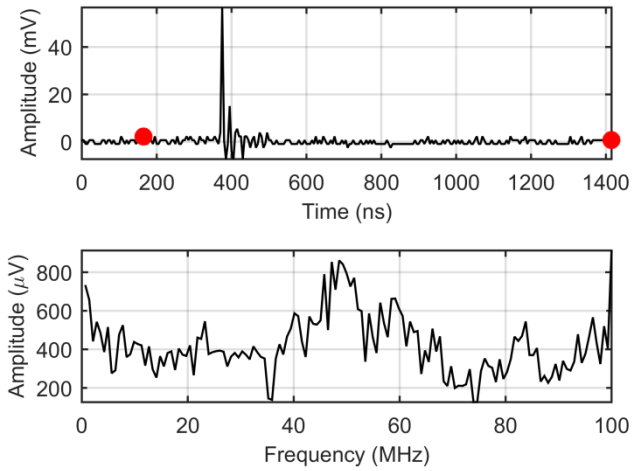

Figure 83: Positively pulsed free-moving particle, pulse 27173.

Figure 82 and Figure 83 show a negatively and positively charged pulse in the time and frequency domains of the free-moving particle defect.

Frequency domain:

- **Concentration: a**round 50 & 60 MHz, decays exponentially
- **Peaks: a**round 50 & 60 MHz

Time domain:

- **Settling time:** settles gradually
- **Signal to noise ratio:** large
- **Oscillation:** yes; more than once
- **Overshoot:** yes; large peaks (±27% of max) and smaller peaks of (±11% of max)

6.1.1.4. Positive and Negative Floating Electrode Pulses

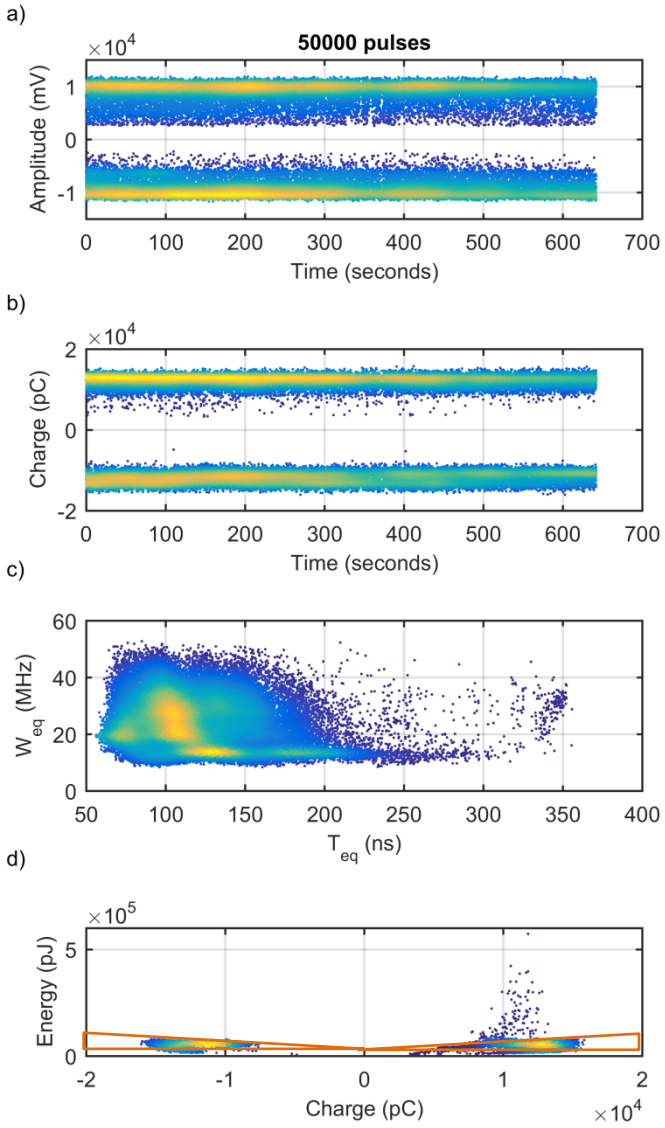

Figure 84: Floating electrode time evolution and clusters.

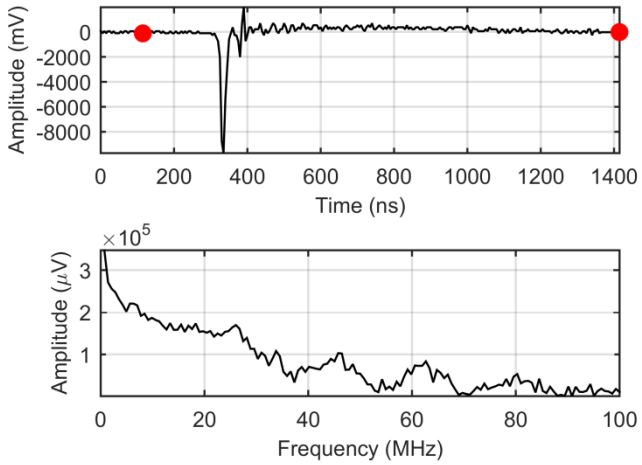

Figure 85: Negatively pulsed floating electrode, pulse 47485.

Magnitude order:

- Voltage: 10^4 mV
- Charge: 10^4 pC

Weq vs. teq cluster floating electrode:

- Single concentration

Energy vs. charge cluster:

- Two concentrations: positive and negative
- Slope: ±46875 pJ/pC

$$Slope = \frac{\Delta Energy}{\Delta Charge} = \frac{93750pJ}{\pm 2pC} = \pm 46875 \frac{pJ}{pC}$$

Figure 85 and Figure 86 show a negatively and positively charged pulse in the time and frequency domains of the floating electrode defect.

Frequency domain:

- **Concentration:** at lower frequencies (f=0), decays exponentially
- **Peaks:** only at beginning (f=0)

Time domain:

- **Settling time:** settles gradually
- **Signal to noise ratio:** large
- **Oscillation:** yes; more than once
- **Overshoot:** yes; large peaks (±21% of max) and smaller peaks of (±4% of max)

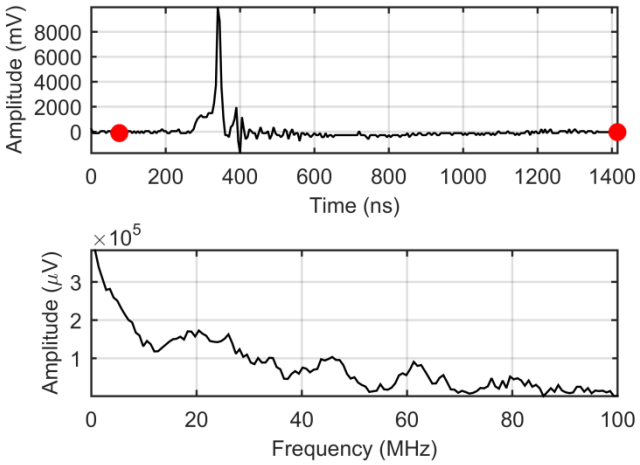

Figure 86: Positively pulsed floating electrode, pulse 10741.

6.1.1.5. Positive and Negative Internal Discharge Pulses

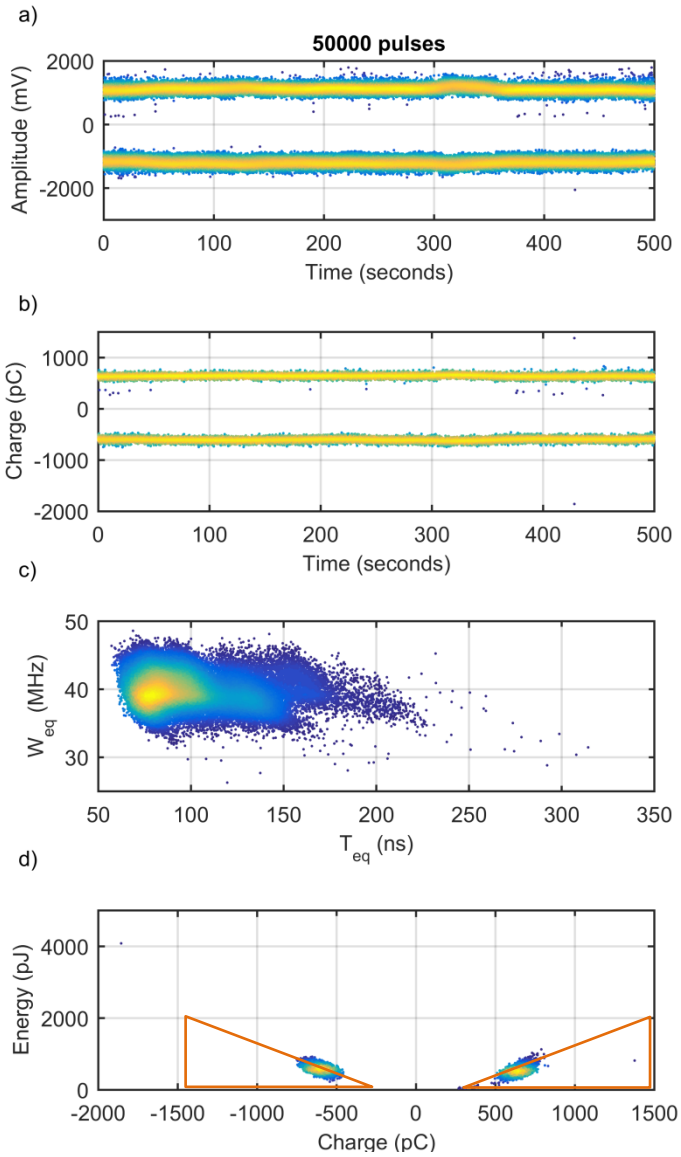

Magnitude order:

- Voltage: 10^3 mV
- Charge: 10^3 pC

Weq vs. teq cluster internal discharge:

- Single concentration

Energy vs. charge cluster:

- Two concentrations: positive and negative
- Slope: ±1.6 pJ/pC

$$Slope = \frac{\Delta Energy}{\Delta Charge} = \frac{2000pJ}{\pm 1250pC} = \pm 1.6\frac{pJ}{pC}$$

Figure 87: Internal discharge time evolution and clusters.

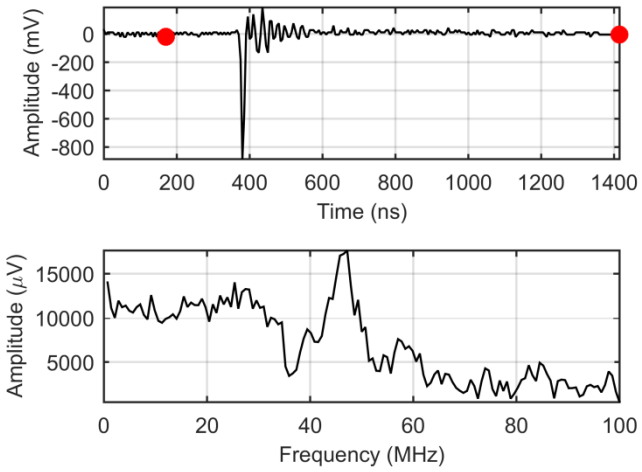

Figure 88: Negatively pulsed internal discharge, pulse 37715.

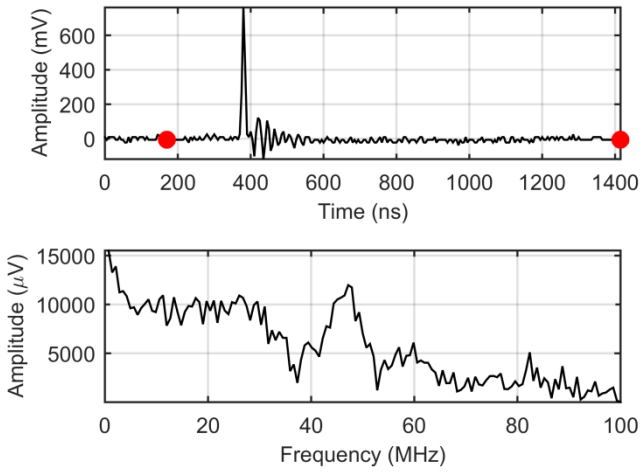

Figure 89: Positively pulsed internal discharge, pulse 36567.

Figure 88 and Figure 89 show a negatively and positively charged pulse from in the time and frequency domains of the internal discharge defect.

Frequency domain:

- **Concentration:** at lower frequencies (f=0 till 30MHz) and around 45MHZ
- **Peaks:** at beginning (f=0) and around 45MHz

Time domain:

- **Settling time:** settles gradually
- **Signal to noise ratio:** large
- **Oscillation:** yes; more than once
- **Overshoot:** yes; large peaks (±17% of max) and smaller peaks of (±4% of max)

6.1.2. Energy per Charge vs. Charge

To get a different view of the defect characteristics it was decided to view the effects of the defect clusters when plotting energy per charge versus the charge. Figure 90 t/m Figure 95 show the graphs of the clusters made by calculating the energy per charge and plotting it versus the charge. The clusters now have shapes that are better to work with (e.g. linear instead of parabolic) when comparing them to energy versus charge graphs. Each individual defect can now be characterized more easily with slopes and magnitudes. Each figure also shows the calculated slope(s) and the “triangle” used for this calculation.

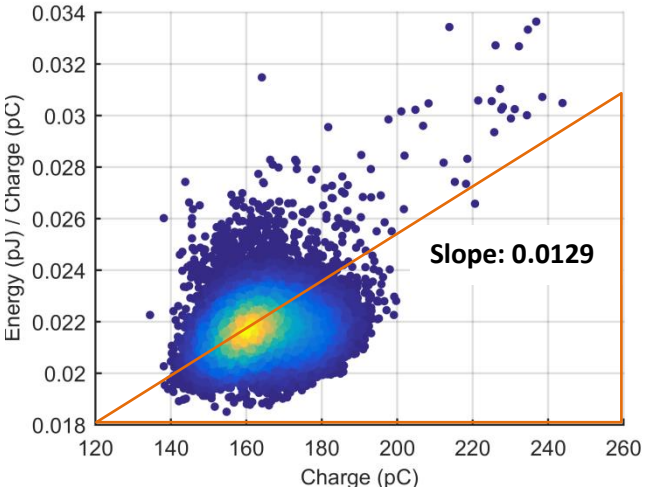

Figure 90: Negative corona - Energy per charge vs. charge.

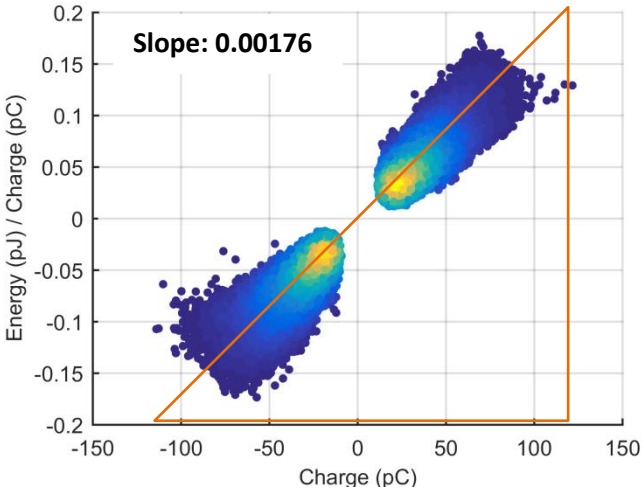

Figure 93: Free-moving particle - Energy per charge vs. charge.

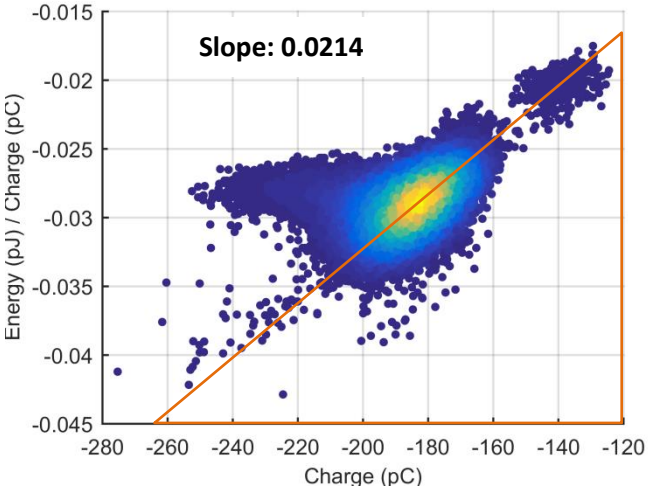

Figure 91: Positive corona - Energy per charge vs. charge.

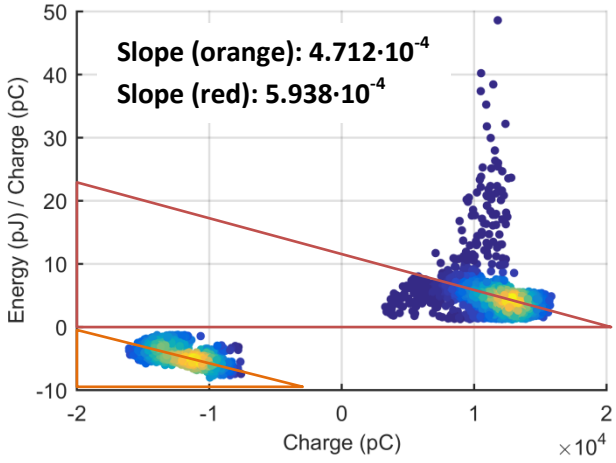

Figure 94: Floating electrode - Energy per charge vs. charge.

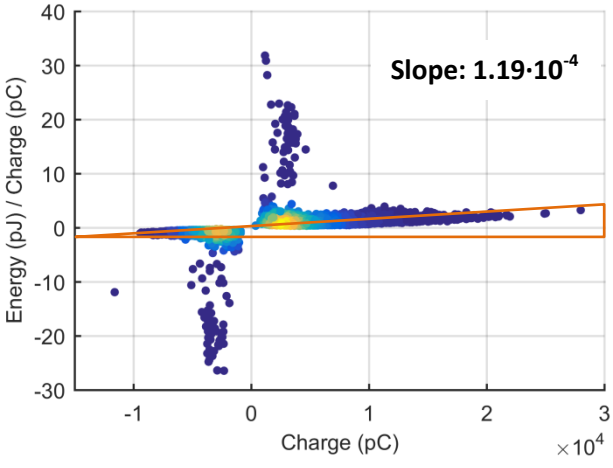

Figure 92: Surface discharge - Energy per charge vs. charge.

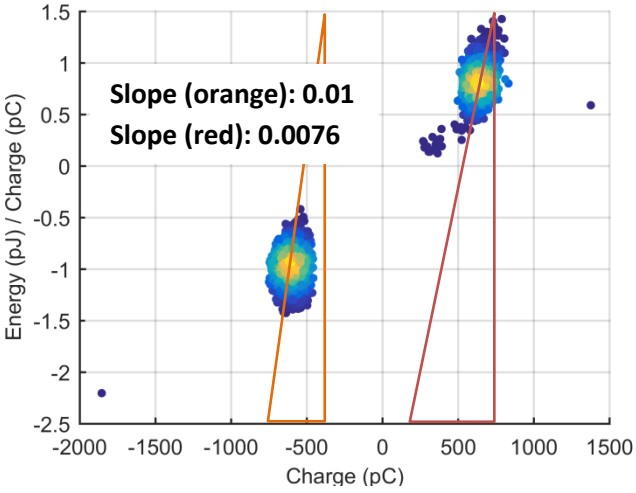

Figure 95: Internal discharge - Energy per charge vs. charge.

Sample Defect	Slope	Magnitude [pJ/pC]
Negative corona	$+129 \cdot 10^{-4} \approx +10^{-2}$	$+10^{-2}$
Positive corona	$+214 \cdot 10^{-4} \approx +10^{-2}$	-10^{-2}
Internal discharge	$+1 \cdot 10^{-2} \approx +10^{-2}$	-10^{1}
	$+76 \cdot 10^{-4} \approx +10^{-3}$	$+10^{1}$
Free-moving particle	$+176 \cdot 10^{-5} \approx +10^{-3}$	$\pm 10^{-1}$
Surface discharge	$+1.19 \cdot 10^{-4} \approx +10^{-4}$	$\pm 10^{1}$
Floating electrode	$-4.712 \cdot 10^{-4} \approx -10^{-4}$	-10^{1}
	$-5.938 \cdot 10^{-4} \approx -10^{-4}$	$+10^{1}$

Table 10: Summary, slopes of energy per charge vs. charge

From these figures and graphs we can conclude that all the defects are distinguishable from each other simply by using this cluster technique. This analysis can be seen in Figure 96 as a flowchart, which shows that all the defects are distinguishable. Only if the defect is not similar to the six samples is the defect not distinguishable, and therefore it is undefined. The colour green shows the defect combinations that were distinguishable, and orange shows the undefined ones.

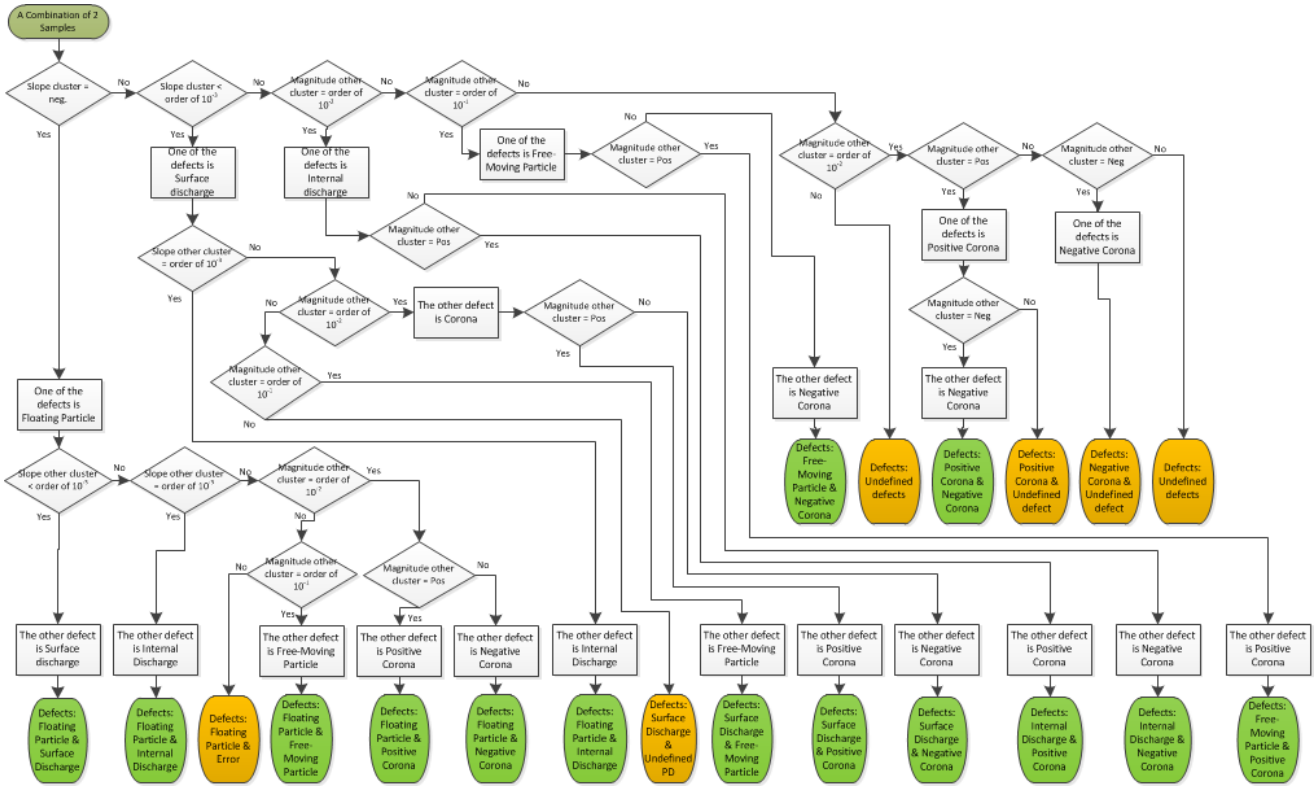

Figure 96: Flowchart: Energy per charge analysis.

6.1.3. Fall- vs. Rise-time of Pulse

As already mentioned in chapter 2, and as will be further elaborated in section 7.2.1, PD pulses are attenuated and distorted when traveling through e.g. the cables. Even though this attenuation and distortion exists, there is a chance that these graphs can be used for clustering. It is definite that they cannot be used for defect origin recognition due to this attenuation and distortion, which occurs in real life. Perhaps in this case, due to the equal path length in the setup, the PDs could be distinguished completely, but this is of no importance. For this cluster, the rise-time is taken from 10% to 90% of the pulse peak and the fall-time is taken from 90% down to 10%, as shown in Figure 10.

Figure 97 and Figure 98 show the clustering graphs of negative and positive corona. They are exactly the same, only reflected over the y-axis (negative to positive), so therefore the rise and fall times are similar for these defects. In these graphs, there is no identifiable shape.

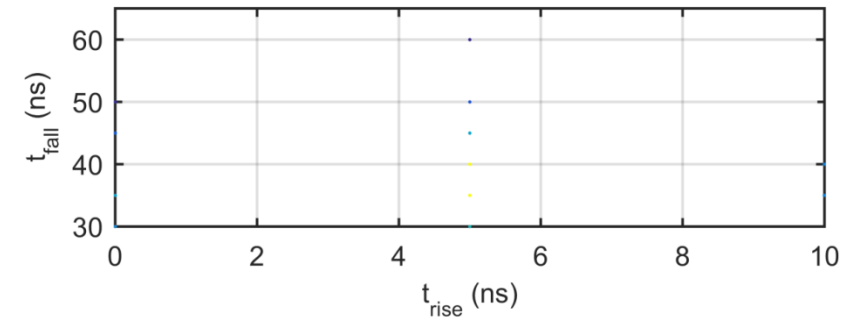

Figure 97: Negative corona – Pulse fall-time vs. rise-time.

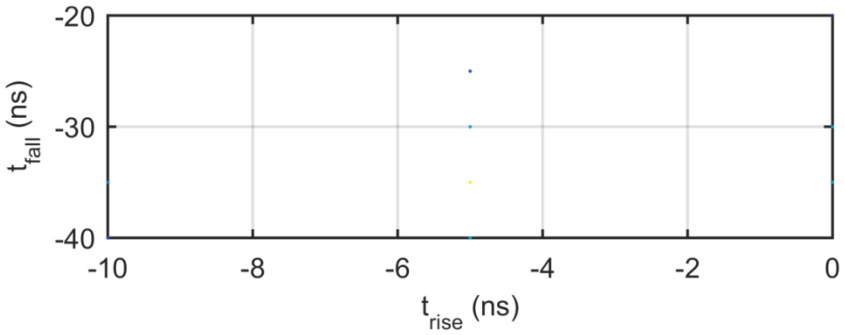

Figure 98: Positive corona – Pulse fall-time vs. rise-time.

The occurring discharges have rise-times of ±10ns, ±5ns and 0ns, which are exactly the same for positive and negative corona. The fall-times of negative corona have a wider range compared to positive corona. Negative corona occur between 30ns and 60ns with steps of 5ns, and positive corona occur between 25ns and 35ns with steps of 5 ns. The 5 ns steps are due to the pre-set sampling rate, which can be adjusted on the oscilloscope.

Figure 99 shows the clustering graph of surface discharge. The shape is like a line through the 0-crossing, with the concentration near this 0-crossing. The range of the rise-time is from -550ns to 300ns, and the fall-time is in the range of -500ns to 300ns.

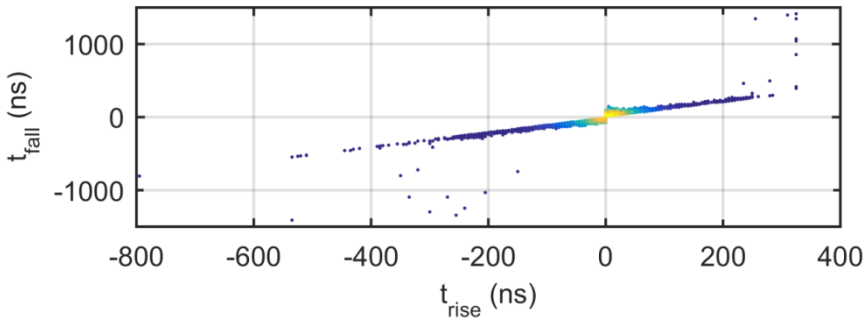

Figure 99: Surface discharge – Pulse fall-time vs. rise-time.

Figure 100 shows the clustering graph of free-moving particles. The shape is like a line through the 0-crossing, with its concentration near the 0-crossing. The range of the rise-time is from -60ns to 200ns, and the fall-time is in the range of -75ns to 200ns.

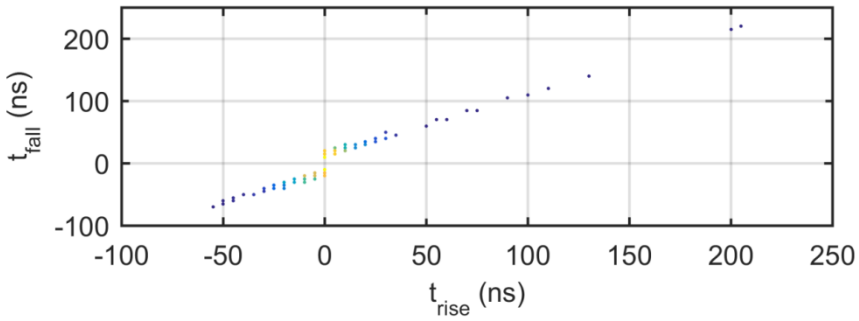

Figure 100: Free-moving particle – Pulse fall-time vs. rise-time.

Figure 101 shows the clustering graph of floating electrodes. The shape is like a line through the 0-crossing, with its concentration near the 0-crossing. The range of the rise-time is from -125ns to 200ns, and the fall-time is in the range of -150ns to 200ns.

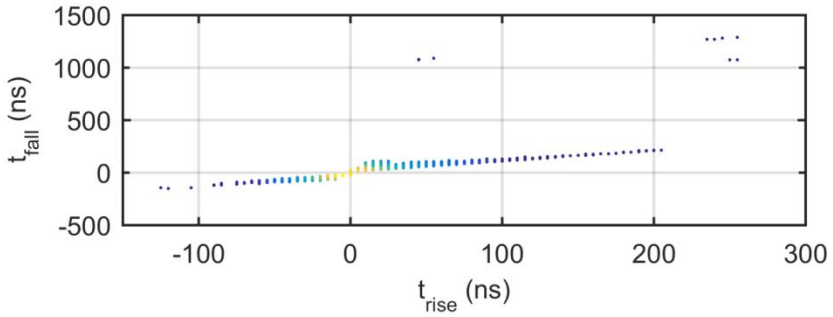

Figure 101: Floating electrode – Pulse fall-time vs. rise-time.

Figure 102 shows the clustering graph of internal discharge. Here, just like the corona discharges, there is no identifiable shape. The occurring discharges have a rise-time of 0, ±5 and 10 ns, with corresponding fall-times of 25, ±20, ±15 and ±10ns.

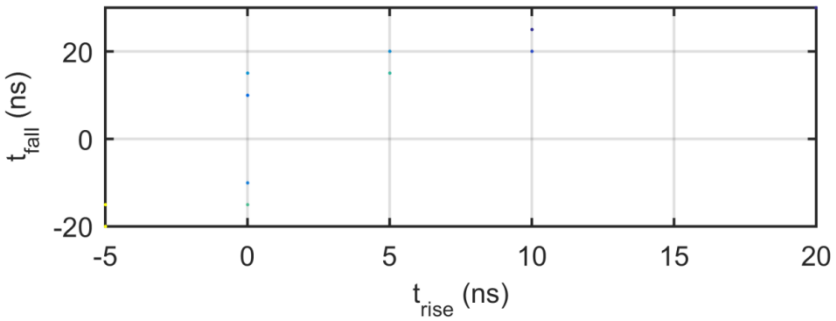

Figure 102: Internal discharge – Pulse fall-time vs. rise-time.

The ns ranges of the pulses are similar to those described in section 2.2. Among the different artificial defects, there are two “shapes” distinguishable: a horizontal line through the 0 axis (for surface discharge, free-moving particle, and floating electrode samples) and some scattered dots not shaped in any way (corona and internal discharge samples).

6.1.4. PRPD Characterization Summary

Since the PRPD characterization was already done in section 5.5, no further characterization is needed. A summary of these characterizations is presented in this section.

Table 11 contains a summary of the analysis done from Figure 68 t/m Figure 73. With this summary, we can more easily use and evaluate the analysis to distinguish the defects. During the analysis of the charge versus phase, we looked at the magnitude order of charge, phase, concentration and shape of the figures.

Analysis Type	Negative Corona	Positive Corona	Surface Discharge	Free-Moving Particle	Floating Electrode	Internal Discharge
Magnitude order	10^2	10^2	10^4	10^2	10^4	10^3
Phase	around 90^0 (maximum of phase signal) with a slight phase shift	around 270^0 (minimum of phase signal) with a slight phase shift	PDs occur within both half cycles of the phase "180^0" (not crossing the zero crossings of phase signal) and have centres around 90^0 and 270^0 (max. and min. of phase signal)	centres of triangles are at 90^0 and 270^0 (max. and min. of phase signal). PDs do not stay inside the half cycle of the phase "180^0" (crosses the zero crossings of phase signal). PDs have phase length of $\pm 225^0$.	around 67^0 and 247^0	along the phase (sinus)
Concentration	horizontal line	horizontal line	middle near x-axis	along the x-axis, near the x-axis	in the middle of the squares	in the beginning of the arcs near the phase signal
Shape	horizontal line	horizontal line	triangle	triangle	square	arc

Table 11: Summary of PRPD analysis.

6.1.5. TRPD Characterization

When analysing PDs in DC-voltage TRPD analysis is used, and when measuring PDs in AC-voltage PRPD is used. It would be very convenient if TRPD could be used for AC-voltage as well. In this case, the final product will be cheaper and probably less complex, because no synchronization is needed. Synchronization is used in PRPD to know where the PDs happen in the phase. Below, Figure 103 t/m Figure 114 show the TRPD graphs of the different defect types.

6.1.5.1. TRPD *Corona*

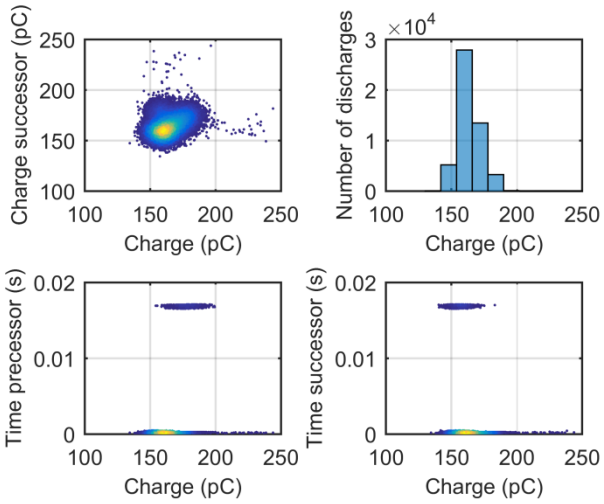

Figure 103: Negative corona TRPD – Positively charged pulses.

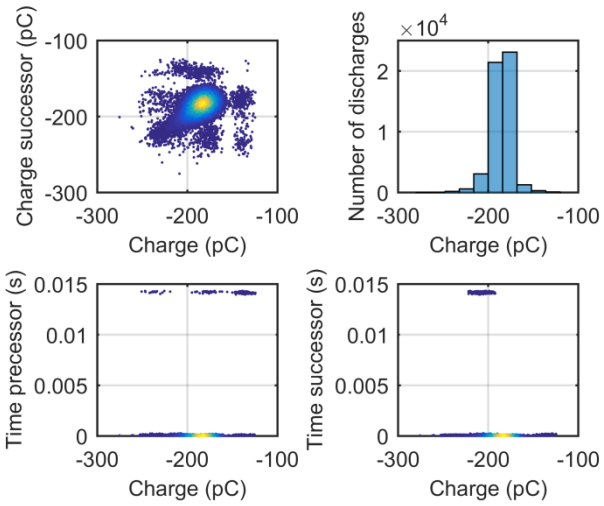

Figure 104: Positive corona TRPD – Negatively charged pulses.

6.1.5.2. TRPD *Surface Discharge*

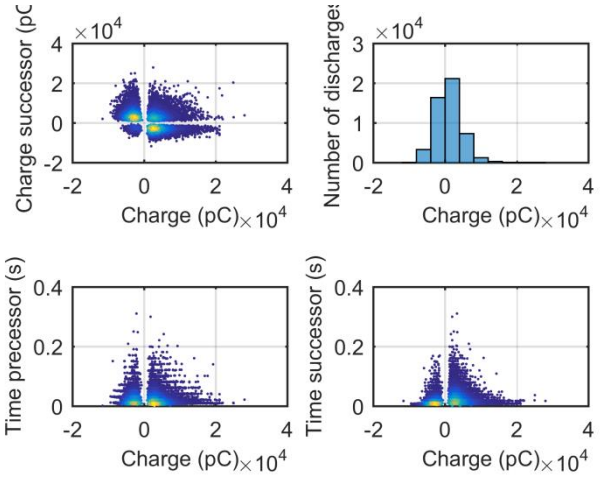

Figure 105: Surface discharge TRPD.

Negative corona PRPD:

- **Qsuc vs. Q:** one concentration spot with a reflection possible around y=x line. PDs occur in the first quadrant, with magnitude order $+10^2$ and one concentration spot on the line y=x, with an oval shape at an angle of 45^0 (on line y=x).
- **Number of discharges vs. Q:** a peak around 160pC
- **Tpre & Tsuc vs. Q:** two horizontal lines, one around t=0s and the other around t=0.016s. Order of 10^2pC and 10^{-2} seconds. The horizontal lines have a thickness of ±0.0004 seconds.

Positive corona PRPD:

- **Qsuc vs. Q:** One concentration spot with a reflection possible around y=x line. PDs occur in third quadrant, with magnitude order -10^2 and one concentration spot (oval shape) on the line y=x.
- **Number of discharges vs. Q:** a peak around -180pC
- **Tpre & Tsuc vs. Q:** two horizontal lines, one around t=0s and the other around t=0.014s. Order of 10^2pC and 10^{-2} seconds. The horizontal lines have a thickness of ±0.0002 seconds.

Surface discharge TRPD:

- **Qsuc vs. Q:** Four concentration spots near the 0-crossing with a reflection possible around y=x line. No PDs on the x and y axes. The farther away from the 0-crossing, the fewer PDs there are. PDs occur in all four quadrants, with magnitude order $\pm10^4$ and four concentration spots near 0-crossing.
- **Number of discharges vs. Q:** a peak around 0pC.
- **Tpre & Tsuc vs. Q:** no PDs on the y-axis. Concentration is near 0-crossing. Order of 10^4pC and 10^{-1} seconds.

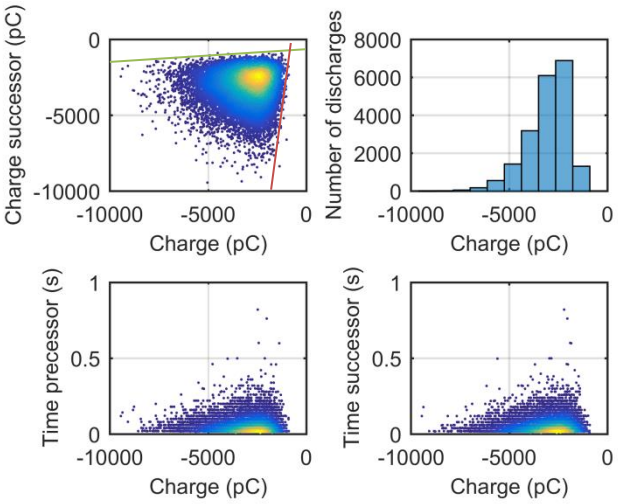

Figure 106: Surface discharge TRPD – Negatively charged pulses.

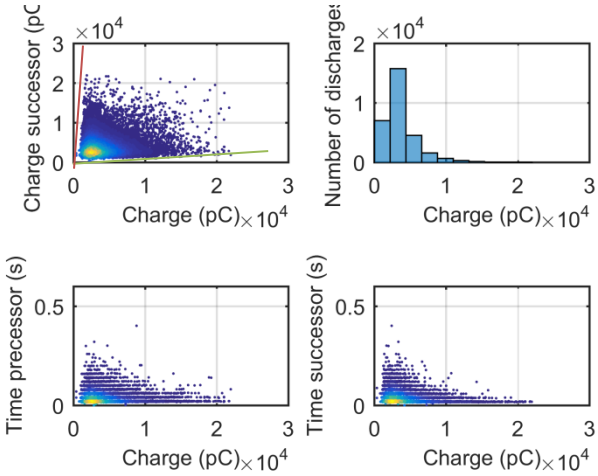

Figure 107: Surface Discharge TRPD – Positively charged pulses.

For a better understanding of the patterns in TRPD analysis, we will also look at the charge polarities separately. Taking the positive charge and the negative charge as separate clusters, we can clearly see different shapes and PD distributions.

Negatively charged pulses of surface discharge in TRPD:

- **Qsuc vs. Q:** triangle shape with concentration in a corner near 0-crossing with an angle of 75^0C (crossing of green and red lines). The PDs appear within two lines that have slopes of 0.1 (green line) and 6.50 (red line).
- **Number of discharges vs. Q:** peak around -2500pC. The slope towards 0 decreases quickly, but away from 0 the slope decreases slowly.
- **Tpre & Tsuc vs. Q:** shape of stacked horizontal lines (triangle-like). The stacked lines are separated by ±0.02 seconds from each other, and they are ±0.004 seconds thick. The further away from the x-axis, the less the concentration. The concentration of the lines is denser closer to the x-axis. The PDs have a time interval on the order of 10^{-1}.

Positively charged pulses of surface discharge in TRPD:

- **Qsuc vs. Q:** triangle shape with concentration in a corner near 0-crossing with an angle of 81^0C (crossing of green and red lines). The PDs appear within two lines that have slopes of 0.1 (green line) and 14.29 (red line).
- **Number of discharges vs. Q:** peak around +3000pC. The slope towards 0 decreases quickly, but away from 0 the slope decreases slowly.
- **Tpre & Tsuc vs. Q:** shape of stacked horizontal lines (triangle-like). The stacked lines are separated by ±0.02 seconds from each other, and they are ±0.004 seconds thick. The further away from the x-axis, the less the concentration. The concentration of the lines is denser closer to the x-axis. The PDs have a time interval on the order of 10^{-1}.

6.1.5.3. TRPD *Free-Moving Particle*

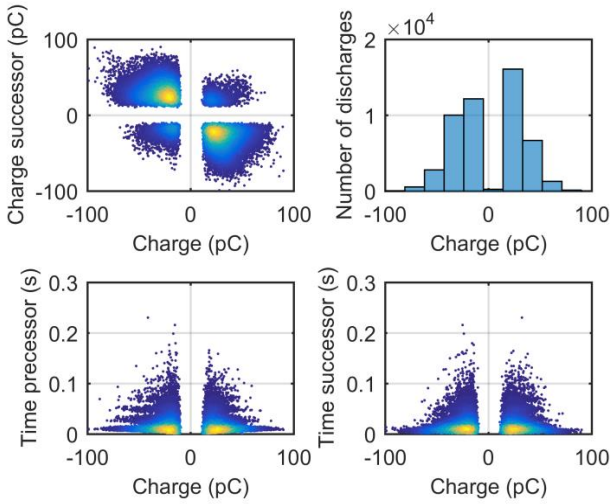

Figure 108: Free-moving particle TRPD.

Free-moving particle TRPD:

- **Qsuc vs. Q:** four concentration spots near the 0-crossing with a reflection possible around y=x, y=-x lines. No PDs on the x- and y-axes. The farther away from the 0-crossing, the fewer PDs there are. PDs occur in all four quadrants, with magnitude order $\pm 10^2$ and four concentration spots near 0-crossing.
- **Number of discharges vs. Q:** peaks around ±10pC
- **Tpre & Tsuc vs. Q:** no PDs on the y-axis. Concentration is near 0-crossing. Order of 10^2pC and 10^{-1} seconds.

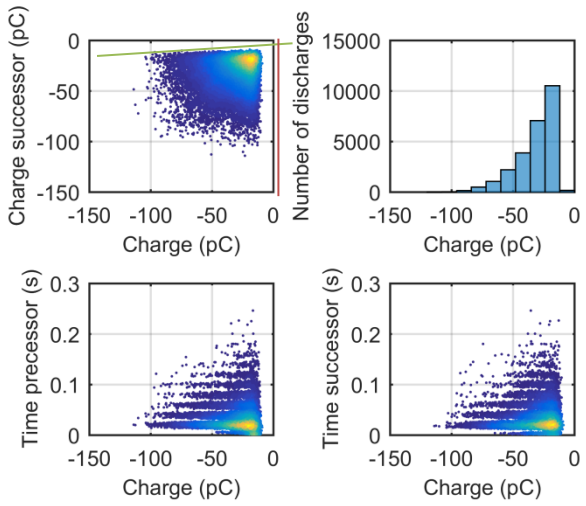

Figure 109: Free-moving particle TRPD – Negatively charged pulses.

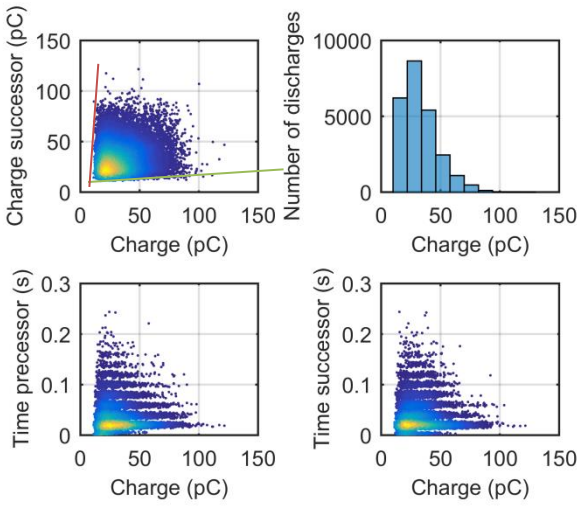

Figure 110: Free-moving particle TRPD – Positively charged pulses.

For a better understanding of the patterns in TRPD analysis, we will also look at the charge polarities separately. Taking the positive charge and the negative charge as separate clusters, we can clearly see different shapes and PD distributions.

Negatively charged pulses of free-moving particles in TRPD:

- **Qsuc vs. Q:** triangle shape with concentration in a corner near 0-crossing with an angle of 85^0C (crossing of green and red lines). The PDs appear within two lines that have slopes of 0.048 (green line) and 24 (red line).
- **Number of discharges vs. Q:** peak around -19pC. The slope towards 0 decreases quickly, but away from 0 the slope decreases slowly.
- **Tpre & Tsuc vs. Q:** shape of stacked horizontal lines (right-angle triangle). The stacked lines are separated by ±0.01 seconds from each other, and they are ±0.006 seconds thick. The further away from the x-axis, the less the concentration. The concentration of the lines is denser closer to the x-axis. The PDs have a time interval on the order of 10^{-1}.

Positively charged pulses of free-moving particles in TRPD:

- **Qsuc vs. Q:** triangle shape with concentration in a corner near 0-crossing with an angle of 83^0C (crossing of green and red lines). The PDs appear within two lines that have slopes of 0.071 (green line) and 16.0 (red line).
- **Number of discharges vs. Q:** peak around +21pC. The slope towards 0 decreases quickly, but away from 0 the slope decreases slowly.
- **Tpre & Tsuc vs. Q:** shape of stacked horizontal lines (right-angle triangle). The stacked lines are separated by ±0.01 seconds from each other, and they are ±0.006 seconds thick. The further away from the x-axis, the less the concentration. The concentration of the lines is denser closer to the x-axis. The PDs have a time interval on the order of 10^{-1}.

6.1.5.4. TRPD Floating Electrode

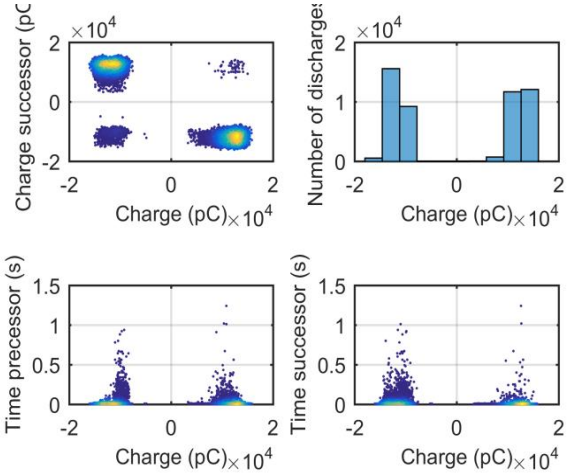

Figure 111: Floating electrode TRPD.

Floating electrode TRPD:

- **Qsuc vs. Q:** Four concentration spots with a reflection possible around y=x line. No PDs on the x- and y-axis. PDs occur in all four quadrants, with magnitude order $\pm10^4$ and four concentration spots (one in each quadrant) occurring on the lines y=x and y=-x.
- **Number of discharges vs. Q:** peaks around ±1pC
- **Tpre & Tsuc vs. Q:** no PDs on the y-axis. Concentration is near x-axis. Order of 10^4pC and 10^{-1} seconds.

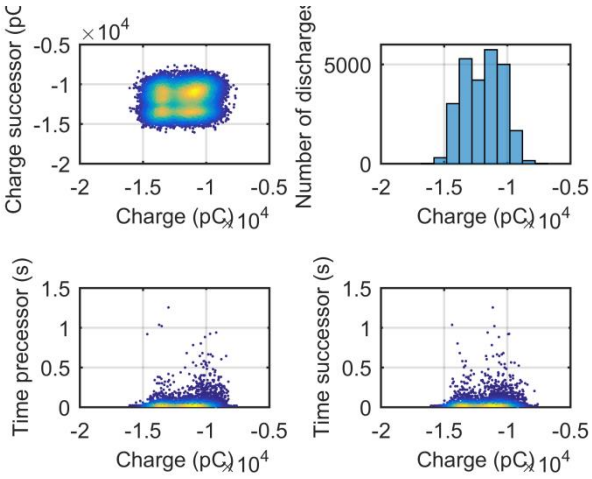

Figure 112: Floating electrode TRPD – Negatively charged pulses.

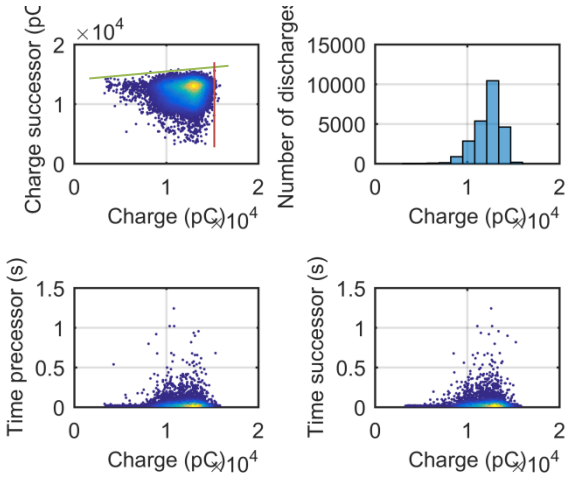

Figure 113: Floating electrode TRPD – Positively charged pulses.

For a better understanding of the patterns in TRPD analysis, we will also look at the charge polarities separately. Taking the positive charge and the negative charge as separate clusters, we can clearly see different shapes and PD distributions.

Negatively charged pulses of floating electrodes in TRPD:

- **Qsuc vs. Q:** square shape with four concentrations, one near each corner of the square.
- **Number of discharges vs. Q:** peak around -12900pC. The slope towards 0 decreases slowly, but away from 0 the slope decreases more quickly.
- **Tpre & Tsuc vs. Q:** concentration is near x-axis and fades slowly in vertical direction (away from x-axis), and looks like a sunset. The PDs have a time interval on the order of 10^{-1}.

Positively charged pulses of floating electrodes in TRPD:

- **Qsuc vs. Q:** triangle shape with concentration in a corner near 0-crossing with an angle of 72^0C (crossing of green and red lines). The PDs appear within two lines that have slopes of 0.0625 (green line) and 6.00 (red line).
- **Number of discharges vs. Q:** peak around +12900pC. The slope towards 0 decreases slowly, but away from 0 the slope decreases more quickly.
- **Tpre & Tsuc vs. Q:** concentration is near x-axis and fades slowly in vertical direction (away from x-axis), and looks like a sunset. The PDs have a time interval on the order of 10^{-1}.

6.1.5.5. TRPD Internal *Discharge*

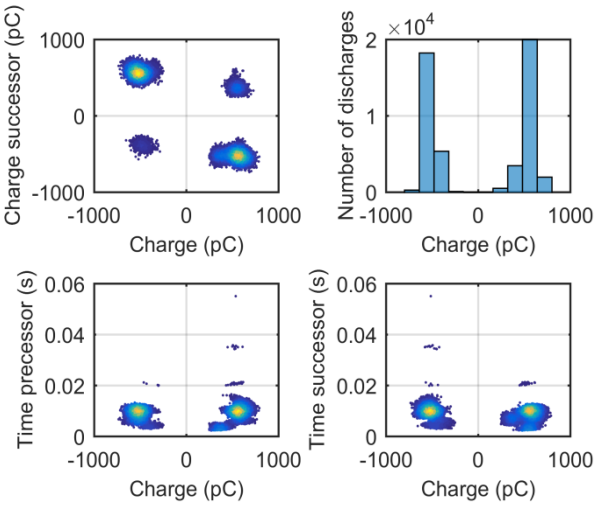

Internal discharge TRPD:

- **Qsuc vs. Q:** four concentration spots with a reflection possible around y=x, y=-x lines. No PDs on the x- and y-axis. PDs occur in all four quadrants, with magnitude order $\pm10^3$ and four concentration spots (one in each quadrant) occurring on the lines y=x and y=-x.
- **Number of discharges vs. Q:** peaks around ±500pC
- **Tpre & Tsuc vs. Q:** no PDs on the y-axis. Concentration is near t=0.01s. Order of 10^3pC and 10^{-2} seconds.

Figure 114: Internal discharge TRPD.

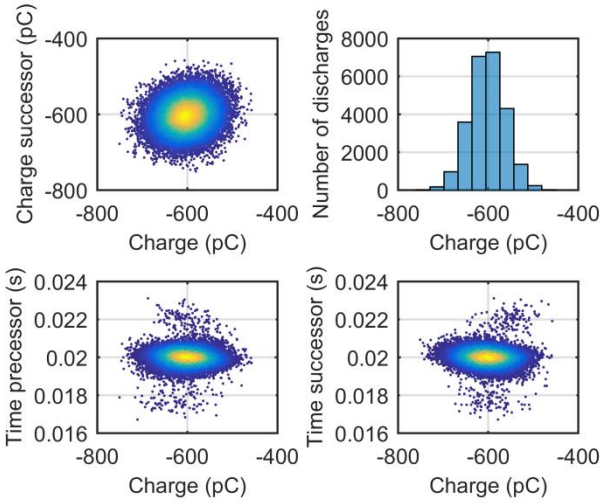

Figure 115: Internal discharge TRPD – Negatively charged pulses.

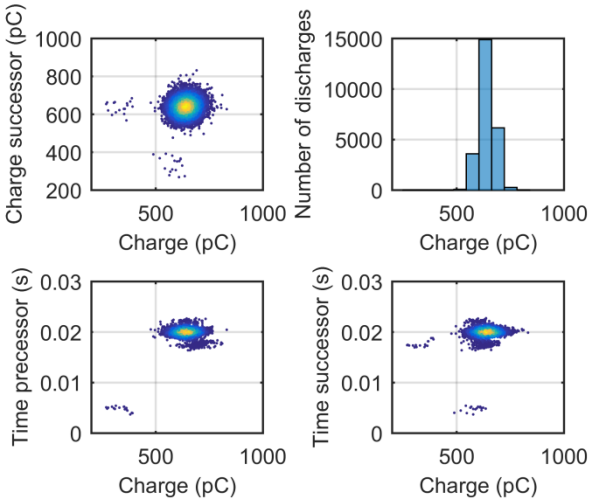

Figure 116: Internal discharge TRPD – Positively charged pulses.

For a better understanding of the patterns in TRPD analysis, we will also look at the charge polarities separately. Taking the positive charge and the negative charge as separate clusters, we can clearly see different shapes and PD distributions.

Negatively charged pulses of internal discharge in TRPD:

- **Qsuc vs. Q:** the shape is circular with a concentration in the centre of the circle.
- **Number of discharges vs. Q:** peak around -600pC. Comparing the slope towards and away from the 0-axis, the slope on both sides of the peak is very similar, but still a bit steeper towards the 0-crossing.
- **Tpre & Tsuc vs. Q:** oval shape, concentration is a horizontal line around 0.02seconds. The concentration fades in all directions, faster in vertical direction compared to horizontal. The PDs have a time interval on the order of 10^{-2}.

Positively charged pulses of internal discharge in TRPD:

- **Qsuc vs. Q:** the shape is circular with a concentration in the centre of the circle.
- **Number of discharges vs. Q:** peak around +600pC. Comparing the slope towards and away from the 0-axis, the slope on both sides of the peak is very similar, but still a bit steeper slope towards the 0-crossing.
- **Tpre & Tsuc vs. Q:** oval shape, concentration is a horizontal line around 0.02seconds. The concentration fades in all directions, faster in vertical direction compared to horizontal. The PDs have a time interval on the order of 10^{-2}.

6.1.5.6. Summary of TRPD Analysis

Table 12, Table 13 and Table 14 present a summary of the analysis done from Figure 103 t/m Figure 114. With this summary, we can more easily use and evaluate the analysis to distinguish the defects. During the analysis of the charge successor versus charge graph, we looked at the magnitudes of charge, polarity of charge, symmetry of the figures and the concentrations.

Analysis Type	Negative Corona	Positive Corona	Surface Discharge	Free-Moving Particle	Floating Electrode	Internal Discharge
Magnitude order	10^2 pC	10^2 pC	10^4 pC	10^2 pC	10^4 pC	10^3 pC
Polarity	+	-	±	±	±	±
Symmetry	y=x line	y=x line	y=x line	y=x & y=-x line	y=x line	y=x & y=-x line
Quadrant occurrence	1st	3rd	all 4	all 4	all 4	all 4
Concentration	one concentration spot on the line y=x	one concentration spot on the line y=x	four concentration spots near 0-crossing	four concentration spots near 0-crossing	four concentration spots (one in each quadrant) occurring on the lines y=x and y=-x	four concentration spots (one in each quadrant) occurring on the lines y=x and y=-x

Table 12: Summary of TRPD analysis – Charge successor vs. charge.

During the analysis of the number of discharges versus charge graph, we looked at the number of peaks and where they occur.

Analysis Type	Negative Corona	Positive Corona	Surface Discharge	Free-Moving Particle	Floating Electrode	Internal Discharge
# peaks	1	1	1	2	2	2
Location of peaks	around +160pC	around -180pC	around 0pC	around ±10pC	around ±1pC	around ±500pC

Table 13: Summary of TRPD analysis – Number of discharges vs. charge.

During the analysis of the charge successor versus charge graph, we looked at the magnitudes of charge and time, the shape of the figures and the concentrations.

Analysis Type	Negative Corona	Positive Corona	Surface Discharge	Free-Moving Particle	Floating Electrode	Internal Discharge
Shape	horizontal lines	horizontal lines	triangle	triangle	half dot	single dot
Concentration	around t=0s and t=0.016s	around t=0s and t=0.014s	near 0-crossing	near 0-crossing	near x-axis and ±1000pC	near 0.01s and ±500pC
Magnitude order	10^2 pC 10^{-2} s	10^2 pC 10^{-2} s	10^4 pC 10^{-1} s	10^4 pC 10^{-1} s	10^4 pC 10^{-1} s	10^3 pC 10^{-2} s

Table 14: Summary of TRPD analysis – Time presessor and successor vs. charge.

Now we look at the similarities and differences of the TRPD when differentiating between the charge polarities.

Analysis Type	Corona		Surface Discharge		Free-Moving Particle		Floating Electrode		Internal Discharge	
	Neg. Charge	Pos. Charge	Neg. Charge	Pos. Charge	Neg. Charge	Pos. Charge	Neg. Charge	Pos. Charge	Neg. Charge	Pos. Charge
Magnitude order	10^{-2} s	10^{-2} s	10^{-1} s	10^{-1} s	10^{-1} s	10^{-1} s	10^{-1} s	10^{-1} s	10^{-2} s	10^{-2} s
Shape	oval	oval	triangle	triangle	triangle	triangle	square	triangle	circle	circle
Angle of spread	-	-	75	81	85	83	-	72	-	-
Slopes of angle	-	-	0.1 6.50	0.1 14.29	0.048 24	0.071 16	-	0.063 6.0	-	-
Concentration	along y=x line; towards 0-crossing	along y=x line; towards 0-crossing	towards 0-crossing	towards 0-crossing	towards 0-crossing	towards 0-crossing	in each corner of square	towards 0-crossing	along y=x line; middle of circle	along y=x line; middle of circle
Magnitude order	10^3 PD's	10^4 PD's	10^3 PD's	10^4 PD's	10^4 PD's	10^4 PD's	10^3 PD's	10^4 PD's	10^3 PD's	10^4 PD's
Peak	+160 pC	-180 pC	-2500 pC	+3000 pC	-19 pC	+21 pC	-12900 pC	+12900 pC	-600 pC	+600 pC
Slope towards 0	steeper	steeper	steeper	steeper	steeper	steeper	flatter	flatter	steeper	steeper
Slope away from 0	flatter	flatter	flatter	flatter	flatter	flatter	steeper	steeper	flatter	flatter
Shape	2 horizontal lines	2 horizontal lines	±12 horizontal lines stacked on top of	±12 horizontal lines stacked on top of	±10 horizontal lines stacked on top of	±12 horizontal lines stacked on top of	>>>12 horizontal lines stacked on top	>>>12 horizontal lines stacked on top	oval, with centre around 0.02s	oval, with centre around 0.02s

			each other (triangle)	each other (triangle)	each other (right-angle triangle)	each other (right-angle triangle)	of each other	of each other		
Time between shapes	±0.017 s	±0.014 s	±0.02	±0.02	±0.01	±0.01	-	-	-	-
Thickness shapes	±0.0004 s	±0.0002 s	±0.004	±0.004	±0.006	±0.006	-	-	±0.006	±0.006
Concentration	horizontal	horizontal	close to x-axis and 0-crossing	close to x-axis and 0-crossing	close to x-axis and 0-crossing	close to x-axis and 0-crossing	along the x-axis	along the x-axis	middle of oval shape at 0.02s	middle of oval shape at 0.02s
Concentration fading	horizontally away from +160 pC	horizontally away from -180 pC	vertically (away from x-axis) and horizontally (away from y-axis)	vertically (away from x-axis) and horizontally (away from y-axis)	vertically (away from x-axis) and horizontally (away from y-axis)	vertically (away from x-axis) and horizontally (away from y-axis)	vertically (away from x-axis)	vertically (away from x-axis)	faster vertically than horizontally	faster vertically than horizontally
Magnitude order	10^{-2} s	10^{-2} s	10^{-1} s	10^{-1} s	10^{-1} s	10^{-1} s	10^{-1} s	10^{-1} s	10^{-2} s	10^{-2} s

Table 15: Summary of TRPD analysis – Positive and negative charges separated.

6.1.6. Number of Discharges Per Cycle

There are differences in the number of discharges that occur per cycle. These differences are examined below, and are presented in Table 16. This can be useful when clustering defects and when trying to distinguish different types of defects from each other.

Sample Defect	Average (pulses per cycle)	Occurring (pulses per cycle)	Concentration order (pulses per cycle)
Positive Corona	250.00	249-254	250
Negative Corona	18.32	17-20	18;19
Surface Discharge	1.41	1-4	1
Internal Discharge	2.00	1-3	2
Free-Moving Particle	1.67	1-6	1
Floating Electrode	1.93	1-3	2

Table 16: Pulses per cycle.

In the case of a defect with origins in surface discharge, internal discharge, free-moving particles and floating electrodes, the number of discharges per cycle is similar. In these cases, the number of discharges per cycle is too close to be able to differentiate them. Positive and negative corona, on the other hand, can be distinguished from the other types of defects.

Positive corona have ±13 times more discharges per cycle compared to negative corona and ±125 times more discharges than the other types of defects. Negative corona have ±13 times fewer discharges per cycle compared to positive corona and ±9 times more discharges than the other types of defects.

We saw a difference in the TRPD analysis when looking at the positive and negative charges separately. Therefore, we will also look into the difference between the number of discharges per cycle of the positive and negative charges. This comparison is presented in Table 17.

Sample Defect	# of Pulses per Cycle	Charge Polarity	# of Pulses per Cycle
Positive Corona	250	Negatively charged pulses	250
		Positively charged pulses	-
Negative Corona	18.32	Negatively charged pulses	-

		Positively charged pulses	18.32
Surface Discharge	1.41	Negatively charged pulses	1.00
		Positively charged pulses	1.01
Internal Discharge	2.00	Negatively charged pulses	1.09
		Positively charged pulses	1.08
Free-Moving Particle	1.67	Negatively charged pulses	1.01
		Positively charged pulses	1.01
Floating Electrode	1.93	Negatively charged pulses	1.01
		Positively charged pulses	1.00

Table 17: Pulses per cycle – Positively and negatively charged pulses.

The differences in the number of pulses per cycle when looking at the different polarities are clearer. All the defects except for the corona discharges have one pulse per cycle. In this way, it is more convenient to distinguish the samples' origins with the use of the number of pulses per cycle. Negative and positive corona still have a difference of ±13 times. But now negative corona have a difference of ±18 compared to the rest of the defects, and positive corona have a difference of ±250 compared to the rest of the defects.

6.2. Influence of Time (Number of Discharges)

In order to know the minimum number of discharges needed to be able to recognize the defect origin we will portray a relationship between the recoded time and the number of discharges recorded. In this way, there is no need to do many consecutive measurements with different time recordings and different numbers of pulses/discharges.

6.2.1. Recoding Time vs. Number of Discharges

At first, the number of discharges needed was not known, so to be sure that the recorded 50,000 discharges were enough we measured 100,000 discharges of some of the defects. The only difference noticed when recording 100,000 instead of 50,000 was that the concentration was more intense, from both the PRPD and the TRPD. Therefore, we decided to do the analysis for all the defects for recordings of 50,000 discharges so that the running time would be shorter when recording data.

Table 18 presents a comparison between the calculated and the real pulse. The recorded time for each sample for 50,000 pulses was taken as a reference. The calculated reference is the ideal case if the number of discharges is directly proportional to the time. From this comparison we calculated the deviation for each interval. Table 19 shows the average deviation from the calculated values and the real values for the direct proportionality of the running time and the number of discharges.

Positive Corona			**Negative Corona**			**Free-Moving Particle**			**Internal Discharge**			**Floating Particle**			**Surface Discharge**		
Time	Cal. # Pulse	Real # Pulse	Time	Cal. # Pulse	Real # Pulse	Time	Cal. # Pulse	Real # Pulse	Time	Cal. # Pulse	Real # Pulse	Time	Cal. # Pulse	Real # Pulse	Time	Cal. # Pulse	Real # Pulse
4	50000	50000	54.5	50000	50000	786	50000	50000	500	50000	50000	642	50000	50000	986	50000	50000
2	25000	25287	30	27523	27744	400	25445	26159	250	25000	25005	300	23364	27016	500	25354	24036
1	12500	12654	15	13761	13995	200	12723	13388	100	10000	10098	100	7788	9195	250	12677	10590
0.5	6250	6283	10	9174	9415	100	6361	6986	50	5000	5016	50	3895	4588	100	5070	5043
0.1	1250	1257	5	4587	4755	50	3181	3489	20	2000	2011	20	1558	1835	50	2536	2532
0.03	375	503	2	1835	1924	20	1272	1463	10	1000	1003	10	779	863	25	1268	1069
0.006	75	252	1	917	969	10	636	728	5	500	502	5	389	474	10	507	427
			0.5	459	492	5	318	357	2	200	202	2	156	185	5	254	207
			0.25	229	247	2	127	118	1	100	101	1	78	86	4	203	173
			0.025	115	38	1	64	55	0.5	50	51	0.5	39	51	3	152	126
			0.0035	16	19										2	101	84

Positive Corona		**Negative Corona**		**Free-Moving Particle**		**Internal Discharge**		**Floating Particle**		**Surface Discharge**	
Time	% Deviation	Time	% Deviation	Time	% Deviation	Time	% Deviation	Time	% Deviation	Time	% Deviation
4	0,00	54.5	0,00	786	0,00	500	0,00	642	0,00	986	0,00
2	0,01	30	0,01	400	0,03	250	0,00	300	-0,14	500	-0,05
1	0,01	15	0,02	200	0,05	100	-0,01	100	-0,15	250	-0,16
0.5	0,01	10	0,03	100	0,10	50	0,00	50	-0,15	100	-0,01

0.1	0,01	5	0,04	50	0,10	20	-0,01	20	-0,15	50	0,00
0.03	0,34	2	0,05	20	0,15	10	0,00	10	-0,10	25	-0,16
0.006	2,36	1	0,06	10	0,14	5	0,00	5	-0,18	10	-0,16
		0.5	0,07	5	0,12	2	-0,01	2	-0,16	5	-0,19
		0.25	0,08	2	-0,07	1	-0,01	1	-0,09	4	-0,15
		0.025	-0,67	1	-0,14	0.5	-0,02	0.5	-0,24	3	-0,17
		0.0035	0,19							2	-0,17

Table 18: Calculation deviation of time vs. recorded pulses.

The average deviation of all the defects is 0.11%. Because of this small deviation, we can say that the running time and the number of discharges are directly proportional to each other. This is only valid if there are no major interferences or disturbances present. Examples of these defects are explained in more detail in section 4.2 above. Therefore, we can conclude that in real-time measurements, this analysis of time and number of discharges is not valid, since there is a great amount of noise and disturbance present. However, in the lab these measurements are valid. Now, because we concluded that the number of discharges is directly proportional to the time, we can use the number of cycles as a standard to estimate the number of pulses/discharges in time.

Defect	Average Deviation (%)
Positive Corona	0.39
Negative Corona	0.03
Free-Moving Particle	0.08
Internal Discharge	0.00
Floating Electrode	0.12
Surface Discharge	0.08
TOTAL:	**0.11%**

Table 19: Average deviation, direct proportionality of time and pulses.

Because the number discharges occur homogeneously in time we could make clusters dependent on time. This saved a significant amount of time, because otherwise each measurement of time or discharges would have been measured separately. After the clusters were made the characteristics were inspected to see the change in PRPD and TRPD because of the change in time (or pulses). The change in time is directly proportional to the number of discharges, as will be proven below in sections 6.2.2 and 6.2.3.

6.2.2. Influence of Time on PRPD

In this section, the analysis is conducted for the PRPD to see the number of discharges needed to still recognize the origin of the defect.

6.2.2.1. Positive Corona

For the analysis of time in positive corona, six clusters have been made. Figure 255 t/m Figure 266 of appendix D1 contain the graphs used with the selection of the time clusters and their characterizations of the PRPD:

- **Up to 0.1 Seconds (1257 pulses):** the concentration and shape are the same.
- **At 0.006 Seconds (252 pulses):** the concentration and the shape are still there, so it is still recognizable.

Positive corona also have groups of pulses when the time frame is very small. One group of pulses has a duration of 0.006 seconds and the time between pulses is 0.014 seconds. This shape can be seen in Figure 265.

6.2.2.2. Negative Corona

For the analysis of time in negative corona, 10 clusters have been made. Figure 267 t/m Figure 286 of appendix D2 show the graphs used with the selection of the time clusters and their characterizations of the PRPD:

- **Up to 1 Seconds (969 pulses):** still recognizable.
- **At 0.5 Seconds (492 pulses):** the shape is still there, though the concentrations are vanishing. Therefore, it is still recognizable.
- **At 0.0035 Seconds (357 pulses):** the shape is still there but there is no longer any concentration present. The concentration is not needed for recognition, so the defect is still recognizable.

Negative corona also have groups of pulses when the time frame is very small. One group of pulses has a duration of 0.0035 seconds, and the time between pulses is 0.014 seconds. This shape can be seen in Figure 281.

6.2.2.3. Free-Moving Particle

For the analysis of time in free-moving particles, 9 clusters were made. Figure 287 t/m Figure 304 of appendix D3 show the graphs used with the selection of the time clusters and their characterizations of the PRPD:

- **Up to 20 Seconds (1463 pulses):** the concentration and shape stay the same.
- **At 10 Seconds (728 pulses):** the concentration at the positive side is lost, but the shape is still present. Therefore, it is still recognizable.
- **At 5 Seconds (357 pulses):** the shape is lost.

Here the pulses are completely homogeneous in time, so there are no discharges in groups when looking at the small time intervals.

6.2.2.4. Internal Discharge

For the analysis of time in internal discharge, 9 clusters were made. Figure 305 t/m Figure 322 of appendix D4 show the graphs used with the selection of the time clusters and their characterizations of the PRPD:

- **Up to 5 Seconds (502 pulses):** still recognizable; the shape and concentrations are still there.
- **At 2 Seconds (202 pulses):** the arc is gone but the concentration is not. Therefore, it is no longer recognizable.
- **At 0.5 Seconds (51 pulses):** the arc is gone but the concentration is not.

Here, the pulses are completely homogeneous in time, so there are no discharges in groups when looking at the small time intervals.

6.2.2.5. Floating Electrode

For the analysis of time in floating electrodes, 9 clusters have been made. Figure 323 t/m Figure 340 of appendix D5 show the graphs used with the selection of the time clusters and their characterizations of the PRPD:

- **Up to 50 Seconds (4588 pulses):** still recognizable.
- **At 20 Seconds (1835 pulses):** the concentration shape is changing but the overall shape is still a square. Therefore, the defect is still recognizable.
- **At 2 Seconds (185 pulses):** the shape is still recognizable.
- **At 1 Second (86 pulses):** The shapes are no longer recognizable.

Here, the pulses are completely homogeneous in time, so there are no discharges in groups when looking at the small time intervals.

6.2.2.6. Surface Discharge

For the analysis of time in surface discharge, 10 clusters were made. Figure 341 t/m Figure 360 of appendix D6 show the graphs used with the selection of the time clusters and their characterizations of the PRPD:

- **Up to 50 Seconds (2532 pulses):** still recognizable.
- **At 25 Seconds (1069 pulses):** the shape of triangle is lost at the positive cycle.
- **At 10 Seconds (427 pulses):** concentrations and shape are lost.

Here, the pulses are completely homogeneous in time, so there are no discharges in groups when looking at the small time intervals.

6.2.3. Influence of Time on TRPD

In this section, the analysis is done for the TRPD to see the number of discharges needed to still recognize the origin of the defect.

6.2.3.1. Positive Corona

Figure 255 t/m Figure 266 of appendix D1 show the graphs used with the selection of the time clusters and their characterizations of the TRPD:

- **Up to 0.03 Seconds (503 pulses):** still recognizable.
- **At 0.006 Seconds (252 pulses):** time precessor and successor versus the charge changes, so it is no longer recognizable.

6.2.3.2. Negative Corona

Figure 267 t/m Figure 286 of appendix D2 show the graphs used with the selection of the time clusters and their characterizations of the TRPD:

- **Up to 2 Seconds (1924 pulses):** still recognizable.
- **At 1 Seconds (969 pulses):** the number of discharge graphs changes, but the peaks are still the same and successor charge versus charge has only one concentration.

6.2.3.3. Free-Moving Particle

Figure 287 t/m Figure 304 of appendix D3 show the graphs used with the selection of the time clusters and their characterizations of the TRPD:

- **Up to 5 Seconds (357 pulse):** the defect is still recognizable.
- **At 2 Seconds (118 pulses):** the concentrations at time precessor and successor versus charge are lost.
- **At 1 Second (55 pulses):** all concentrations are lost and the time precessor and successor versus charge reflecting over the y=x and y=-x lines are also lost.

6.2.3.4. Internal Discharge

Figure 305 t/m Figure 322 of appendix D4 show the graphs used with the selection of the time clusters and their characterizations of the TRPD:

- **Up to 10 Seconds (1003 pulses):** the defect is still recognizable.
- **At 5 Seconds (502 pulses):** the charge successor versus charge has lost two concentration spots.
- **At 1 Seconds (101 pulses):** the concentration of time precessor and successor versus charge is lost.

6.2.3.5. Floating Electrode

Figure 323 t/m Figure 340 of appendix D5 show the graphs used with the selection of the time clusters and their characterizations of the TRPD:

- **Up to 50 Seconds (4588 pulses)**: the defect is still recognizable.
- **At 20 Seconds (1835 pulses)**: the charge successor versus charge has lost a concentration spot.

6.2.3.6. Surface Discharge

Figure 341 t/m Figure 360 of appendix D6 show the graphs used with the selection of the time clusters and their characterizations of the TRPD:

- **Up to 500 Seconds (24036 pulses):** there are 2 peaks around 0 charge in the number of discharges versus charge, which is acceptable because the peak should be at or around 0 charge.
- **At 10 Seconds (427 pulses):** all still recognizable (still 2 peaks around 0 charge).
- **At 5 Seconds (207 pulses):** all concentrations in the graphs are lost.

6.2.4. Minimum Running Time or Pulses Needed for PD Measurements

Depending on the type of analysis, there could be a difference in running time or pulses needed for recognizing the defects. Table 20 presents the minimum running time and pulses needed for recognition of the defects in PRPD and TRPD analysis.

Sample Defects	PRPD		TRPD		Minimum Needed	
	Running Time(s)	# Discharges (Pulses)	Running Time(s)	# Discharges (Pulses)	Running Time(s)	# Discharges Pulses)
Positive Corona	0.006	252	0.03	503	**0.03**	**503**
Negative Corona	0.0035	357	2	1924	**2**	**1924**
Free-Moving Particle	10	728	3	357	**10**	**728**
Internal Discharge	5	502	10	1003	**10**	**1003**
Floating Electrode	2	185	20	1835	**20**	**1835**
Surface Discharge	25	1069	10	427	**25**	**1069**
Minimum Needed:	**25**	**1069**	**20**	**1924**	**25**	**1924**

Table 20: Minimum running time or number of discharges (pulses) needed.

With this information we could artificially create more data as needed; only the minimum data is needed from the sample. Minimum data is the minimum number of discharges and recoding time needed to still be able to recognize the defect origin.

These numbers are only valid when one sample is measured individually. The minimum number of discharges and time can change when multiple samples are recorded simultaneously.

6.3. Restrictions in Defect Analysis

To be able to better distinguish between the different types of defects and to recognize the origins of PDs, it is important to know their similarities in all ways so that we know to what extent we can use each of the analysis methods.

When making clusters, it will be easier to distinguish between different types of defects by looking at the pulses. Therefore, it is important to know which of the pulses are similar in which ways. When we know these similarities, we will know to what extent we can use them. Table 21 presents a summary of the pulse restrictions, which are divided into characteristics of the pulse itself, the voltage magnitude and the charge magnitude. The analysed data used for this table is shown in Figure 74 t/m Figure 89 of section 6.1.1 above.

PD Pulse		
Shape		
Undistinguishable		**Distinguishable**
➢ Floating electrode ➢ Free-moving particle ➢ Internal discharge		➢ Not Valid
Voltage Magnitude		
Undistinguishable		**Distinguishable**
➢ Surface discharge ➢ Internal discharge		➢ Corona ➢ Surface discharge & internal discharge ➢ Free-moving particle ➢ Floating electrode
Charge Magnitude		
Undistinguishable		**Distinguishable**
➢ Corona ➢ Free-moving particle	➢ Surface discharge ➢ Floating electrode	➢ Corona & free-moving particle ➢ Surface discharge & floating electrode ➢ Internal discharge

Table 21: PD pulse restrictions.

Not only are the differences and similarities in pulses important, but the differences and similarities of the clusters and analysis methods must also be kept in mind when analysing data and making multiple combinations, so that we know exactly to what extent we can use the data and the analysis of the data. Table 22 t/m Table 27 present the restrictions summaries of each cluster and analysis. Each cluster or analysis is divided into smaller sections for a better understanding of the restrictions.

In the cluster of energy versus charge, there are clear differences between the slopes of the cluster. Not all the slopes of the samples were calculable; some of the clusters have a parabolic shape. The analysed data used for this table are shown in Figure 74 t/m Figure 89 of section 6.1.1 above.

Cluster: Energy vs. Charge		
No slope	**Undistinguishable in slope**	**Distinguishable in slope**
➢ Surface discharge ➢ Free-moving particle	➢ Surface discharge ➢ Free-moving particle	➢ Negative corona ➢ Positive corona ➢ Floating electrode ➢ Internal discharge

Table 22: Energy vs. charge cluster restrictions.

As mentioned above, a logarithmic scale was implemented to better calculate the slopes of the clusters. As shown in Table 23, all the slopes of the defects were calculable, unlike in cases in which a logarithmic scale was not implemented. However, two defects, surface discharge and free-moving particles, are not distinguishable by slope, because the magnitudes are of the same order. The analysed data used for this table are shown in Figure 90 t/m Figure 96 of section 6.1.2 above.

Cluster: Energy vs. Charge in Logarithmic Scale	
Undistinguishable in slope	**Distinguishable in slope**
➢ Surface discharge ➢ Free-Moving particle	➢ Negative corona ➢ Positive corona ➢ Floating electrode ➢ Internal discharge

Table 23: Energy vs. charge cluster in logarithmic scale restrictions.

We will discuss the restrictions of the PRPD analysis in four different characteristics. The analysed data used for this table are shown in Figure 68 t/m Figure 73 of section 6.1.4 above. With these four different characteristics we can easily distinguish between all the different defects/samples:

- **Magnitude:** Negative corona, positive corona, free-moving particles and internal discharge have the same magnitude, while surface discharge and floating electrodes have the same magnitude. Therefore, these two groups of discharges are distinguishable from each other.
- **Shape:** Positive corona and negative corona have the same shape, but they are still distinguishable from each other by polarity and by phase. Surface discharge and free-moving particles have the same shape but are also distinguishable by phase.
- **Phase:** There are three sets of defects with PDs that occur around the same phase. When the defects occur around the same phase, it could be difficult to distinguish them.
- **Charge polarity:** Most of the defects have positive and negative PDs occurring on the positive and negative polarity (of charge), except positive and negative corona.

PRPD Analysis			
Undistinguishable magnitude			**Distinguishable magnitude**
➢ Negative corona ➢ Positive corona ➢ Free-moving particle ➢ Internal discharge	➢ Surface discharge ➢ Floating electrode		➢ Negative corona, positive corona, free-moving particle & internal discharge ➢ Surface discharge & floating electrode
Undistinguishable shape			**Distinguishable shape**
➢ Negative corona ➢ Positive corona	➢ Surface discharge ➢ Free-moving particle		➢ Corona ➢ Surface discharge & free-moving particle ➢ Floating electrode ➢ Internal discharge
Undistinguishable phase			**Distinguishable phase**
➢ Negative corona ➢ Floating electrode	➢ Positive corona ➢ Floating electrode	➢ Surface discharge ➢ Free-moving particle	➢ Negative corona & floating electrode ➢ Positive corona & floating electrode ➢ Surface discharge & free-moving particle ➢ Internal discharge
Undistinguishable charge polarity			**Distinguishable charge polarity**
➢ Positive corona ➢ Surface discharge ➢ Free-moving particle ➢ Floating electrode ➢ Internal discharge	➢ Negative corona ➢ Surface discharge ➢ Free-moving particle ➢ Floating electrode ➢ Internal discharge		➢ Positive corona ➢ Negative corona

Table 24: PRPD analysis restrictions.

When discussing the restrictions of the TRPD analysis, we will do do so based on four different figures. The analysed data used for this table is shown in Figure 103 t/m Figure 114 of section 6.1.5 above. With these four different figures we can easily distinguish between all the different defects/samples:

- **Charge successor vs. charge:**
  Information for this part of the analysis of TRPD was taken from Table 12.
  - Magnitude: We can clearly see that positive corona, negative corona and free-moving particles have similar orders of magnitude, as do surface discharge and floating electrodes. Therefore, there are three groups of magnitude orders, which we can distinguish from each other.
  - Polarity: All defects have positive and negative charges except for positive and negative corona.

- Symmetry: When looking at the symmetry of the figures, positive corona, negative corona, surface discharge and floating electrodes all reflect over the y=x line. Free-moving particles and internal discharge can both reflect over the y=x and y=-x lines. Therefore, we can distinguish between the two defects with two reflections (free-moving particles and internal discharge) and the rest of the defects.
- Quadrant: The PDs occur in all quadrants for surface discharge, free-moving particles, floating electrodes and internal discharge. Positive corona occur in the first quadrant and negative corona occur in the third quadrant. Therefore, we can distinguish both corona discharges separately from the rest of the defects.
- Concentration: Both positive and negative corona have one concentration spot on the y=x line. Both surface discharge and free-moving particles have four concentration spots with their concentrations near 0. Both floating electrodes and internal discharge have four concentration sports (one in each quadrant) that occur on the lines y=x and y=-x.

➢ **Number of discharges vs. charge:**
Information for this part of the analysis of TRPD was taken from Table 13.

- Peaks: Both positive and negative corona have peaks around 170pC, but of opposite polarity. Surface discharge and free-moving particles both have peaks close to 0pC. Floating electrode and internal discharge both have symmetry over the y-axis but of different magnitudes, so they are distinguishable.

➢ **Time presessor vs. charge & time successor vs. charge:**
Information for this part of the analysis of TRPD was taken from Table 14.

- Magnitude: Positive corona, negative corona and internal discharge all have the same order of magnitude, and surface discharge, free-moving particles and floating electrodes also have the same order of magnitude. Therefore, we can distinguish between two groups when looking at the magnitudes.
- Shape: There are three types of shapes. Positive and negative corona have a horizontal line shape, while surface discharge and free-moving particles both have triangle shapes (four in total). Floating electrodes and internal discharge both have one concentration point, like a circle.
- Concentration: Positive and negative corona both have two concentrations as the horizontal lines. Surface discharge and free-moving particles both have concentrations near the 0-crossing. Floating electrodes and internal discharge have concentrations near the x-axis.

<table>
<tr><th colspan="3">TRPD Analysis</th></tr>
<tr><th colspan="3">Charge successor vs. charge</th></tr>
<tr><th colspan="2">Undistinguishable in magnitude</th><th>Distinguishable in magnitude</th></tr>
<tr><td>➢ Negative corona
➢ Positive corona
➢ Free-moving particle</td><td>➢ Surface discharge
➢ Floating electrode</td><td>➢ Internal discharge
➢ Corona & free-moving particle
➢ Surface discharge & floating electrode</td></tr>
<tr><th colspan="2">Undistinguishable in polarity</th><th>Distinguishable in polarity</th></tr>
<tr><td>➢ Positive corona
➢ Surface discharge
➢ Free-moving particle
➢ Floating electrode
➢ Internal discharge</td><td>➢ Negative corona
➢ Surface discharge
➢ Free-moving particle
➢ Floating electrode
➢ Internal discharge</td><td>➢ Positive corona
➢ Negative corona</td></tr>
<tr><th colspan="2">Undistinguishable in symmetry analysis</th><th>Distinguishable in symmetry analysis</th></tr>
</table>

<table>
<tr><td colspan="2">➢ Corona
➢ Surface discharge
➢ Floating electrode
➢ Free-moving particle
➢ Internal discharge</td><td>➢ Free-moving particle
➢ Internal discharge</td><td>➢ Free-moving particle & internal discharge
➢ Corona, surface discharge & floating electrode</td></tr>
<tr><td colspan="3">Undistinguishable in quadrant occurrence</td><td>Distinguishable in quadrant occurrence</td></tr>
<tr><td colspan="3">➢ surface Discharge
➢ Free-moving particle
➢ Floating electrode
➢ Internal discharge</td><td>➢ Positive corona
➢ Negative corona
➢ Surface discharge, free-moving particle, floating electrode and internal discharge</td></tr>
<tr><td colspan="3">Undistinguishable in concentration</td><td>Distinguishable in concentration</td></tr>
<tr><td>➢ Positive corona
➢ Negative corona</td><td>➢ Surface discharge
➢ Free-moving particle</td><td>➢ Floating electrode
➢ Internal discharge</td><td>➢ Positive corona & negative corona
➢ Surface discharge & free-moving particle
➢ Floating electrode & internal discharge</td></tr>
<tr><td colspan="4">Number of discharges vs. charge</td></tr>
<tr><td colspan="3">Undistinguishable by peaks</td><td>Distinguishable by peaks</td></tr>
<tr><td colspan="3">➢ Surface discharge
➢ Free-moving particle</td><td>➢ Positive corona
➢ Negative corona
➢ Floating electrode
➢ Internal discharge</td></tr>
<tr><td colspan="4">Time pressessor & successor vs. charge</td></tr>
<tr><td colspan="2">Undistinguishable in magnitude</td><td>Distinguishable in magnitude</td></tr>
<tr><td>➢ Positive corona
➢ Negative corona
➢ Internal discharge</td><td>➢ Surface discharge
➢ Free-moving particle
➢ Floating electrode</td><td>➢ Positive corona, negative corona & internal discharge
➢ Surface discharge, free-moving particle & floating electrode</td></tr>
<tr><td colspan="3">Undistinguishable in shape
(charge successor vs. charge)</td><td>Distinguishable in shape
(charge successor vs. charge)</td></tr>
<tr><td>➢ Positive corona
➢ Negative corona</td><td>➢ Surface discharge
➢ Free-moving particle</td><td>➢ Floating electrode
➢ Internal discharge</td><td>➢ Positive corona & negative corona
➢ Surface discharge & free-moving particle
➢ Floating electrode & internal discharge</td></tr>
<tr><td colspan="3">Undistinguishable in shape
(time pre&suc vs. charge)</td><td>Distinguishable in shape
(time pre&suc vs. charge)</td></tr>
<tr><td colspan="3">➢ Positive corona
➢ Negative corona</td><td>➢ Corona
➢ Surface discharge
➢ Free-moving particle
➢ Floating electrode
➢ Internal discharge</td></tr>
<tr><td colspan="3">Undistinguishable in concentration</td><td>Distinguishable in concentration</td></tr>
<tr><td>➢ Positive corona
➢ Negative corona</td><td>➢ Surface discharge
➢ Free-moving particle</td><td>➢ Floating electrode
➢ Internal discharge</td><td>➢ Positive corona & negative corona
➢ Surface discharge & free-moving particle
➢ Floating electrode & internal discharge</td></tr>
</table>

Table 25: TRPD analysis restrictions.

In the cluster of energy per charge versus the charge, there are clear differences between the slopes of the cluster. The analysed data used for this table is shown in Figure 90 t/m Figure 95 and in Table 10 of section 6.1.2 above. Table 10 presents a summary of all the defects' slopes in the graphs of energy per charge versus charge ordered by the magnitude of the slopes. These slopes can be used to make distinctions between the origins of the defects. We also looked to the magnitude order and the charge polarity. With these three different characteristics we can easily distinguish between all the different defects/samples.

<table>
<tr><th colspan="5">Cluster: Energy per Charge vs. Charge</th></tr>
<tr><th colspan="3">Similar in magnitude order</th><th colspan="2">Distinguishable in magnitude order</th></tr>
<tr><td colspan="2">➢ Positive corona
➢ Negative corona</td><td>➢ Internal discharge
➢ Free-moving particle
➢ Surface discharge
➢ Floating electrode</td><td colspan="2">➢ Corona
➢ Internal discharge, free-moving particle, surface discharge & floating electrode</td></tr>
<tr><th colspan="3">Similar in magnitude polarity</th><th colspan="2">Distinguishable in magnitude polarity</th></tr>
<tr><td colspan="2">➢ Negative corona
➢ Internal discharge
➢ Free-moving particle
➢ Surface discharge
➢ Floating electrode</td><td>➢ Positive corona
➢ Internal discharge
➢ Free-moving particle
➢ Surface discharge
➢ Floating electrode</td><td colspan="2">➢ Positive corona
➢ Negative corona</td></tr>
<tr><th colspan="3">Slope</th><th colspan="2">Slope</th></tr>
<tr><td>➢ Positive corona
➢ Negative corona
➢ Free-moving particle
➢ Internal discharge</td><td>➢ Surface discharge
➢ Floating electrode</td><td>➢ Internal discharge
➢ Free-moving particle</td><td>➢ Corona, free-moving particle & internal discharge
➢ Surface discharge & floating electrode</td><td>➢ Internal discharge
➢ Corona, free-moving particle, surface discharge & floating electrode</td></tr>
</table>

Table 26: Energy per charge vs. charge cluster restrictions.

Table 27 shows the restrictions of the discharges per cycle. The analysed data used for this table is from Table 16 of section 6.1.6 above. It is clear that we can distinguish between positive corona, negative corona and the rest of the defects when looking at the number of discharges per cycle.

Discharges Per Cycle Analysis	
Similar	**Distinguishable**
➢ Surface discharge ➢ Internal discharge ➢ Free-moving particle ➢ Floating electrode	➢ Positive corona ➢ Negative corona ➢ Surface discharge, Internal discharge, free-moving particle & floating electrode

Table 27: Discharges per cycle analysis restrictions.

6.4. Discussion of Defect Characterization, Analysis and Recognition

Based on the characteristics of the individual defects and the restrictions made in section 6.3, there are many different possible ways for recognizing the defect origin. Some are simpler than others; for instance, the simplest detected method recognized was with shapes. With the shapes I mean the basic shape patterns that are created by the distribution of the discharges (pulses). These

shapes and method will be further elaborated and confirmed in chapter 7 and 8 below. In this section, some other aspects are discussed that seem more promising.

6.4.1. Charge Polarity

The corona discharges are easy distinguishable from the rest of the discharges by their polarity occurrence. This is due to the fact that PDs from the negative corona occur only in the first quadrant of TRPD and PDs from positive corona occur only in the third quadrant of TRPD. The question is now whether this is also the case when multiple discharges are measured at the same time or when there is a significant amount of noise or interference.

6.4.2. Number of Discharges Per Cycle

In the different types of analysis conducted above, we repeatedly saw that more positively charged PDs occur compared to negatively charged PDs. We will explain this phenomenon in this section using the corona discharges as an example. We can use corona discharges for this explanation because we can easily differentiate between positive and negative corona. As seen in the figures above, PDs in negative corona occur only on the positive half side (only positively charged pulses) and PDs in positive corona occur only on the negative half (only negatively charged pulses).

Secondary avalanches, are the source of the formation of corona discharges. When comparing negative corona (positively charged pulses) to positive corona (negatively charged pulses), more discharges in a certain time period occur with positive corona, which is when the pulses are negatively charged. This could also be verified with the number of PDs per cycle for each defect, which can be seen in Table 16 of section 6.1.6. This is due to a lack of non-ionizing plasma regions between the inner and outer regions in positive corona. In negative corona the electrons can drift out of the ionising region, and therefore there is a larger plasma region in the negative corona. In negative corona there are much more electrons compared to positive corona; negative corona have a larger electron density. However, these electrons have less energy compared to positive corona. In positive corona the electrons are concentrated near the surface of the conductor in a high potential gradient region. Because of this, these negatively charged pulses (positive corona) have a higher energy compared to the many positively charged pulses from negative corona, which are located in the outer and lower field areas. Due to the difference in electron density, the reaction rate will also increase or decrease with the increased or decreased electron density. Therefore, for electrons with a lower energy, reactions can take place at a lower rate if the reaction requires electrons with higher energy levels [59].

Therefore, the corona discharges are likely also easily distinguishable from the rest of the discharges by the number of discharges occurring during a cycle. The question is now whether this is also the case when multiple discharges are measured at the same time or when there is a significant amount of noise or interference.

6.4.3. TRPD Analysis

Most conventional measuring systems use PRPD analysis for defect recognition, and our artificially created defects/samples all have the proper PRPD graphs. These graphs are distinguishable from each other by means of their shapes. A disadvantage of using this type of analysis is that the recorded PD pulse must be linked to the phase so that we know where in the phase this PD occurs. Therefore, if this synchronization of phase is not needed, we can achieve a final product that is much simpler and cheaper.

The figures of the TRPD graphs are complex and therefore not easy to make sense of in order to use for defect origin detection. The figures become much simpler when the charge polarities are separated and plotted separately.

7. Multiple Sample Combinations Analysis

7.1. Defect Combinations 1-12

To confirm the characterizations of the individual defects and the conclusions made in chapter 4 above, we measured all possible combinations of defects (combinations of two defect types). Table 57 in appendix G shows all the possible combinations when paring two samples together. However, after seeing that positive and negative corona are clearly distinguishable (this analysis is conducted below in defect combination 1) and because for all other defects there are recordings of negatively and positively charged pulses, we decided to consider these two defects (positive and negative corona) as one defect (corona). This decreased the number of measurements significantly, and will make the analysis of the defects combinations easier. The analysis between the separate charge polarities is also possible in this way. All possible combinations are now visible in Table 28.

	Internal Discharge	**Corona**	**Floating Electrode**	**Surface Discharge**	**Free-Moving Particle**
Internal Discharge					
Corona	Combination 2: Internal discharge & corona (positive & negative)	Combination 1: Positive & negative corona			
Floating Electrode	Combination 6: Internal discharge & floating electrode	Combination 3: Corona (positive & negative) & floating electrode			
Surface Discharge	Combination 7: Internal discharge & surface discharge	Combination 4: Corona (positive & negative) & surface discharge	Combination 9: Floating electrode & & surface discharge		
Free-Moving Particle	Combination 8: Internal discharge & free-moving particle	Combination 5: Corona (positive & negative) & free-moving particle	Combination 10: Floating electrode & free-moving particle	Combination 11: Surface discharge & free-moving particle	

Table 28: Measured defect combinations.

Below we will cover all the defect combinations and look at the distinction possibilities. In our analysis we will look at different methods for cluster detection, PRPD, TRPD and the number of discharges per cycle.

Originally, when looking at the different defects, we thought that making a distinction between the defects based on magnitudes differences was possible. This was not the case. The oscilloscope that we used for recordings has an 8-bit vertical resolution, and distinguishing between the magnitudes requires at a minimum a 12-bit vertical resolution oscilloscope. Therefore, when looking at the defect combinations, we will only be able to differentiate between defects with the same magnitudes order. All of this can be seen in the analysis below.

Defect Combination 1: Positive & Negative Corona

The graphs of this combination of defects appear in appendix F below. Each of these graphs is compared with the graphs of the “pure” defects in section 6.1 above:

Defect Combination 1, Time Evolution and Clusters Analysis

Figure 362 shows the time evolution, the cluster Weq vs. Teq and the cluster of energy vs. charge. In the cluster Weq vs. Teq there is only one cluster, so no distinctions can be made. In the cluster energy vs. charge there are only two clusters, so the defects are distinguishable.

Defect Combination 1, Energy per Charge vs. Charge

Figure 410 of appendix F shows the graph of this cluster. The distinguishable clusters have a slope of $6.67 \cdot 10^{-5}$ [pJ/pC] (positive corona) and 0.1 [pJ/pC] (negative corona).

Defect Combination 1, Rise-time vs. Fall-time

Figure 422 shows the graph of this cluster, in which there is no clear distinction possible between the two artificially created defects.

Defect Combination 1, PRPD Analysis

Figure 386 in appendix F shows the graph of the defects in PRPD. The two defects are both clearly recognizable and distinguishable in the PRPD analysis. Because positive and negative corona are clearly recognizable and distinguishable, and all the other defects have positive and negative charges in the PRPD, we decided to consider positive and negative corona as one defect to compare with the rest of the defects.

Defect Combination 1, TRPD Analysis

As shown in Figure 117, two clusters are clearly visible. Figure 398 in appendix F shows the TRPD of these two clusters.

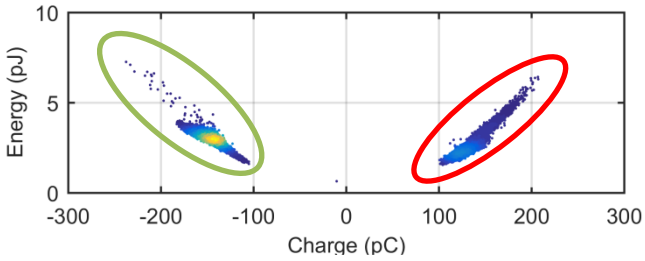

Figure 117: Defect combination 1: Clusters green and red.

The TRPD graph of the green cluster is shown in Figure 119 and of the red cluster in Figure 118. When all the defects are together in one graph (Figure 398 of appendix F4) it is more difficult to distinguish between defects, as the time versus charge graphs change drastically. When looking at the TRPD graphs of the clusters individually we can distinguish between the defect origins.

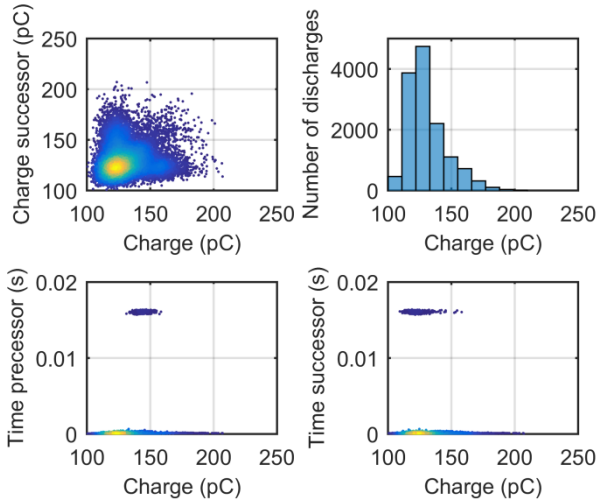

Figure 118: Defect combination 1: Red cluster.

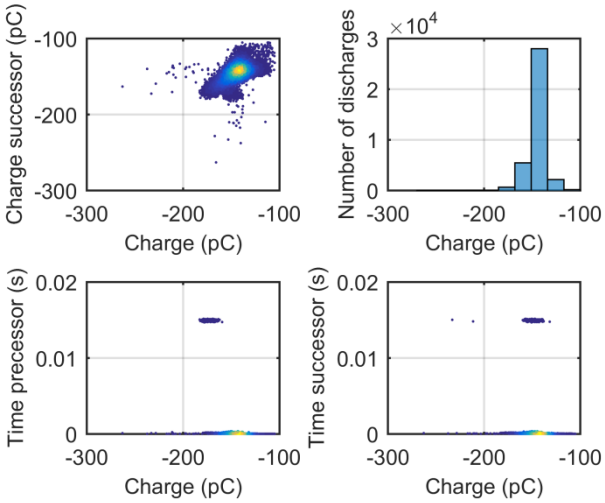

Figure 119: Defect combination 1: Green cluster.

Looking at the red cluster in Figure 119 and the green cluster in Figure 118 and comparing them to the original defects in section 6.1.5 above, we can clearly see that they are defects with origins in corona discharges – positive corona in the green cluster and negative corona in the red cluster. They are oval-shaped clusters at an angle of 45^0 (on the line y=x). The original defect can be seen in Figure 103 (negative corona) and Figure 104 (positive corona).

Defect Combination 1, Number of Discharges per Cycle

The graph of the number of discharges per cycle is shown in Figure 374 in appendix F2.

Average: 147.06 pulses/cycle
Red cluster (positively charged pulses): 39.86 pulses/cycle
Green cluster (negatively charged pulses): 107.19 pulses/cycle

Positive corona (negatively charged pulses) have an average of 250 pulses/cycle, though in this combination case it is 107.19 pulses/cycle. It is significantly reduced but it is still a lot compared to the rest of the types of discharges. Negative corona (positively charged pulses) have an average of 18.32 pulses/cycle, though in this case it is 39.86 pulses/cycle. Even though this is more than the original defect, it is still much less than the positive corona and more than the other defects origins.

Defect Combination 2: Corona & Internal Discharge

The graphs of this combination of defects are in appendix F below. Each of these graphs is compared with the graphs of the "pure" defects in section 6.1 above:

Defect Combination 2, Time Evolution and Clusters Analysis

Figure 363 of appendix F shows the time evolution, the cluster Weq vs. Teq and the cluster Energy vs. Charge. In the cluster Weq vs. Teq there is only one cluster, so no distinctions can be made. In the cluster energy vs. charge there are four clusters. When checking the pulses of the clusters we can see that the pulses from the cluster with a higher slope are of an ungrounded metal near the sample. The other clusters have pulses of a proper PD. Therefore, the defects are not distinguishable in origin, although the polarity is distinguishable.

Defect Combination 2, Energy per Charge vs. Charge

Figure 411 of appendix F shows the graph of this cluster. The distinguishable clusters have a slope of $3.68 \cdot 10^{-4}$ [pJ/pC] and 55 [pJ/pC].

Defect Combination 2, Rise-time vs. Fall-time

Figure 423 shows the graph of this cluster, where there is no clear distinction possible between the two artificially created defects.

Defect Combination 2, PRPD Analysis

Figure 387 of appendix F shows the graph of the defects in PRPD. There is clearly only one cluster visible, but neither one of the defects is recognizable. The shape is neither a horizontal line nor an arc, but a triangle. The defect actually looks more like surface discharge, so it could be that the sample is aged and needs replacing (speaking of the internal discharge sample). The reasoning for why corona are not visible is because of the difference in pulse magnitude: the pulses of corona are

negligible compared to the pulses from internal discharge. Because of the large order of magnitude of internal discharge, corona are treated as noise in this analysis. This difference in magnitude can be seen clearly in Table 11. This is because the vertical resolution is limited. This can be solved by measuring with a 12-bit resolution oscilloscope instead of the current 8-bit resolution oscilloscope.

Defect Combination 2, TRPD Analysis

Since the defect was not distinguishable in PRPD analysis, we cannot learn anything from the graphs constructed for TRPD analysis, shown in Figure 399. By doing the TRPD analysis we can confirm that this method used for defect origin recognition will provide similar results to the PRPD analysis and can be trusted. The shape of the graph of charge successor versus charge is a triangle, which is similar to a defect with origins in surface discharge and free-moving particles. The charge magnitudes, on the other hand, are similar to that of surface discharges. In the graph of time versus charge we can see a figure of a triangle, similar to that of surface discharge. This analysis is similar in both positively and negatively charged pules.

	Possible origin # 1	**Possible origin # 2**
Charge successor vs. charge	Surface discharge	Free-moving particle
Number of discharges vs. charge	Surface discharge	-
Time pre & suc vs. charge	Surface discharge	-

Table 29: Defect combination 2, negatively charged: Summary of TRPD analysis.

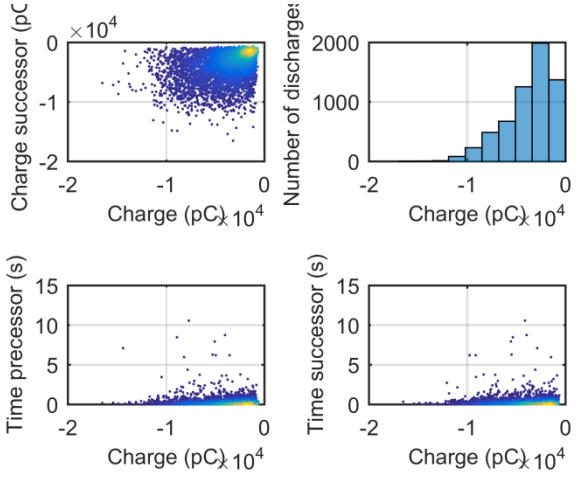

Figure 120: Defect combination 2: Negatively charged pulses TRPD.

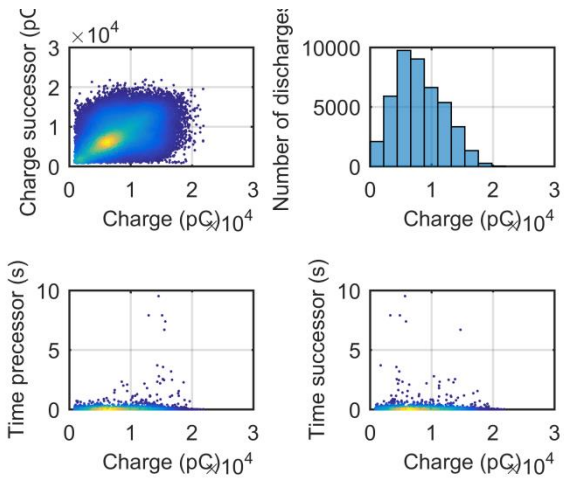

Figure 121: Defect combination 2: Positively charged pulses TRPD.

The analysis above shows that TRPD analysis leads to the same conclusion as PRPD analysis – that no corona or internal discharges are present, but only surface discharges.

Defect Combination 2, Number of Discharges per Cycle

The graph of the number of discharges per cycle is shown in Figure 375 in appendix F2.

Average: 1.12 pulses/cycle
Positively charged pulses: 1.01 pulses/cycle
Negatively charged pulses: 1.00 pulses/cycle

Here, both positively and negatively charged pulses are more or less the same. Internal discharge has an average of 2.00 pulses/cycle and surface discharge of 1.41 pulses/cycle. Positive

corona (negatively charged pulses) have an average of 250 pulses/cycle, and negative corona (positively charged pulses) have an average of 18.32 pulses/cycle. The measured discharges are nowhere near the number of discharges that occur in corona discharges. This is confirmation that there are no corona discharges in this set of recorded pulses.

Defect Combination 3: Corona & Floating Electrode

The graphs of this combination of defects are in appendix F below. Each of these graphs is compared with the graphs of the “pure” defects in section 6.1 above:

Defect Combination 3, Time Evolution and Clusters Analysis

Figure 364 of appendix F shows the time evolution, the cluster Weq vs. Teq and the cluster energy vs. charge. In the cluster Weq versus Teq there is only one cluster, so no distinctions can be made. In the cluster energy versus charge there are four clusters. The pulses of the two clusters closest to the y-axis look like the pulses of an ungrounded metal near the sample. However, this does not have to be the case; the pulse could also be misshapen because of the coupling capacitor limit. In the experimental setup we use a CC of 1nF (two 2nF capacitor in series); the shape of the pulse can be misshapen if the sample(s) have a larger capacitance than the CC. The pulse of this cluster is shown in Figure 122.

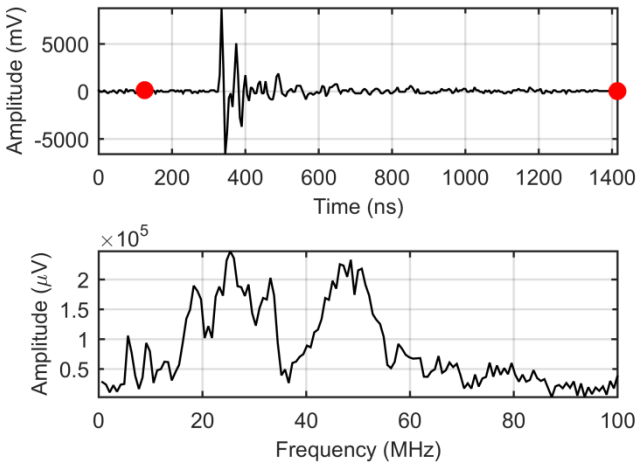

Figure 122: Defect combination 3: Red cluster pulse.

The other two clusters further away from the y-axis have pulses from a proper PD (few oscillations). Therefore, the defects are distinguishable in origin and by polarity.

Defect Combination 3, Energy per Charge vs. Charge

Figure 412 of appendix F shows the graph of this cluster. The distinguishable clusters have a slope of $7.5 \cdot 10^{-4}$ [pJ/pC], $-4.175 \cdot 10^{-4}$ [pJ/pC] (2x) and 0.0032 [pJ/pC] (2x).

Defect Combination 3, Rise-time vs. Fall-time

Figure 424 shows the graph of this cluster, where there is no clear distinction possible between the two artificially created defects.

Defect Combination 3, PRPD Analysis

Figure 388 of appendix F shows the graph of the multiple defects in PRPD. The two defects are recognizable and distinguishable. Floating electrode is clearly visible, but positive and negative corona are not; there are few recorded corona pulses compared to floating electrode. The charge magnitude difference could have some influence on this.

Defect Combination 3, TRPD Analysis

Figure 400 in appendix F shows the complete TRPD with all the defects together. As we have already shown, the fewer defects in the graphs, the simpler the TRPD figures become. The two clusters as will be mentioned in the analysis below can be seen in Figure 123.

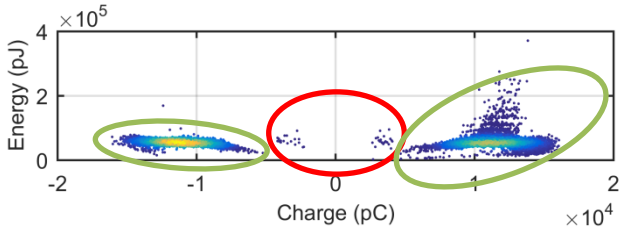

Figure 123: Defect combination 3: Clusters, green and red.

The TRPD graph of the green cluster is shown in Figure 124. When looking at the TRPD graphs of the green cluster, we can clearly see similar graphs as the original defect (floating electrode), as described in section 6.1.5 above. The TRPD graph of the red cluster is shown in Figure 125. When looking at the TRPD graphs of the red cluster, we can clearly see similar graphs as the original defect (floating electrode), but with a different charge magnitude.

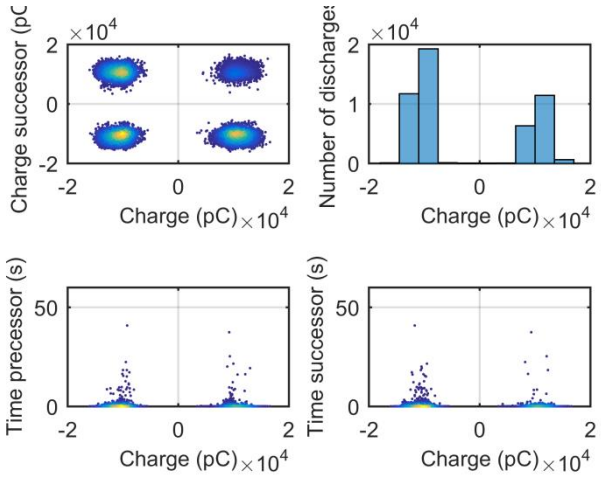

Figure 124: Defect combination 3: Green cluster TRPD.

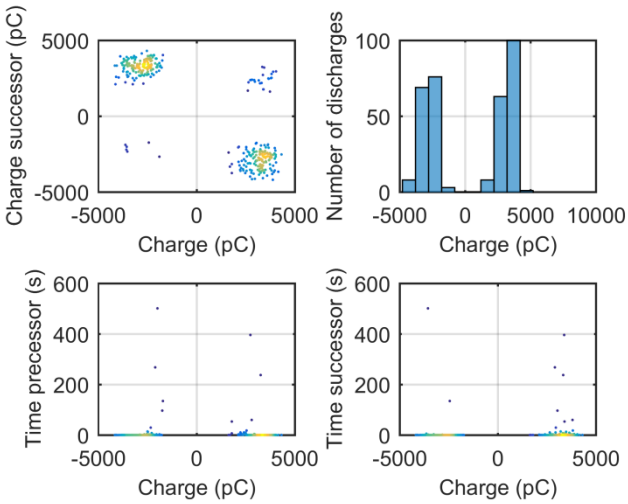

Figure 125: Defect combination 3: Red cluster TRPD.

To confirm that both clusters are from the original defect floating electrode, we will look at the TRPD figures of the different polarities of charges. Below, Figure 126 and Figure 127 show the negatively and positively charged pulses from the green cluster.

Looking at the charge successor versus charge graph in both the positively and negatively charged clusters, there are figures that look like misshapen circles, which can be seen as squares. Squares can be traced back to the original defect of floating electrode, but circles can be traced back to the original defect of internal discharge. Looking at the graph of the number of discharges per

charge we have a magnitude around 10^3 and 10^4 discharges and 10^4 coulomb; the slopes of the graph are steeper away from 0 and flatter towards 0. This part of the analysis is similar to the original defect of floating electrode, but it also has some similarities to surface discharge. The time precessor and successor versus charge have a concentration near the x-axis and fade vertically slower than horizontally. There are no horizontally stacked lines, so no time distinction between the groups can be made. The time between occurring PD pulses is on the order of 10^2 but most of the pulses (more than 95%) occur on the order of 10^1. Therefore, the defect origin can be traced with this graph to floating electrode.

	Possible origin # 1	**Possible origin # 2**	**Possible origin # 3**
Charge successor vs. charge	Floating electrode	Internal discharge	Corona
Number of discharges vs. charge	Floating electrode	Surface discharge	-
Time pre & suc vs. charge	Floating electrode	-	-

Table 30: Defect combination 3, green cluster: Summary of TRPD analysis.

Table 30 shows a summary of the analysis conducted. Floating electrode can be recognized in all of the graphs; therefore, we can conclude that the green cluster is a defect with origins in floating electrode.

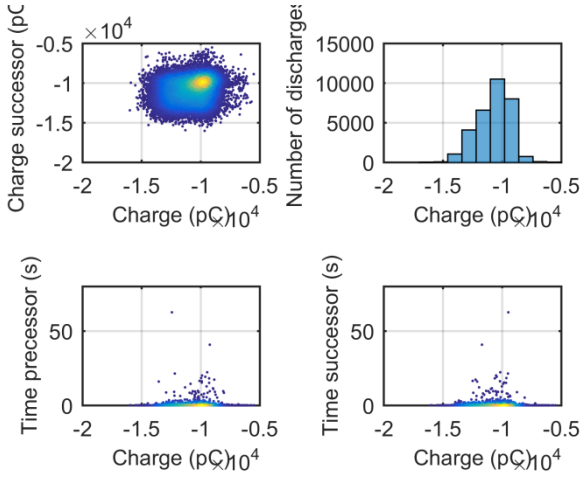

Figure 126: Defect combination 3: Green negatively charged cluster TRPD.

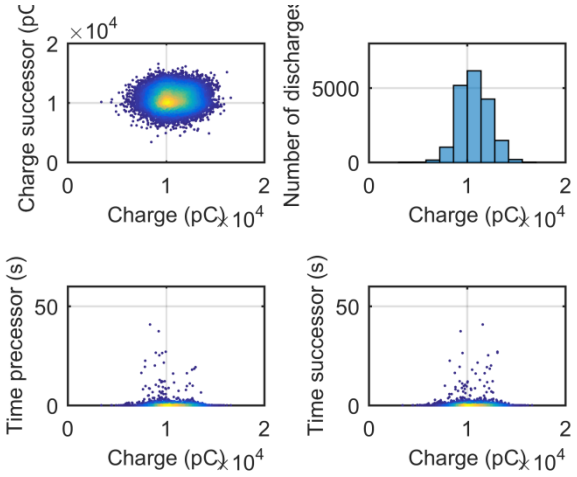

Figure 127: Defect combination 3: Green positively charged cluster TRPD.

Figure 128 and Figure 129 show the negatively and positively charged pulses from the red cluster. There are few pulses recorded compared to the green cluster. In the charge successor versus charge graph, the recorded pulses are not enough to distinguish between the possible shapes – it can look like a circle, an oval at an angle, a triangle or a misshapen square. In the graph of number of discharges versus charge there is a peak around -2500pC and +3500pC. The slope toward 0 is steeper and away from 0 flatter in the red negatively charged cluster, and in the red positively charged cluster it is the opposite. In the individual original defects there is no such combination, so therefore we cannot use this graph either. The shape of the time versus charge graphs looks most like the floating electrode graph. The conclusion that can be drawn from these graphs is that the number of pulses is not enough to distinguish them.

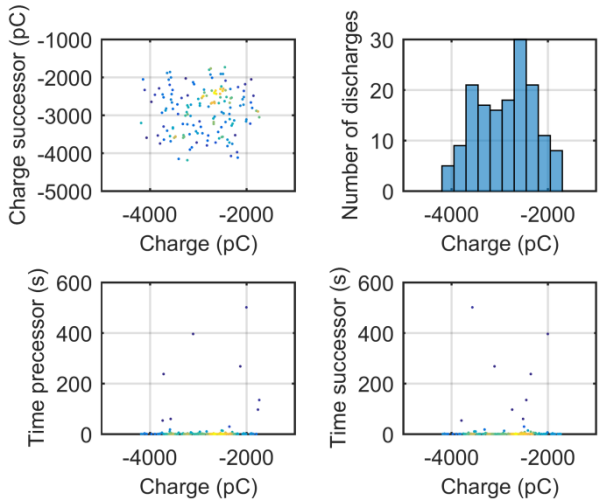

Figure 128: Defect combination 3: Red negatively charged cluster TRPD.

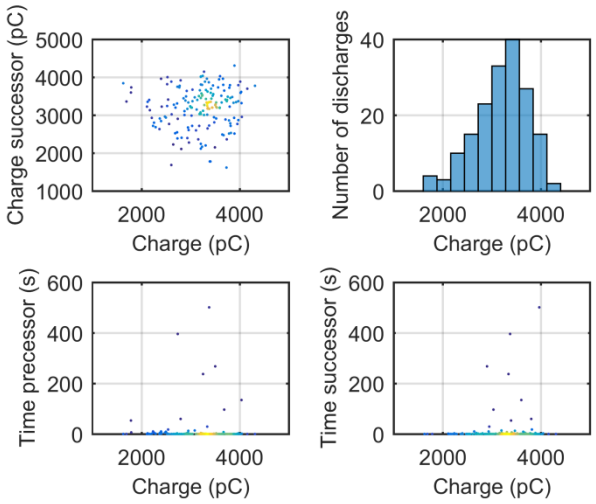

Figure 129: Defect combination 3: Red positively charged cluster TRPD.

Defect Combination 3, Number of Discharges per Cycle

The graph of the number of discharges per cycle is shown in Figure 376 in appendix F2.

Average: 1.36 pulses/cycle
Red cluster: 1.58 pulses/cycle
Red positively charged cluster: 1.03 pulses/cycle
Red negatively charged cluster: - pulses/cycle
Green cluster: 1.35 pulses/cycle
Green positively charged cluster: 1.00 pulses/cycle
Green negatively charged cluster: 1.01 pulses/cycle

There is little difference between the number of pulses/cycle of the green and red clusters. Normally, we would see for positive corona (negatively charged pulses) an average of 250 pulses/cycle, and with negative corona (positively charged pulses) an average of 18.32 pulses/cycle. For floating electrode we saw an average of 1.93 pulses/cycle. The number of pulses/cycle that were recorded for this defect combination is nowhere near the number of pulses/cycle for the corona discharges. This finding is similar to the analysis above; we saw only a few corona pulses, and therefore corona were not very recognizable.

Defect Combination 4: Corona & Surface Discharge

The graphs of this combination of defects are in appendix F below. Each of these graphs is compared with the graphs of the “pure” defects in section 6.1 above:

Defect Combination 4, Time Evolution and Clusters Analysis

Figure 365 of appendix F shows the time evolution, the cluster Weq vs. Teq and the cluster energy vs. charge. In the cluster Weq versus Teq there are three clusters, as shown in Figure 130.

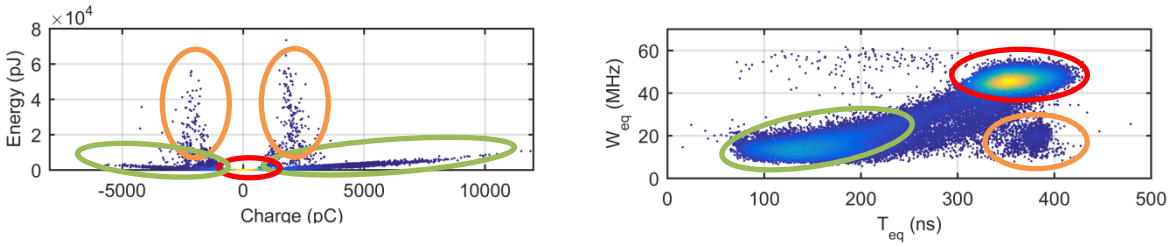

Figure 130: Defect combination 4: Clusters.

The orange clusters are created by pulses that are not properly recorded by the oscilloscope. An example of such a pulse can be seen in Figure 131.

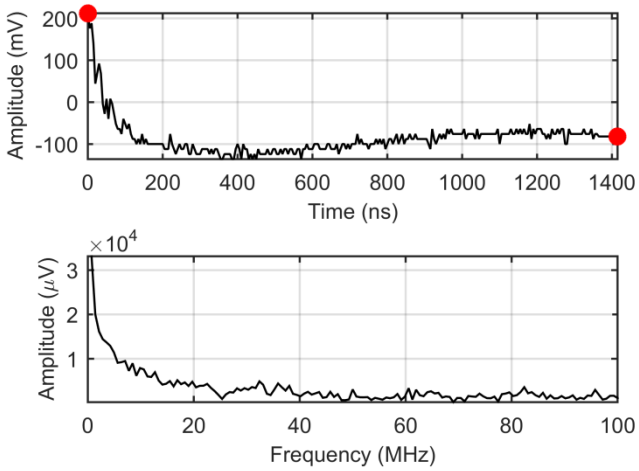

Figure 131: Defect combination 4, pulse 24379.

In the cluster energy versus charge, there are four clusters. The red and the green clusters are not distinguishable in this graph. The red and green clusters have pulses of a proper PD.

Defect Combination 4, Energy per Charge vs. Charge

Figure 413 shows the graph of this cluster. The distinguishable clusters have a slope of 0.00156 [pJ/pC], $1.187 \cdot 10^{-5}$ [pJ/pC] and a vertical slope.

Defect Combination 4, Rise-time vs. Fall-time

Figure 425 shows the graph of this cluster, where there is no clear distinction possible between the two artificially created defects. The second group of PDs are PD pulses that are not properly measured, so no conclusion can be drawn from this part.

Defect Combination 4, PRPD Analysis

Figure 389 of appendix F shows the graph of the defects in PRPD. Figure 132 shows the PRPD of the green cluster and Figure 133 shows the PRPD of the red cluster. Comparing these PRPD graphs to the original defect PRPD graphs in section 6.1.3 above, the red cluster is positive corona

and the green cluster is surface discharge. They are similar in shape, magnitude and concentration when compared to the original defects.

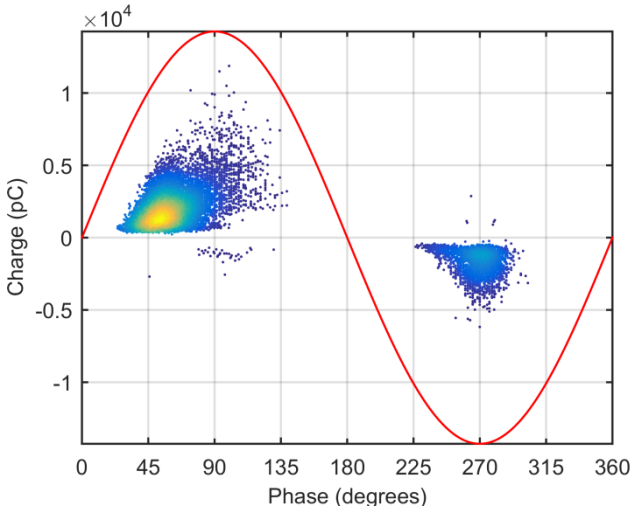

Figure 132: Defect combination 4: Green clusters PRPD.

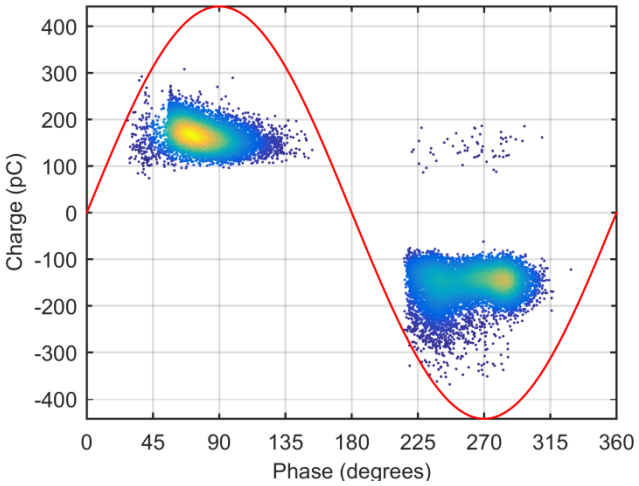

Figure 133: Defect combination 4: Red clusters PRPD.

There are some pulses that are on the opposite polarity than they should be, but they can be neglected because they are pulses that were not recorded properly by the oscilloscope. Looking at these graphs, we can see that the discharges are distinguishable with PRPD analysis. However, the clusters selections are not optimal. With frequency-equivalent versus time-equivalent we can distinguish between the defect origins but not their polarity, and with the energy versus coulomb clusters we can distinguish between the polarities but not the defect origins.

Defect Combination 4, TRPD Analysis

Figure 401 of appendix F shows the TRPD graph of defect combination 4. The TRPD graph of the green cluster is shown in Figure 134. When looking at the TRPD graphs of the green cluster we can clearly see similar graphs as the original defect of surface discharge, as described in section 6.1.5 above. The TRPD graph of the red cluster is shown in Figure 135. When looking at the TRPD graphs of the red cluster we can clearly see similar graphs as the original defect of corona (positive and negative).

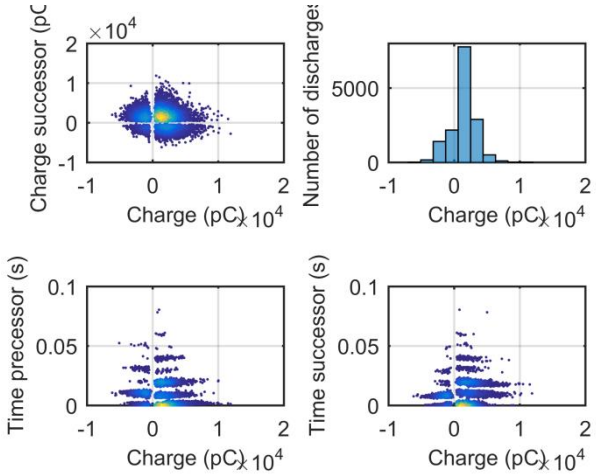

Figure 134: Defect combination 4: TRPD green cluster.

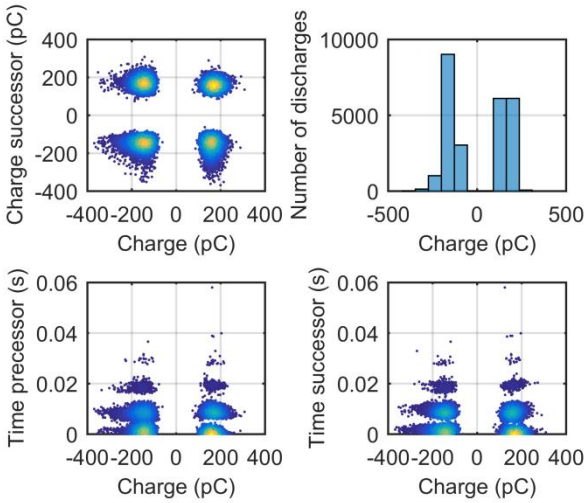

Figure 135: Defect combination 4: TRPD red cluster.

In this analysis we cannot separate between the positively and negatively charged pulses for a simpler TRPD analysis. This because the clusters are not separable in the cluster of energy versus charge.

Defect Combination 4, Number of Discharges per Cycle

The graph of the number of discharges per cycle is shown in Figure 377 in appendix F2.

Average: 7.32 pulses/cycle
Red cluster: 3.71 pulses/cycle (1-9)
Green cluster: 2.35 pulses/cycle (1-8)
Orange cluster: 1.10 pulses/cycle (1,2)

Here, corona and surface discharge were clearly distinguishable, but the red cluster (corona discharges) is nowhere near the number of pulses/cycle that are supposed to occur with corona discharges. We can now conclude that the number of pulses per cycle cannot be used for defect recognition, as they are inconsistent.

Defect Combination 5: Corona & Free-Moving Particle

The graphs of this combination of defects are in appendix F below. Each of these graphs is compared with the graphs of the “pure” defects in section 6.1 above:

Defect Combination 5, Time Evolution and Clusters Analysis

Figure 366 of appendix F shows the time evolution, the cluster Weq vs. Teq and the cluster energy vs. charge. In the cluster Weq versus Teq there are two clusters, so a distinction can be made between the two defects but not between their polarities. In the cluster energy versus charge there are four clusters, so the defects are distinguishable in origin and polarity.

Defect Combination 5, Energy per Charge vs. Charge

Figure 414 of appendix F shows the graph of this cluster. The distinguishable clusters have a slope of 254.5 [pJ/pC], 0.00118 [pJ/pC] and $3.368 \cdot 10^{-4}$ [pJ/pC].

Defect Combination 5, Rise-time vs. Fall-time

Figure 426 shows the graph of this cluster, where there is no clear distinction possible between the two artificially created defects.

Defect Combination 5, PRPD Analysis

Figure 390 of appendix F shows the graph of the defects in PRPD. The two defects are clearly recognizable and distinguishable, even if free-moving particle has many fewer recorded pulses compared to corona. We can clearly see the triangles that are larger than the half cycles as free-moving particle. Corona have clearly two horizontal lines near the minimum and maximum of the phase signal.

Defect Combination 5, TRPD Analysis

As shown in Figure 136, two clusters are clearly visible. Figure 402 of appendix F shows the TRPD of these two clusters.

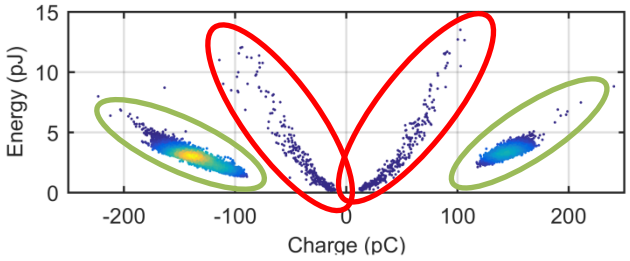

Figure 136: Defect combination 5: Clusters, green and red.

The TRPD graph of the green cluster is shown in Figure 141 and Figure 142 and of the red cluster in Figure 137. When all the defects are together in one graph (Figure 402 of appendix F4), it is more difficult to distinguish between defects. When looking at the TRPD graphs of the clusters individually, we can distinguish between the defect origins.

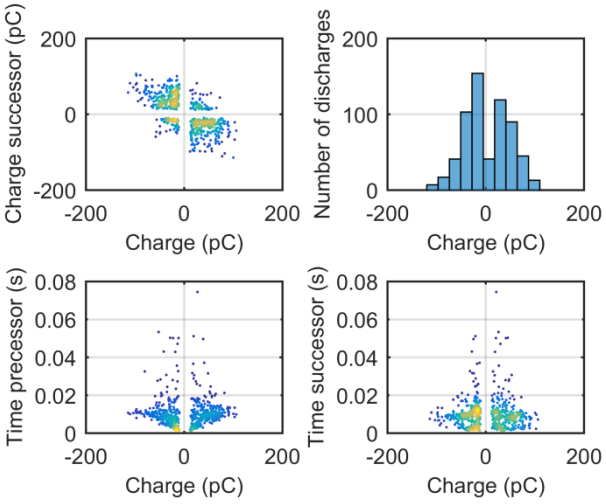

Figure 137: Defect combination 5: TRPD red cluster.

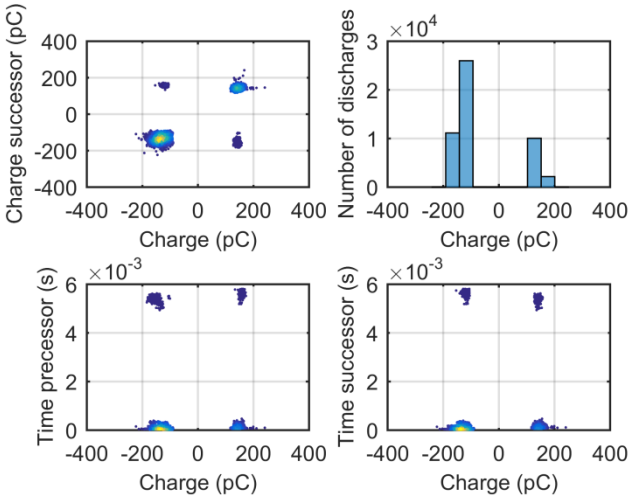

Figure 138: Defect combination 5: TRPD green cluster.

Looking at the red cluster in Figure 137 and comparing it to the original defects in section 6.1.5 above, we can clearly see that it is a defect with a free-moving particle origin. Comparing the green

cluster in TRPD (Figure 138) to the original defect in section 6.1.5 above, we can see corona discharges (positive and negative corona).

Figure 139 and Figure 140 show the negatively and positively charged pulses from the red cluster. Analysing the negatively charged pulses, we see that the shape of the charge successor versus the charge is a triangle, which the original defects surface discharge and free-moving particle have. The number of discharges versus charge has a peak around -25pC, a steep slope towards 0 and a flatter slope away from 0. This is comparable to surface discharge and free-moving particle. However, the magnitudes of the charge are comparable to the defect origin free-moving particle. In the time versus charge graph there are not enough pulses recorded to make a proper shape (though it is beginning to look like a triangle). But looking at the distances between the horizontally stacked lines, they are separated by ±0.01 seconds; this resembles a defect with origins in free-moving particle.

	Possible origin # 1	**Possible origin # 2**	**Possible origin # 3**
Charge-successor vs. charge	Free-moving particle	Surface discharge	-
Number of discharges vs. charge	Free-moving particle	Surface discharge	Internal discharge
Time pre & suc vs. charge	Free-moving particle	-	-

Table 31: Defect combination 5, red cluster negatively charged: Summary of TRPD analysis.

Analysing the positively charged pulses, we see that the shape of the charge successor versus charge is a triangle, like the shape of the original defects surface discharge and free-moving particle. The number of discharges versus charge has a peak around +25pC, a steep slope towards 0 and a flatter slope away from 0. This is comparable to surface discharge and free-moving particle. However, the magnitudes of the charge are comparable to the defect origin free-moving particle. In the time versus charge graph there are not enough pulses recorded to make a proper shape (though it is beginning to look like a triangle). But looking at the distances between the horizontally stacked lines, they are separated by ±0.01 seconds; this resembles a defect with origins in free-moving particle. From the conclusions drawn above, we can say that the red cluster is definitely a defect with origins in free-moving particle.

	Possible origin # 1	**Possible origin # 2**	**Possible origin # 3**
Charge-successor vs. charge	Free-moving particle	Surface discharge	-
Number of discharges vs. charge	Free-moving particle	Surface discharge	Internal discharge
Time pre & suc vs. charge	Free-moving particle	-	-

Table 32: Defect combination 5, red cluster positively charged: Summary of TRPD analysis.

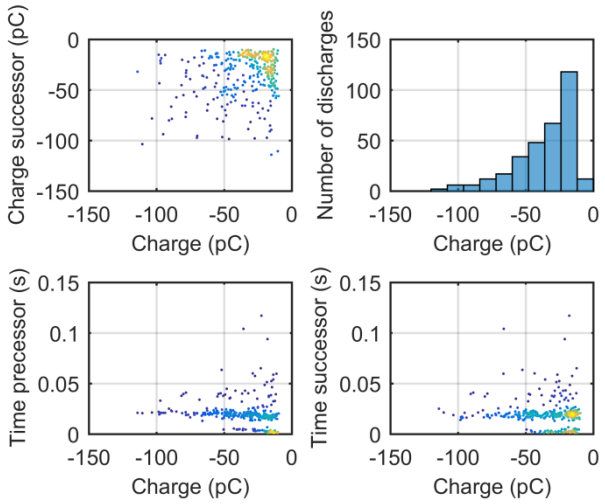

Figure 139: Defect combination 5: TRPD red cluster negatively charged pulses.

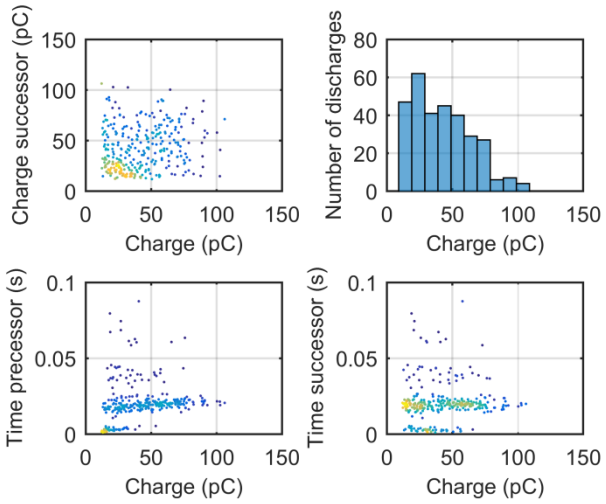

Figure 140: Defect combination 5: TRPD red cluster positively charged pulses.

Figure 141 and Figure 142 show the negatively and positively charged pulses from the green cluster. Analysing the negatively charged pulses, the shape of the charge successor versus the charge can be seen as a square but also as an oval-shaped concentration at an angle of 45^0 (on the line y=x). These shapes can be seen as a defect with an origin in floating electrode or corona discharges. The number of discharges versus charge has a peak around ±140pC, a steep slope towards 0 and a flatter slope away from 0. However, at the positively charged green cluster it is the opposite, and therefore we cannot use the slopes to detect the defect origin. The magnitudes of the charge are comparable to the defect origin corona. In the time versus charge graph of the negatively charged green cluster we can clearly see two horizontal lines, one at 0 and the other around 0.014 seconds.

	Possible origin # 1	**Possible origin # 2**
Charge-successor vs. charge	Floating electrode	Positive corona
Number of discharges vs. charge	Positive corona	-
Time pre & suc vs. charge	Positive corona	-

Table 33: Defect combination 5, green cluster negatively charged: Summary of TRPD analysis.

Analysing the negatively charged pulses, the shape of the charge successor versus the charge is an oval-shaped concentration at an angle of 45^0 (on the line y=x). This shape can be seen as a defect with an origin in corona discharges. In the time versus charge graph of the negatively charged green cluster we can clearly see two horizontal lines, one at 0 and the other around 0.017 seconds.

	Possible origin # 1
Charge-successor vs. charge	Negative corona
Number of discharges vs. charge	Negative corona
Time pre & suc vs. charge	Negative corona

Table 34: Defect combination 5, green cluster positively charged: Summary of TRPD analysis.

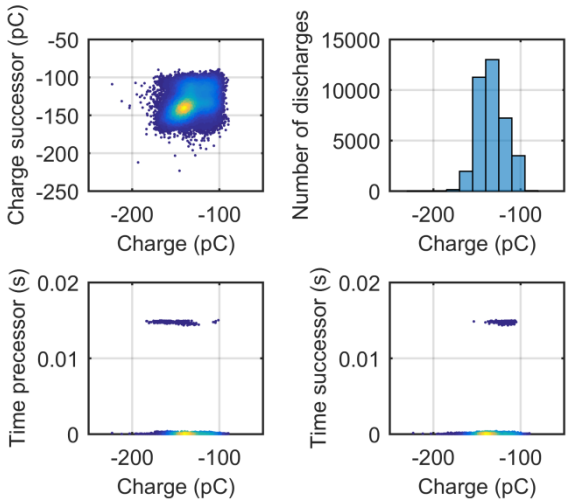

Figure 141: Defect combination 5: TRPD green cluster negatively charged.

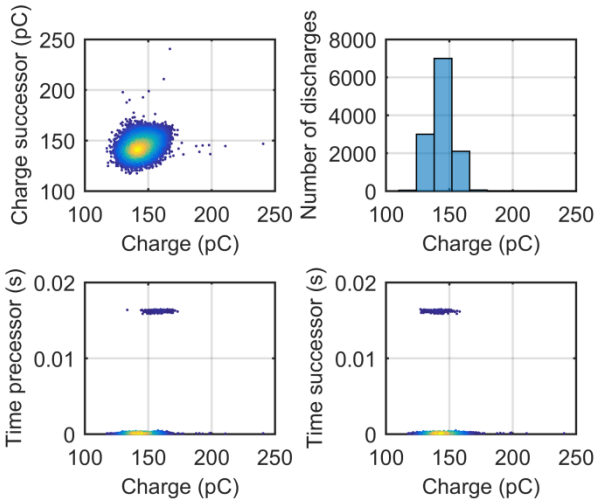

Figure 142: Defect combination 5: TRPD green cluster positively charged.

Looking at the positively and negatively charged pulses of the green cluster (Figure 141 and Figure 142) and comparing them to the original defects in section 6.1.5 above, we can clearly see that it is a defect with origin in corona discharges: positive corona in the negatively charged cluster and negative corona in the positively charged cluster. The original defect can be seen in Figure 103 (negative corona) and Figure 104 (positive corona).

Defect Combination 5, Number of Discharges per Cycle

The graph of the number of discharges per cycle is shown in Figure 378 in appendix F2.

Average: 154.80 pulses/cycle
Red cluster: 2.13 pulses/cycle
Red positively charged cluster: 1.16 pulses/cycle
Red negatively charged cluster: 1.35 pulses/cycle
Green cluster: 152.85 pulses/cycle
Green positively charged cluster: 37.92 pulses/cycle
Green negatively charged cluster: 115.04 pulses/cycle

Here we can see a clear difference between the number of pulses/cycle of the selected clusters. For the original defects, the free-moving particle has an average of 1.67 pulses/cycle, positive corona (negatively charged pulses) has an average of 250 pulses/cycle and negative corona (positively charged pulses) has an average of 18.32 pulses/cycle. In the green cycle we can clearly distinguish between positive and negative corona. The red cluster must therefore be the free-moving particle. The number of pulses per cycle of this recorded defect combination is not exactly the same as the original defect, but they are close to each other.

Defect Combination 6: Internal Discharge & Floating Electrode

The graphs of this combination of defects are in appendix F below. Each of these graphs is compared with the graphs of the “pure” defects in section 6.1 above:

Defect Combination 6, Time Evolution and Clusters Analysis

Figure 367 shows the time evolution, the cluster Weq vs. Teq and the cluster energy vs. charge. In the cluster Weq versus Teq there is only one cluster, so no distinctions can be made. In the cluster

energy versus charge there are four clusters that are reflections over the y-axis. Looking at the graph of clusters in Figure 143, we can clearly distinguish more than one cluster. On the negative charge part of the graph (left side) there are two clear and distinguishable clusters, but on the right side (positive charge) there seems to be an interference of some sort, so no proper distinction can be made. Therefore, we will look at Figure 144, which is zoomed in on the negative charge region (left side of the graph).

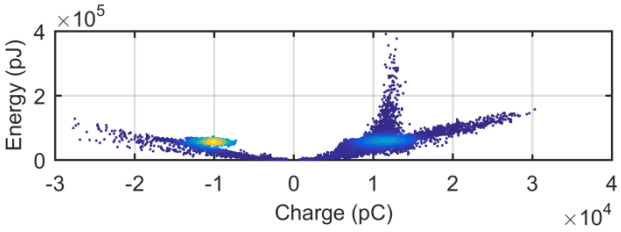

Figure 143: Defect combination 6: Clusters.

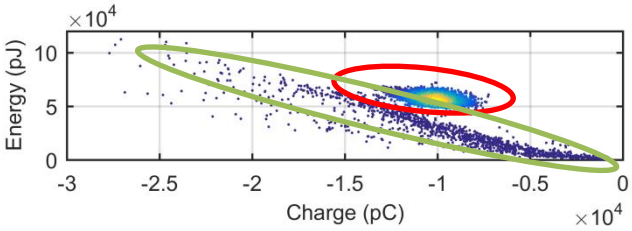

Figure 144: Defect combination 6, left part: Clusters, green and red.

Defect Combination 6, Energy per Charge vs. Charge

Figure 415 shows the graph of this cluster. The distinguishable cluster has a slope of $2.04 \cdot 10^{-4}$ [pJ/pC].

Defect Combination 6, Rise-time vs. Fall-time

Figure 427 shows the graph of this cluster, where there is no clear distinction possible between the two artificially created defects.

Defect Combination 6, PRPD Analysis

Figure 391 shows the graph of the defects in PRPD. The two defects are clearly recognizable and distinguishable, even if internal discharge has many fewer recorded pulses compared to the floating electrode. The triangle that stays within the half cycles of the defect internal discharge is clearly visible, but the square of the floating electrode has become a bit flatter. The floating electrode could be confused with corona when looking at the shapes, but the magnitudes are different.

Defect Combination 6, TRPD Analysis

Since the defect was not distinguishable in PRPD analysis, we cannot learn anything from the graphs constructed for TRPD analysis, shown in Figure 403.

The TRPD of the negatively charged red cluster is shown in Figure 145 and the TRPD of the negatively charged green cluster in Figure 146. The red cluster of defect combination 6 is clearly an internal discharge defect. Visible in the charge-successor versus charge graph is a circle and in the time versus charge graph a horizontal oval line around 0.02 seconds with a concentration in the centre of the oval shape. The number of discharges versus charge graph has a flatter slope towards 0 and a steeper slope away from 0. These slopes are not equal to the original defect slopes.

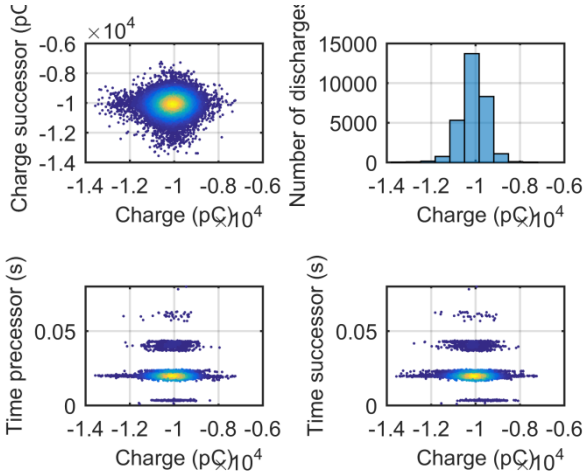

Figure 145: Defect combination 6: TRPD red cluster negatively charged.

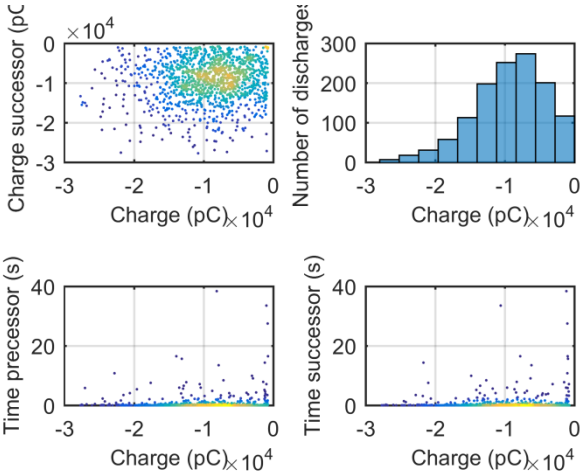

Figure 146: Defect combination 6: TRPD green cluster negatively charged.

In the analysis above we saw that even if there is a disturbance present, we only need to distinguish the defects in one of the charge polarities to be able to distinguish between defect origins.

Defect Combination 6, Number of Discharges per Cycle

The graph of the number of discharges per cycle is shown in Figure 379 in appendix F2.

Average: 1.70 pulses/cycle
Red negatively charged cluster: 1.02 pulses/cycle
Green negatively charged cluster: 1.01 pulses/cycle

Here, both positively and negatively charged pulses are more or less the same. Internal discharge has an average of 2.00 pulses/cycle and floating electrode 1.93 pulses/cycle. The recorded pulses per cycle are close to the original defect number of pulses per cycle, but these numbers of discharges per cycle are too close to be able to distinguish them from each other.

Defect Combination 7: Internal Discharge & Surface Discharge

The graphs of this combination of defects are in appendix F below. Each of these graphs is compared with the graphs of the “pure” defects in section 6.1 above:

Defect Combination 7, Time Evolution and Clusters Analysis

Figure 368 shows the time evolution, the cluster Weq vs. Teq and the cluster energy vs, charge. This is a similar case, like defect combination 6, in which the energy versus charge graph cannot be used for cluster selection. The clusters can be selected in the frequency-equivalent versus time-equivalent. Figure 147 shows the selected green and red clusters in the frequency-equivalent versus time-equivalent. It is clear that the clusters are not distinguishable in the energy versus charge graph. Here we are also unable to distinguish between polarities, though we can distinguish between the defect origins.

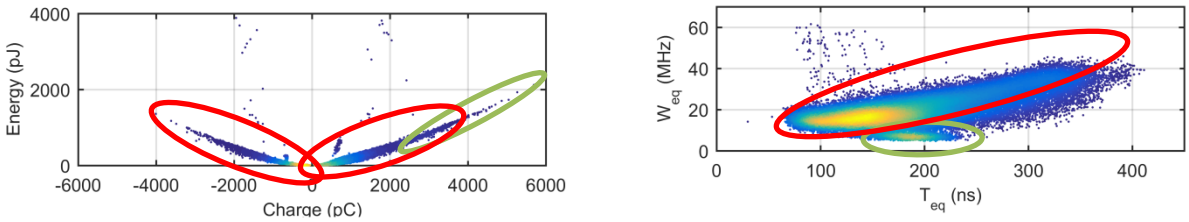

Figure 147: Defect combination 7: Clusters.

Defect Combination 7, Energy per Charge vs. Charge

Figure 416 shows the graph of this cluster. The distinguishable clusters have a slope of 0.00116 [pJ/pC] and $7.225 \cdot 10^{-5}$ [pJ/pC].

Defect Combination 7, Rise-time vs. Fall-time

Figure 428 shows the graph of this cluster, where there is no clear distinction possible between the two artificially created defects.

Defect Combination 7, PRPD Analysis

Figure 392 shows the graph of the defects in PRPD. Below, Figure 148 and Figure 149 show the selected clusters. Looking at the shapes, we can say that the green cluster is the defect with origin in internal discharge and the red cluster is the deft defect with origin in surface discharge. The arc of internal discharge is not a nice arc, as it was previously, but it is still an arc. Surface discharge is recognizable and internal discharge is recognizable and distinguishable.

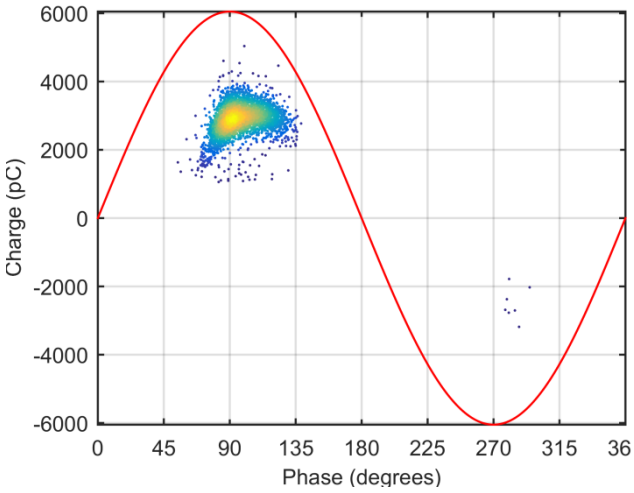

Figure 148: Defect combination 7: PRPD green cluster.

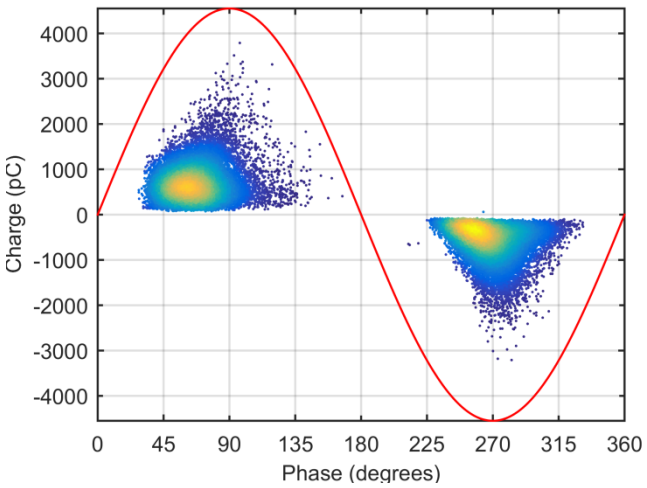

Figure 149: Defect combination 7: PRPD red cluster.

Defect Combination 7, TRPD Analysis

The TRPD analysis of both defects is shown in Figure 404. Figure 150 and Figure 151 show the selected clusters (green and red). We must keep in mind that the green cluster has only positively charged pulses and the red cluster has both positively and negatively charged pulses. The charge-successor versus charge of the green cluster has the shape of a circle, which corresponds to internal discharge. The shape of the graph of time versus charge cannot be compared to any of the defects, perhaps because there are a few negative pulses within the graph that disturb the shape. The red

cluster, on the other hand, is similar to Figure 105, which corresponds to surface discharge. It is similar to it in shape for both charge-successor versus charge and time versus charge.

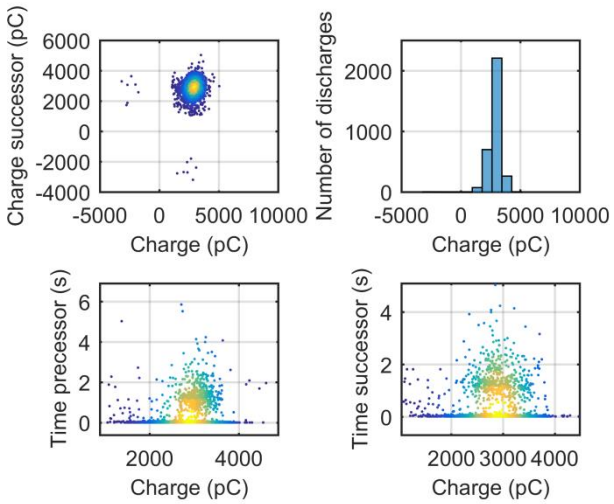

Figure 150: Defect combination 7: TRPD green cluster.

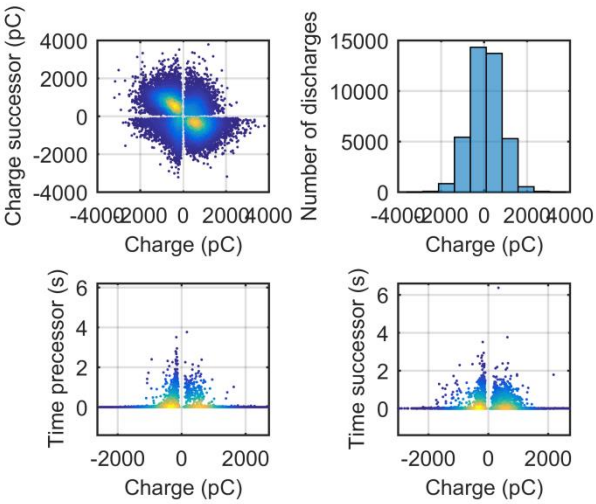

Figure 151: Defect combination 7: TRPD red cluster.

The green cluster is internal discharge and the red cluster is surface discharge.

Defect Combination 7, Number of Discharges per Cycle

The graph of the number of discharges per cycle is shown in Figure 380 in appendix F2.

Average: 2.22 pulses/cycle
Red cluster: 2.08 pulses/cycle
Green cluster: 1.01 pulses/cycle

This is the same case as in defect combination 6. The numbers of discharges per cycle are too close to each other and therefore cannot be used for defect distinction.

Defect Combination 8: Internal Discharge & Free-Moving Particle

The graphs of this combination of defects are in appendix F below. Each of these graphs is compared with the graphs of the “pure” defects in section 6.1 above:

Defect Combination 8, Time Evolution and Clusters Analysis

Figure 369 shows the time evolution, the cluster Weq vs. Teq and the cluster energy vs. charge. In the cluster Weq versus Teq there is only one cluster, so no distinctions can be made. In the cluster energy versus charge there are two clusters that are reflections over the y-axis, so while the defects are not distinguishable, the polarity is of one defect origin.

Defect Combination 8, Energy per Charge vs. Charge

Figure 417 shows the graph of this cluster. The distinguishable cluster has a slope of 0.0016 [pJ/pC].

Defect Combination 8, Rise-time vs. Fall-time

Figure 429 shows the graph of this cluster, where there is no clear distinction possible between the two artificially created defects.

Defect Combination 8, PRPD Analysis

Figure 393 shows the graph of the defects in PRPD. Only free-moving particle is visible; there is no sign of internal discharge. Free-moving particle is recognizable but internal discharge not, so no distinction can be made. This could be due to the limited vertical resolution of the oscilloscope or an aged internal discharge sample.

Defect Combination 8, TRPD Analysis

Since the defect was not distinguishable in PRPD analysis, we cannot learn anything from the graphs constructed for TRPD analysis. These TRPD graphs are shown in Figure 405.

Defect Combination 8, Number of Discharges per Cycle

The graph of the number of discharges per cycle is shown in Figure 381 in appendix F2.

Average: 2.38 pulses/cycle

Defect Combination 9: Floating Electrode & Surface Discharge

The graphs of this combination of defects are in appendix F below. Each of these graphs is compared with the graphs of the “pure” defects in section 6.1 above:

Defect Combination 9, Time Evolution and Clusters Analysis

Figure 370 shows the time evolution, the cluster Weq vs. Teq and the cluster energy vs. charge. In the cluster Weq versus Teq there are two clusters, so a distinction can be made between the two defects but not between their polarities. In the cluster energy versus charge there are four clusters. When checking the pulses of the clusters we can see that the pulses from the cluster with a higher slope (closest to y-axis) are of an ungrounded metal near the sample. The other clusters have pulses of a proper PD. Therefore, the defects are not distinguishable in origin, but the polarity is distinguishable.

Defect Combination 9, Energy per Charge vs. Charge

Figure 418 shows the graph of this cluster. The distinguishable clusters have a slope of 0.016 [pJ/pC], 0.01829 [pJ/pC], $-3.429 \cdot 10^{-4}$ [pJ/pC] and $-2.286 \cdot 10^{-4}$ [pJ/pC].

Defect Combination 9, Rise-time vs. Fall-time

Figure 430 shows the graph of this cluster, where there is no clear distinction possible between the two artificially created defects.

Defect Combination 9, PRPD Analysis

Figure 394 shows the graph of the defects in PRPD. Floating electrode and surface discharge are clearly distinguishable. The defect floating electrode is clearly recognizable and still looks like a

square, but surface discharge no longer has a triangle shape. This could be because the resolution of the oscilloscope is not set to accurately measure one defect, but rather two defects; the oscilloscope does not have a vertical resolution high enough to measure both defects accurately.

Defect Combination 9, TRPD Analysis

Figure 406 shows the complete TRPD with all the defects together. As previously shown, the fewer defects in the graphs, the simpler the TRPD figures become. The two clusters, as will be mentioned in the analysis, are shown in Figure 152.

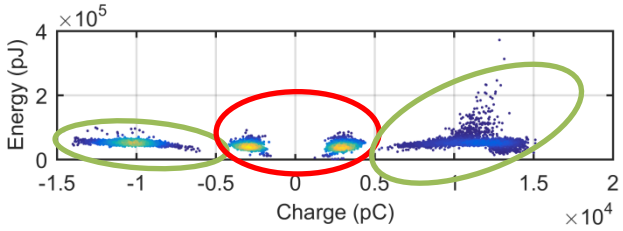

Figure 152: Defect combination 9: TRPD green and red clusters.

The TRPD graph of the green cluster is shown in Figure 153 and of the red cluster in Figure 154.

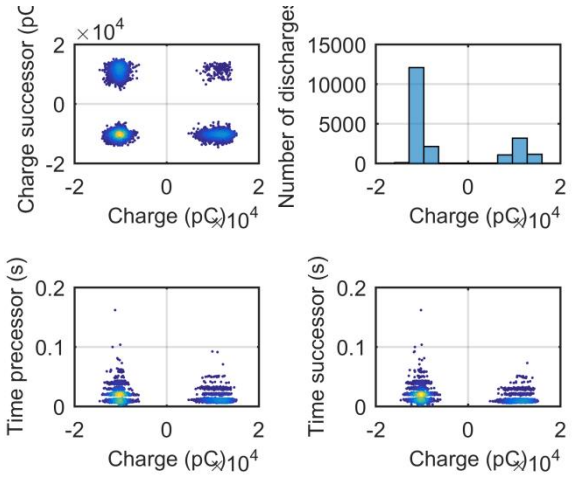

Figure 153: Defect combination 9: TRPD green cluster.

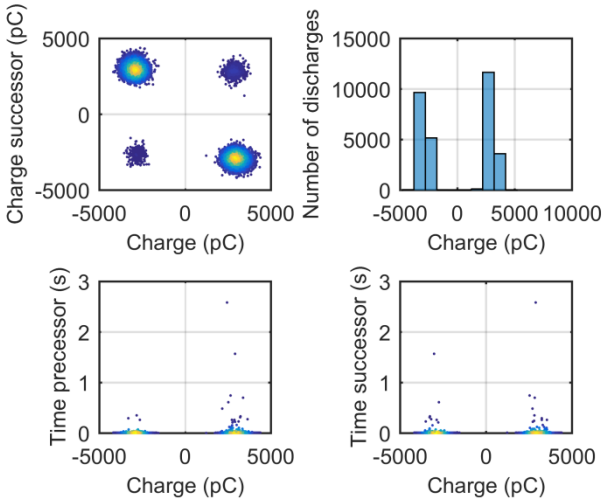

Figure 154: Defect combination 9: TRPD red cluster.

Figure 155 and Figure 156 show the negatively and positively charged pulses from the red cluster. In the graphs of charge-successor versus charge for positively and negatively charged pulses, there is a circle, which resembles a defect with origin in internal discharge. However, the magnitudes of the charges resemble those of surface discharge. In the graph of number of discharges versus charge, the slope towards 0 is flatter compared to away from 0, and in negatively charged pulses the same slopes are present. These slopes happened in the original defect for internal discharge and for floating particle. The magnitudes of these graphs are comparable to surface discharge. The figure of the time versus charge graph looks like the original defect of floating particle.

	Possible origin # 1	Possible origin # 2	Possible origin # 3
Charge-successor vs. charge	Internal discharge	Surface discharge	-
Number of discharges vs. charge	Surface discharge	Internal discharge	Floating particle
Time pre & suc vs. charge	Floating particle	-	-

Table 35: Defect combination 9, red cluster negatively charged: Summary of TRPD analysis.

	Possible origin # 1	Possible origin # 2	Possible origin # 3
Charge-successor vs. charge	Internal discharge	Surface discharge	-
Number of discharges vs. charge	Surface discharge	Internal discharge	Floating particle
Time pre & suc vs. charge	Floating particle	-	-

Table 36: Defect combination 9, red cluster positively charged: Summary of TRPD analysis.

When making the clusters we could select different PD types (different artificially created defects), but looking at the analysis from this red cluster we cannot conclude which defect it is (it is supposed to be surface discharge). In PRPD analysis we also were unable to recognize this surface discharge defect in this sample combination.

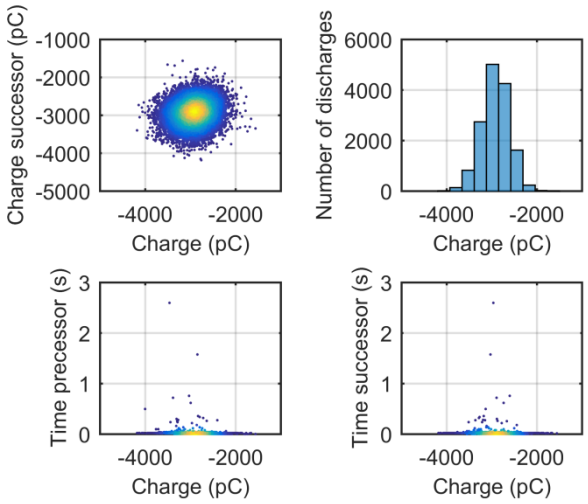

Figure 155: Defect combination 9: TRPD red cluster negatively charged pulses.

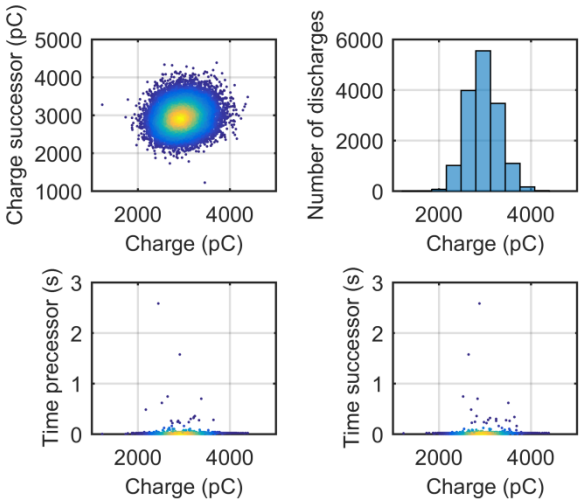

Figure 156: Defect combination 9: TRPD red cluster positively charged pulses.

Figure 157 and Figure 158 show the negatively and positively charged pulses from the green cluster. In the graphs of charge-successor versus charge for negatively charged pulses there is a circle, which can also be seen as a square rotated at an angle. A circle resembles a defect with origin in internal discharge, and a square resembles a defect with origin in floating electrode. The magnitudes are comparable to the defect of floating electrode. The figure of the time versus charge graph looks like the original defect of floating electrode, because the concentration is centred on the horizontal lines, it is near the x-axis and it is fading vertically and horizontally.

	Possible origin # 1	Possible origin # 2	Possible origin # 3
Charge-successor vs. charge	Floating electrode	Internal discharge	-
Number of discharges vs. charge	Floating electrode	-	-
Time pre & suc vs. charge			

Table 37: Defect combination 9, green cluster negatively charged: Summary of TRPD analysis.

In the graphs of charge-successor versus charge for positively charged pulses there is a square, which resembles a defect with origin floating electrode. The figure of the time versus charge graph looks like the original defect of floating electrode.

	Possible origin
Charge-successor vs. charge	Floating electrode
Number of discharges vs. charge	Floating electrode
Time pre & suc vs. charge	Floating electrode

Table 38: Defect combination 9, green cluster positively charged: Summary of TRPD analysis.

The green cluster is therefore a defect with origin in floating particle.

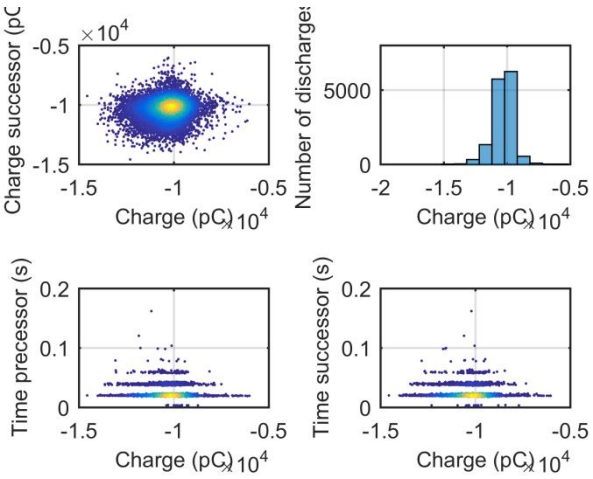

Figure 157: Defect combination 9: TRPD green cluster negatively charged pulses.

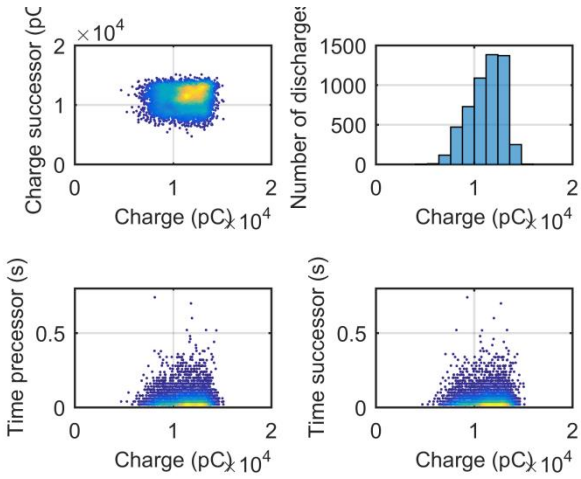

Figure 158: Defect combination 9: TRPD green cluster positively charged pulses.

Defect Combination 9, Number of Discharges per Cycle

The graph of the number of discharges per cycle is shown in Figure 382 in appendix F2.

Average: 3.25 pulses/cycle
Red cluster: 2.05 pulses/cycle
Red positively charged cluster: 1.05 pulses/cycle
Red negatively charged cluster: 1.02 pulses/cycle
Green cluster: 1.36 pulses/cycle
Green positively charged cluster: 1.01 pulses/cycle
Green negatively charged cluster: 1.01 pulses/cycle

This is the same case as in defect combination 6. The numbers of discharges per cycle are too close to each other and therefore cannot be used for defect distinction.

Defect Combination 10: Floating Electrode & Free-Moving Particle

The graphs of this combination of defects are in appendix F below. Each of these graphs is compared with the graphs of the “pure” defects in section 6.1 above:

Defect Combination 10, Time Evolution and Clusters analysis

Figure 371 shows the time evolution, the cluster Weq vs. Teq and the cluster energy vs. charge. In the cluster Weq versus Teq there are clusters, so a distinction can be made between the two

defects but not between their polarities. In the cluster energy versus charge there are four clusters. When checking the pulses of the clusters, we can see that the pulses from the cluster with a higher slope (closest to y-axis) are of an ungrounded metal near the sample. The other clusters have pulses of a proper PD. Therefore, the defects are not distinguishable in origin, but the polarity is distinguishable.

Defect Combination 10, Energy per Charge vs. Charge

Figure 419 shows the graph of this cluster. The distinguishable clusters have a slope of $3.2 \cdot 10^{-4}$ [pJ/pC], $5.3 \cdot 10^{-4}$ [pJ/pC], $6 \cdot 10^{-4}$ [pJ/pC] and $8 \cdot 10^{-4}$ [pJ/pC].

Defect Combination 10, Rise-time vs. Fall-time

Figure 431 shows the graph of this cluster, where there is no clear distinction possible between the two artificially created defects.

Defect Combination 10, PRPD Analysis

Figure 395 shows the graph of the defects in PRPD. There are clearly four clusters visible, so they are distinguishable. However, the shape of the free-moving particle defect is lost, as it looks more like an arc now instead of a triangle. Therefore, floating electrode is distinguishable from free-moving particle; floating electrode is recognizable but free-moving particle is not.

Defect Combination 10, TRPD Analysis

Figure 407 shows the complete TRPD with all the defects together. As already shown, the fewer defects in the graphs, the simpler the TRPD figures become. The two clusters, as will be mentioned in the analysis, are shown in Figure 159.

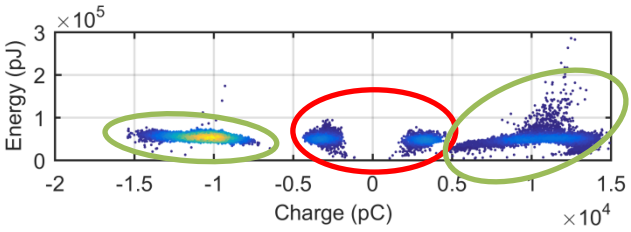

Figure 159: Defect combination 10: TRPD green and red clusters.

The TRPD graph of the green cluster is shown in Figure 160 and of the red cluster in Figure 161.

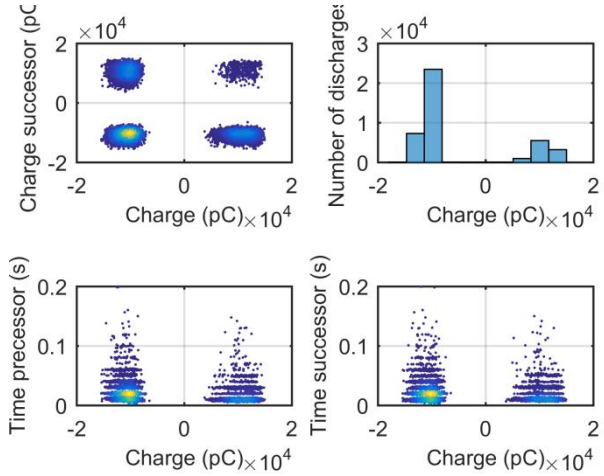

Figure 160: Defect combination 10: TRPD green cluster.

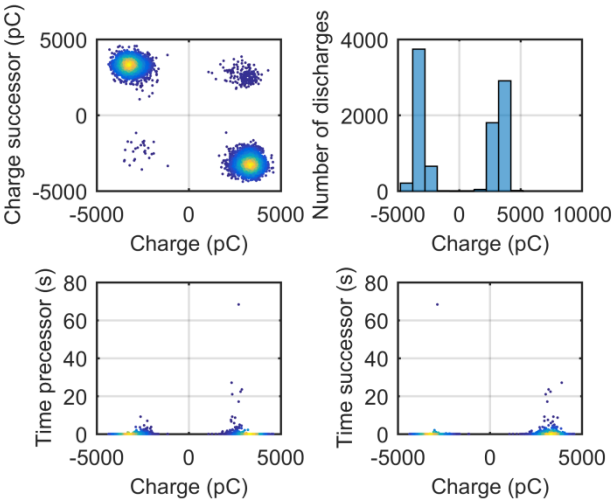

Figure 161: Defect combination 10: TRPD red cluster.

Figure 162 and Figure 163 show the negatively and positively charged pulses from the red cluster. In the graphs of charge-successor versus charge for negatively and positively charged pulses, there is a circle. A circle resembles a defect with origin in internal discharge. However, the magnitudes are comparable to the defects surface discharge and floating electrode. The figure of the time versus charge graph looks like the original defect of floating electrode, because the concentration is centred on the horizontal lines, it is near the x-axis and it is fading vertically and horizontally. The magnitudes are also similar to the original defect.

	Possible origin # 1	**Possible origin # 2**	**Possible origin # 3**
Charge-successor vs. charge	Internal discharge	Floating electrode	Surface discharge
Number of discharges vs. charge	Surface discharge	-	-
Time pre & suc vs. charge	Floating electrode	-	-

Table 39: Defect combination 10, red cluster negatively charged: Summary of TRPD analysis.

	Possible origin
Charge-successor vs. charge	Internal discharge
Number of discharges vs. charge	Surface discharge
Time pre & suc vs. charge	Floating electrode

Table 40: Defect combination 10, red cluster positively charged: Summary of TRPD analysis.

Looking at the analysis above, we can say that the red cluster has origins in either internal discharge, floating electrode or surface discharge.

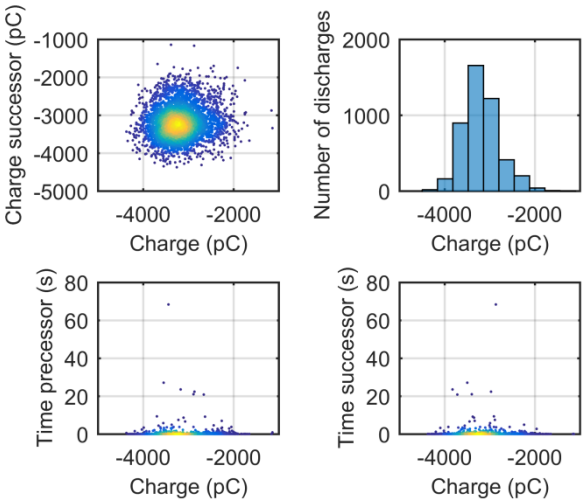

Figure 162: Defect combination 10: TRPD red cluster negatively charged pulses.

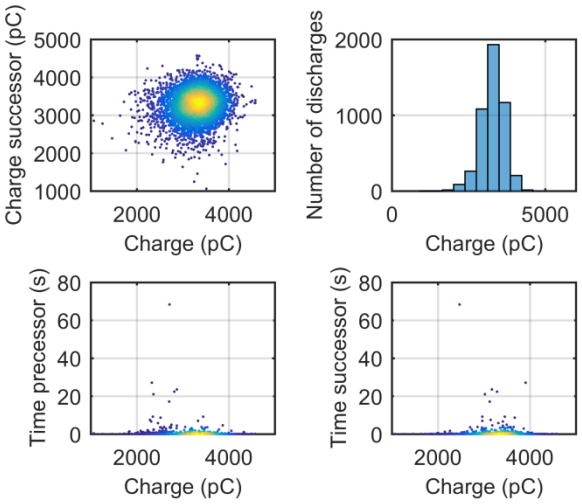

Figure 163: Defect combination 10: TRPD red cluster positively charged pulses.

Figure 164 and Figure 165 show the negatively and positively charged pulses from the green cluster. In the graphs of charge-successor versus charge for negatively and positively charged pulses, there is a square. A square resembles a defect with origin in floating electrode. The time versus charge graphs also have figures that look like a defect with origin in floating electrode.

	Possible origin
Charge-successor vs. charge	Floating electrode
Number of discharges vs. charge	Floating electrode
Time pre & suc vs. charge	Floating electrode

Table 41: Defect combination 10, green cluster negatively charged: Summary of TRPD analysis.

	Possible origin
Charge-successor vs. charge	Floating electrode
Number of discharges vs. charge	Floating electrode
Time pre & suc vs. charge	Floating electrode

Table 42: Defect combination 10, green cluster positively charged: Summary of TRPD analysis.

From the analysis above we can conclude that the green cluster is a defect with origin in floating electrode.

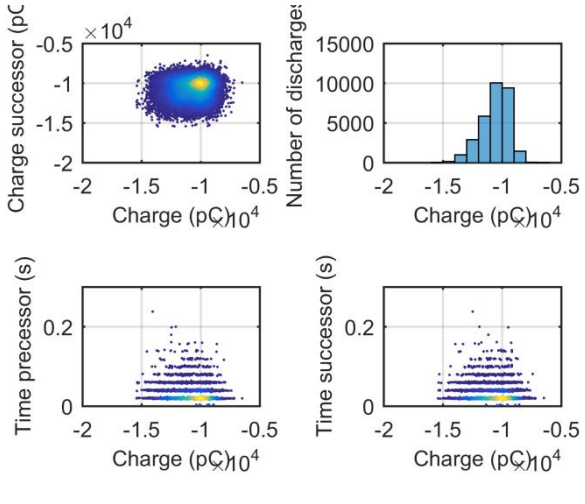

Figure 164: Defect combination 10: TRPD green cluster negatively charged pulses.

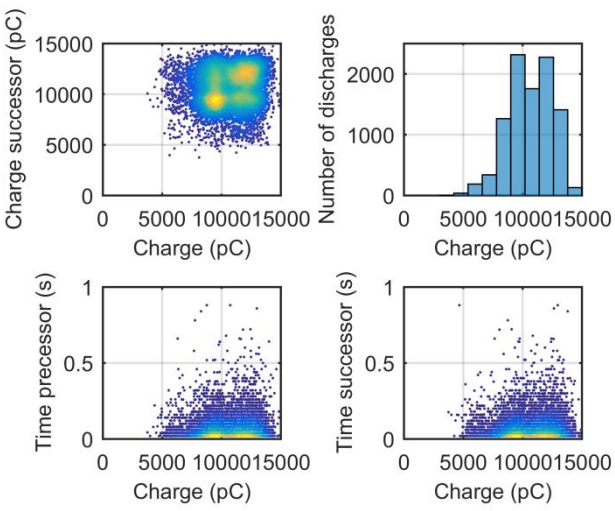

Figure 165: Defect combination 10: TRPD green cluster positively charged pulses.

The green cluster is defined, but the red cluster not. In the PRPD analysis we also saw that there were two clusters, one with origins in floating electrode and one that looks like an internal discharge (arc). The arcs are supposed to be triangles of free-moving particles. Therefore, we can assume that the pulses were not measured properly.

Defect Combination 10, Number of Discharges per Cycle:

The graph of the number of discharges per cycle is shown in Figure 383 in appendix F2.

Average: 1.52 pulses/cycle
Red cluster: 1.96 pulses/cycle
Red positively charged cluster: 1.02 pulses/cycle
Red negatively charged cluster: 1.00 pulses/cycle
Green cluster: 1.27 pulses/cycle
Green positively charged cluster: 1.00 pulses/cycle
Green negatively charged cluster: 1.00 pulses/cycle

This is the same case as in defect combination 6. The numbers of discharges per cycle are too close to each other and therefore cannot be used for defect distinction.

Defect Combination 11: Surface Discharge & Free-Moving Particle

The graphs of this combination of defects are in appendix F below. Each of these graphs is compared with the graphs of the "pure" defects in section 6.1 above:

Defect Combination 11, Time Evolution and Clusters Analysis

Figure 372 shows the time evolution, the cluster Weq vs. Teq and the cluster energy vs. charge. In the cluster Weq versus Teq there are two clusters, so a distinction can be made between the two defects, but not between their polarities. In the cluster energy versus charge there are four clusters, so the defects are distinguishable in origin and polarity.

Defect Combination 11, Energy per Charge vs. Charge

Figure 420 shows the graph of this cluster. The distinguishable clusters have a slope of 0.0012 [pJ/pC], 0.00632 [pJ/pC], 0.06 [pJ/pC] and $1.5 \cdot 10^{-4}$ [pJ/pC].

Defect Combination 11, Rise-time vs. Fall-time

Figure 432 shows the graph of this cluster, where there is no clear distinction possible between the two artificially created defects.

Defect Combination 11, PRPD Analysis

Figure 396 of appendix F3 shows the graph of the defects in PRPD. Only free-moving particle is recognizable; surface discharge is not visible. Therefore, no distinctions can be made.

Defect Combination 11, TRPD Analysis

The graph in TRPD is shown in Figure 408 of appendix F4. The charge-successor versus charge graph has a figure of a triangle, similar to the defect with origin in free-moving particle. The time

versus charge graphs is also similar to the defect with origin in free-moving particle. Positively and negatively charged pulses have similar shapes in this analysis in TRPD.

	Possible origin
Charge-successor vs. charge	Free-moving particle
Number of discharges vs. charge	Free-moving particle
Time pre & suc vs. charge	Free-moving particle

Figure 166: Defect combination 11: Negatively and positively charged pulses.

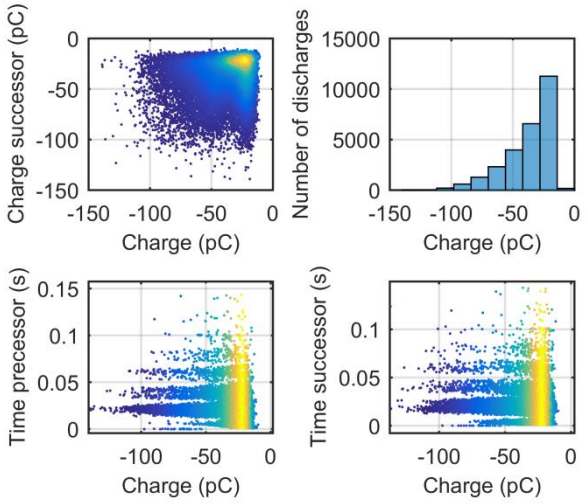

Figure 167: Defect combination 11: Negatively charged pulses.

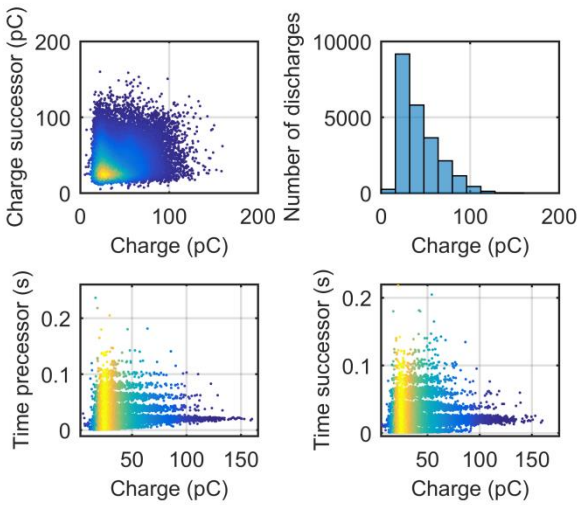

Figure 168: Defect combination 11: Positively charged pulses.

The defect combination 11 has only PDs with origins in free-moving particle. The TRPD analysis provides the same conclusion as PRPD.

Defect Combination 11, Number of Discharges per Cycle

The graph of the number of discharges per cycle is shown in Figure 384 in appendix F2. PRPD and TRPD analysis show that this is a free-moving particle defect, with no other defects present.

Average: 2.32 pulses/cycle
Positively charged pulses: 1.27 pulses/cycle
Negatively charges pulses: 1.41 pulses/cycle

This is the same case as in defect combination 6. The numbers of discharges per cycle are too close to each other and therefore cannot be used for defect distinction.

Defect Combination 12: All 6 Defects

The graphs of this combination of defects are in appendix F below. Each of these graphs is compared with the graphs of the “pure” defects in section 6.1 above. Figure 373 shows the time evolution, the cluster Weq vs. Teq and the cluster energy vs. charge. In the cluster Weq versus Teq there is only one cluster, so no distinctions can be made. In the cluster energy versus charge there are four clusters, so more than one defect is distinguishable in origin and polarity.

Clustering here is more difficult compared to when only one or two defects are being measured. Figure 421 shows the graph of the energy per charge versus charge cluster. Figure 433 shows the graph of the rise-time versus fall-time cluster, where there is no clear distinction possible between the six artificially created defects – not even a distinction between two of them is possible here.

Figure 397 shows the graph of the defects in PRPD. We can recognize a triangle, two horizontal lines, and something that looks like a flatter square. The triangle is within the half cycles. Therefore, we can say that we recognize surface discharge and floating electrode. The flat line is not particularly distinguishable because it is too close to the x-axis, which means it could be corona (positive and negative), internal discharge or free-moving particle. Figure 409 shows the TRPD graphs of all six samples. The graph of the number of discharges per cycle is shown in Figure 385 in appendix F2. Table 43 presents the summary of the defect recognition for the different clusters.

Defects Combinations	Cluster: Weq vs. Teq		Cluster: Energy vs. Charge		Cluster: Energy per Charge vs. Charge	
	Defect recognition	Polarity recognition	Defect recognition	Polarity recognition	Defect recognition	Polarity recognition
12: All 6 Defects	no	no	Not all 6	yes	Not all 6	yes

Table 43: Summary cluster analysis of multiple defects.

7.2. Cluster Detection Comparison

Looking at the summary of the analysis of the different clusters we can conclude that the cluster of Weq vs Teq is less effective in recognizing the clusters compared to the cluster of energy versus charge. Also in the cluster of energy versus the charge we can distinguish between the polarities of the charge which is not possible with the cluster Weq versus Teq. But to be able to distinguish between all of the defects we will need both; as we have seen above sometimes WT-clusters can't distinguish but WT-clusters can.

Aside from this, we tried making clusters using logarithmic scales, to hopefully better see a difference between the defects, but this was not possible. The drawn conclusions from these graphs were too similar to the original graphs.

7.2.1. Clusters Not for Pattern Recognition of Defect Origin

The clusters that use energy in order for the PDs to be clustered cannot be used for recognizing the defect origin, because the energy in the pulse is not constant but rather dependent on the path that the pulse travelled. However, this method is useful for recognizing the origin of the pulse defect. These clusters of energy can be used for making clusters, not for recognizing the defect origins, because the energy of a pulse is not constant. Cables can be represented as a series of inductors and capacitors. This can be done because the E-fields between the conductors can be seen as a capacitance for each length of the pair of conductors, and the H-fields surrounding the conductors can be seen as an inductance. Therefore, the longer the cable, the larger these values will be. A representation of a long cable is shown in Figure 169(a); here the cable is represented as a series of incremental (small) LC elements chained together [31]. As a PD pulse travels through the cable, there will be attenuation. This can be seen schematically in Figure 169(b) and (c), where the pulse attenuation increases as the distance increases (orange to red is increasing distance and attenuation).

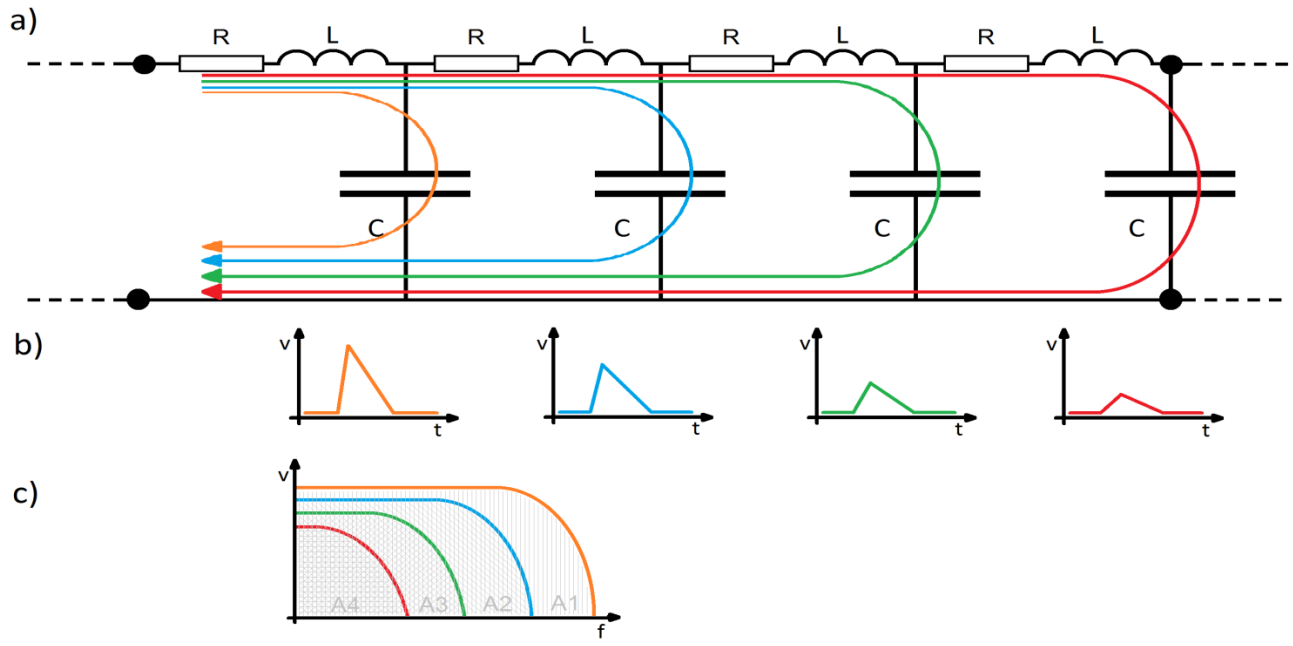

Figure 169: (a) Cable represented as a series of inductors and capacitors; (b) PD pulse attenuation time-domain; (c) PD pulse attenuation frequency-domain.

The amount of F/m and H/m is dependent on the conductor size and shape. The inductance relates the amount of energy stored in the magnetic field around the cable to the current level. The capacitance relates the amount of energy stored in the electric field to the potential difference between the conductors [31]. The energy in a pulse is the area underneath the pulse, as shown in Figure 169(c) as A1 – A4. As can be seen, the energy of the pulse is not constant; it therefore cannot be used for defect origin recognition, only for clustering.

7.3. Summary of PRPD Analysis

The table below presents a summary of the PRPD analysis on two defects (considering that positive and negative corona are one defect). A distinction is made between recognizing a defect, meaning knowing what the defect origin of the cluster is, and distinguishing between defects, meaning being able to distinguish between the number of clusters (defects) that there are.

Defect Combinations	Defect Recognition	Defect Distinction
1: Positive & Negative Corona	Both	Yes
2: Corona & Internal Discharge	None	No
3: Corona & Floating Electrode	Both	Yes
4: Corona & Surface Discharge	Both	Yes (but with Weq vs. Teq)
5: Corona & Free-Moving Particle	Both	Yes
6: Internal Discharge & Floating electrode	Both	Yes
7: Internal Discharge & Surface Discharge	both	Yes (but with Weq vs. Teq)
	No internal discharges are measured.	
8: Internal Discharge & Free-	Free-Moving Particle	No

Moving Particle		
	No internal discharges are measured.	
9: Floating electrode & Surface Discharge	Floating electrode	Yes
10: Floating electrode & Free-Moving Particle	Floating electrode	No
	Arcs are seen for the other electrode, so it looks like internal discharge and not like free-moving particle.	
11: Surface Discharge & Free-Moving Particle	Free-Moving Particle	No
12: All 6 Defects	Surface Discharge & Floating Electrode	3 of 6

Table 44: Summary of PRPD analysis of multiple defects.

7.4. Summary of TRPD Analysis

With the single defect combinations in chapter 4, we saw that there are many ways to distinguish between the defects origins and in the end to differentiate between defects.

Defect Combinations	Defect Recognition
1: Positive & Negative Corona	Both
2: Corona & Internal Discharge	None
	A defect that looks like surface discharge.
3: Corona & Floating Electrode	Floating Electrode
	The cluster of corona does not have enough recorded PD's to make out a proper shape.
4: Corona & Surface Discharge	Both
	The use of Weq vs. Teq cluster detection is needed. A distinction was possible but not for separate charges, because cluster selection was not straightforward here.
5: Corona & Free-Moving Particle	Both
6: Internal Discharge & Floating electrode	Both
7: Internal Discharge & Surface Discharge	Both
	The use of Weq vs. Teq cluster detection is needed. A distinction was possible but not for separate charges, because cluster selection was not straightforward here.
8: Internal Discharge & Free-Moving Particle	Free-Moving Particle
	No internal discharges are measured.
9: Floating Electrode & Surface Discharge	Floating Electrode
	In defect combinations 7-9 the defect recognitions were also not possible with PRPD.
10: Floating Electrode & Free-Moving Particle	Floating Electrode
	There is a second defect recognizable, but the origin of the defect is either floating particle or internal discharge. It should be free-moving particle, but in PRPD arcs are seen that correspond to internal discharge.
11: Surface Discharge	

& Free-Moving Particle	
12: All 6 Defects	

Table 45: Summary of TRPD analysis of multiple defects.

7.5. Summary of Energy Per Charge vs. Charge

Table 46 presents the different slopes of the graphs from the defect combinations; we are looking for any indication of similarity with the original defect to see if the defects are distinguishable by slope for PD origin recognition. The slopes are compared to the values in Table 10 of section 6.1.2 above, which are also shown in Table 46 below.

Defect Combinations	Slope of Individual Defects	Slopes from Multiple Defect Analysis	Relation of Slopes Between Origin Defect and Multiple Defects
1: Positive & Negative Corona	Positive Corona: 0.0214 Negative Corona: 0.0129	$6.67 \cdot 10^{-5}$ 0.1	No relation, completely different magnitude order. Magnitude difference: 10^1 & 10^3
2: Corona & Internal Discharge	Positive Corona: 0.0214 Negative Corona: 0.0129 Internal Discharge: 0.0076 & 0.01	$3.68 \cdot 10^{-4}$ 55	No relation, completely different magnitude order.
3: Corona & Floating Electrode	Positive Corona: 0.0214 Negative Corona: 0.0129 Floating Electrode: $5.938 \cdot 10^{-4}$	$7.5 \cdot 10^{-4}$ $-4.175 \cdot 10^{-4}$ (2x) 0.0032 (2x)	Floating electrode slope was more or less the same (recognizable), but this was not the case for corona discharges.
4: Corona & Surface Discharge	Positive Corona: 0.0214 Negative Corona: 0.0129 Surface Discharge: $1.19 \cdot 10^{-4}$	0.00156 $1.187 \cdot 10^{-5}$ Vertical	No relation, completely different magnitude order.
5: Corona & Free-Moving Particle	Positive Corona: 0.0214 Negative Corona: 0.0129 Free-Moving Particle: 0.00176	254.5 0.00118 $3.368 \cdot 10^{-4}$	No relation, completely different magnitude order.
6: Internal Discharge & Floating Electrode	Internal Discharge: 0.0076 & 0.01 Floating Electrode: $5.938 \cdot 10^{-4}$	$2.04 \cdot 10^{-4}$	Floating electrode slope was more or less the same (recognizable), but this was not the case for internal discharge.
7: Internal Discharge & Surface Discharge	Internal Discharge: 0.0076 & 0.01 Surface Discharge: $1.19 \cdot 10^{-4}$	0.00116 $7.225 \cdot 10^{-5}$	No relation, completely different magnitude order.
8: Internal Discharge & Free-Moving Particle	Internal Discharge: 0.0076 & 0.01 Free-Moving Particle: 0.00176	0.0016	Free-moving particle slope was the same (recognizable), but this was not the case for internal discharge.
9: Floating Electrode & Surface Discharge	Floating Electrode: $5.938 \cdot 10^{-4}$ Surface Discharge: $1.19 \cdot 10^{-4}$	0.016 0.01829 $-3.429 \cdot 10^{-4}$ $-2.286 \cdot 10^{-4}$	Floating electrode slope was more or less the same (recognizable), but this was not the case for surface discharges.
10: Floating Electrode & Free-Moving Particle	Floating Electrode: $5.938 \cdot 10^{-4}$ Free-Moving Particle: 0.00176	$3.2 \cdot 10^{-4}$ $5.3 \cdot 10^{-4}$ $6 \cdot 10^{-4}$ $8 \cdot 10^{-4}$	Floating electrode slope was more or less the same (recognizable), but this was not the case for free-moving particle.
11: Surface Discharge & Free-Moving Particle	Surface Discharge: $1.19 \cdot 10^{-4}$ Free-Moving Particle: 0.00176	0.0012 0.00632 0.06 $1.5 \cdot 10^{-4}$	Surface discharge slope was more or less the same (recognizable), but this was not the case for free-moving particle.

Table 46: Slope relations of energy per charge versus charge.

The only relation that was found was for floating electrode defect, in which the magnitude of the slopes was repeatedly more or less the same (with more or less a mean a factor of 2-3 of difference). Therefore, we can conclude that there is **no relation between the slope of the clusters** (in the graphs of energy per discharge versus charge) **and the sample origins**. This method cannot be used for defect distinction because the slopes are not constant, and to be able to recognize the defect by a slope with the same order of magnitude is not enough – it is not something concrete.

7.6. Renewed Internal Discharge Sample (Aging)

7.6.1. Detection of Aged Sample

What was noticeable in all the analyses of the multiple sample combinations above in Table 43 t/m Table 45 is that nearly every time internal discharge was measured, no distinction could be made. Internal discharge has the same magnitude as free-moving particle, negative corona and positive corona, so magnitude is not the problem. Additionally, the shape (in PRPD) is completely different compared to the rest of the defects. In sample combination 7 the number of PDs measured was extremely low, and in sample combinations 6 and 8 no internal discharge was recorded at all.

In defect combination 2 there are clearly two different types of clusters (cluster A in green and cluster B in red). One has origins in ungrounded metal near the sample, described in section 4.1 above. We can confirm this by looking at the pulse from cluster A (green) of Figure 170, an example of which is shown in Figure 171. Cluster A (green) is therefore identical to the pulses from the disturbance “ungrounded metal near the samples”, as described in section 4.1 above.

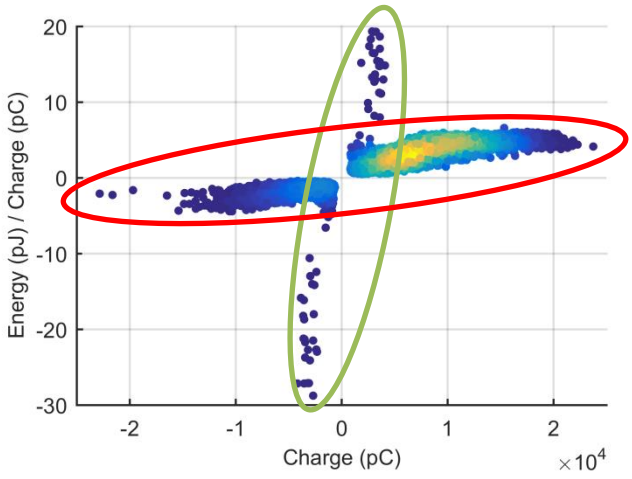

Figure 170: Defect combination 2; energy per charge.

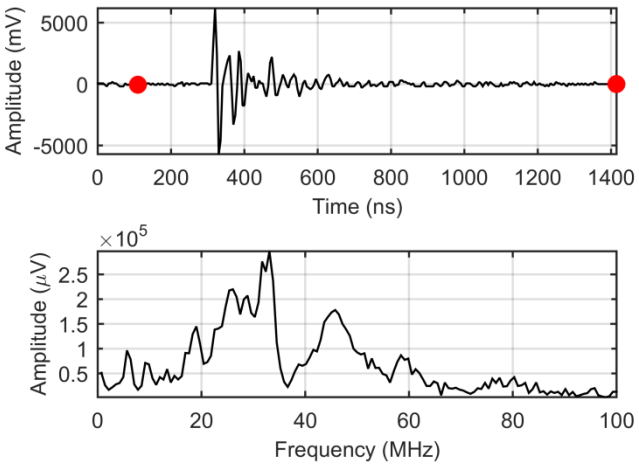

Figure 171: Cluster A (green), pulse 116.

The other cluster (red) has origins in surface discharge. We can confirm this by looking at a pulse from cluster B (red) of Figure 170, for example, pulse 116 shown in Figure 172, and comparing it to the pulses in Figure 79 and Figure 80 of section 6.1 above; the pulses are identical in magnitude, shape, time domain and frequency domain. Cluster B is therefore identical to the surface discharge defect.

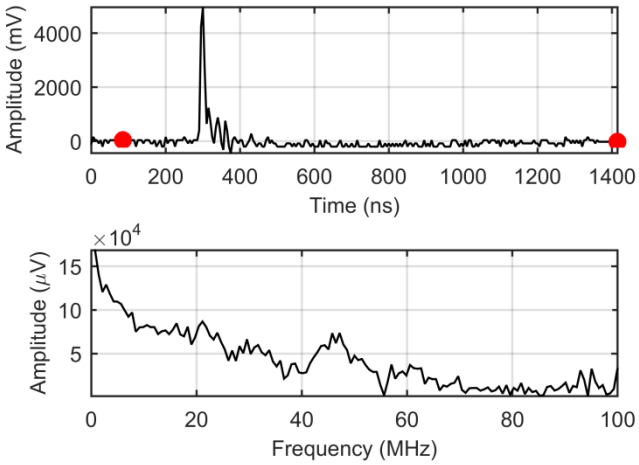

Figure 172: Cluster B, pulse 3922.

Therefore, we can also say that in this defect combination no internal discharge is present. Surface discharge could overlap corona discharge, which could be a reason for it not to be visible. Surface discharge is one of the interferences that can happen easily with internal discharge. Therefore, it can be said that the defect is aged and that the PDIV has likely been raised above 10kV so that no PDs were measured from the internal discharge defect.

The defect has a lifetime of ±1hour (excluding the aging process before PDs occur) with 10kV AC applied on the sample. This lifetime was estimated by adding all the measurement times together and adding an extra 10 minutes (estimated) for the time it took to save the data and for unforeseen extra time when voltage was applied on the sample.

7.6.2. Defect Combinations with Renewed Internal Discharge

Below, the defect combinations with internal discharge are measured again, but this time with the renewed internal discharge.

Defect Combination 2: Corona & Renewed Internal Discharge Sample

The graphs of this combination of defects are in appendix F below. Each of these graphs is compared with the graphs of the "pure" defects in section 6.1 above:

➢ Defect Combination 2 Time evolution and clusters analysis:

Figure 434 of appendix G1 shows the time evolution, the cluster Weq vs. Teq and the cluster energy vs. charge. Below, Figure 173 shows the selected clusters (green and red) that will be used during this analysis.

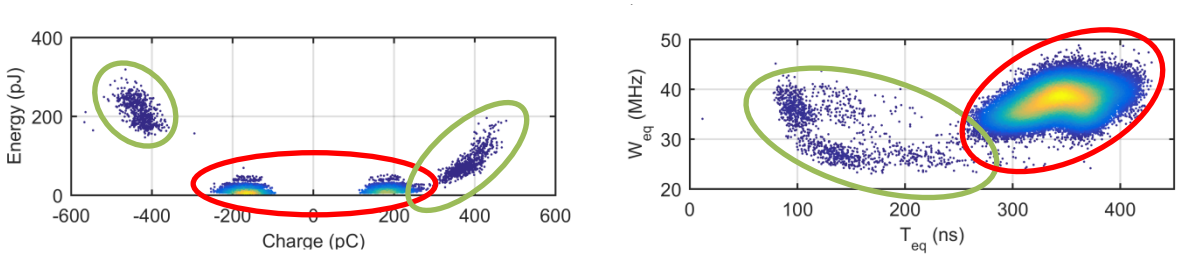

Figure 173: Defect combination 2 (renewed internal discharge sample); Left: Energy versus charge cluster; Right: Frequency-equivalent versus time-equivalent cluster.

➢ Defect Combination 2 PRPD Analysis:

Figure 442 of appendix G3 shows the graph of the defects in PRPD and TRPD. We can clearly see the two defects with different origins. There is one shaped like an arc, which is the internal discharge, and the other is a horizontal line, which resembles positive and negative corona. Both defects are now clearly recognizable and distinguishable.

➢ Defect Combination 2 TRPD Analysis:

Figure 446 of appendix G4 shows the graph of the defects in PRPD and TRPD. The positively and negatively charged pulses of the red cluster are shown in Figure 174 and Figure 175. In the charge-successor versus charge graph there is a shape of a circle, which corresponds to a defect with origins in internal discharge. We must keep in mind that corona discharges also have a circle-like shape, an oval at an angle of 45 degrees. The discharge magnitudes are similar to those of corona discharges. In the graph of time versus charge there are two horizontal lines, with a distance of ±0.017 seconds. This shape is similar to corona discharges.

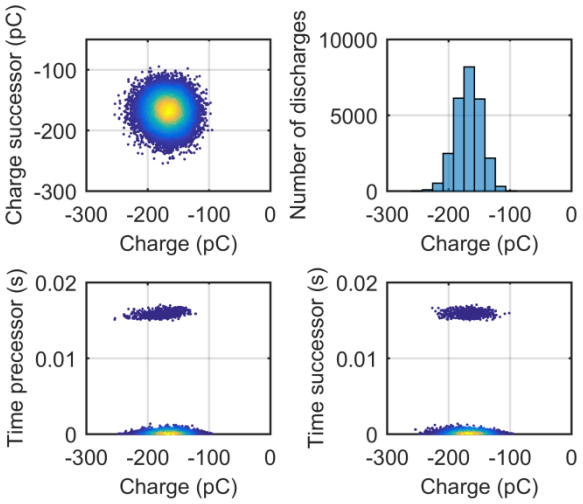

Figure 174: Defect combination 2 with renewed internal discharge sample: TRPD red cluster negatively charged pulses.

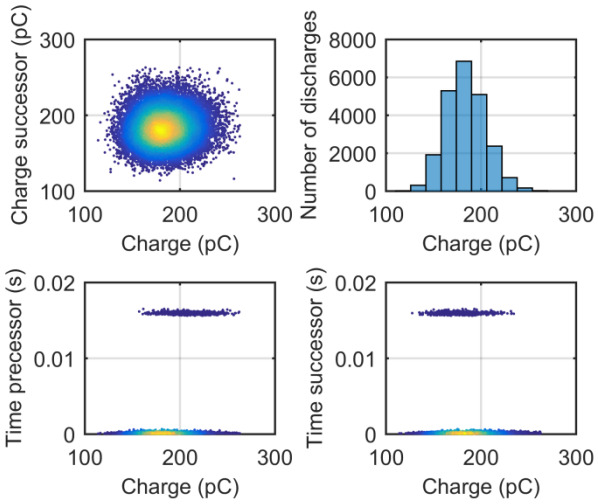

Figure 175: Defect combination 2 with renewed internal discharge sample: TRPD red cluster positively charged pulses.

The positively and negatively charged pulses of the green cluster are shown in Figure 176 and Figure 177. In the charge successor versus charge graph there is a misshapen circle. The time versus charge graphs have a shape of a line around 0.02 seconds, which corresponds to a defect with origins in internal discharge. The charge magnitude is also similar to the original defect of internal discharge. If more pulses of the green cluster were recorded, it would have been easier to recognize the defect.

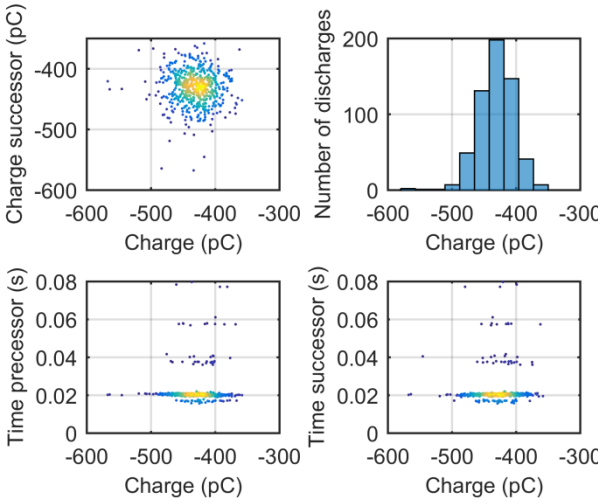

Figure 176: Defect combination 2 with renewed internal discharge sample: TRPD green cluster negatively charged pulses.

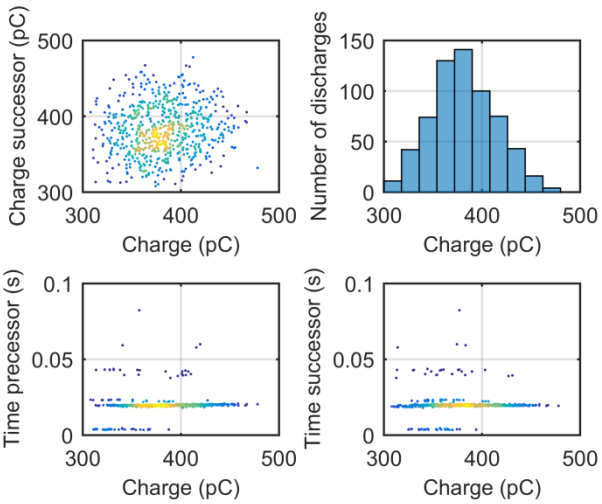

Figure 177: Defect combination 2 with renewed internal discharge sample: TRPD green cluster positively charged pulses.

In the analysis above we saw that the red cluster has origins in corona discharges and the green cluster in internal discharges.

Defect Combination 6: Floating Electrode & Renewed Internal Discharge Sample

The graphs of this combination of defects are in appendix F below. Each of these graphs is compared with the graphs of the “pure” defects in section 6.1 above:

- Defect Combination 6 Time evolution and clusters analysis:

Figure 435 of appendix G1 shows the time evolution, the cluster Weq vs. Teq and the cluster energy vs. charge. There are clearly two different defects; the selected clusters can be seen in Figure 178 (red and green clusters).

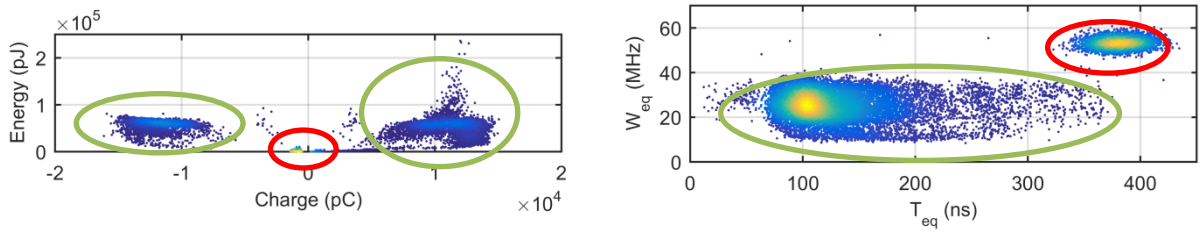

Figure 178: Defect combination 6 (renewed internal discharge sample); Left: Energy versus charge cluster; Right: Frequency-equivalent versus time-equivalent cluster.

➢ Defect Combination 6 PRPD Analysis:

Figure 443 of appendix G3 shows the graph of the defects in PRPD and TRPD. There are clearly two different defects, but the shapes are not clearly visible. Looking at the red (Figure 179) and green (Figure 180) clusters separately in PRPD analysis, we can see that all three shapes look like squares (corresponding to floating electrode). The green cluster has a defect with origins in floating electrode, because the magnitudes are also identical to the original floating electrode defect. The red cluster, on the other hand, has a magnitude of ±2 times larger than the original internal discharge defect. This could be because of the large difference in the magnitudes of internal discharge and floating electrode, and a limited vertical resolution of the oscilloscope could mean that the pulses of the internal discharge defect (smaller in magnitude) are not measured properly.

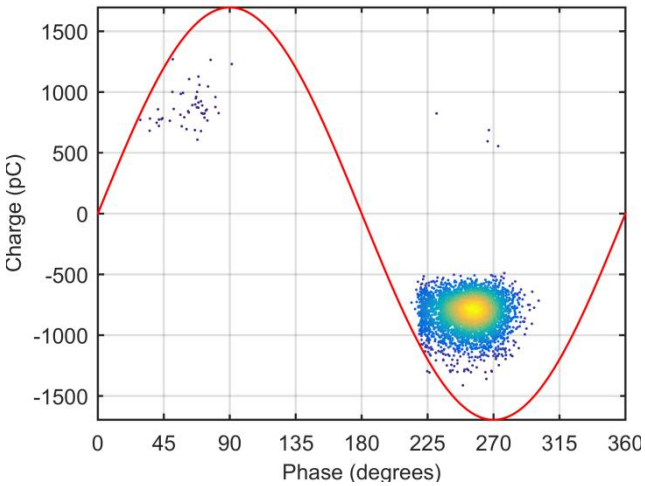

Figure 179: Defect combination 6: PRPD red cluster.

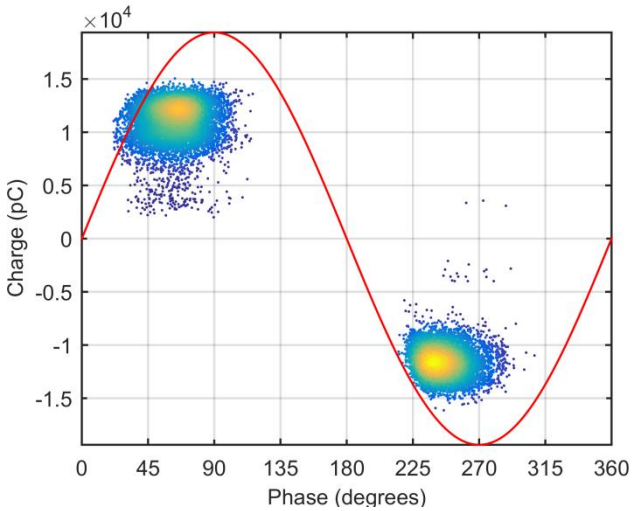

Figure 180: Defect combination 6: PRPD green cluster.

➢ Defect Combination 6 TRPD Analysis:

Figure 447 of appendix G4 shows the graph of the defects in PRPD and TRPD. The two clusters can be seen in Figure 181 (red) and Figure 182 (green). These graphs are difficult to use for defect origin recognition, so we will look at their positively and negatively charged pulses separately.

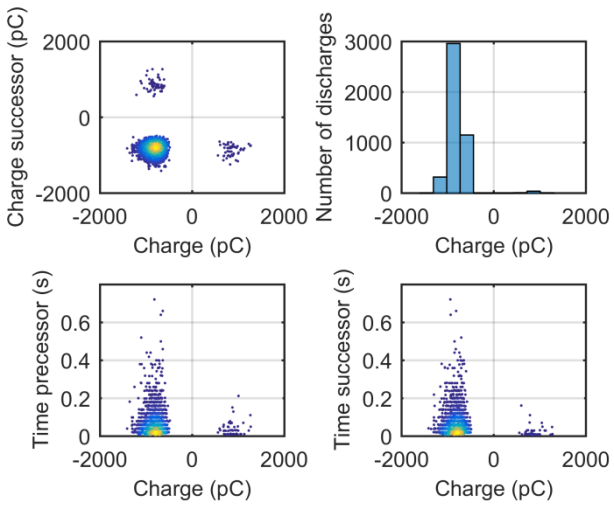

Figure 181: Defect combination 6: TRPD red cluster.

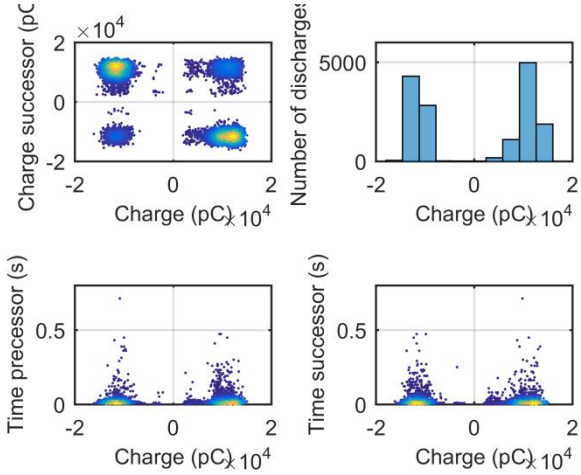

Figure 182: Defect combination 6: TRPD green cluster.

The positively and negatively charged pulses of the green cluster are shown in Figure 183 and Figure 184. In the charge-successor versus charge graphs there is a shape of a square corresponding to the floating electrode defect. The charge magnitudes are also similar to the original defect of floating electrode. In the time versus charge graph there is a triangle shape, with a concentration near the x-axis that fades vertically and horizontally. This shape corresponds to the defect with origins in floating electrode.

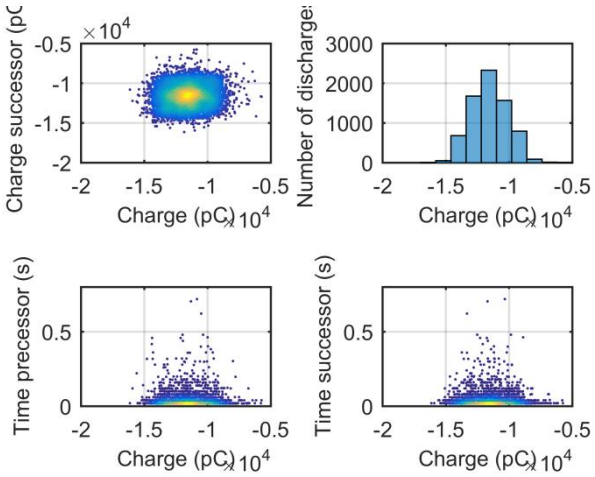

Figure 183: Defect combination 6: TRPD green cluster negatively charged pulses.

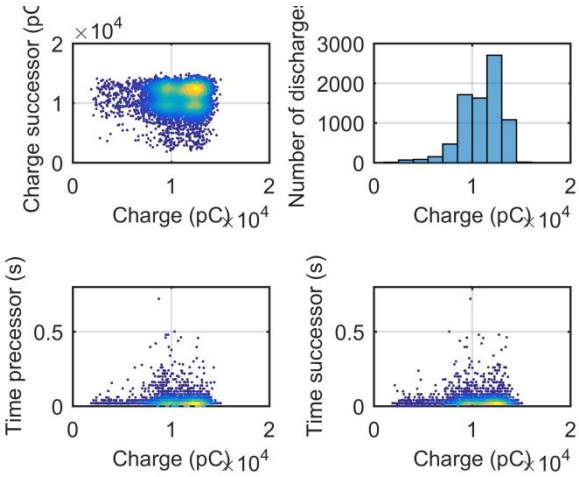

Figure 184: Defect Combination 6: TRPD green cluster positively charged pulses.

The positively and negatively charged pulses of the red cluster are shown in Figure 185 and Figure 186. There are few positively charged pulses recorded in this cluster. They are not enough to distinguish between shapes, so no analysis can be done here. On the other hand, there are enough negatively charged pulses. In the charge-successor versus charge graph there is a shape that looks like a misshapen circle, which corresponds to the defect with origins in internal discharge. The charge magnitudes are similar to the original defect of internal discharge. In the time versus charge graph there is a shape that is similar to that of floating electrode.

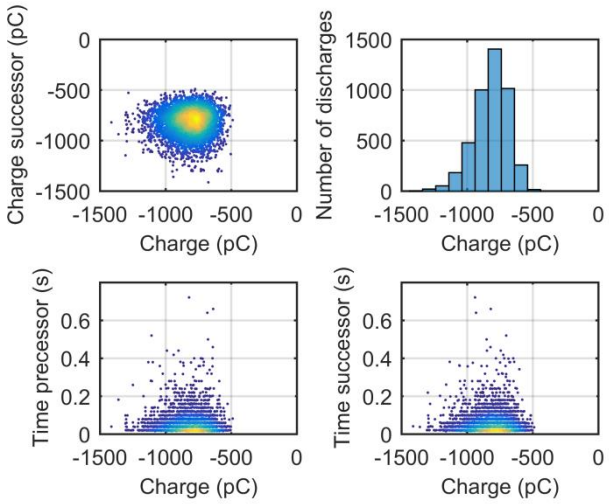

Figure 185: Defect combination 6: TRPD red cluster negatively charged pulses.

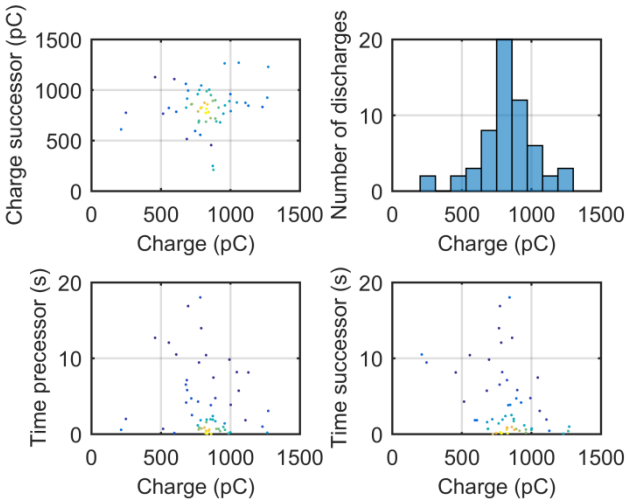

Figure 186: Defect Combination 6: TRPD red cluster positively charged pulses.

Looking at the analysis above we can conclude that the green cluster has origins in the defect floating electrode. This conclusion is similar to the PRPD analysis. With the red cluster, on the other hand, we were not able to identify the origin of this defect. Though the TRPD analysis did not provide a definite answer, it did provide some clues that it should be a defect with origins in internal discharge or floating electrode.

Defect Combination 7: Surface Discharge & Renewed Internal Discharge Sample

There graphs of this combination of defects are in appendix F below. Each of these graphs is compared with the graphs of the "pure" defects in section 6.1 above:

➢ Defect Combination 7 Time evolution and clusters analysis:

Figure 436 of appendix G1 shows the time evolution, the cluster Weq vs. Teq and the cluster energy vs. charge. Below, Figure 187 shows the selected clusters (green and red) that will be used during this analysis.

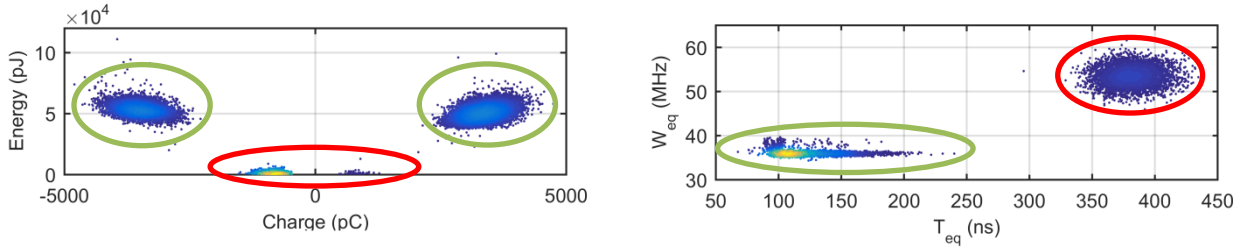

Figure 187: Defect combination 7 with renewed internal discharge; Left: Energy versus charge cluster; Right: Frequency-equivalent versus time-equivalent cluster.

➢ Defect Combination 7 PRPD Analysis:

Figure 444 of appendix G3 shows the graph of the defects in PRPD. There are clearly two defects visible (red and green cluster), and there are also clearly two other clusters that are improperly detected/processed pulses. We will neglect these two clusters because they do not provide any valuable information for the analysis. The red cluster has a square shape in PRPD, which corresponds to floating electrode. Neither of the two clusters (red and green) has the shape of an arc or a triangle, which correspond to the internal and surface discharge samples. The defects are therefore distinguishable but not recognizable in this case.

➢ Defect Combination 7 TRPD Analysis:

Figure 448 of appendix G4 shows the graph of the defects in TRPD. In these graphs, the analysis is difficult, and therefore we will look at each polarity of the cluster separately. The positively and negatively charged pulses of the green cluster can be seen in Figure 188 and Figure 189. In the charge-successor versus charge of the green cluster there is clearly a circle, which corresponds to the internal discharge defect. The charge, on the other hand, is a factor of five larger than the original internal discharge defect. The time-precessor versus charge is zoomed in and the time-successor versus charge is zoomed out. Normally, the internal discharge sample has a shape in these graphs that looks like a horizontal oval with a concentration in the centre. The shape that we see in this graph is similar: the oval shape is stretched out, and multiple oval shapes are stacked on top of each other. None of the other defects has similar a shape, so therefore we can conclude that the defect definitely has origins in internal discharge.

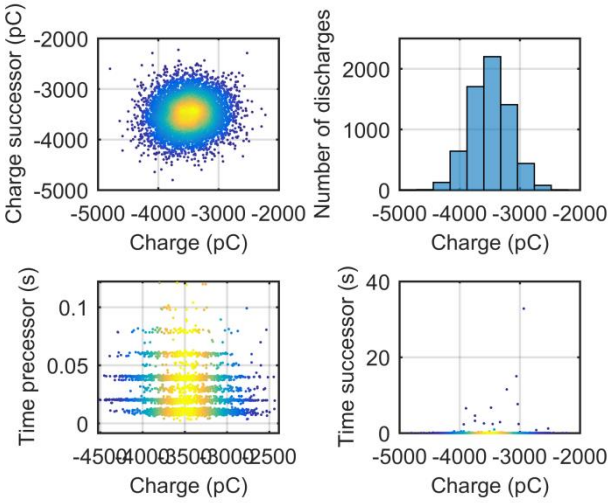

Figure 188: Defect combination 7 with renewed internal discharge sample: TRPD reen cluster negatively charged pulses.

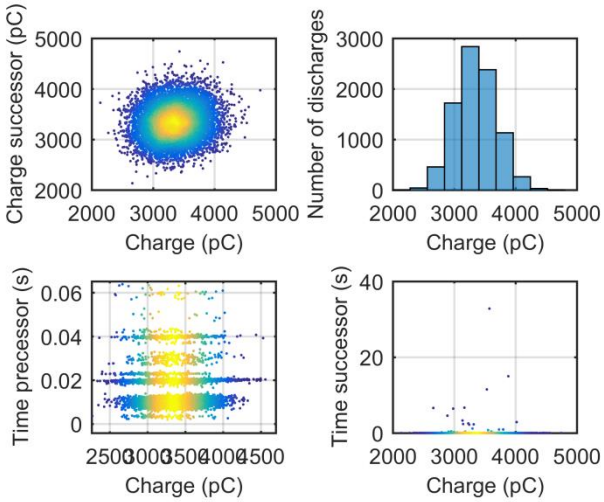

Figure 189: Defect combination 7 with renewed internal discharge sample: TRPD green cluster positively charged pulses.

The positively and negatively charged pulses of the red cluster can be seen in Figure 190 and Figure 191. There are few recorded positively charged pulses for this defect combination, so no analysis can be done on this part. Looking at the negatively charged pulses, there is a triangle shaped like a defect with origins in surface discharge and free-moving particle. The charge magnitudes are ±10 times smaller than the original surface discharge sample, and ±10 times larger than the original free-moving particle sample. The time versus charge graph is shaped like a triangle that looks like a defect with origins in surface discharge. We can now conclude that the red cluster is a defect with origins in surface discharge.

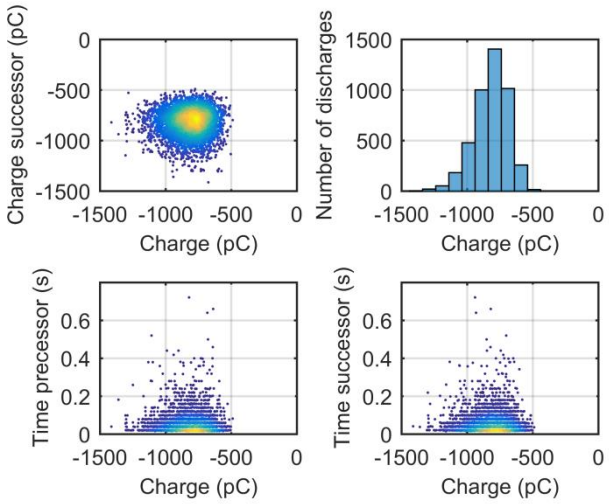

Figure 190: Defect combination 7 with renewed internal discharge sample: TRPD red cluster negatively charged pulses.

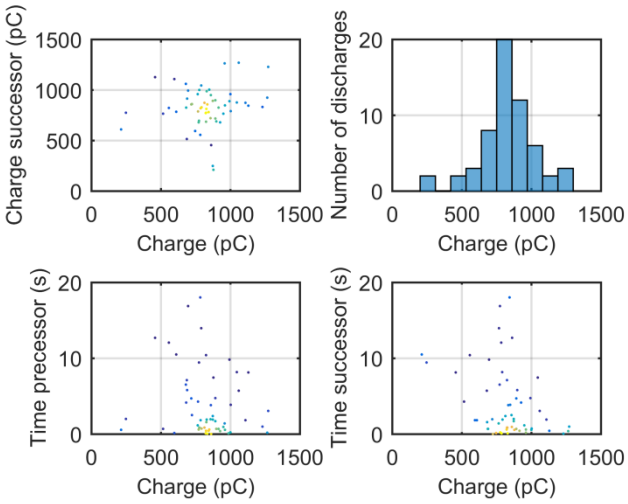

Figure 191: Defect combination 7 with renewed internal discharge sample: TRPD red cluster positively charged pulses.

This is another example in which TRPD analysis provides more information than PRPD analysis. The defect origins are recognizable in this case with TRPD analysis but not with PRPD analysis.

Defect Combination 8: Free-Moving Particle & Renewed Internal Discharge Sample

The graphs of this combination of defects are in appendix F below. Each of these graphs is compared with the graphs of the "pure" defects in section 6.1 above:

➢ Defect Combination 8 Time evolution and clusters analysis:

Figure 437 of appendix G1 shows the time evolution, the cluster Weq vs. Teq and the cluster energy vs. charge. Figure 192 shows the selected clusters (green and red) that will be used during this analysis.

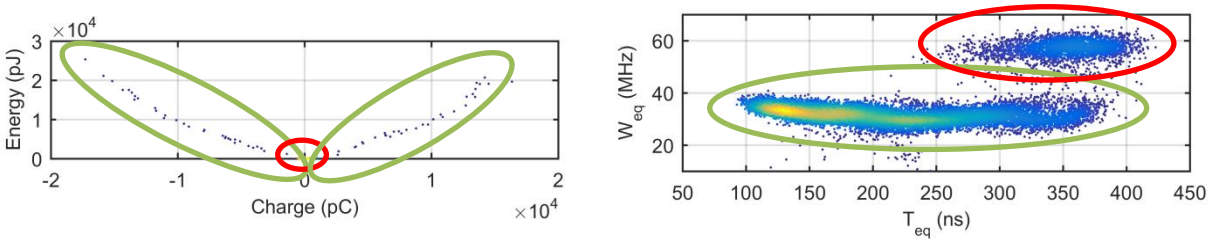

Figure 192: Defect combination 8 with renewed internal discharge; Left: Energy versus charge cluster; Right: Frequency-equivalent versus time-equivalent cluster.

➢ Defect Combination 8 PRPD Analysis:

Figure 445 of appendix G3 shows the graph of the defects in PRPD. In order to be able to distinguish more easily between the defects, we will look at them separately. Figure 193 shows the green cluster in PRPD and Figure 194 the red cluster. The shape of the green cluster is clearly an arc, which resembles a defect with origins in internal discharge. The shape of the red cluster is a triangle similar to that of a defect with origins in free-moving particle.

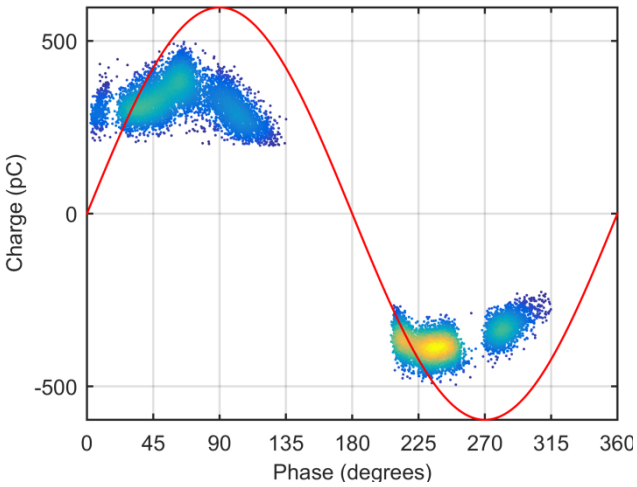

Figure 193: Defect combination 8 with renewed internal discharge sample: PRPD green cluster.

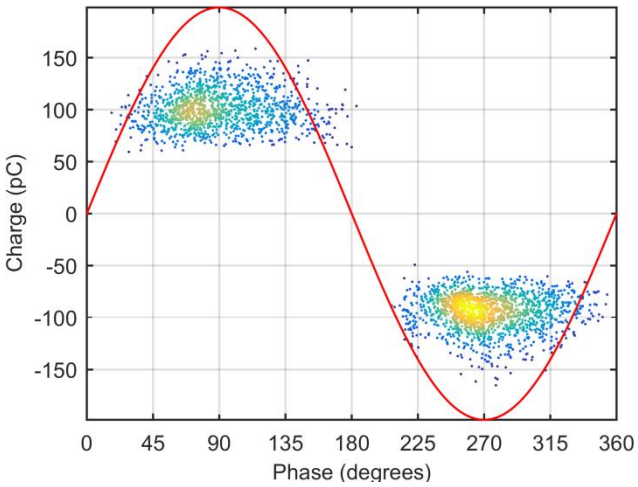

Figure 194: Defect combination 8 with renewed internal discharge sample: PRPD red cluster.

➢ Defect Combination 8 TRPD Analysis:

Figure 449 of appendix G4 shows the graph of the defects in PRPD and TRPD. The positively and negatively charged pulses of the green cluster are shown in Figure 195 and Figure 196. In the green cluster there is a figure of something that looks like a misshapen circle or a misshapen square, which resembles a defect with origins in internal discharge or floating particle. The charge magnitude, however, is similar to that of an internal discharge defect. In the time versus charge graph there are multiple stacked horizontal oval shapes (lines) with the concentration in the centre. These shapes represent a defect with origins in internal discharge.

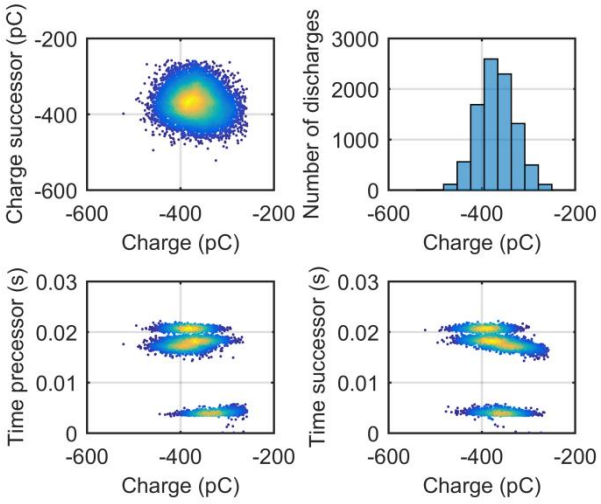

Figure 195: Defect combination 8 with renewed internal discharge sample: TRPD green cluster negatively charged pulses.

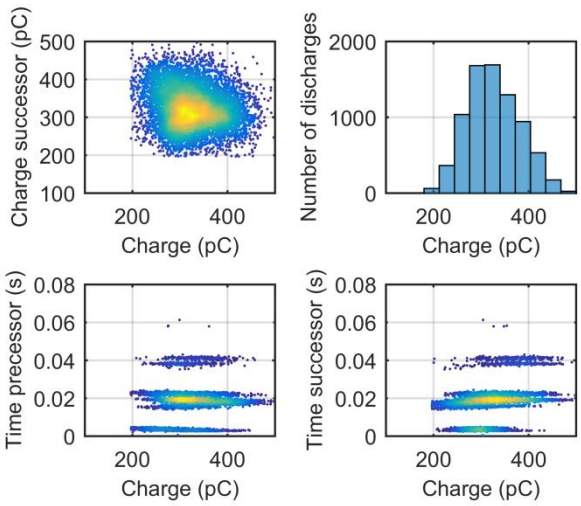

Figure 196: Defect combination 8 with renewed internal discharge sample: TRPD green cluster positively charged pulses.

The positively and negatively charged pulses of the red cluster are shown in Figure 197 and Figure 198. In the charge-successor versus charge graphs there is a triangle with a charge magnitude similar to the defect with origins in free-moving particle. The time versus charge graph shows a triangle shape that is similar to a defect with origins in free-moving particle and in floating electrode. To make a conclusion here would be a bit confusing, because the negatively charged pulses clearly show a defect with origins in free-moving particle and the positively charged pulses show a defect that could have origins in both floating electrode and

in free-moving particle. However, since the defect free-moving particle is recognizable at least somewhat nearly everywhere, we can say that the defect has origins in free-moving particle.

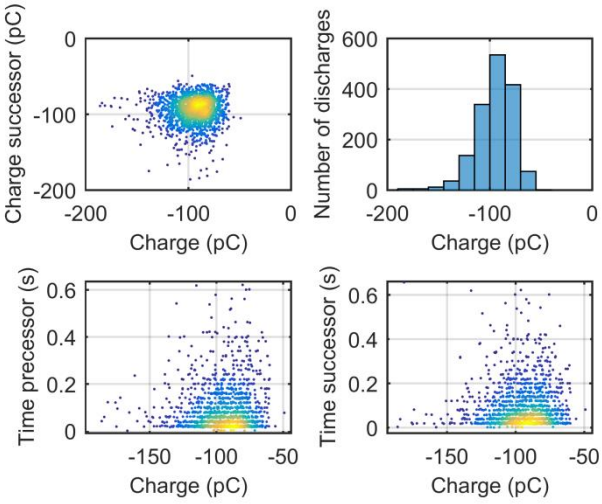

Figure 197: Defect combination 8 with renewed internal discharge sample: TRPD red cluster negatively charged pulses.

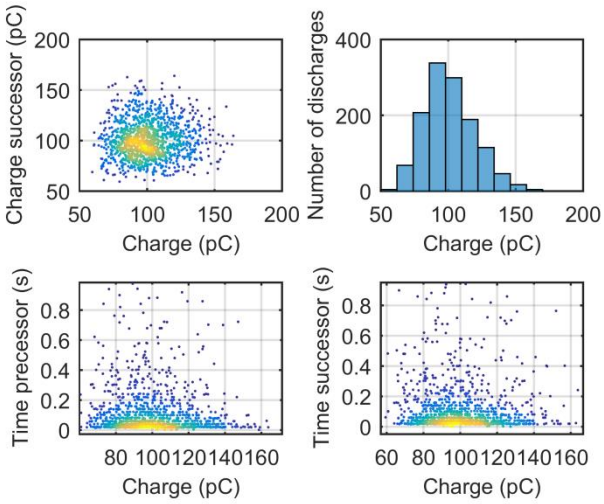

Figure 198: Defect combination 8 with renewed internal discharge sample: TRPD red cluster positively charged pulses.

7.7. Results and Evaluation of Multiple Sample Analysis

This section provides a brief summary the conclusions drawn in this chapter while analysing the multiple sample combinations. Some of these conclusions are also either verifications or contradictions of the conclusions drawn in chapter 4. Here, conclusions will be drawn about the magnitudes, clusters, TRPD analysis, number of discharges per cycles and the lifetimes of the artificially created defects.

7.7.1. Magnitudes

In section 6.3 above we assumed that some of the defects are distinguishable by magnitude. However, this was not always the case, because the oscilloscope used cannot record both PDs with a large difference in magnitude properly; the vertical resolution is limited. The resolution of the oscilloscope is not large enough, and instead of an 8-bit we should use a 12- or 24-bit vertical resolution oscilloscope.

7.7.2. Clusters

During the analysis of the PDs we used five types of clustering techniques:

- Frequency-equivalent vs. time-equivalent
- Energy vs. charge
- Energy vs. charge (in logarithmic scale)
- Energy per charge vs. charge
- Rise-time vs, fall-time

The cluster rise-time versus fall-time was not able to distinguish between any of the artificially created defect combinations. This could have been due to the uniformly created PD test platform (equal path length); therefore, if the defects were not located at the same distance and were placed further from each other, it might have been possible to distinguish defects using this cluster.

None of these clusters could identify the defect (make a separate cluster) on its own for all defects. The clustering techniques of energy versus charge, energy versus charge in logarithmic

scale and energy per charge versus charge are similar in making clusters (they differentiate between the same cluster combinations). The only difference is the shape and slope of the cluster itself. The defect combinations 1, 3 and 9 are only distinguishable with the clustering technique of energy versus charge. The defect combinations 4 and 8 (renewed internal discharge sample) are only distinguishable with the use of the clustering technique of frequency-equivalent versus time-equivalent. The defect combinations 5, 2 (renewed internal discharge sample) and 10 are distinguishable by both, frequency-equivalent versus time-equivalent and energy versus charge, clustering techniques. Defect combinations 6 and 7 are an exception; they were recognized by both and also not recognizable by both (looking at the defect combination with and without the renewed internal discharge sample). Therefore, we can say that we clearly need both, frequency-equivalent versus time-equivalent and energy versus charge, clustering techniques to differentiate between all the defects.

Therefore, we can conclude with the analysis conducted above that for making clusters (defect distinction) we cannot use only one of the two described methods. We need a minimum of two clustering techniques to be able to distinguish between all the defect combinations, e.g. the clustering technique of frequency-equivalent versus time-equivalent and energy versus charge.

None of these clustering techniques can be used for PD defect origin recognition in the aspect of shapes and magnitudes. Looking at the clustering technique of energy per charge versus charge, we can conclude that the slopes of these figures cannot be used for defect origin recognition, because the slopes are not constant for each individual defect.

7.7.3. PRPD vs. TRPD

It would be useful to know that we can detect the origin of the defect by using TRPD analysis, because then there is no need to synchronize the measured PDs with the phase signal. As a consequence, the final product can be cheaper and much simpler, compared to the final product that uses PRPD analysis. With final product I mean the PD measuring instrument that can detect the PD defect type, location, etc. and can be used in practice.

We saw that when analysing data from multiple sample combinations with the use of TRPD analysis, the defects were recognizable. The TRPD analysis originally provided complex figures, but when the TRPD analysis was plotted with the charge polarity separated the figures became much simpler. With these simpler shapes we could also recognize the defect origins.

Additionally, when looking at the graphs of time between the discharges versus charge, we sometimes saw horizontally stacked lines, which can be used for defect origin distinction/separation. The distance between the defects is constant but the thickness of the horizontal lines is not; it depends on the number of pulses recorded.

In the TRPD analysis, when looking at the graph of the number of discharges versus charge, the slopes of the graph cannot be used for defect recognition, because the slopes change significantly. However, the charges can be used as an indication for defect recognition.

In TRPD analysis conducted above we saw that even if there is a disturbance present, we only need to recognize the defects in one of the charge polarities to be able to recognize the defect origin.

Based on the analysis conducted above, we can say that TRPD analysis is as good or even better than PRPD analysis when analysing the data for defect origin recognition. This is because the TRPD analysis provides the same results, compared to the PRPD analysis, when the pulses of the defects were or were not properly measured (e.g. defect combinations 2, 6 and 8). In some cases the TRPD analysis provided even more information compared to the PRPD (e.g. defect combination 6 with renewed internal discharge sample). TRPD analysis can also sometimes

recognize defects in cases that PRPD analysis cannot (e.g. defect combination 7 with renewed internal discharge sample).

It was not always easier to recognize the defect in TRPD analysis (e.g. defect combination 2 with renewed internal discharge sample). In this case, the internal discharge sample was easily recognizable by the shape of an arc in the PRPD analysis, but with TRPD the pulses were just barely enough to be able to determine the defect origin.

7.7.4. Number of Discharges per Cycle

The number of discharges per cycle cannot be used for defect distinction. When combining multiple samples, the number of pulses per cycle of each individual defect is affected by the other defects. The number of discharges per cycle can sometimes be used to make a distinction between positive corona, negative corona and all the other types of discharges. However, this is irregular and not always possible. Therefore, we can conclude that the number of discharges per cycle cannot be used for defect distinction.

8. PD Pattern Recognition

From the conclusions drawn in the previous chapter, we see that the easiest way to recognize the PD origin is by differentiating between the shapes of the different artificial defects in TRPD analysis when separating the charge polarities. When the charge polarities are separated, the shapes of the graphs become very simple.

There are different ways of using these shapes for recognizing their origins. In the following section an idea for PD shape recognition is proposed, including the use of edge detection. Afterwards the shapes are characterized for each artificial defect, checked for their consistency, to see if they are constant and can actually be used for defect origin/source recognition. In the end a flowchart is presented on how to recognize each PD defect origin with the proposed shapes.

8.1. Edge Detection

For recognition of the original shapes we can make use of the edges of the data. After edge detection, we will try to match the known shapes to the data. We will also rotate, centre, flip, resize and reflect vertically and horizontally to see what matches the data best. As an illustration an example is give: Figure 199 presents an example of negatively charged pulses of surface discharge. Figure 199(a) shows the edges of the data. The y- and x-axis have a minimum and a maximum, shown in red. Graphs (b) t/m (f) of Figure 199 show how we placed all the possible shapes within the minimum and maximum borders. Figure 199(b) and (f) have the best fit compared to the rest. These best-matched shapes are resized, rotated and centred, and the result can be seen in Figure 200.

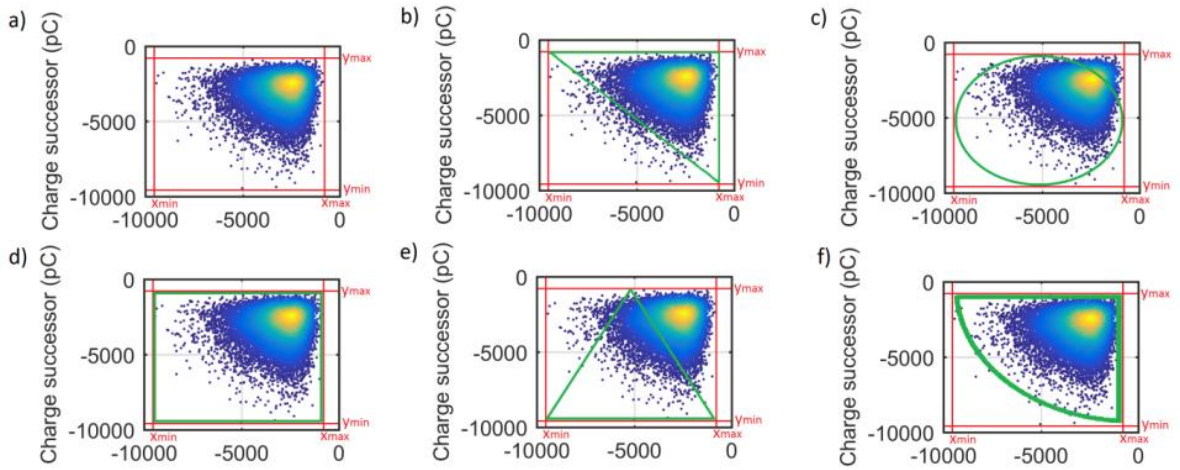

Figure 199: Edge detection and shape matching.

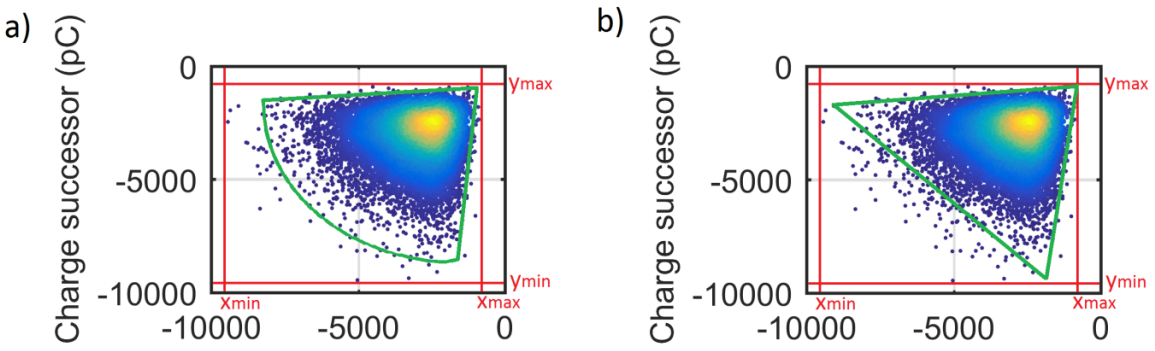

Figure 200: Shape matching (resizing, centring, rotating, flipping, reflecting and cropping).

Comparing Figure 200(a) and (b), the shape of (b) has a better fit than (a). For this method to actually work, the shapes of all the artificially created defects, all the different PD types, have to be characterized and checked for consistency.

8.2. Shape Characterization

As demonstrated in chapter 4 above, the shapes of the graphs of the number of discharges versus charge are not constant. Therefore, this graph will not be used for the individual defect shape characterization. Chapter 4 above also showed that the graphs of time-precessor versus charge are identical to time-successor versus charge. Therefore, we will consider only the time-precessor versus charge graph when characterizing the shapes of the defects.

Because of the simpler shapes and shape differences (as shown in chapter 4 above) when looking at the positively and negatively charged pulses separately, we will also make a distinction between the positively and negatively charged pulses when characterizing the shapes of the individual defects.

8.2.1. Shape Characterization of Negatively Charged Pulses

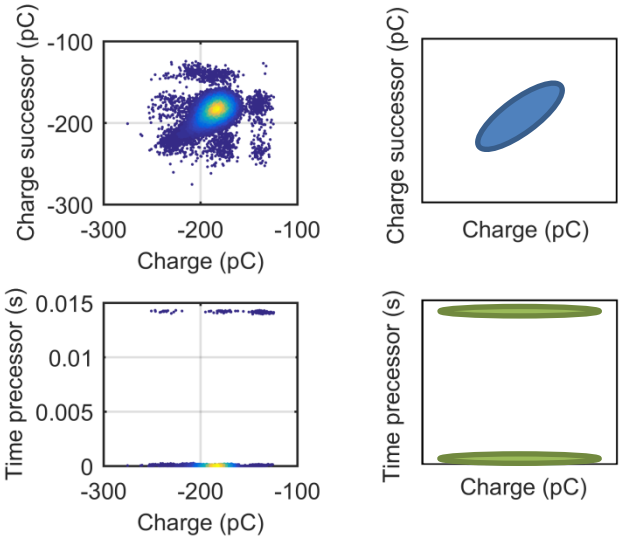

Figure 201: Positive corona, shapes of negatively charged pulses.

Figure 201 shows the shapes of the positive corona defect with negatively charged pulses.

Blue:
Oval-shaped at an angle of 45^0.

Green:
Two lines.

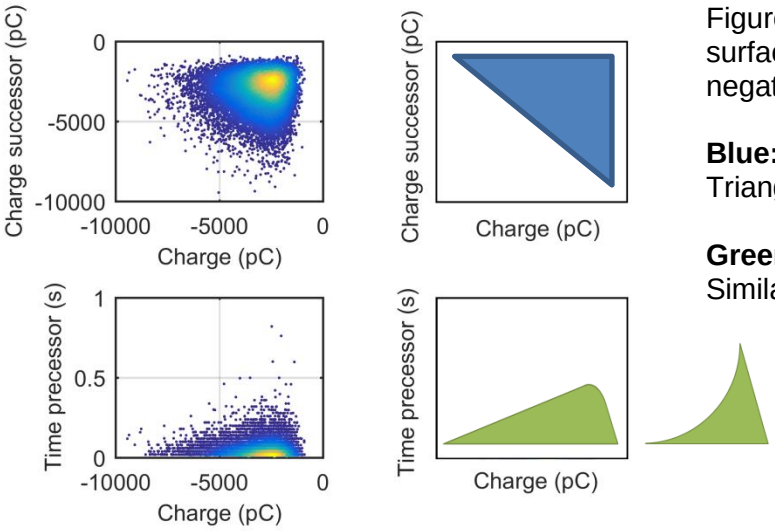

Figure 202: Surface discharge, shapes of negatively charged pulses.

Figure 202 shows the shapes of the surface discharge defect with negatively charged pulses.

Blue:
Triangle with 90^0 corner at 0-crossing.

Green:
Similar to a triangle shape.

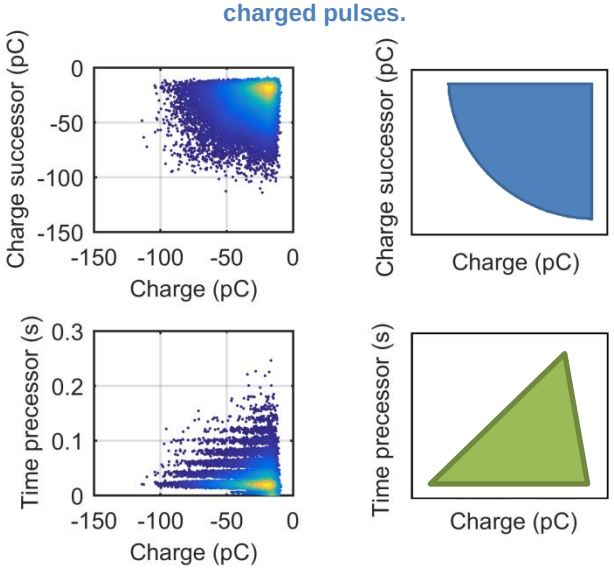

Figure 203: Free-moving particle, shapes of negatively charged pulses.

Figure 203 shows the shapes of the free-moving particle defect with negatively charged pulses.

Blue:
Similar to a triangle shape with 90^0 corner at 0-crossing.

Green:
Triangle shape.

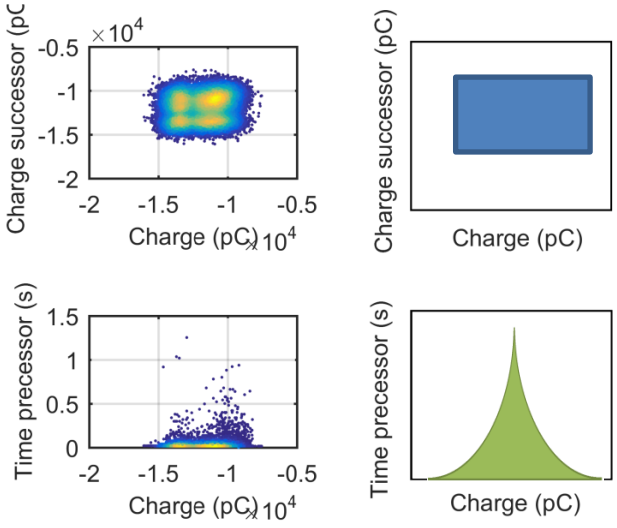

Figure 204: Floating electrode, shapes of negatively charged pulses.

Figure 204 shows the shapes of the floating electrode defect with negatively charged pulses.

Blue:
Rectangle.

Green:
Similar to a triangle shape.

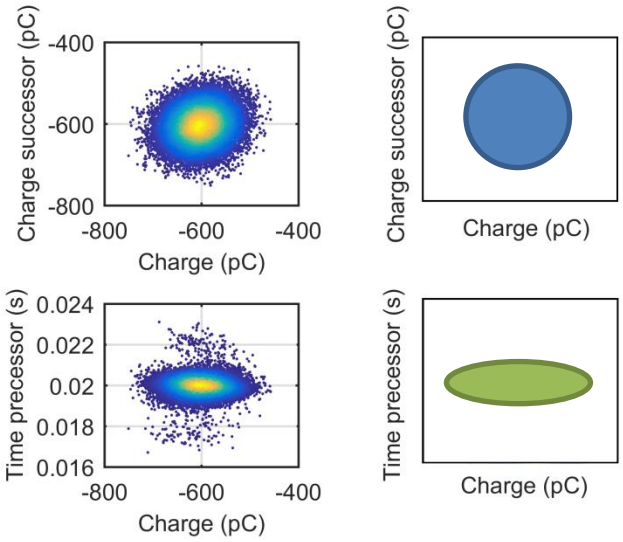

Figure 205: Internal discharge, shapes of negatively charged pulses.

Figure 205 shows the shapes of the internal discharge defect with negatively charged pulses.

Blue:
Circle.

Green:
Horizontal oval.

8.2.2. Shape Characterization of Positively Charged Pulses

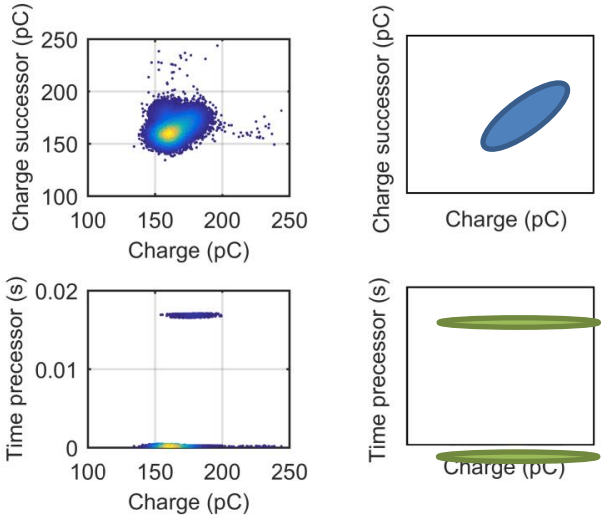

Figure 206: Negative corona, shapes of positively charged pulses.

Figure 206 show the shapes of the negative corona defect with positively charged pulses.

Blue:
Oval-shaped at an angle of 45^0.

Green:
Two lines.

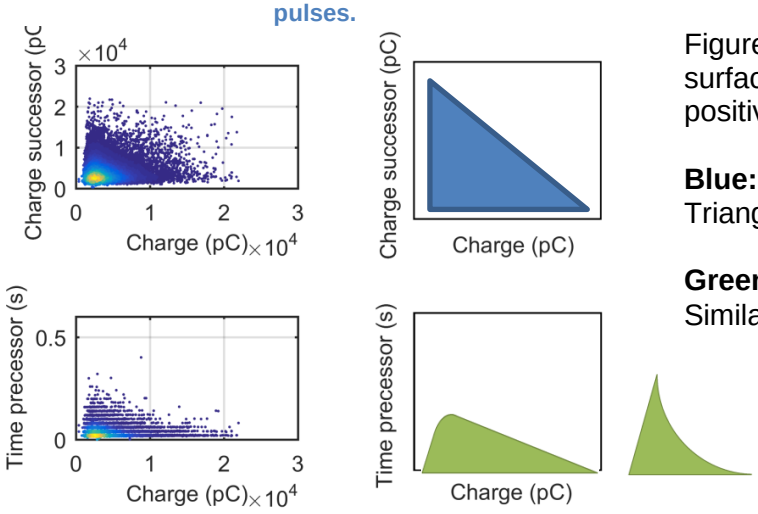

Figure 207: Surface discharge, shapes of positively charged pulses.

Figure 207 shows the shapes of the surface discharge defect with positively charged pulses.

Blue:
Triangle with 90^0 corner at 0-crossing.

Green:
Similar to a triangle shape.

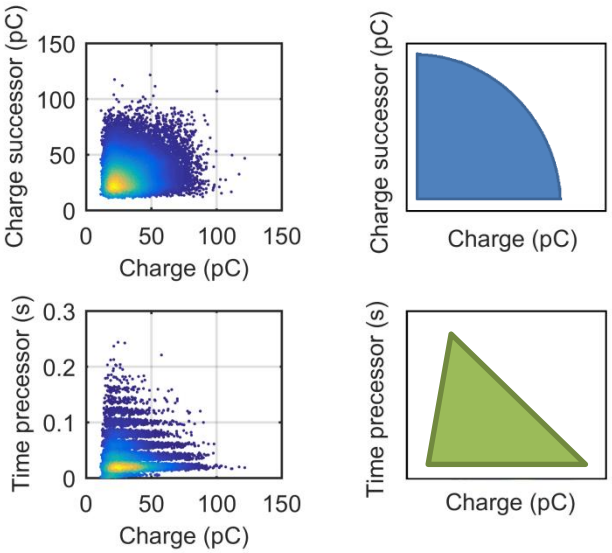

Figure 208: Free-moving particle, shapes of positively charged pulses.

Figure 208 shows the shapes of the free-moving particle defect with positively charged pulses.

Blue:
Similar to a triangle shape with 90^0 corner at 0-crossing.

Green:
Triangle shape.

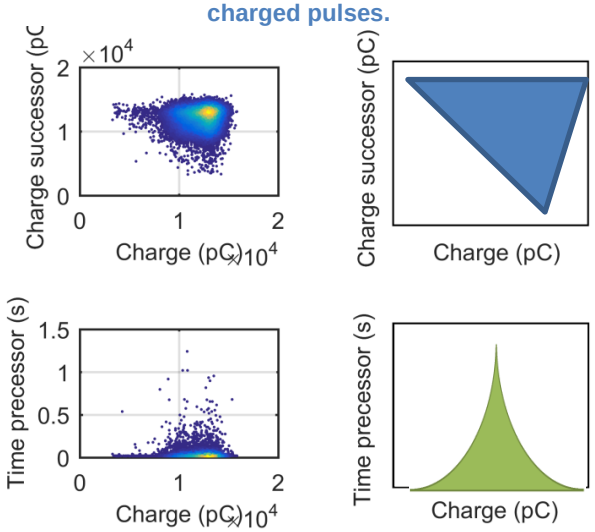

Figure 209: Floating electrode, shapes of positively charged pulses.

Figure 209 shows the shapes of the floating electrode defect with positively charged pulses.

Blue:
Triangle.

Green:
Similar to a triangle shape.

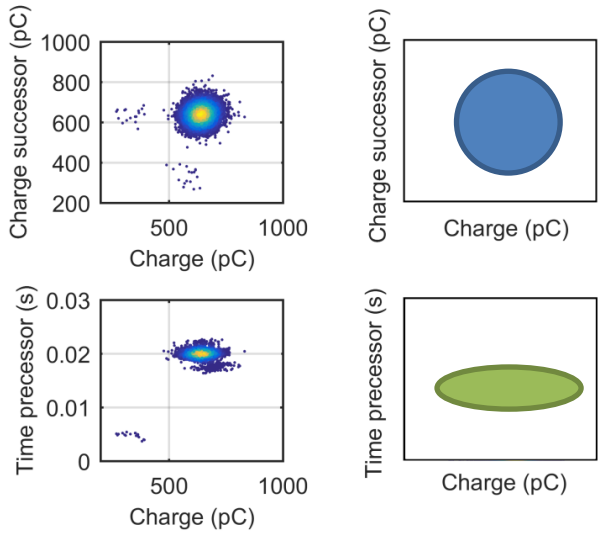

Figure 210: Internal discharge, shapes of positively charged pulses.

Figure 210 shows the shapes of the internal discharge defect with positively charged pulses.

Blue:
Circle.

Green:
Horizontal oval.

8.2.3. Summary of Shape Characterization

	Charge Polarity	Qsuc vs. Q	Tpre vs. Q
Negative Corona	-Q	-	-
Positive Corona	-Q		
Surface Discharge	-Q		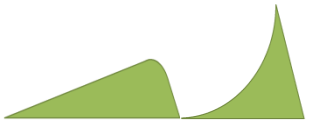
Free-Moving Particle	-Q		
Floating Electrode	-Q		
Internal Discharge	-Q		

Table 47: Shapes for recognition of negatively charged artificially created defects.

	Charge Polarity	Qsuc vs. Q	Tpre vs. Q
Negative Corona	+Q		
Positive Corona	+Q	-	-
Surface Discharge	+Q	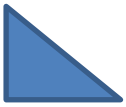	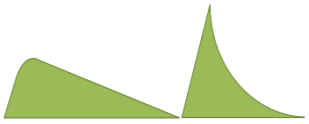
Free-Moving Particle	+Q		
Floating Electrode	+Q		
Internal Discharge	+Q		

Table 48: Shapes for recognition of positively charged artificially created defects

8.3. Consistency of Characterized Shapes

In section 8.2 above we characterized all the shapes of the artificial defects (samples) of the TRPD patterns with the charge polarities separated. To be sure that these shapes can be used for pattern recognition, we will consider different measurements done with the artificial defects (samples) to see if the shapes are constant. The charge polarities are considered separately since the shapes will be compared to the other artificially created defects (samples) of the same polarity. Each artificial defect polarity has its own assigned shape; if needed, the shaped can be adjusted if it is not consistent.

8.3.1. Negatively Charged Pulses

We will first address the shape consistency of all the negatively charged PD pulses for each artificially created defect.

Negative Corona

Negative corona do not have any negatively charged pulses, so no consistency check could be conducted here.

Positive Corona

The shape that will be used for recognition of the artificial defect positive corona is shown in Table 47 of section 8.2 above, including the second samples for internal discharge and floating electrode defects.

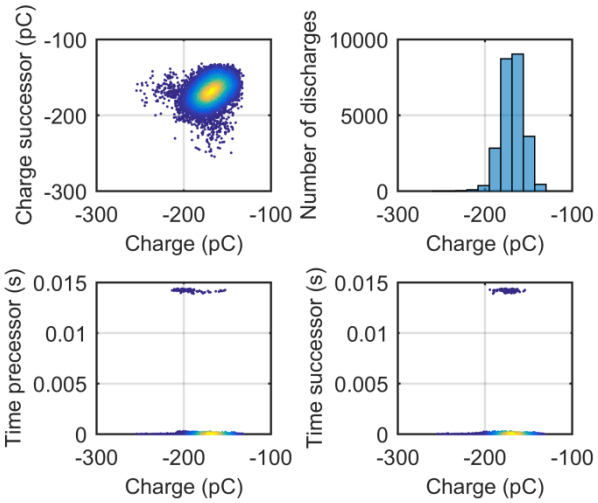

Figure 211: Negatively charged pulses: Positive corona, consistency check 1.

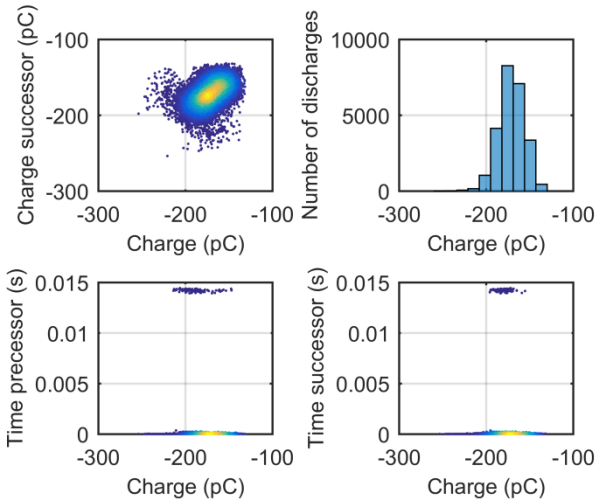

Figure 212: Negatively charged pulses: Positive corona, consistency check 2.

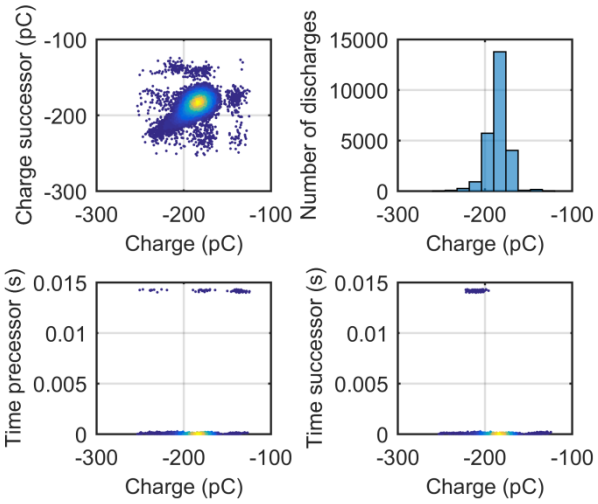

Figure 213: Negatively charged pulses: Positive corona, consistency check 3.

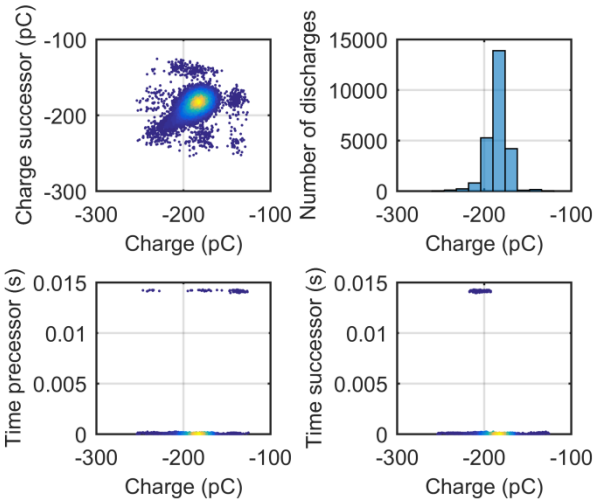

Figure 214: Negatively charged pulses: Positive corona, consistency check 4.

As shown in Figure 211 t/m Figure 214, the shape remains the same: it is a misshapen circle/oval (at an angle of 45 degrees) for the Qsuc vs. Q (charge-successor versus charge) graph and two horizontal lines for the Tsuc vs. Q (time-precessor versus charge) graph. These findings are similar to those from section 8.2.

Internal Discharge

The shape that will be used for recognition of the artificial defect internal discharge is found in Table 47 of section 8.2 above.

Internal Discharge Sample I: Based on the layers of dielectric material (see section 5.3.1):

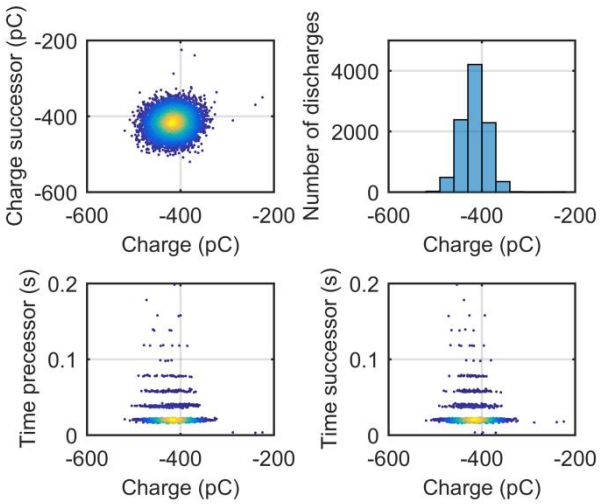

Figure 215: Negatively charged pulses: Internal discharge sample 1, consistency check 1.

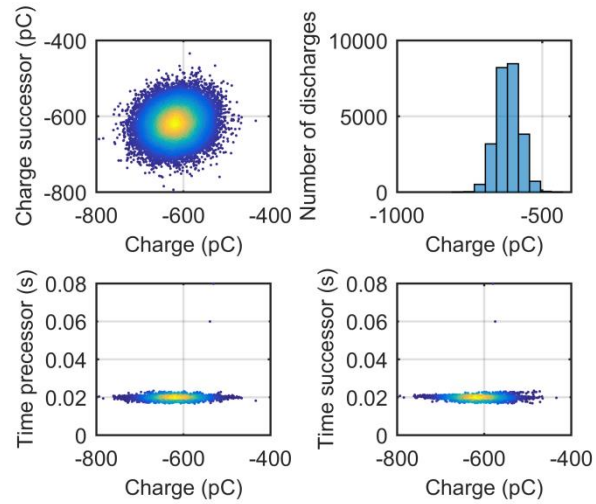

Figure 216: Negatively charged pulses: Internal discharge sample 1, consistency check 2.

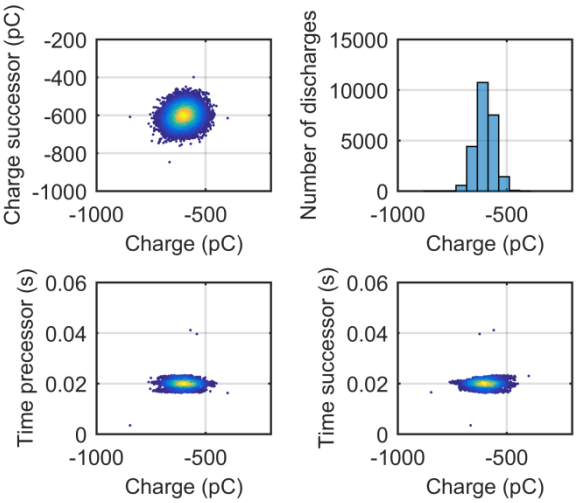

Figure 217: Negatively charged pulses: Internal discharge sample 1, consistency check 3.

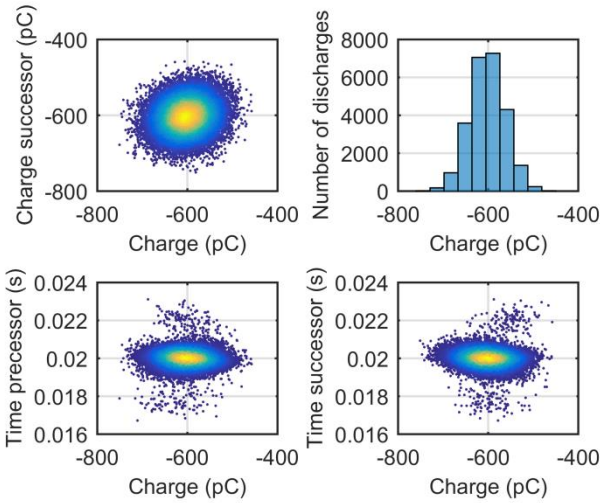

Figure 218: Negatively charged pulses: Internal discharge sample 1, consistency check 4.

As shown in Figure 215 t/m Figure 218, the shape remains the same: a circle for the Qsuc vs. Q (charge-successor versus charge) graph and a (horizontal) oval for the Tsuc vs. Q (time-precessor versus charge) graph.

Internal Discharge Sample II: Based on the void on the bottom of the glass jar (see section 5.2.1):

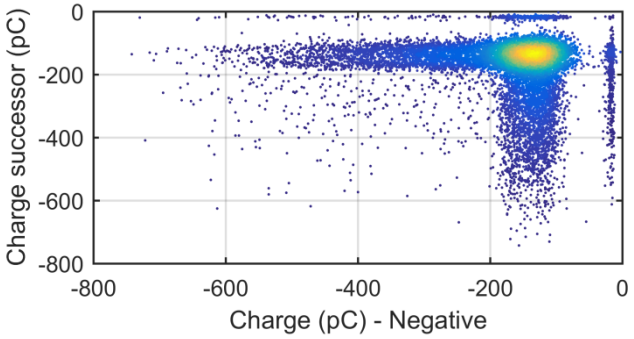

Figure 219: Negatively charged pulses: Internal discharge sample 2, consistency check 1.

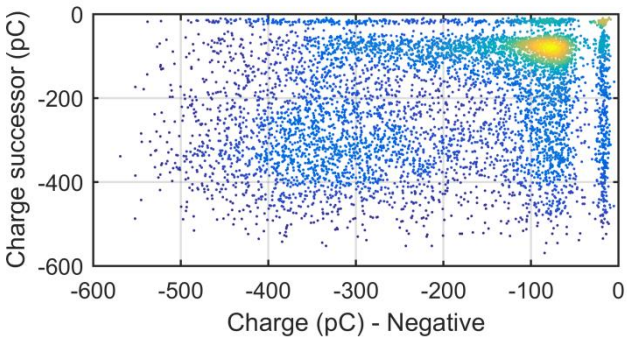

Figure 220: Negatively charged pulses: Internal discharge sample 2, consistency check 2.

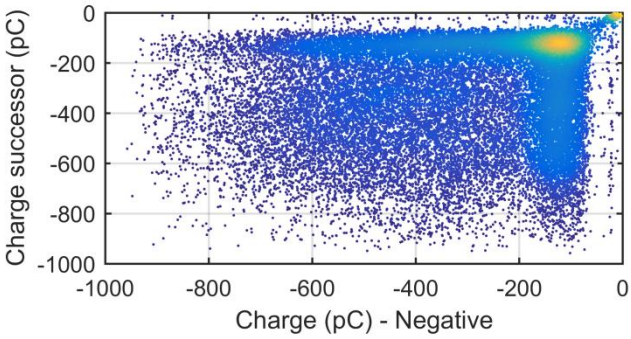

Figure 221: Negatively charged pulses: Internal discharge sample 2, consistency check 3.

Figure 219 to Figure 221 show the graphs of the Qsuc vs. Q (charge successor versus negative charge) of the second internal discharge sample. The shapes here are slightly different compared to the first internal discharge defect; the oval shape is still there, in the upper right-hand corner, but now the overall shape looks more like an “L” with the corner near the 0-crossing.

In the graph of check 3, Figure 221, it looks slightly more like a square, but here all the PDs filling up the middle of the “L” shape are pulses that are not properly measured.

Free-Moving Particle

The shape that will be used for recognition of the artificial defect free-moving particle is found in Table 47 of section 8.2 above.

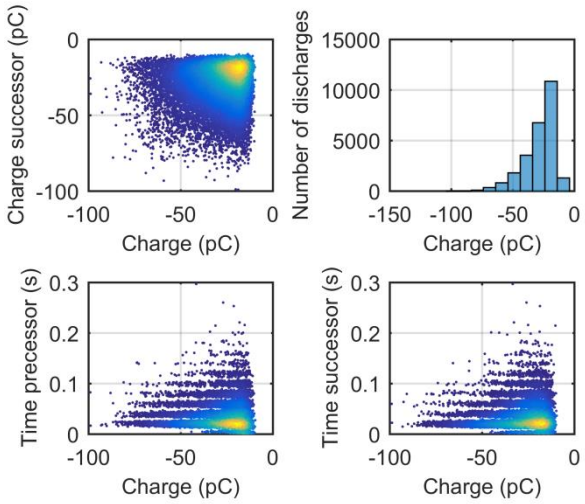

Figure 222: Negatively charged pulses: Free-moving particle, consistency check 1.

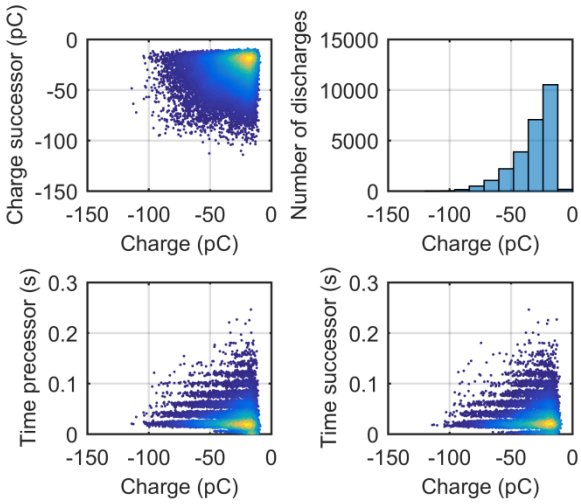

Figure 223: Negatively charged pulses: Free-moving particle, consistency check 2.

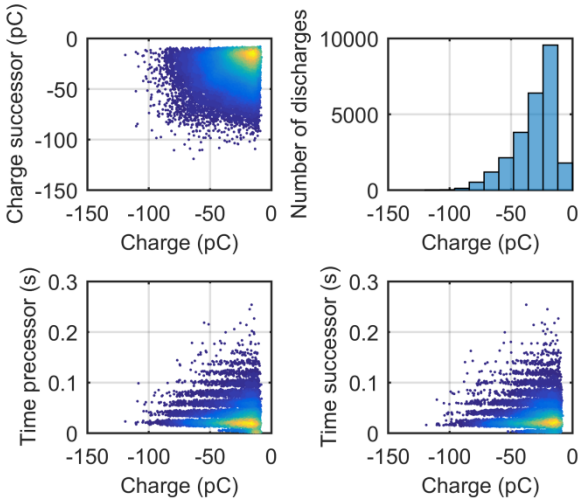

Figure 224: Negatively charged pulses: Free-moving particle, consistency check 3.

As shown in Figure 222 t/m Figure 224, the shape remains the same: a triangle with an arc at the side connecting the two axes for the Qsuc vs. Q (charge-successor versus charge) graph and a triangle for the Tsuc vs. Q (time-precessor versus charge) graph.

Floating Electrode

The shape that will be used for recognition of the artificial defect floating electrode is found in Table 47 of section 8.2 above.

Floating Electrode Sample I: Based on the metal floating with the dielectric ring (see section 5.3.3):

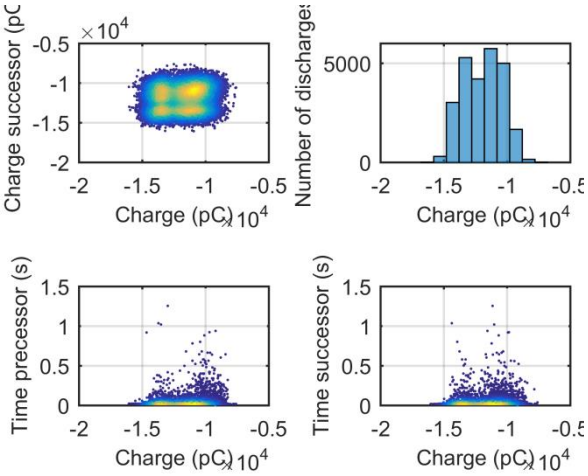

Figure 225: Negatively charged pulses: Floating electrode sample 1, consistency check 1.

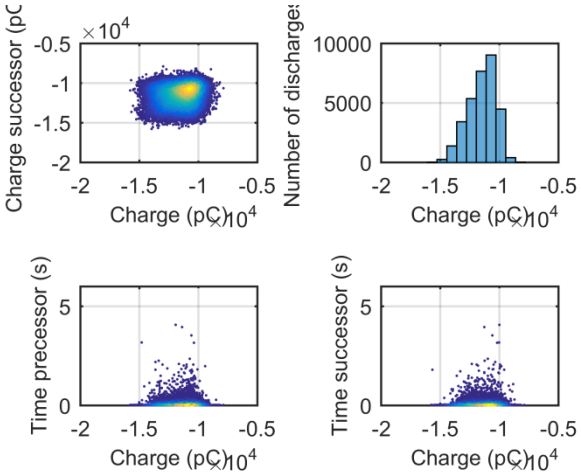

Figure 226: Negatively charged pulses: Floating electrode sample 1, consistency check 2.

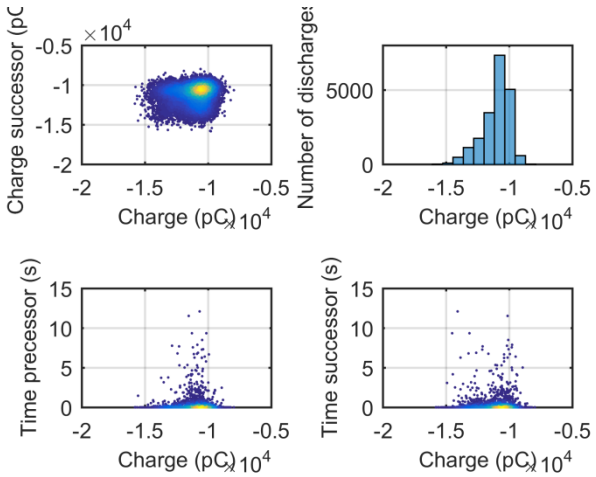

Figure 227: Negatively charged pulses: Floating electrode sample 1, consistency check 3.

As shown in Figure 225 t/m Figure 227, the shape remains the same: a square for the Qsuc vs. Q (charge-successor versus charge) graph and a shape described in section 8.3.1 for the Tsuc vs. Q (time-precessor versus charge) graph.**Floating Electrode Sample II: Based on the metal floating with the use of magnets (see section 5.2.1):**

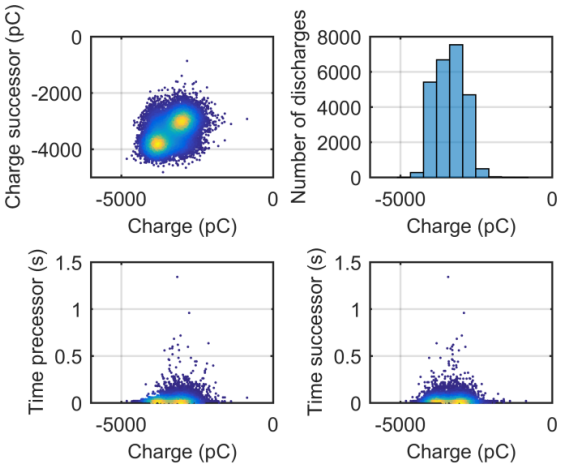

Figure 228: Negatively charged pulses: Floating electrode sample 2, consistency check.

As shown in Figure 228, the shape from the Tpre vs. Q graph from sample 2 is exactly the same as that in sample 1 (see Figure 225 t/m Figure 227). However, the shape from the Qsuc vs. Q is slightly different compared to sample 1: the shape is still a square but now tilted at an angle of 45 degrees.

Surface Discharge

The shape that will be used for recognition of the artificial defect surface discharge is found in Table 47 of section 8.2 above.

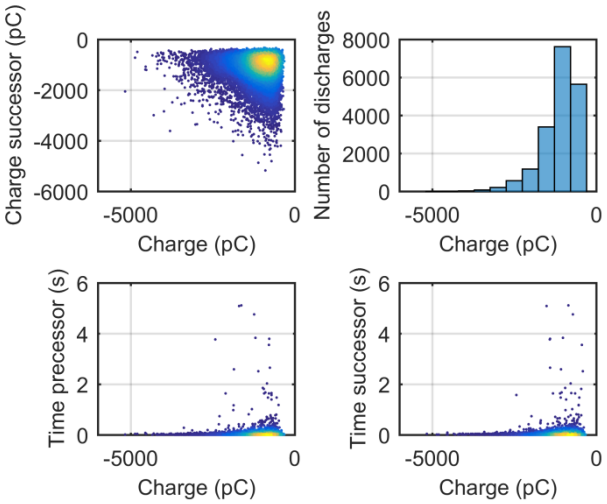

Figure 229: Negatively charged pulses: Surface discharge, consistency check 1.

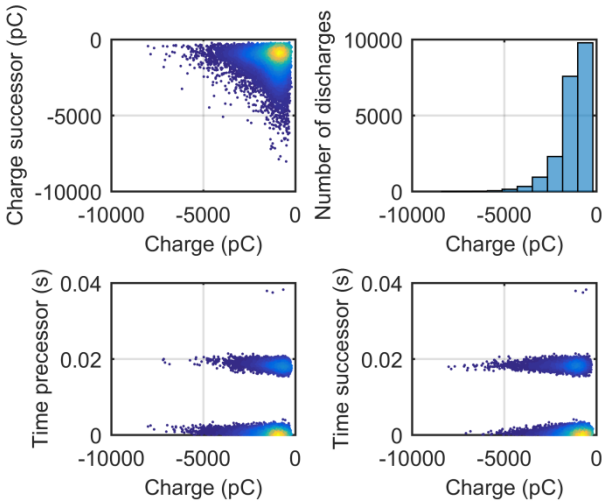

Figure 230: Negatively charged pulses: Surface discharge, consistency check 2.

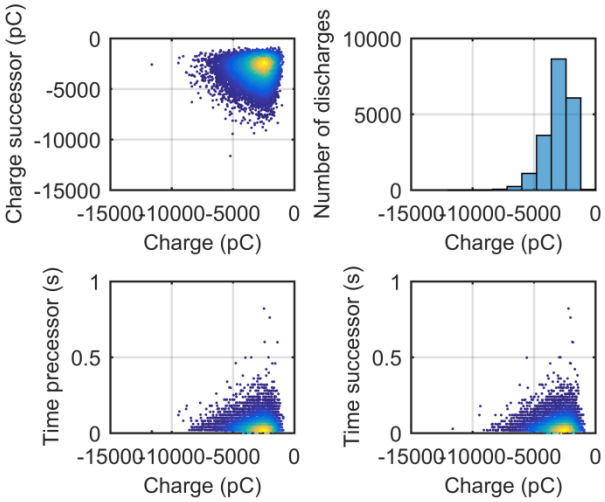

Figure 231: Negatively charged pulses: Surface discharge, consistency check 3.

As shown in Figure 229 t/m Figure 231, the shape remains the same: a triangle for the Qsuc vs. Q (charge-successor versus charge) graph and a misshapen triangle (shown in section 8.2.3) for the Tsuc vs. Q (time-precessor versus charge) graph.

8.3.2. Positively Charged Pulses

In this section we will consider the shape consistency of all the positively charged PD pulses for each artificially created defect, including the second samples for internal discharge and floating electrode defects.

Negative Corona

The shape that will be used for recognition of the artificial defect negative corona is found in Table 48 of section 8.2 above.

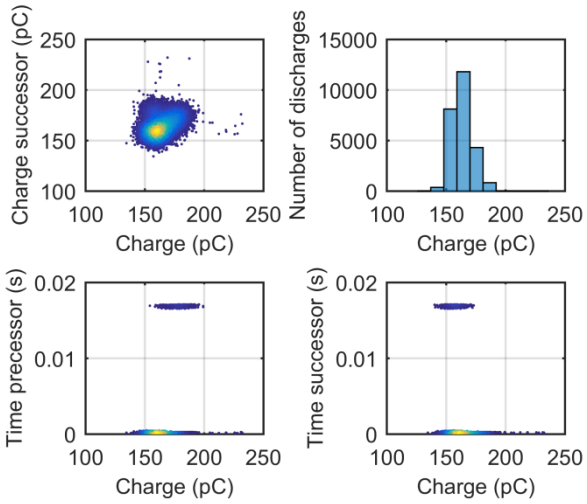

Figure 232: Positively charged pulses: Negative corona, consistency check 1.

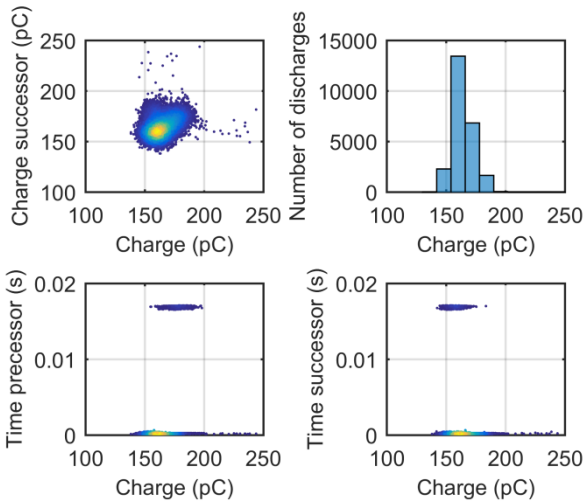

Figure 233: Positively charged pulses: Negative corona, consistency check 2.

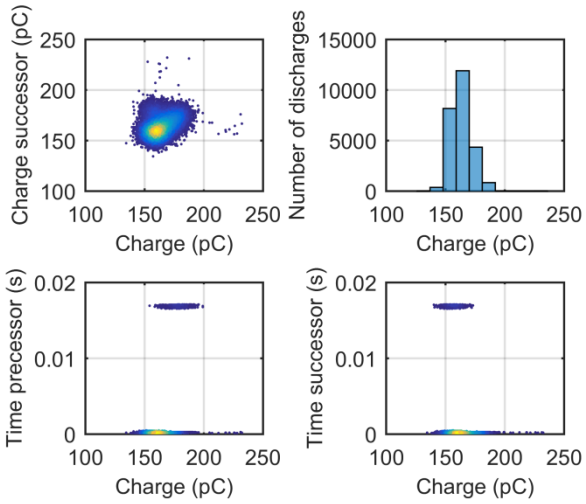

Figure 234: Positively charged pulses: Negative corona, consistency check 3.

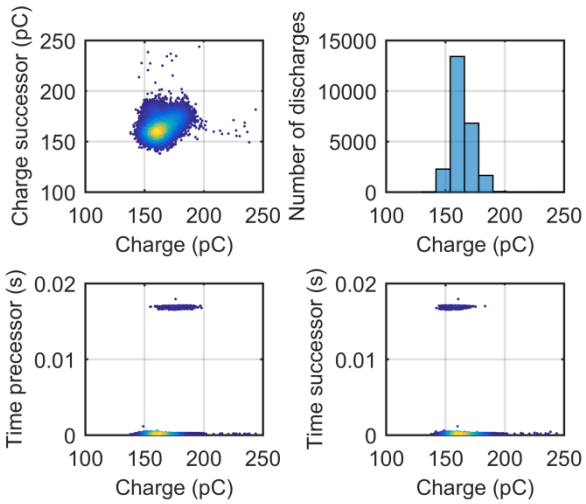

Figure 235: Positively charged pulses: Negative corona, consistency check 4.

As shown in Figure 232 t/m Figure 235, the shape remains the same: a misshapen circle/oval (at an angle of 45 degrees) for the Qsuc vs. Q (charge-successor versus charge) graph and two horizontal lines for the Tsuc vs. Q (time-precessor versus charge) graph. These findings are similar to those in section 8.2.

Positive Corona

Positive corona do not have any positively charged pulses, so no consistency check could be conducted here.

Internal Discharge

The shape that will be used for recognition of the artificial defect internal discharge is found in Table 48 of section 8.2 above.

Internal Discharge Sample I: Based on the layers of dielectric material (see section 5.2):

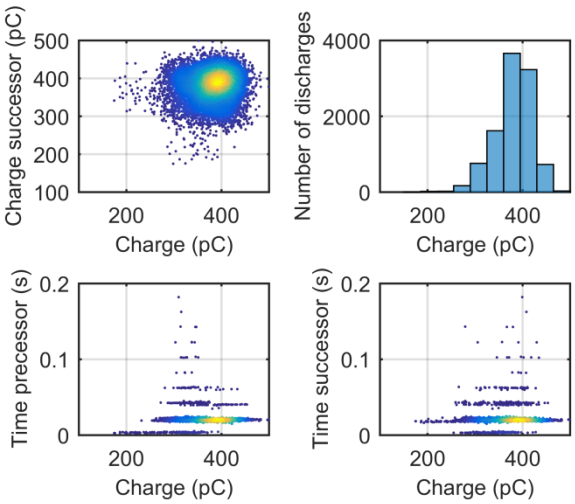

Figure 236: Positively charged pulses: Internal discharge sample 1, consistency check 1.

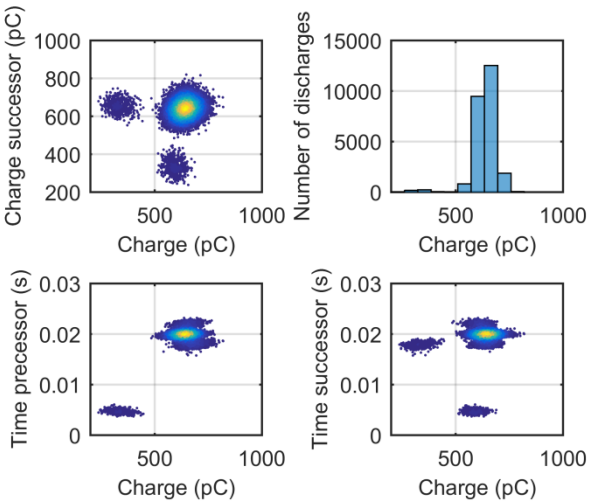

Figure 238: Positively charged pulses: Internal discharge sample 1, consistency check 3.

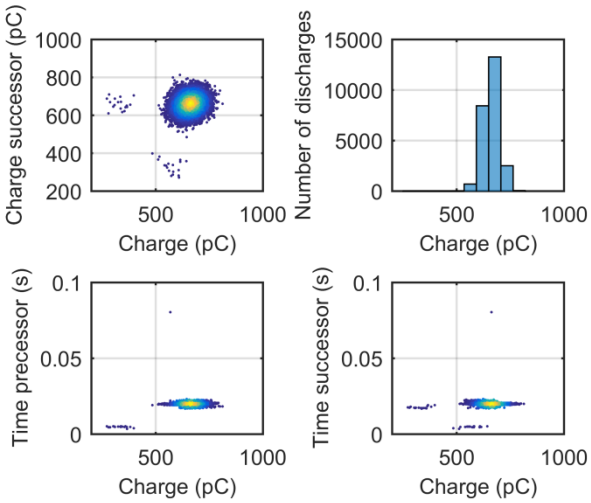

Figure 237: Positively charged pulses: Internal discharge sample 1, consistency check 2.

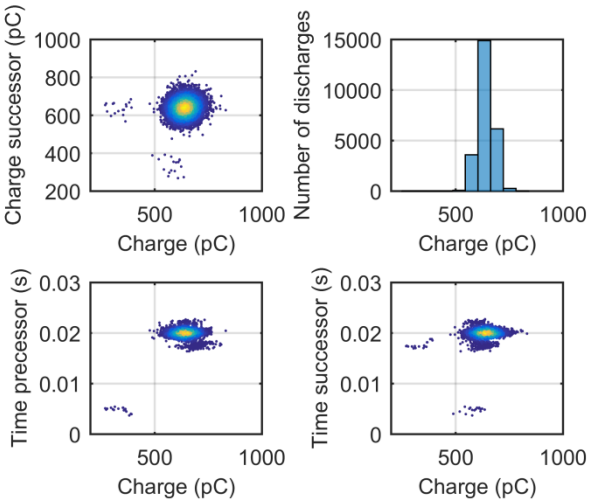

Figure 239: Positively charged pulses: Internal discharge sample 1, consistency check 4.

As shown in Figure 236 t/m Figure 239, the shape remains the same: a circle for the Qsuc vs. Q (charge-successor versus charge) graph and a (horizontal) oval for the Tsuc vs. Q (time-precessor versus charge) graph.

Internal Discharge Sample II: Based on the void on the bottom of the glass jar (see section 5.2.1):

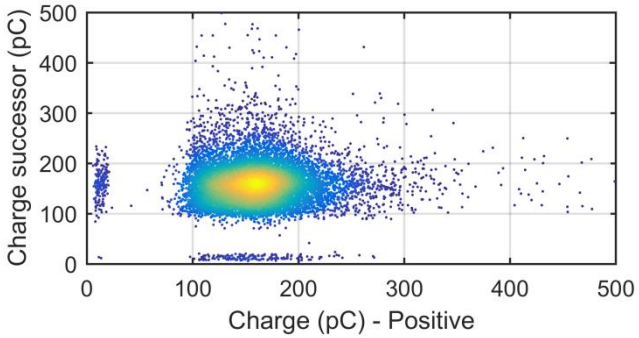

Figure 240: Positively charged pulses: Internal discharge sample 2, consistency check 1.

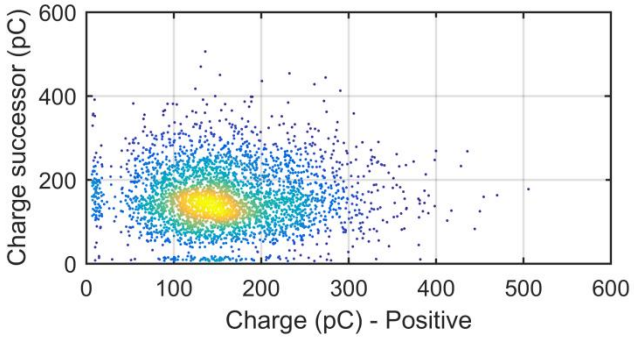

Figure 241: Positively charged pulses: Internal discharge sample 2, consistency check 2.

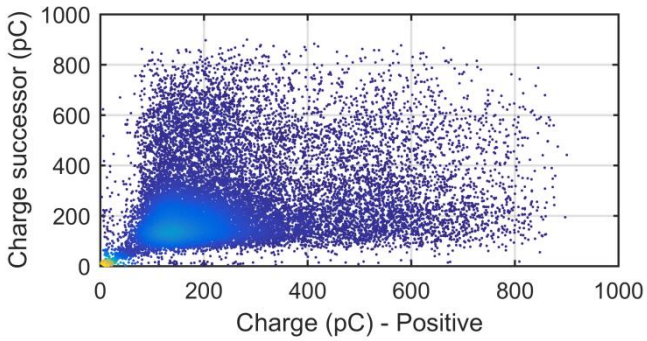

Figure 242: Positively charged pulses: Internal discharge sample 2, consistency check 3.

Figure 240 to Figure 242 show the graphs of the Qsuc vs. Q (charge successor versus negative charge) of the second internal discharge sample. The shapes here are slightly different compared to the first internal discharge defect, but similar to the negatively charged pulses of the second sample. The oval shape is still there in the upper right-hand corner, and the overall shape also looks more like an “L” with the corner near the 0-crossing. In the graph of check 3, Figure 242, it looks slightly more like a square, but here all the PDs filling up the middle of the “L” shape are pulses that are not properly measured.

Free-Moving Particle

The shape that will be used for recognition of the artificial defect free-moving particle is found in Table 48 of section 8.2 above.

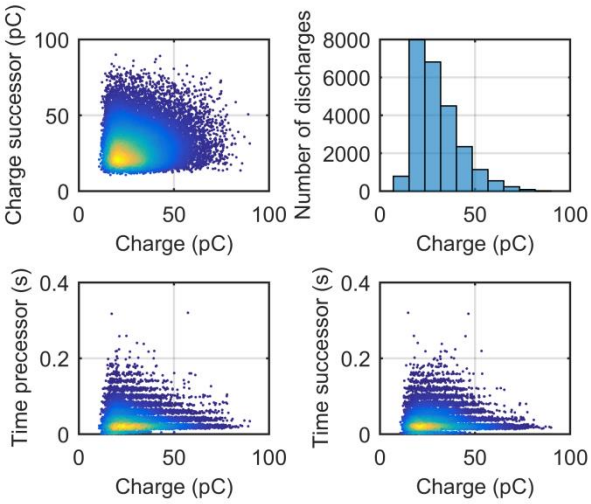

Figure 243: Positively charged pulses: Free-moving particle, consistency check 1.

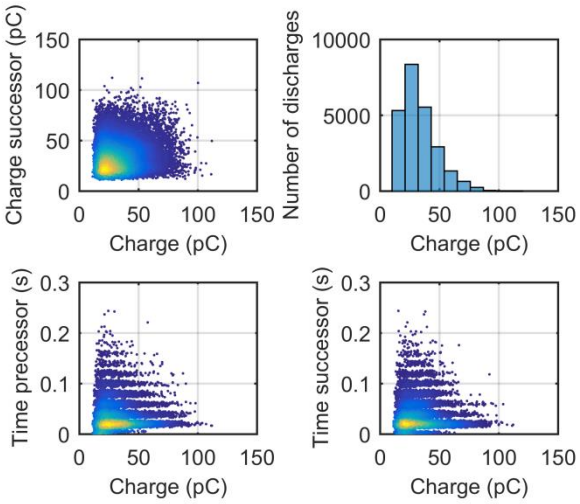

Figure 244: Positively charged pulses: Free-moving particle, consistency check 2.

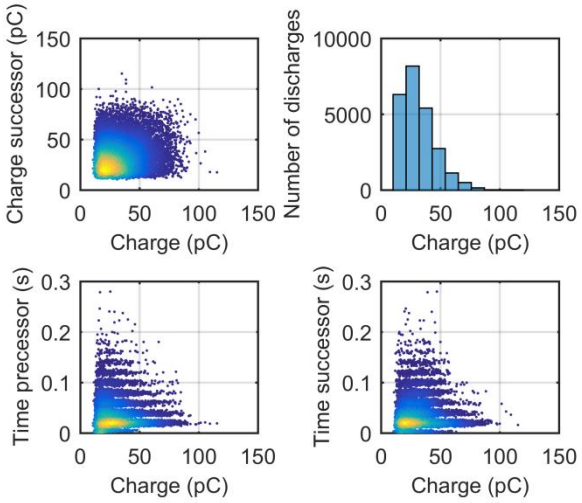

Figure 245: Positively charged pulses: Free-moving particle, consistency check 3.

As shown in Figure 243 t/m Figure 245, the shape remains the same: a triangle with an arc at the side connecting the two axes for the Qsuc vs. Q (charge-successor versus charge) graph and a triangle for the Tsuc vs. Q (time-precessor versus charge) graph.

Floating Electrode

The shape that will be used for recognition of the artificial defect floating electrode is found in Table 48 of section 8.2 above.

Floating Electrode Sample I: Based on the metal floating with the dielectric ring (see section 5.3.3):

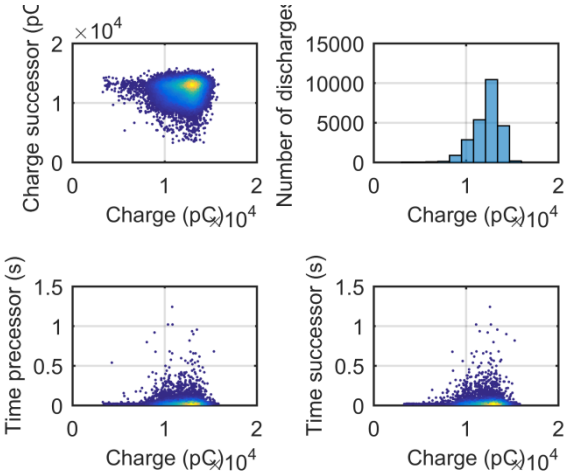

Figure 246: Positively charged pulses: Floating electrode, consistency check 1.

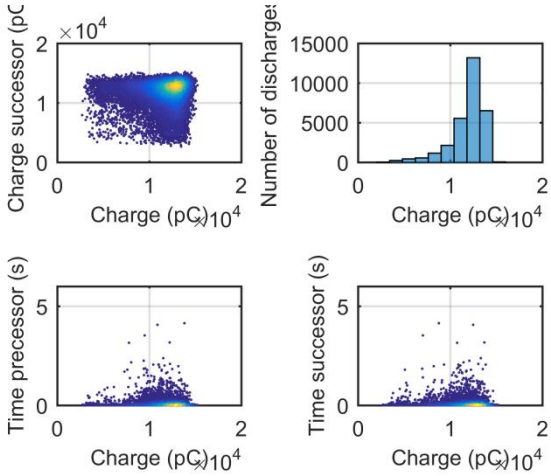

Figure 247: Positively charged pulses: Floating electrode, consistency check 2.

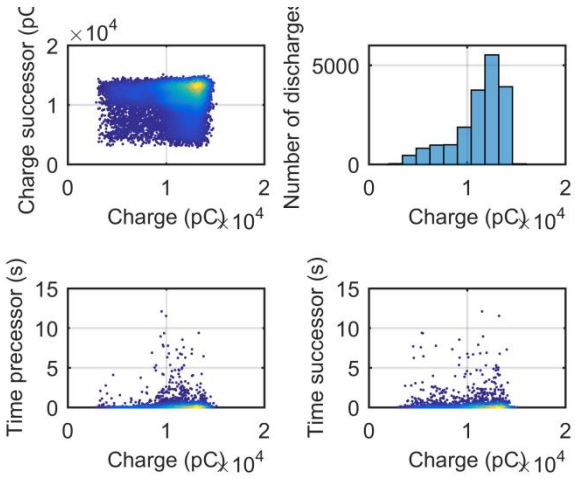

Figure 248: Positively charged pulses: Floating electrode, consistency check 3.

As shown in Figure 246 t/m Figure 248, the shape remains the same: a square/triangle for the Qsuc vs. Q (charge-successor versus charge) graph and a shape described in section 8.3.1 for the Tsuc vs. Q (time-precessor versus charge) graph.

Floating Electrode Sample II: Based on the metal floating with the use of magnets (see section 5.2.1):

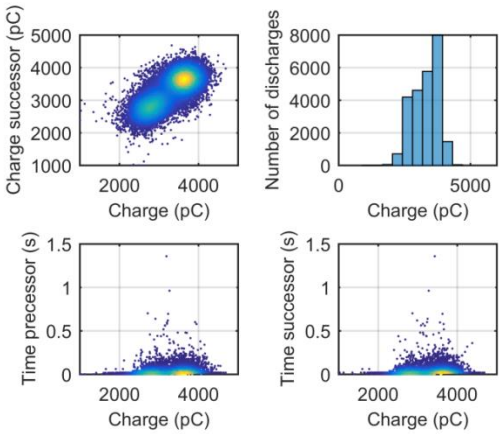

Figure 249: Positively charged pulses: Floating electrode sample 2, consistency check.

As shown in Figure 249, the shape from the Tpre vs. Q graph from sample 2 is exactly the same as that in sample 1 (see Figure 225 t/m Figure 227). However, the shape from the Qsuc vs. Q is slightly different compared to sample 1: the shape is still a square but now tilted at an angle of 45 degrees.

Surface Discharge

The shape that will be used for recognition of the artificial defect surface discharge is found in Table 48 of section 8.2 above.

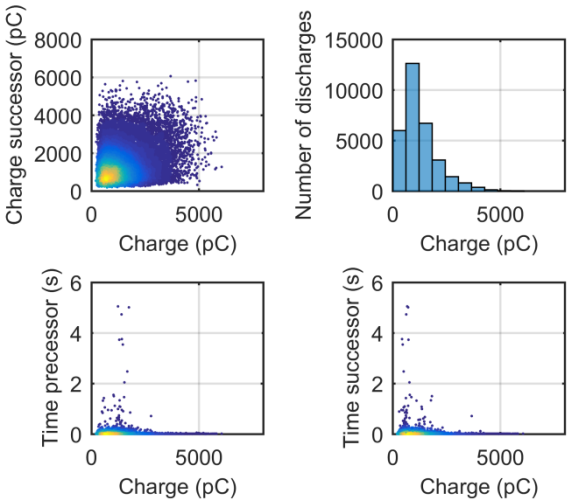

Figure 250: Positively charged pulses: Surface discharge, consistency check 1.

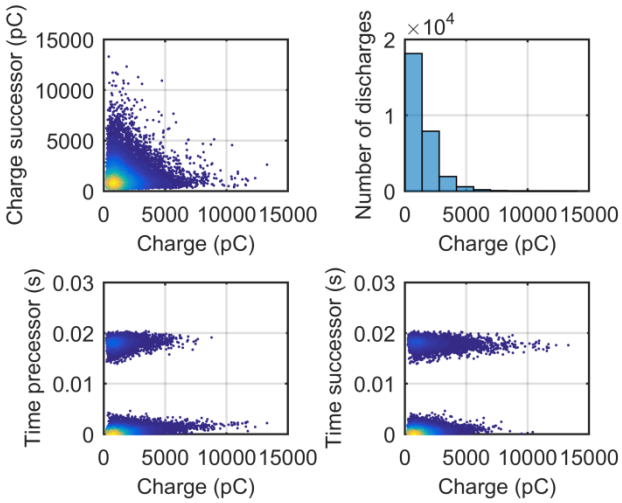

Figure 251: Positively charged pulses: Surface discharge, consistency check 2.

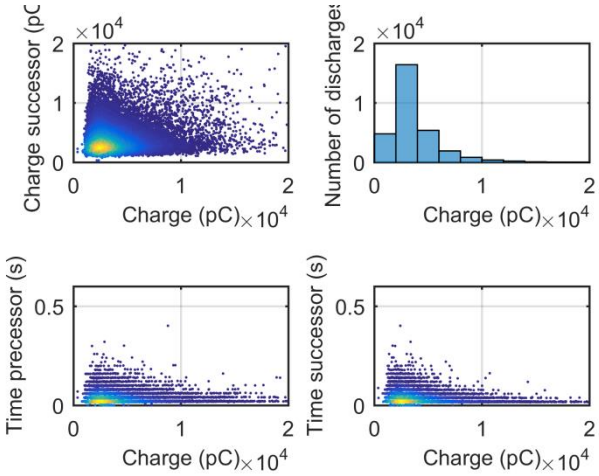

Figure 252: Positively charged pulses: Surface discharge, consistency check 3.

As shown in Figure 250 t/m Figure 252, the shape remains the same: a triangle for the Qsuc vs. Q (charge-successor versus charge) graph and a misshapen triangle (shown in section 8.2.3) for the Tsuc vs. Q (time-precessor versus charge) graph.

8.4. Summary and Discussion of Shape Consistency

In this section we will discuss the similarities and differences found in sections 8.3.1 and 8.3.2, and if needed the chosen characterization shapes for each artificial defect will be changed or adjusted.

Corona Discharge Defect(s)

Both the positively and negatively charged pulses are consistent for both graphs. The final shape for this defect is an oval/circle at an angle of 45 degrees (on the y=x line) for the Qsuc vs. Q (charge-successor versus charge) graph and two horizontal lines for the Tsuc vs. Q (time-precessor versus charge) graph. These final shapes are presented below in Table 49.

	Charge Polarity	Qsuc vs. Q	Tpre vs. Q
Negative Corona	-Q	-	-
	+Q		
Positive Corona	-Q		
	+Q	-	-

Table 49: Corona discharge shapes for TRPD pattern recognition.

Internal Discharge Defect(s)

Looking at the Qsuc vs. Q graph, for the first sample the shape is a circle, while for the second sample the shapes are slightly different: the graphs still show an oval shape, in the upper right-hand corner, but now the overall shape looks more like an “L” with the corner near the 0-crossing. Comparing these findings, we can conclude that in the first sample we actually can see an “L” shape beginning to form for positively charged pulses (see e.g. Figure 236 - Figure 239). The negatively charged pulses, on the other hand, do not have the starting phase of this “L” shape. The Tsuc vs. Q graph has, for the first sample, the shape of a (horizontal) oval for all the checks. These final shapes are presented below in Table 50.

Charge Polarity	Qsuc vs. Q	Tpre vs. Q
-Q		
+Q		

Table 50: Internal discharge shapes for TRPD pattern recognition.

Free-Moving Particle Defect

For this sample, the shapes are similar to the initial shape, shown in section 8.2.3. The final shape is a triangle with an arc at the side connecting the two axes for the Qsuc vs. Q (charge-successor versus charge) graph and a triangle for the Tsuc vs. Q (time-precessor versus charge) graph. These final shapes are presented below in Table 51.

Charge Polarity	Qsuc vs. Q	Tpre vs. Q
-Q		
+Q		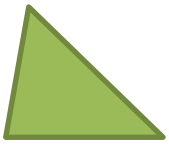

Table 51: Free-moving particle shapes for TRPD pattern recognition.

Floating Electrode Defect(s)

For the first defect we found that for both positively and negatively charged pulses the Qsuc vs. Q graphs showed the shape of a square, but in positively charged pulses there is also a possibility of a triangle. In the second sample this shape is slightly different: it is still a square but now tilted at an angle of 45 degrees.

When looking at the Tpre vs. Q graphs, we saw for both positively and negatively charged pulses the shapes described in section 8.3.1, and for sample 2 this shape is exactly the same. These final shapes are presented below in Table 52.

Charge Polarity	Qsuc vs. Q	Tpre vs. Q
-Q	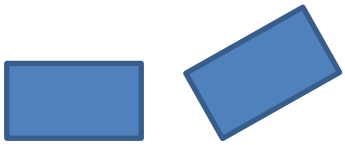	
+Q	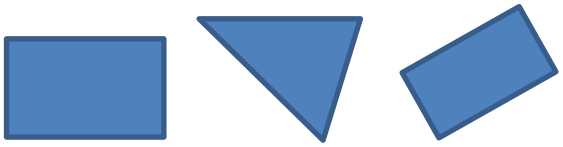	

Table 52: Floating electrode shapes for TRPD pattern recognition.

Surface Discharge

For this sample the shapes are similar to the initial shape, shown in section 8.2.3. The final shape is a triangle for the Qsuc vs. Q (charge-successor versus charge) graph and a misshapen triangle for the Tsuc vs. Q (time-precessor versus charge) graph. These final shapes are presented below in Table 53.

Charge Polarity	Qsuc vs. Q	Tpre vs. Q
-Q		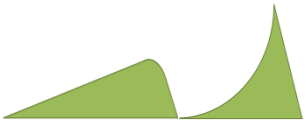
+Q	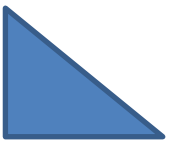	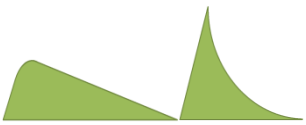

Table 53: Surface discharge shapes for TRPD pattern recognition.

8.5. PD Shape Recognition

In this section ideas for PD shape recognition are proposed, including the use of edge detection and statistical distribution. In the end a flowchart is presented on how to recognize each PD defect origin with the proposed shapes from the previous section.

8.5.1. Flowchart PD Origin Recognition

By analysing the similarities and the differences between the different types of defects, we can make flowcharts of how to recognize the origin of the defect. Figure 253 presents a sample of such a flowchart.

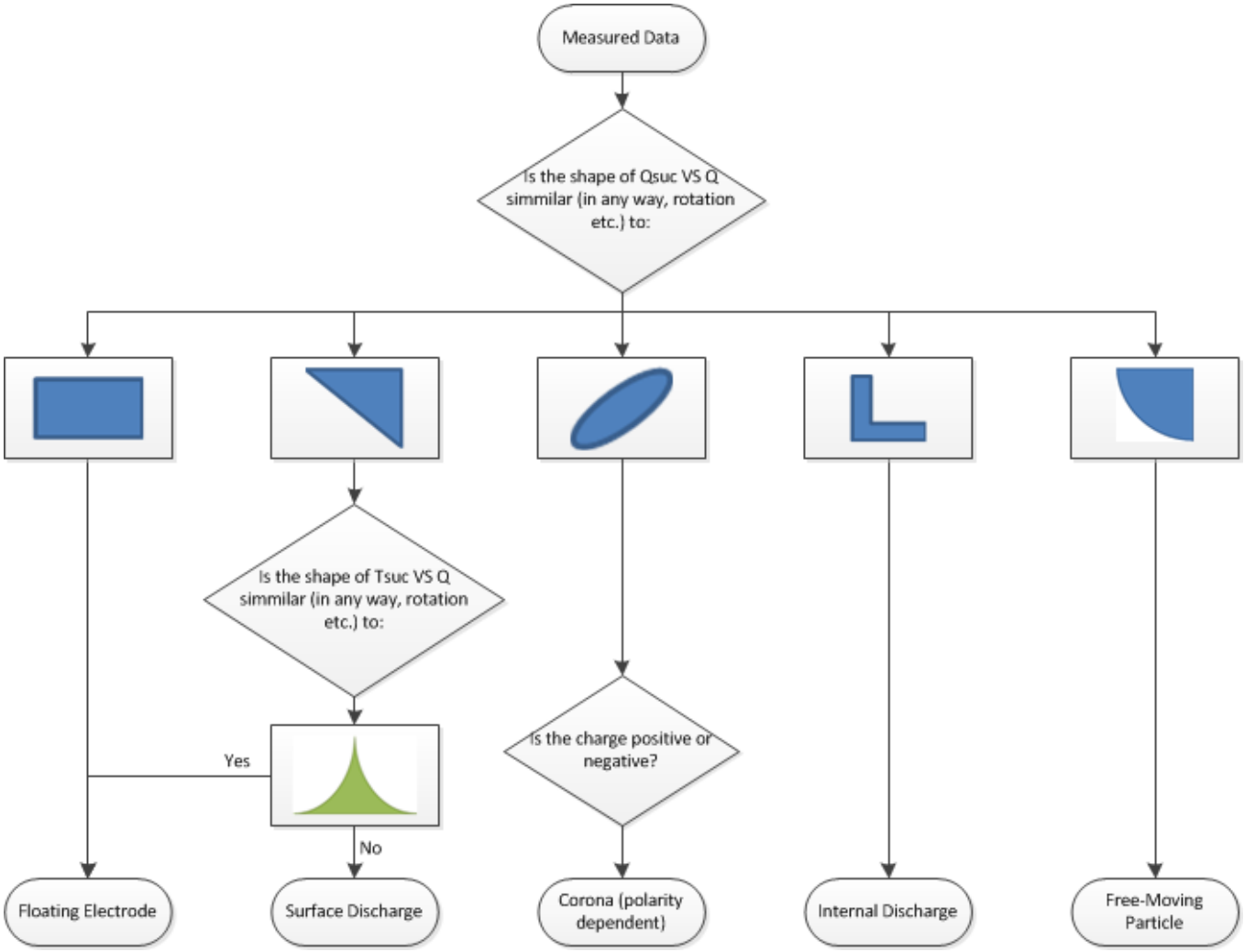

Figure 253: Example TRPD defect recognition flowchart.

By applying edge detection techniques on the characterized shapes, the origins of the artificially created defects are ascertainable. The shapes achieved from both the charge successor versus charge graph and the time processor (or successor) versus charge graph, can both be used individually for defect recognition. The shapes of the different graphs can also be used as a confirmation of the one and other.

By using these pattern recognition techniques in combination with the time-resolved partial discharge (TRPD) analysis there is no need to synchronize the discharges with the phase anymore, no phase dependency. From the analysis in this thesis, it can be concluded that the TRPD analysis for PD recognition under AC voltage is as good as, or even better than, phase-resolved partial discharge (PRPD) analysis. For most of the data analysed, the TRPD analysis provides the same results compared to the PRPD analysis. However, further checking is needed, such as validating the findings with mathematical models.

9. Conclusions and Future Work

9.1. Conclusions

During this master's thesis research project, a PD test platform was created with six artificially created defects with origins in positive and negative corona, internal discharges, free-moving particles, floating electrodes and surface discharges. These defects were designed to have a partial discharge inception voltage (PDIV) of around 10kV, and could easily be connected or disconnected from the setup. Therefore, it was possible to measure individual defects or a combination of them. This PD test platform simulated not only medium- to high-voltage AC cables but also other HV apparatus where the PDs of the artificially created defects occur, e.g. in gas insulated systems (GIS), bushings, etc. Chapter 4 and 5 provided a good and elaborate description of this PD test platform and the process of creating its details.

The weaknesses of this PD test platform included the samples, specifically internal discharge and surface discharge. The internal discharge sample is the most unstable of them all and has the shortest lifetime. This sample is most affected by aging: the higher the applied voltage, the shorter the lifetime of the sample. The internal discharge defect has a lifetime of ±1hour (excluding the aging process before PDs occur) with 10kV AC applied on the sample. When an internal discharge sample is newly constructed and no surface discharge is present, it needs an average aging time of ±25min before internal discharges appear. On the other hand, if surface discharges disappear, they can easily be brought back by moving the electrode on the sample or the sample itself (see section 7.6 for more details on the internal discharge sample).

For each type of defect (and combinations of them), measurements were done with the PD test platform in order to characterize different aspects of each PD type or defect combination. Analysing the data in such a way provided the opportunity to investigate the best methods for PD defect origin recognition. During this process, each type of defect was characterized, analysed, confirmed with defect combinations and verified with more samples and measurements.

The most promising technique for PD pattern classification of defects in on-line monitoring is TRPD analysis in which the charges are separated. In this method, the location of the PD occurrence on the phase voltage does not need to be measured, making the measurement simpler and less expensive and thus easier to implement on a larger scale.

The shapes of each defect type for the charge-separated TRPD patterns are described in section 8.4. These final shapes can be used for PD defect origin recognition, as described in section 8.5.

In addition to these findings there are some other important conclusions that can be drawn. These conclusions are summarized below:

Charge polarity:

The corona discharges are easily distinguishable from the rest of the discharges by their polarity occurrence. This is due to the fact that PDs from negative corona only occur in the first quadrant of TRPD and PDs from positive corona only occur in the third quadrant of TRPD.

TRPD analysis:

We saw that when analysing data from multiple sample combinations with the use of TRPD analysis, the defects were recognizable. The TRPD analysis originally provided complex figures, it is my addition to use only the charge polarity separated. When the TRPD analysis was plotted

with the charge polarity separated, the figures became much simpler. With these simpler shapes, we could recognize the defect origins.

Additionally, when looking at the graphs of time between the discharges versus charge we sometimes saw horizontally stacked lines, which can be used for defect origin distinction/separation. The distances between the defects are constant, but the thickness of the horizontal lines is not; is depends on the number of pulses recorded.

In TRPD analysis, when looking at the graph of the number of discharges versus charge, the slopes of the graph cannot be used for defect recognition, because the slopes change significantly. However, the charge magnitudes can be used as an indication for defect recognition.

Even in the presence of a disturbance, we only need to recognize the defects in one of the charge polarities to be able to recognize the defect origin, which makes it much easier to recognize the defect origin.

From all the analysis conducted during this thesis, it can be concluded that TRPD analysis for PD recognition under AC voltage is as good as, or even better than, PRPD analysis. This is due to the fact that for most of the data analysed, the TRPD analysis provides the same results as PRPD analysis. In some cases when some of the PD pulses were or were not properly measured we even get more information with TRPD analysis compared to PRPD. TRPD analysis can also sometimes recognize defects in cases that PRPD analysis cannot. Therefore, TRPD analysis is as good as or even better than PRPD analysis.

However, it was not always easier to recognize the defect in TRPD analysis. There was a case during the measurements in which the sample was easily recognizable by the shape in the PRPD analysis, but with the TRPD there were barely enough pulses to be able to determine the defect origin.

By applying edge detection techniques on the characterized shapes, the origins of the artificially created defects are ascertainable. The shapes achieved from both the charge successor versus charge graph and the time processor (or successor) versus charge graph, can both be used individually for defect recognition. The shapes of the different graphs can also be used as a confirmation of the one and other. By using these pattern recognition techniques in combination with the time-resolved partial discharge (TRPD) analysis there is no need to synchronize the discharges with the phase anymore, no phase dependency.

Clusters:

Different clustering techniques were analysed, not only with the purpose of clustering but also of defect origin recognition. None of these clustering techniques can be used for PD defect origin recognition in the aspect of shapes, slopes and magnitudes.

The cluster rise-time versus fall-time was not able to distinguish between any of the artificially created defect combinations. This could have been due to the uniformly created PD test platform (equal path length); therefore, if the defects were not located at the same distance and were placed further from each other, it might have been possible to use this cluster.

None of the clusters could identify the defect (make a separate cluster) on its own for all the different defect types. We need a minimum of two clustering techniques to be able to distinguish between all the defect combinations. From the analysis conducted during this thesis, we can therefore say that for making clusters (defect distinction) we must use a combination of the two clustering techniques, one from group A and one from group B, in order to be able to distinguish between all the defect types. Groups A and B are:

A. Frequency-equivalent versus time-equivalent.

B. Energy versus charge, Energy versus charge in logarithmic scale or Energy per charge versus charge.

A proper clustering example of discharges done by “group A” can be seen in Figure 130 and Figure 147 of defect combination 3 and 7. Here the Frequency-equivalent versus time-equivalent graphs show distinction possibilities between the defects while no distinction is possible in the Energy versus Charge graph. As a contradiction, a proper clustering example of discharges done by “group B” can be seen in e.g. Figure 159 of defect combination 10. Here the Energy versus Charge graphs show distinction possibilities between the defects while no distinction is possible in the Frequency-equivalent versus time-equivalent graph. The Frequency-equivalent versus time-equivalent graph can be appreciated in Figure 371.

Number of discharges per cycle

The number of discharges per cycle cannot be used for defect distinction. When combining multiple samples the number of pulses per cycle of each individual defect is affected by the other defects. The number of discharges per cycle can sometimes be used to make a distinction between positive corona, negative corona and all the other types of discharges. However, this is irregular and not always possible. Therefore, we can conclude that the number of discharges per cycle cannot be used for defect distinction.

9.2. Recommendations for Future Research

In this thesis research project, the “initial step” towards PD defect origin recognition for AC voltage without any phase dependency was done with the use of TRPD analysis. It was shown that it is possible to do the time analysis and recognition for AC voltage for the artificially created defects. In future research projects it would be beneficial to test this theory with more data, e.g. more types of samples for each PD type/source, with e.g. different materials, shapes and sizes so that more definite conclusions can be drawn.

In addition to this extension of the data and verification of the thesis, the program for PD pattern recognition could be extended and perfected so it would eventually even work in the field, where there are many disturbances like noise and interferences. The program could also be adjusted so that when selecting data (clustering) it immediately shows the percentage of the selected cluster that is one or all of the PD types. In this way, the program and PD test platform could not only work for educational and research purposes but also for non-specialized staff that need to do e.g. maintenance for HV apparatus.

Instead of focusing on all the possible PD types/sources at once, it may be useful to consider studying this topic in an equipment-dependent manner. In addition to this, looking at the best ways for detecting, recognizing and originating PDs for each type of HV equipment where PDs occur, then each type of apparatus can be tuned and monitored optimally for its specific use.

Appendix

A. Dimensions Electrodes

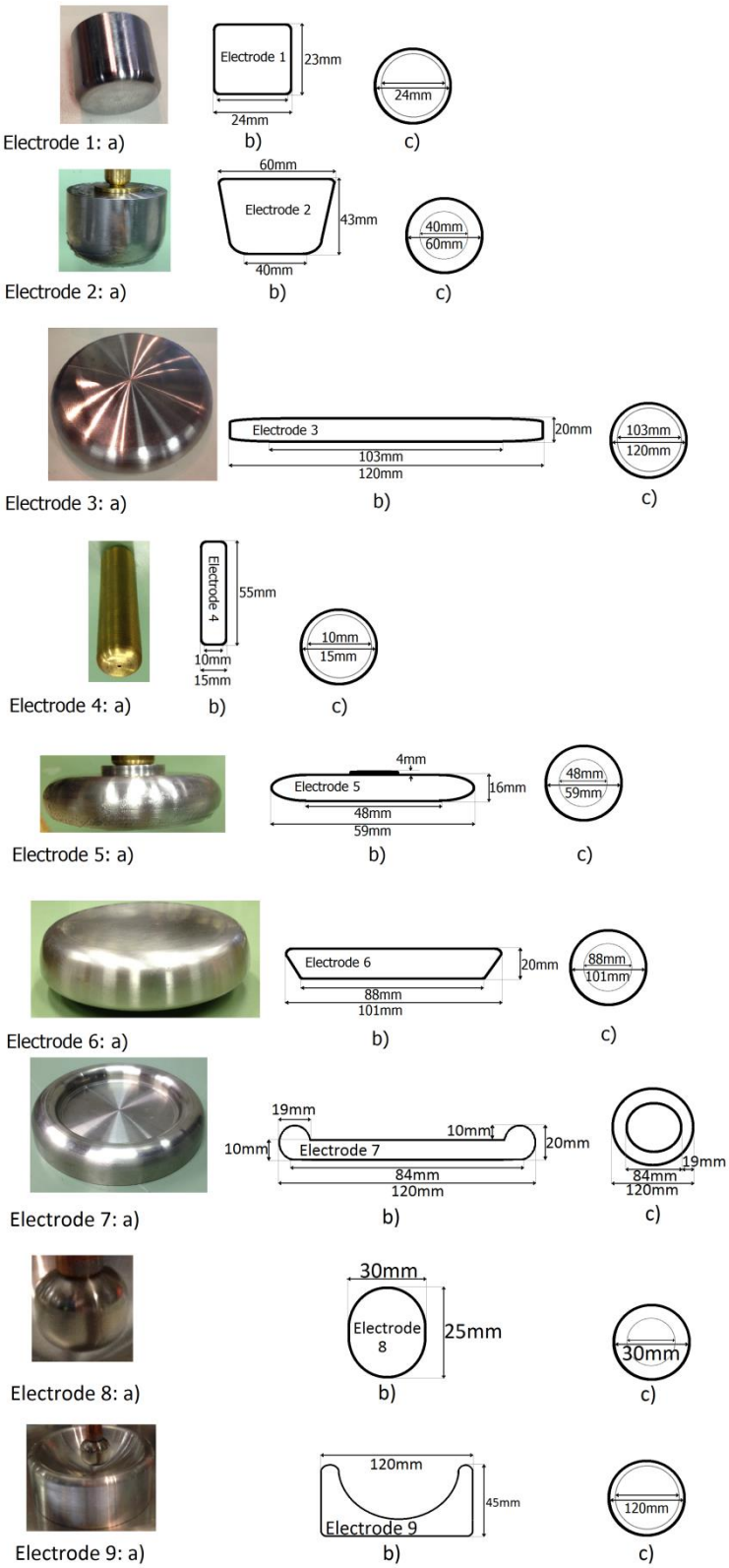

Figure 254: Dimensions Electrodes; (a) Picture; (b) Schematic: Cross Section; (c) Schemtic: Contact Side (Dielectric side view).

B. PD graphs of final individually measured samples

The Samples were measured with the PD Detector and TECHimp PDBase II connected in parallel, according to.

B1. Positive Corona

Sample 3

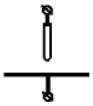

Applied Volt. [kV]	10
# of pulses	50735
Acuisition time [s]	7.38
Bandwidth	WB
Trigger [pC]	0.0024

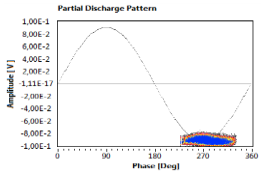

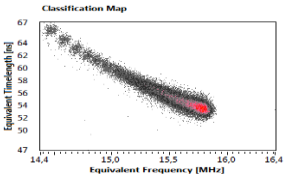

Applied Volt. [kV]	10
# of pulses	10000
Acuisition time [s]	4.35
Bandwidth	WB
Trigger	0.0024

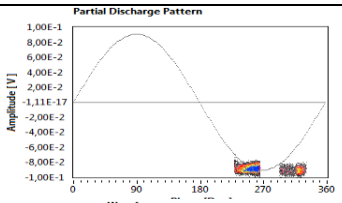

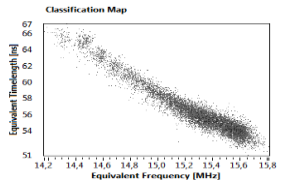

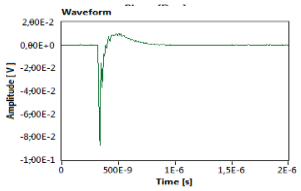

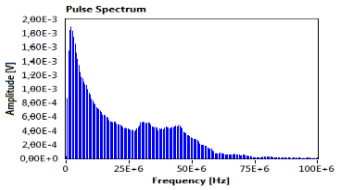

Applied Volt. [kV]	10
# of pulses	48662
Acuisition time [s]	11.17
Bandwidth	IEC
Trigger [V]	105

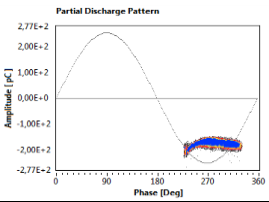

Applied Volt. [kV]	10
# of pulses	10000
Acuisition time [s]	50.56
Bandwidth	IEC
Trigger [pC]	13

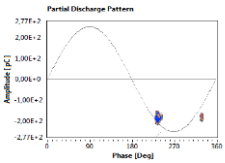

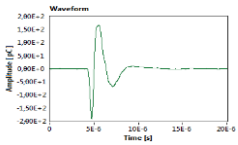

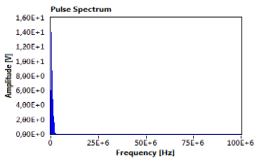

B2. Negative Corona

Sample 3

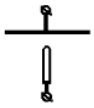

Applied Volt. [kV]	10
# of pulses	1697
Acuisition time [s]	224.17
Bandwidth	WB
Trigger [pC]	0.0070

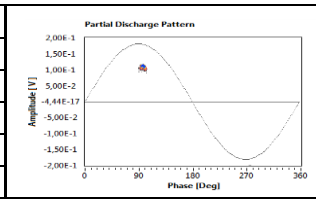

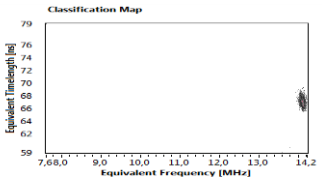

Applied Volt. [kV]	11,9
# of pulses	2000
Acuisition time [s]	18086
Bandwidth	WB
Trigger	0,014

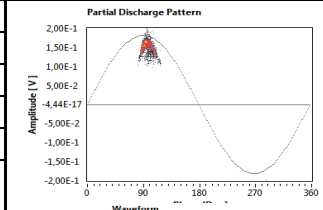

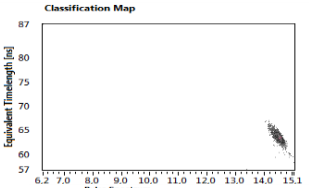

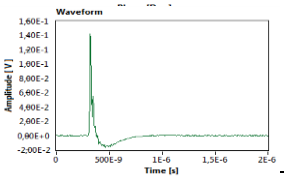

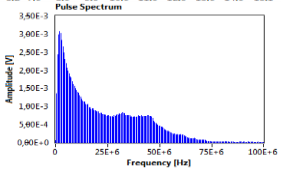

Applied Volt. [kV]	11,9
# of pulses	9870
Acuisition time [s]	126,44
Bandwidth	IEC
Trigger [V]	22

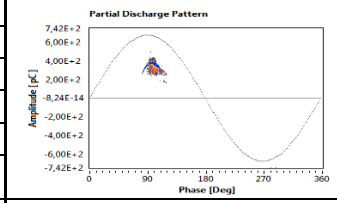

Applied Volt. [kV]	11,9
# of pulses	2000
Acuisition time [s]	26,71
Bandwidth	IEC
Trigger [pC]	22

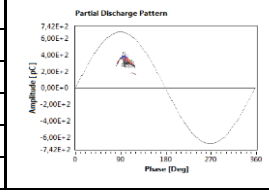

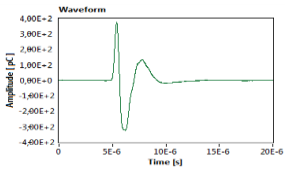

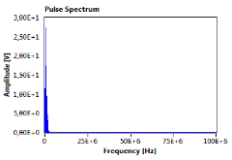

B3. Internal Discharge (Void)

In the tables below you can see clearly the progress of aging of the void in time (top to bottom).

Electrode 1: Polished and Flat surface Sample: Coarsen with Brasso With Big Spring & 2 Rings of Grease

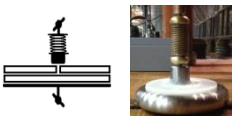

Applied Volt. [kV]	10
# of pulses	10000
Acuisition time [s]	110,25
Bandwidth	WB
Trigger [pC]	0,12
PD Magnitude	0,5nC

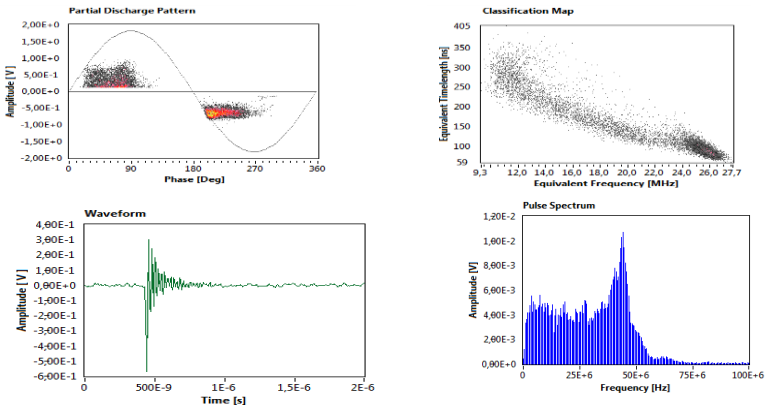

Applied Volt. [kV]	10
# of pulses	6554
Acuisition time [s]	55,05
Bandwidth	IEC
Trigger	0,0005
PD Magnitude	0,5nC

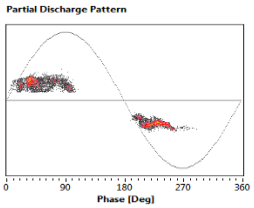

Applied Volt. [kV]	10
# of pulses	10000
Acuisition time [s]	95,52
Bandwidth	IEC
Trigger [V]	0,0005
PD Magnitude	0,5nC

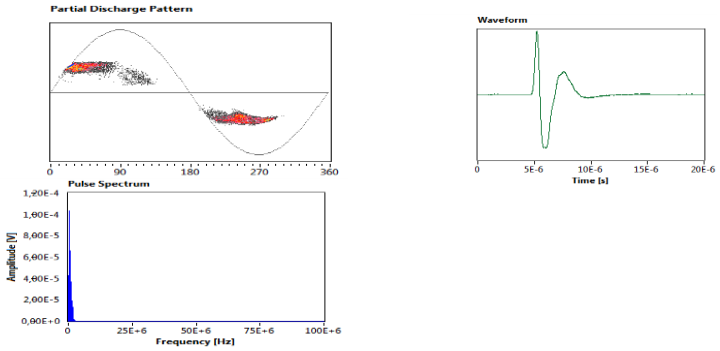

Applied Volt. [kV]	10
# of pulses	15609
Acuisition time [s]	152,44
Bandwidth	IEC
Trigger [pC]	0,0005
PD Magnitude	0,5nC

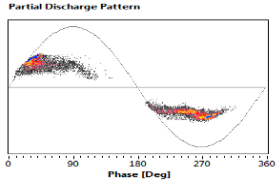

Applied Volt. [kV]	10
# of pulses	1652
Acuisition time [s]	27,71
Bandwidth	WB
Trigger	0,12
PD Magnitude	0,5nC

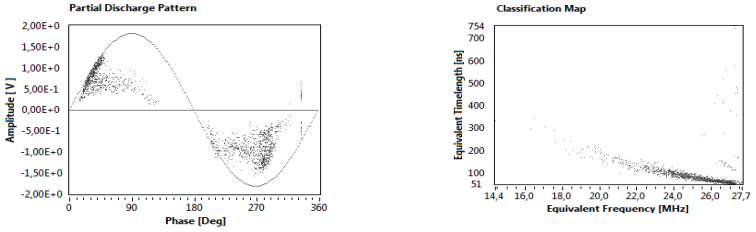

B4. Floating electrode

a=2mm
b=10
c=20,8

Applied Volt. [kV]	10
# of pulses	902
Acuisition time [s]	140,94
Bandwidth	WB
Trigger [pC]	0,95
PD Magnitude	

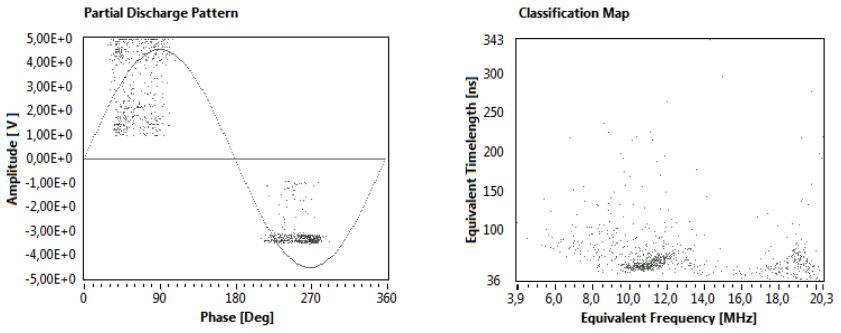

Applied Volt. [kV]	10
# of pulses	5461
Acuisition time [s]	500
Bandwidth	WB
Trigger	0,95
PD Magnitude	

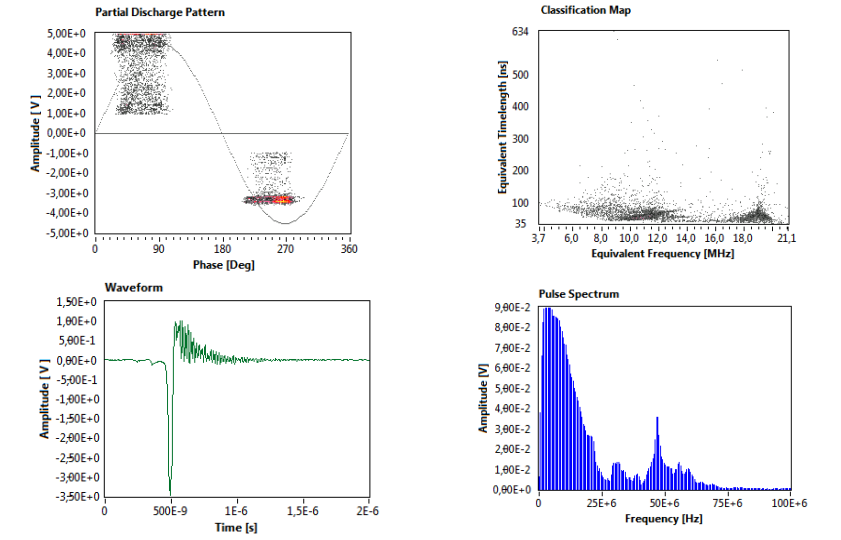

B5. Surface Charge

a=52mm; dikte 12,5mm; gnd=electrode3; pos=electrode1

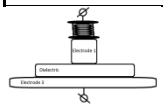

Applied Volt. [kV]	10
# of pulses	26700
Acuisition time [s]	36,02
Bandwidth	WB
Trigger	0,006

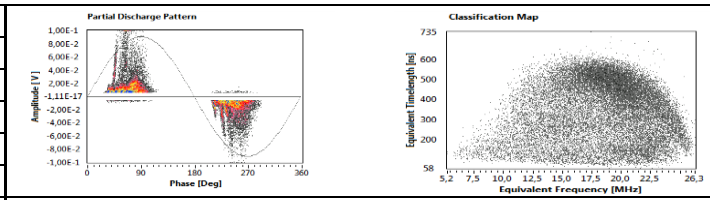

Applied Volt. [kV]	10
# of pulses	2000
Acuisition time [s]	1,22
Bandwidth	WB
Trigger [V]	0,006

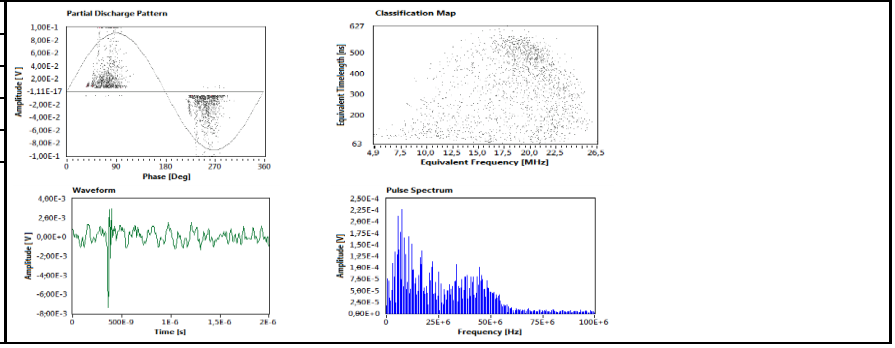

a=52mm; dikte 12,5mm; gnd=electrode7; pos=electrode1

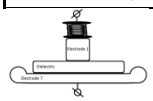

Applied Volt. [kV]	10
# of pulses	21080
Acuisition time [s]	52,96
Bandwidth	WB
Trigger	0,05

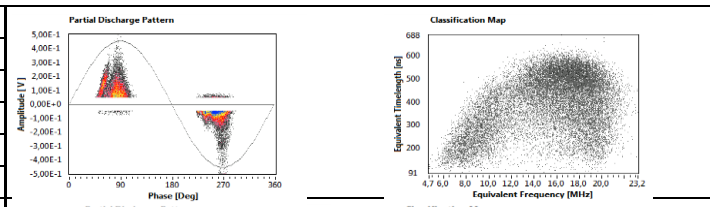

Applied Volt. [kV]	10
# of pulses	4000
Acuisition time [s]	10,09
Bandwidth	WB
Trigger [V]	0,05

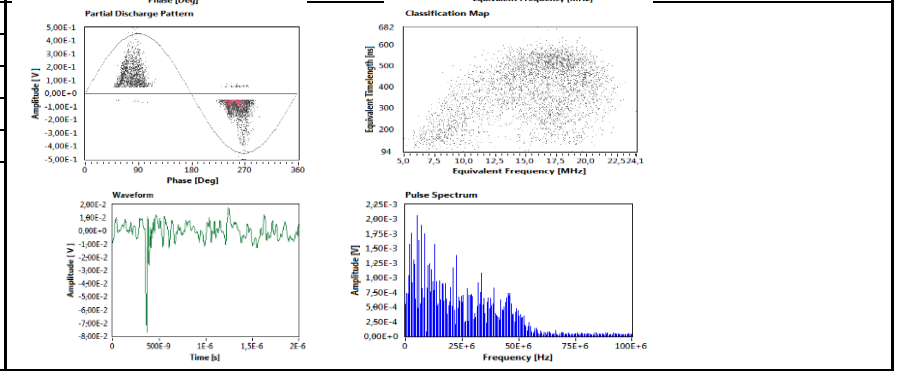

C. Partial Discharge Inception Voltage of Internal Discharge Sample

C1. Estimation of PDIV based on [21]

Field strength in voids at discharge inception

Eqn 1 and 4 from appendix of [20]

Estimation of PDIV based on [21]

To calculate the PDIV, many parameters must be taken into consideration [21]:

- Type of gas in void
- Gas pressure
- Surface properties of the void
- Size and shape of the void
- Location of the void
- Dielectric constant of the surrounding medium

Exact calculation is nearly impossible, which is why we will estimate the PDIV.
During this estimation we will use the following limitations:

- Pressure range [21]: 0.00067-1.01333 bar

(The standard Atmospheric Pressure: 1 Atm = 1.01325 Bar)

- Paschen's Curve [21]: Valid for the whole range

A technique was developed in [21] to evaluate the PDIV in the case of discharges occurring at the interface as well as in voids in the ambient medium of air. This estimation is based on the analysis of Townsend breakdown criterion.

By making a table with estimated PDIV occurring in different sizes of voids for different sample thicknesses and materials, the right sample can be calculated and afterwards compared with actual observations.

Based on the Townsend breakdown criterion we have for breakdown voltage:

$$V_b = \frac{B * p * t'}{\ln[\frac{A * p * t'}{\ln(1 + {}^{1}/_{\gamma})}]}$$

The constants A and B can be evaluated from the Townsend equation:

$$\alpha = A * p * e^{[-\frac{B*p}{E}]}$$

With the parameters:

- p Pressure
- t' Gap spacing
- α Primary ionization coefficient
- γ Secondary ionization process
- A (Constant) Saturation ionization in the gas at a particular E/p (electric stress/pressure)
- B (Constant) Related to the excitation and ionization energies
- E Electric stress

The equations from above are simplified, because we have accurate breakdown voltages available air (the gas in our case) for a wide range of p*t' values (pressure * gap spacing). So according to [21] we therefore get:

$$V_b = \frac{B * p * t'}{\ln[p * t'] + k}$$

Where k is:

$$k = \ln[\frac{A}{\ln(1 + {}^{1}/_{\gamma})}]$$

The values A and B for air are: [21]

- A (Ionization/kPa-cm) 112.50
- B (V/kPa-cm) 2737.50

Gas	**P*t'(kPa –cm)**	**k = M*(p*t')^{N}**
Air	0.0133 - 0.2	$2.0583(p*t)^{-0.1724}$
	0.2 - 100	$3.5134(p*t)^{0.0599}$
	100 - 1400	4.6295 [corresponding to p*t'=100kPa-cm in $k=3.5134(p*t)^{0.0599}$]

The electric strength of the gap at pressure p:

$$E_g = \frac{V_b}{t'} = \frac{B * p}{\ln[p * t'] + k}$$

Based on the capacitive voltage distribution law, the PDIV for discharges occurring in voids is: [21]

$$PDIV = V_i = \frac{E_g * [t + t'(\varepsilon_r - 1)]}{\varepsilon_r}$$

Substituting the last two equations into each other, the PDIV becomes:

$$PDIV = V_i = \frac{B * p}{\ln[p * t'] + k} * \frac{[t + t'(\varepsilon_r - 1)]}{\varepsilon_r}$$

where $k = M * (p * t')^N$

with the parameters:

- E_g Electric strength of the gap at pressure p
- t Thickness of insulation/dielectric sample
- t' Thickness of the discharge gap included within the thickness of t
- ε_r Relative permittivity of dielectric sample
- M Constant
- N Constant

C2. Estimation of PDIV based on [22]

Estimation of PDIV based on [22]

In [22] an integral equation method is presented that provides a general approach for calculating the electric field inside the void (shapes are arbitrary). With this, the analysis of PDIV is possible.

Establishment of integral equation with matrix representations:
Parallel plane electrodes containing dielectrics & gaseous void

With the parameters [22]:

- S_t Inner surface of positive electrode
- S_b Inner surface of grounded electrode

Dimensions of S_t and S_b are assumed to be much larger than the thickness of the sample. This must be such that the electrostatic field normal to the circumferential surface S_0 is negligible.

- S_0 Circumferential surface surrounding the dielectric sample/slab
- d Thickness of sample
- V_2 The bounden domain of gaseous void
- V_1 The domain filled with a dielectric medium of permittivity ε_r
- S The regular surface of V_2
- n^ The unit normal vector to the surfaces S, S_t and S_b
- $ø_1$ Electric potential function in V_1

In [22] they start with the two equations

$$\nabla^2 \phi_1 = 0$$
$$\nabla^2 g_1(\bar{r}, \bar{\bar{r}}') = -\delta(\bar{r}, \bar{\bar{r}}')$$

By applying mathematical modifications and theorems we get according to [22] to the three equations that provide an approach to the computation of electric potential in voids:

$$\phi_2(\bar{r}) = \sum_m \alpha_m \tilde{\psi}_m(\bar{r})$$

$$Q_{nm} = \int_S ds \left[\left(\frac{1}{\varepsilon_r}\right)\tilde{\psi}_n(\bar{r})\hat{n} \cdot \nabla\tilde{\psi}_m(\bar{r}) - \tilde{\psi}_m(\bar{r})\hat{n} \cdot \nabla\tilde{\psi}_n(\bar{r})\right]$$

$$A_n = \left(\frac{V_0}{d}\right)\int_{St+Sb} ds\, \tilde{\psi}_n(\bar{r}) + V_0 \int_{St} ds\hat{n} \cdot \tilde{\psi}_n(\bar{r})$$

with the parameters:

- $\phi_2(\bar{r})$ The potential function in region 2
- A_n The surface integral over S
- V_0 The voltage applied across the electrodes

The electric potential:

$$\bar{E}_2(\bar{r}) = -\nabla\phi_2(\bar{r})$$

C3. Table Internal PDIV Sample

In Table 54, Table 55 and Table 56 you can see all most promising combinations used for choosing the right sample. With most promising I mean that the inception voltage is as close to the 10kV as possible. The tables are taking the limitations described in paragraph 5.3.1 into account for void depth, permittivity, and sample thickness.

εr (permittivity)	t [cm] (thickness sample)	Vi [kV] (Inception Voltage)
2	0,4	10,80
2,5	0,4	9,51
3	0,5	10,08
3,5	0,5	9,26
3,5	0,6	10,49
4	0,6	9,72
4,5	0,6	9,12
4	0,7	10,80
4,5	0,7	10,08
5	0,7	9,51
5,5	0,7	9,03
5	0,8	10,37
5,5	0,8	9,82
6	0,8	9,36

Table 54: PDIV for Void Depth 1mm

εr (permittivity)	t [cm] (thickness sample)	Vi [kV] (Inception Voltage)
2	0,3	10,65
2,5	0,3	10,65
3	0,3	10,65
3,5	0,3	10,65
4	0,3	10,65
4,5	0,3	10,65
5	0,3	10,65
5,5	0,3	10,65
6	0,3	10,65
6,5	0,3	10,65
7	0,3	10,65
7,5	0,3	10,65
8,5	0,3	10,65
9	0,3	10,65
9,5	0,3	10,65
10	0,3	10,65

Table 55: PDIV for Void Depth 3mm

εr (permittivity)	t [cm] (thickness sample)	Vi [kV] (Inception Voltage)
2	0,3	9,51
2,5	0,3	9,13
2,5	0,4	10,65
3	0,4	10,14
3,5	0,4	9,78
4	0,4	9,51
4,5	0,4	9,29
5	0,4	9,13
3,5	0,5	10,86
4	0,5	10,46
4,5	0,5	10,14
5	0,5	9,89
5,5	0,5	9,68
6	0,5	9,51
6,5	0,5	9,36
7	0,5	9,23
7,5	0,5	9,13
8	0,5	9,03
4,5	0,6	10,98
5	0,6	10,65
5,5	0,6	10,37
6	0,6	10,14
6,5	0,6	9,94
7	0,6	9,78
7,5	0,6	9,63
8	0,6	9,51
9,5	0,6	9,21
10	0,6	9,13
6	0,7	10,77
6,5	0,7	10,53
7	0,7	10,32
7,5	0,7	10,14
8	0,7	9,98
8,5	0,7	9,84
9,5	0,7	9,61
10	0,7	9,51
7	0,8	10,86
7,5	0,8	10,65
8	0,8	10,46
8,5	0,8	10,29
9	0,8	10,14
9,5	0,8	10,01
10	0,8	9,89

Table 56: PDIV for Void Depth 2mm

From these tables three observations can be made:

- As you can see in Table 54, Table 56 and Table 55 the IV decreases with increasing permittivity. But this is only valid if the void is not completely through the sample. These observations can be seen e.g. in the orange selected rows in Table 54, Table 56 and Table 55.
- As the sample thickness increases, the IV also increases. These observations can be seen e.g. in the yellow selected rows in Table 54, Table 56 and Table 55.
- As the void depth increases, the IV also increases. . These observations can be seen e.g. in the green selected rows in Table 54, Table 56 and Table 55.

D. Influence of time in PRPD & TRPD

D1. Positive Corona time influence

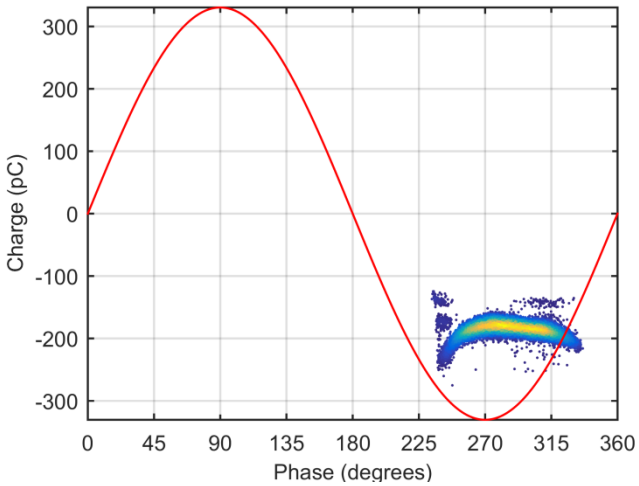

Figure 255: Positive Corona PRPD cluster 1; 0-2 seconds; 25287 discharges.

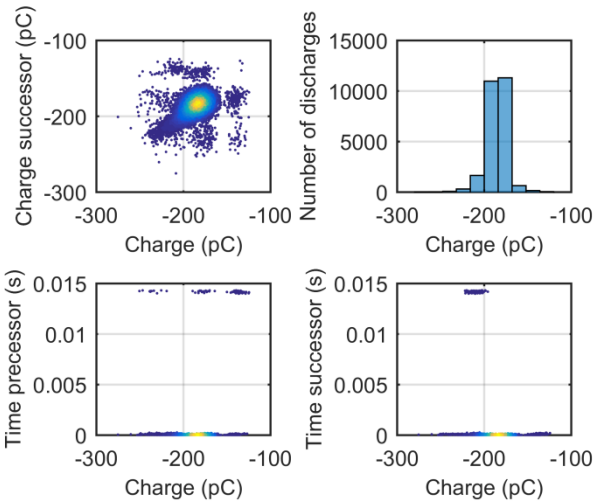

Figure 256: Positive Corona TRPD cluster 1; 0-2 seconds; 25287 discharges.

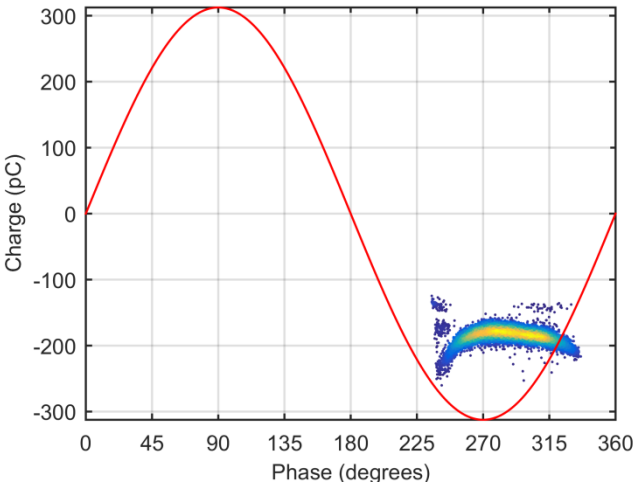

Figure 257: Positive Corona PRPD cluster 2; 0-1 seconds; 12654 discharges.

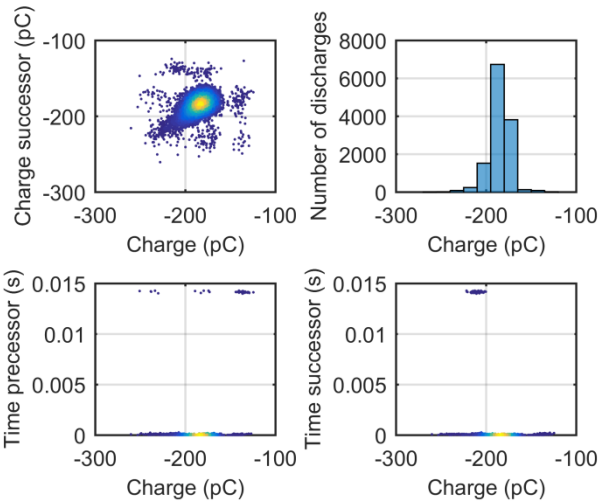

Figure 258: Positive Corona TRPD cluster 2; 0-1 seconds; 12654 discharges.

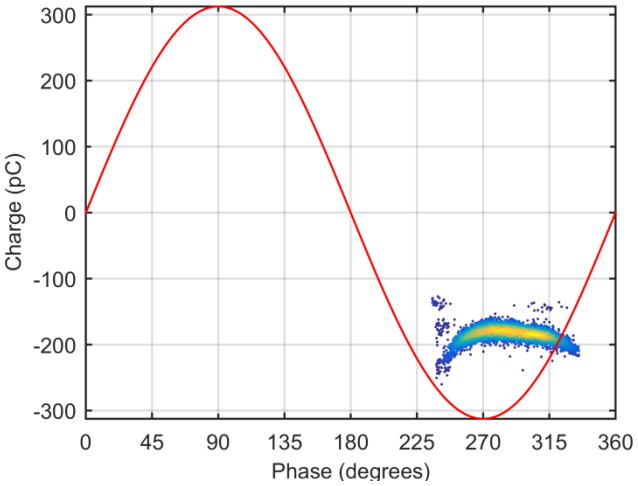

Figure 259: Positive Corona PRPD cluster 3; 0-0.5 seconds; 6283 discharges.

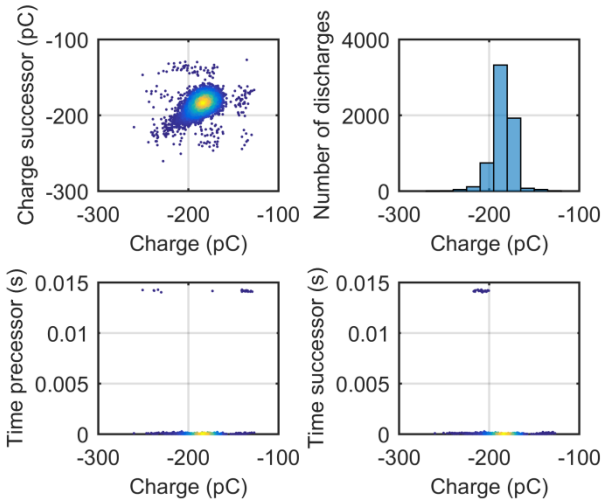

Figure 260: Positive Corona TRPD cluster 3; 0-0.5 seconds; 6283 discharges.

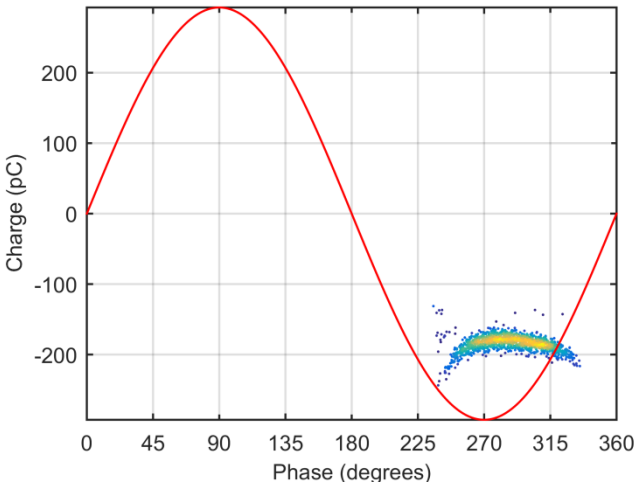

Figure 261: Positive Corona PRPD cluster 4; 0-0.1 seconds; 1257 discharges.

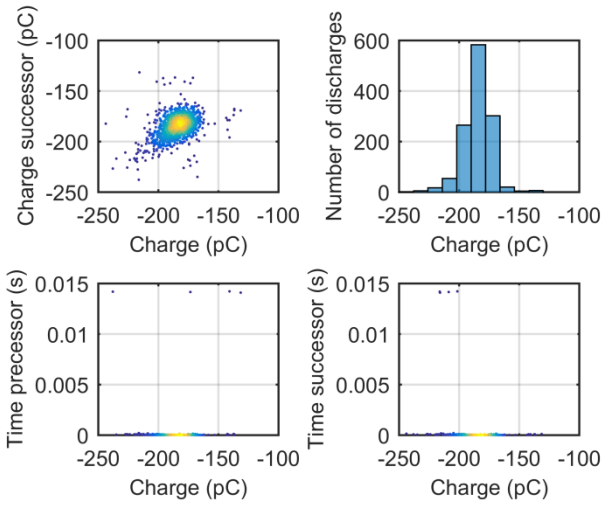

Figure 262: Positive Corona TRPD cluster 4; 0-0.1 seconds; 1257 discharges.

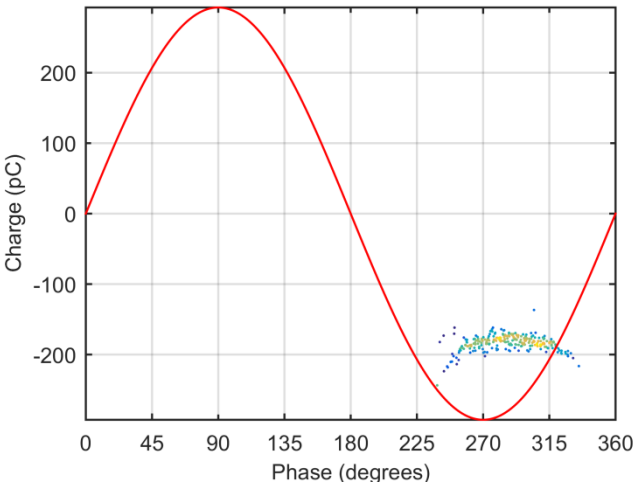

Figure 263: Positive Corona PRPD cluster 5; 0-0.006 seconds; 252 discharges.

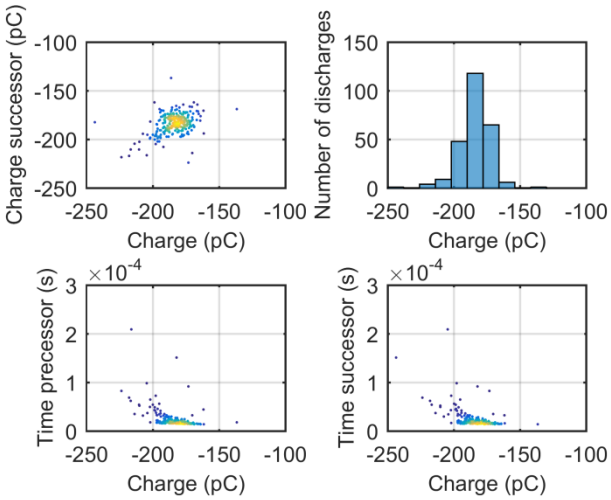

Figure 264: Positive Corona TRPD cluster 5; 0-0.006 seconds; 252 discharges.

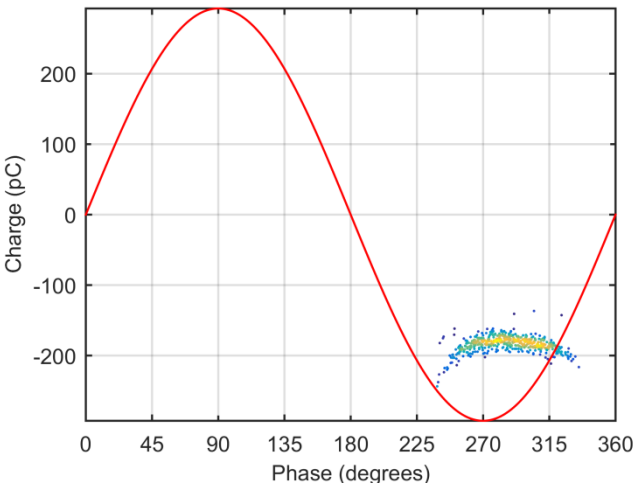

Figure 265: Positive Corona PRPD cluster 6; 0-0.03 seconds; 503 discharges.

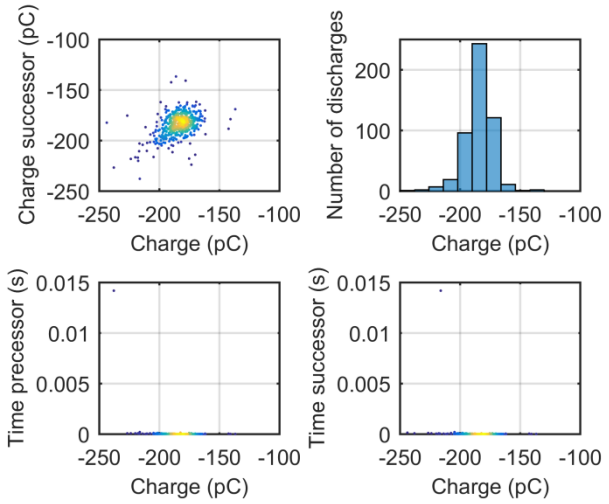

Figure 266: Positive Corona TRPD cluster 6; 0-0.03 seconds; 503 discharges.

D2. Negative Corona time influence

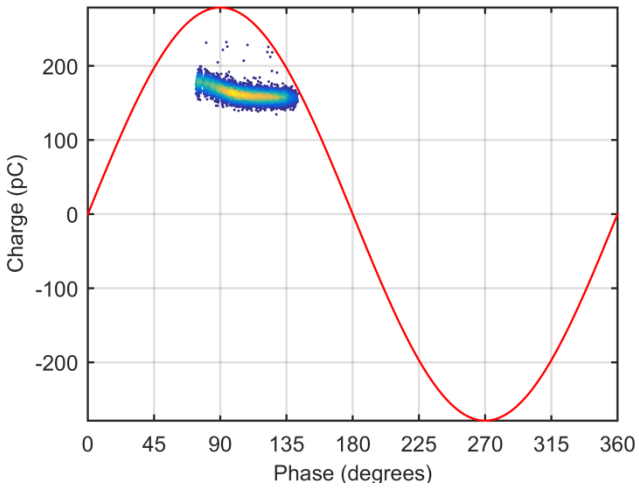

Figure 267: Negative Corona PRPD cluster 1; 0-30 seconds; 27744 discharges.

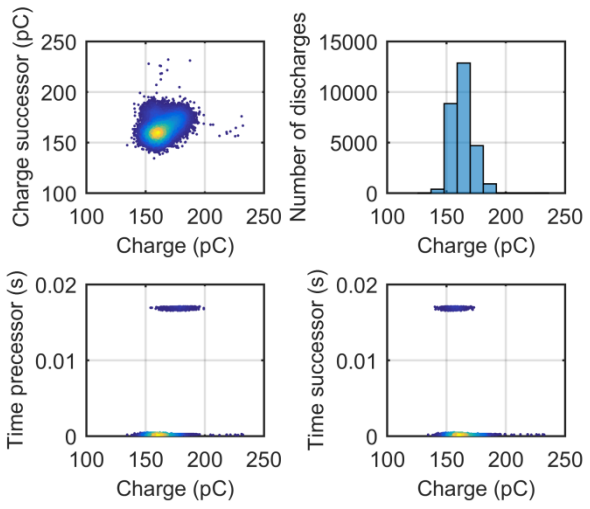

Figure 268: Negative Corona TRPD cluster 1; 0-30 seconds; 27744 discharges.

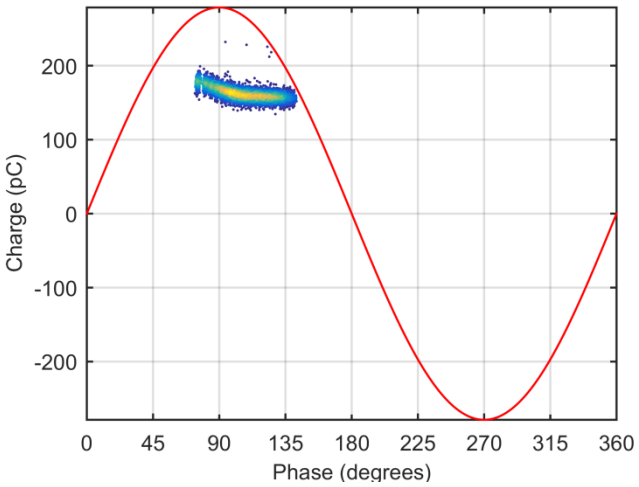

Figure 269: Negative Corona PRPD cluster 2; 0-15 seconds; 13995 discharges.

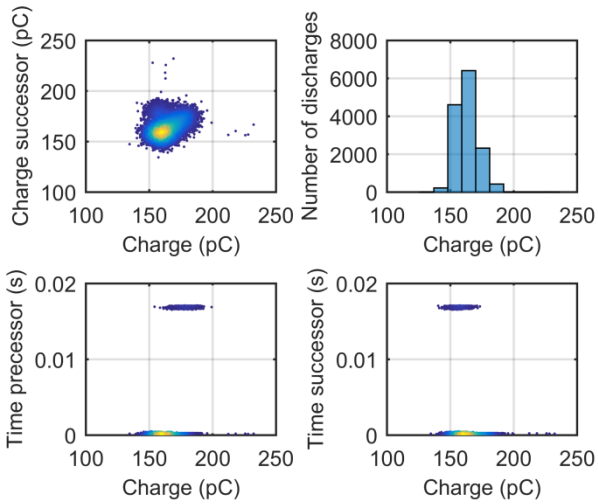

Figure 270: Negative Corona TRPD cluster 2; 0-15 seconds; 13995 discharges.

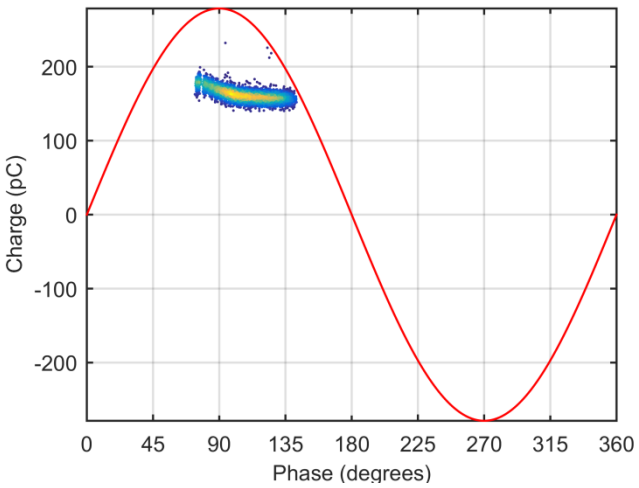

Figure 271: Negative Corona PRPD cluster 3; 0-10 seconds; 9415 discharges.

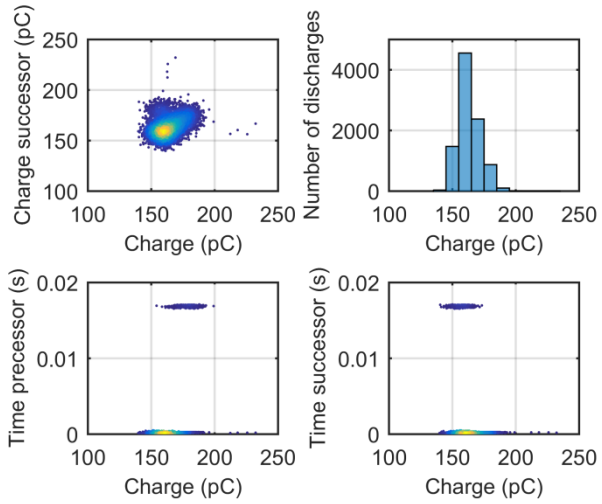

Figure 272: Negative Corona TRPD cluster 3; 0-10 seconds; 9415 discharges.

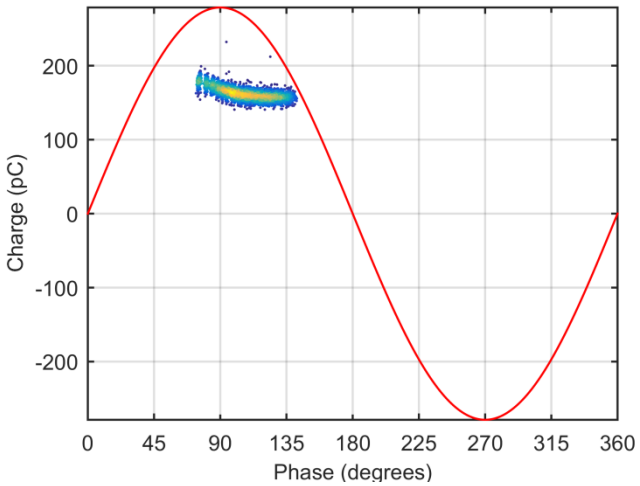

Figure 273: Negative Corona PRPD cluster 4; 0-5 seconds; 4755 discharges.

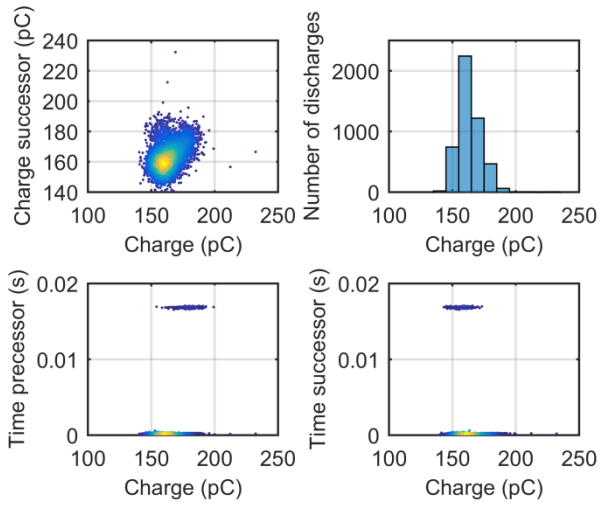

Figure 274: Negative Corona TRPD cluster 4; 0-5 seconds; 4755 discharges.

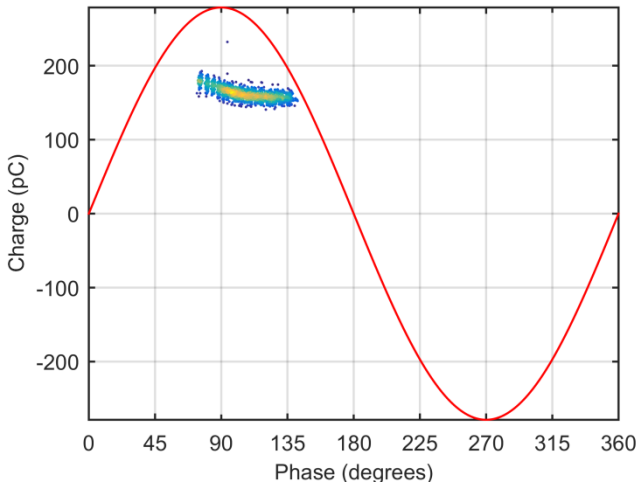

Figure 275: Negative Corona PRPD cluster 5; 0-2 seconds; 1924 discharges.

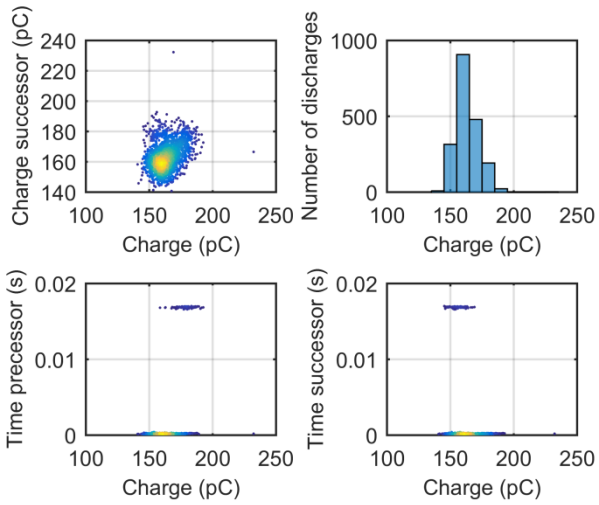

Figure 276: Negative Corona TRPD cluster 5; 0-2 seconds; 1924 discharges.

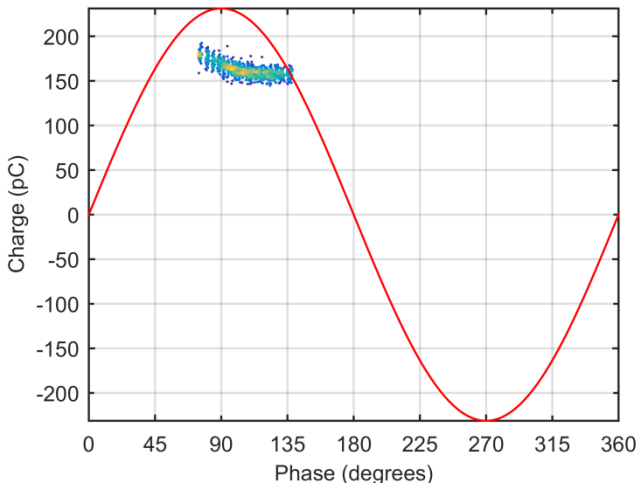

Figure 277: Negative Corona PRPD cluster 6; 0-1 seconds; 969 discharges.

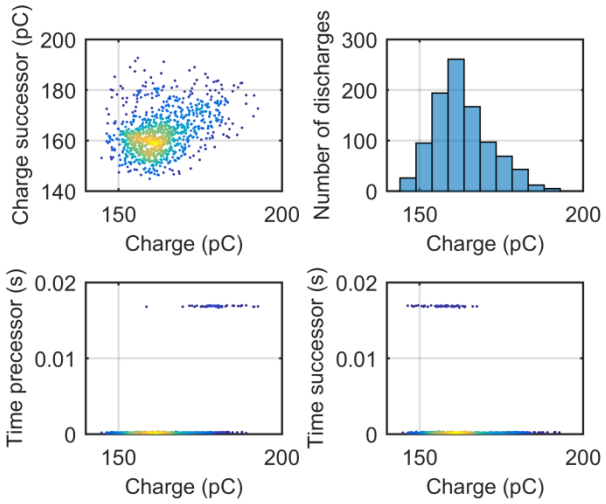

Figure 278: Negative Corona TRPD cluster 6; 0-1 seconds; 969 discharges.

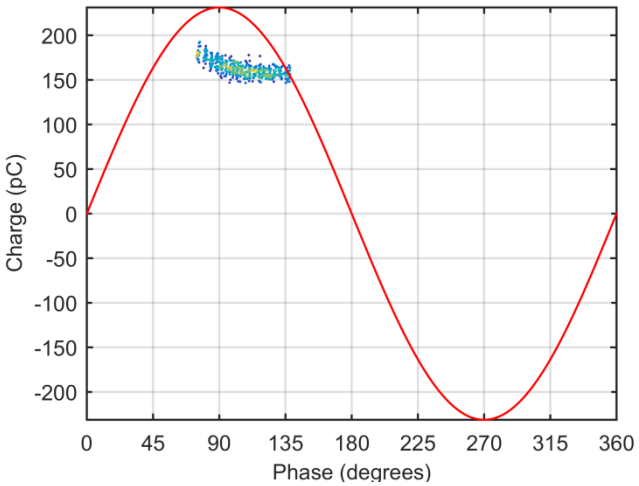

Figure 279: Negative Corona PRPD cluster 7; 0-0.5 seconds; 492 discharges.

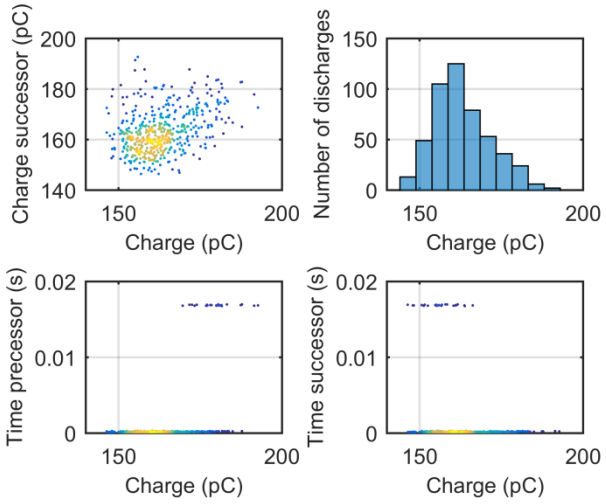

Figure 280: Negative Corona TRPD cluster 7; 0-0.5 seconds; 492 discharges.

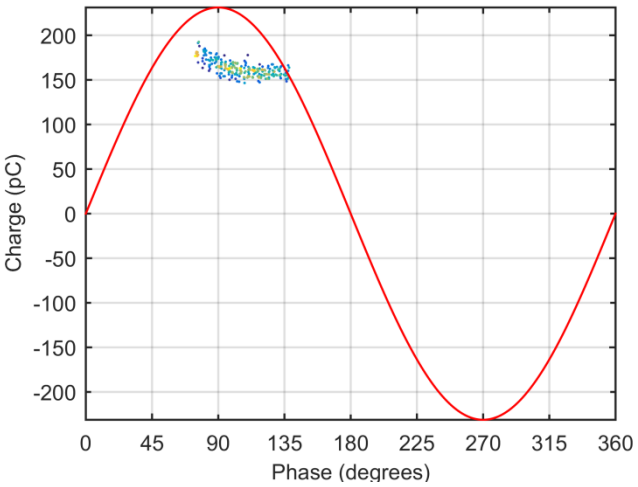

Figure 281: Negative Corona PRPD cluster 8; 0-0.25 seconds; 247 discharges.

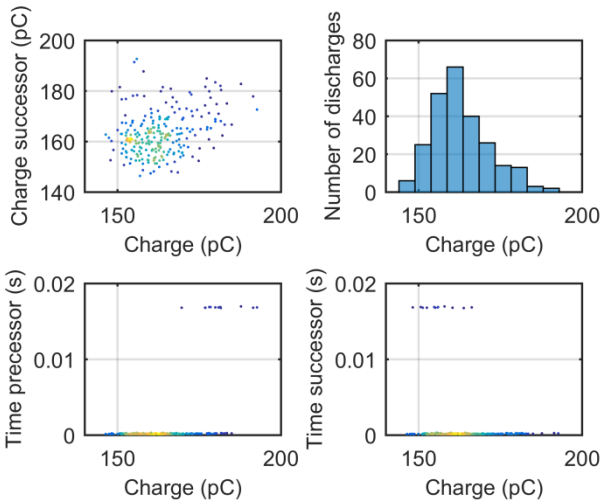

Figure 282: Negative Corona TRPD cluster 8; 0-0.25 seconds; 247 discharges.

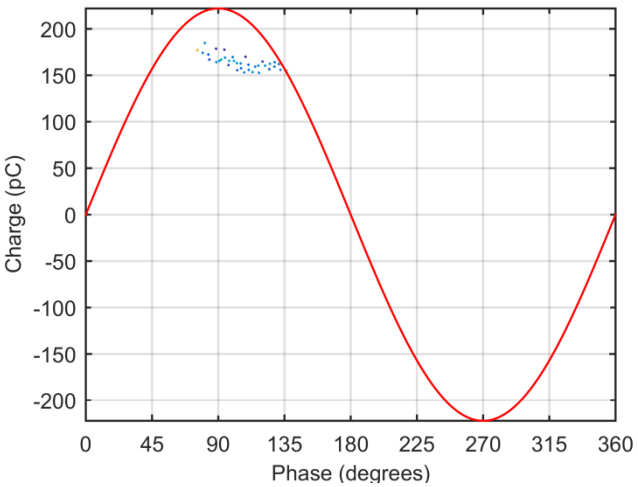

Figure 283: Negative Corona PRPD cluster 9; 0-0.025 seconds; 38 discharges.

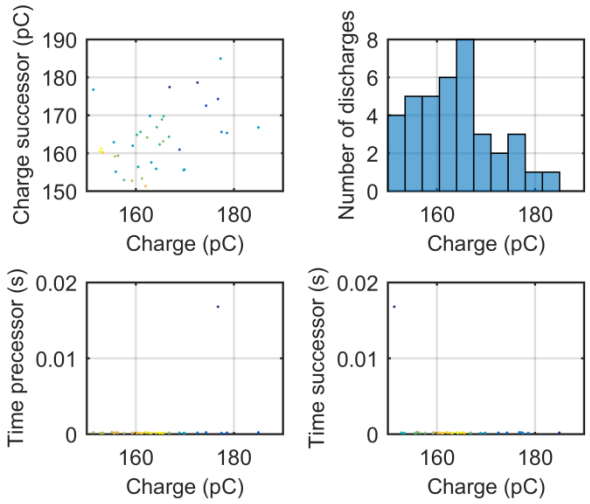

Figure 284: Negative Corona TRPD cluster 9; 0-0.025 seconds; 38 discharges.

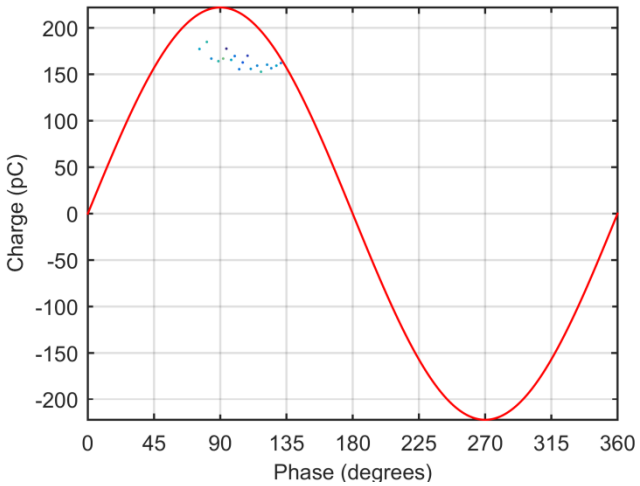

Figure 285: Negative Corona PRPD cluster 10; 0-0.0035 seconds; 19 discharges.

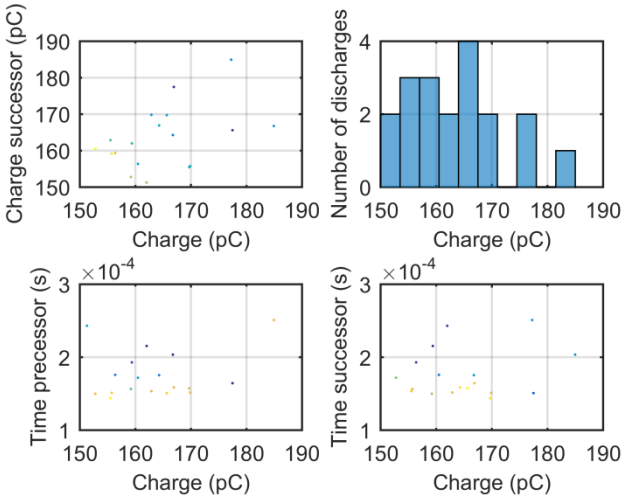

Figure 286: Negative Corona TRPD cluster 10; 0-0.0035 seconds; 19 discharges.

D3. Free-Moving Particle

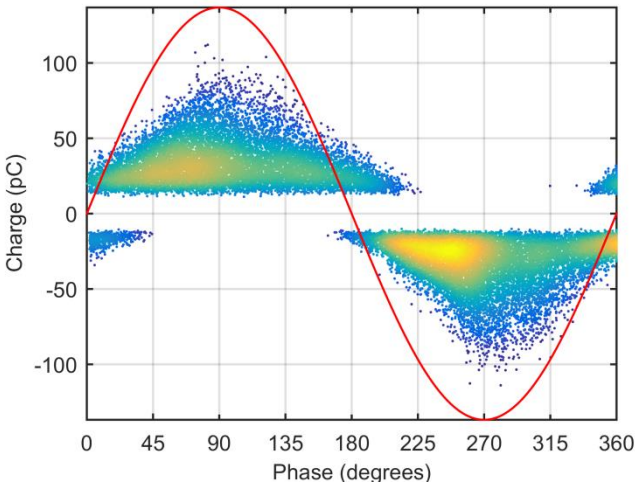

Figure 287: Free-Moving Particle PRPD cluster 1; 0-400 seconds; 26159 discharges.

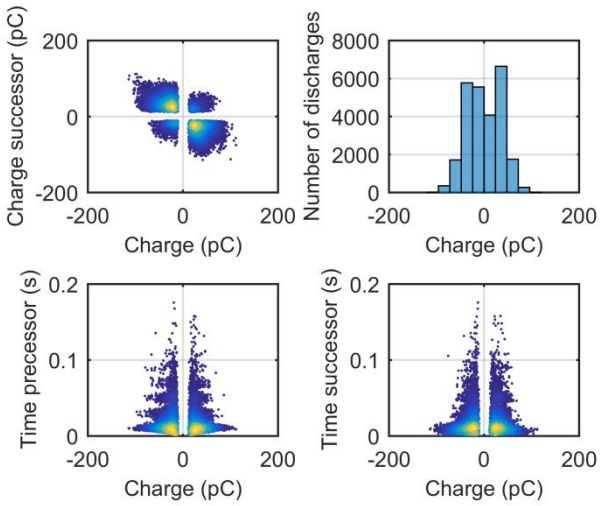

Figure 288: Free-Moving Particle TRPD cluster 1; 0-400 seconds; 26159 discharges.

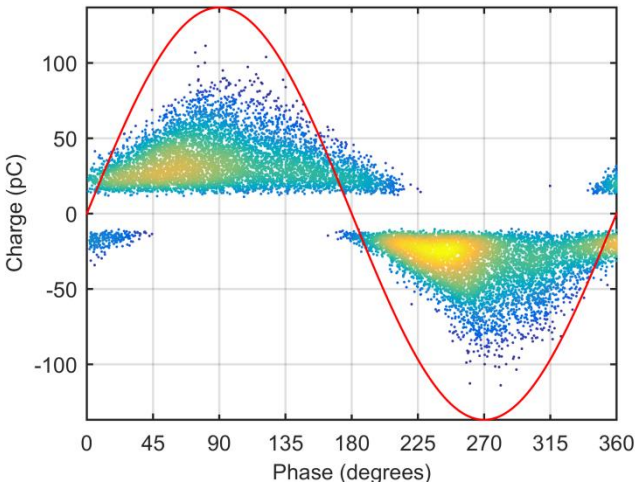

Figure 289: Free-Moving Particle PRPD cluster 2; 0-200 seconds; 13388 discharges.

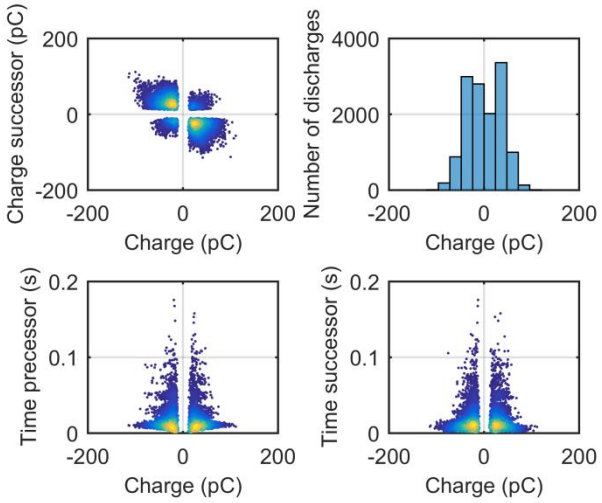

Figure 290: Free-Moving Particle TRPD cluster 2; 0-200 seconds; 13388 discharges.

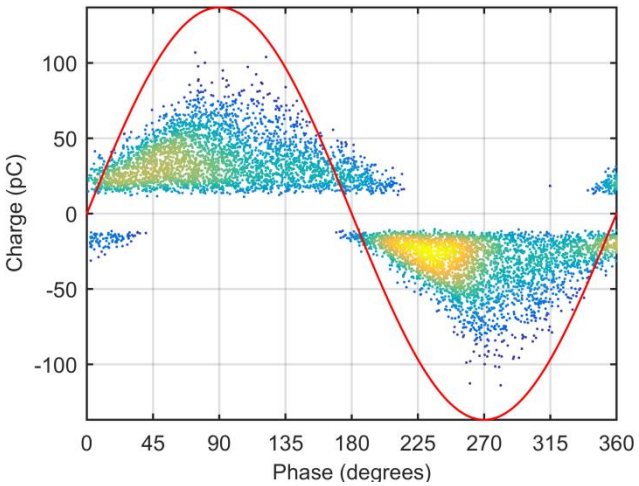

Figure 291: Free-Moving Particle PRPD cluster 3; 0-100 seconds; 6986 discharges.

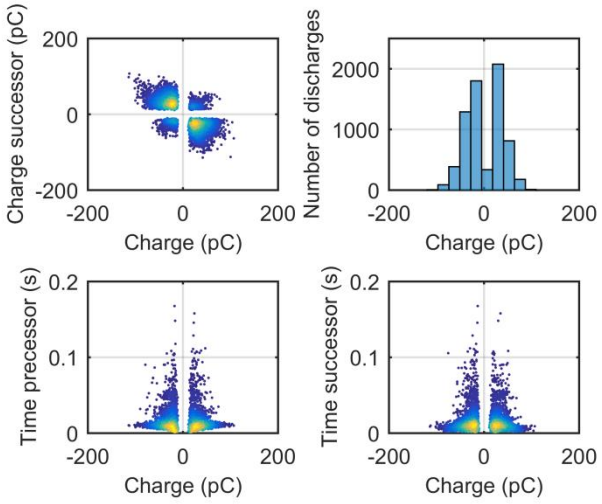

Figure 292: Free-Moving Particle TRPD cluster 3; 0-100 seconds; 6986 discharges.

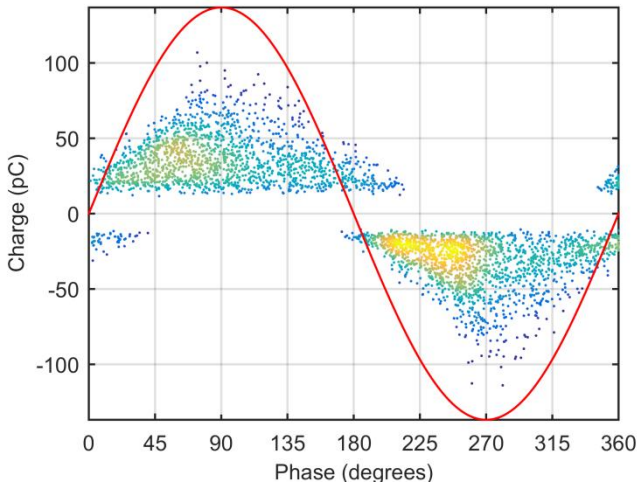

Figure 293: Free-Moving Particle PRPD cluster 4; 0-50 seconds; 3489 discharges.

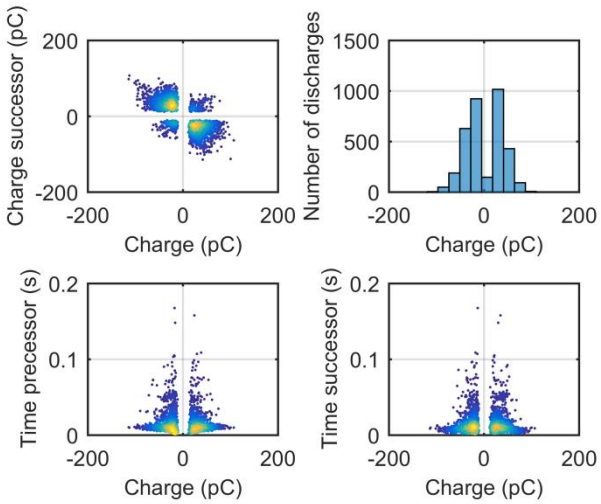

Figure 294: Free-Moving Particle TRPD cluster 4; 0-50 seconds; 3489 discharges.

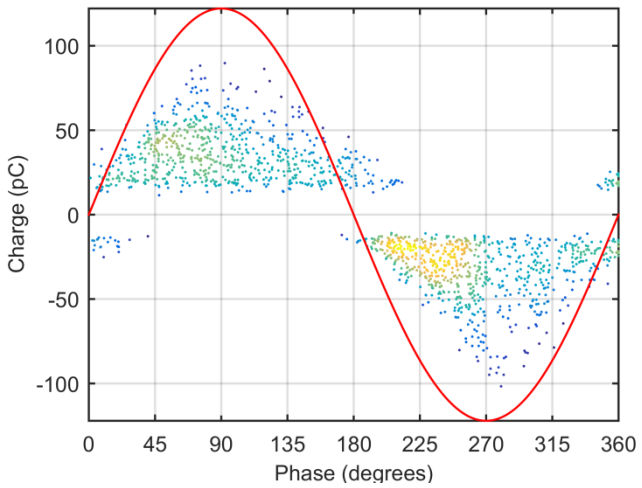

Figure 295: Free-Moving Particle PRPD cluster 5; 0-20 seconds; 1463 discharges.

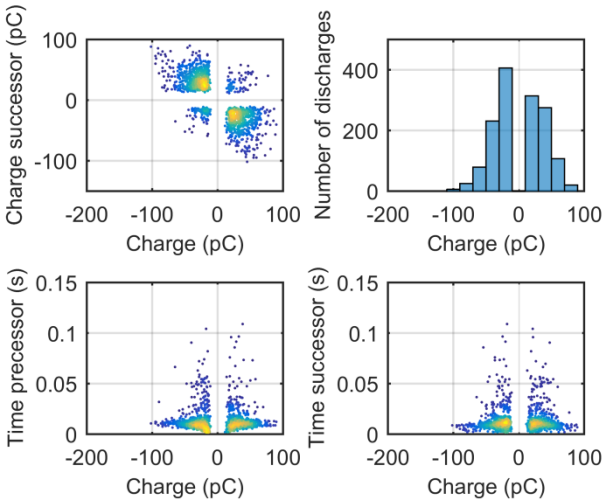

Figure 296: Free-Moving Particle TRPD cluster 5; 0-20 seconds; 1463 discharges.

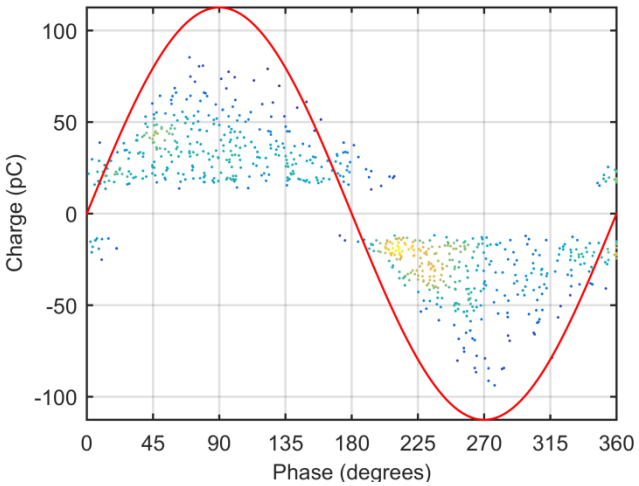

Figure 297: Free-Moving Particle PRPD cluster 6; 0-10 seconds; 728 discharges.

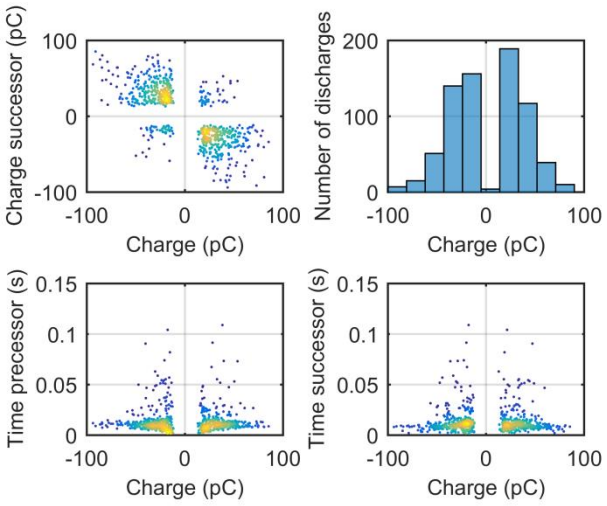

Figure 298: Free-Moving Particle TRPD cluster 6; 0-10 seconds; 728 discharges.

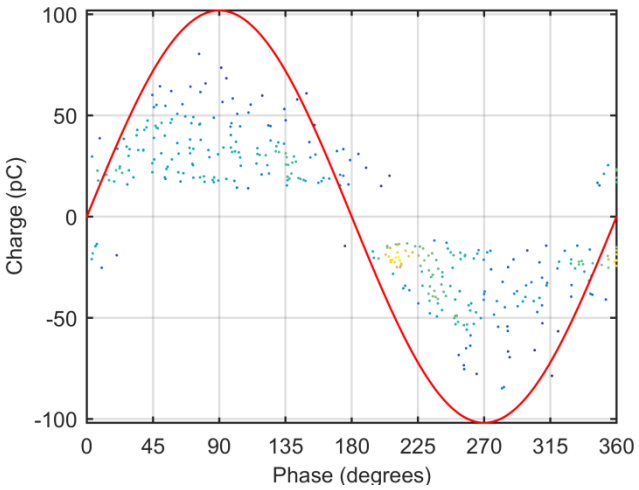

Figure 299: Free-Moving Particle PRPD cluster 7; 0-5 seconds; 357 discharges.

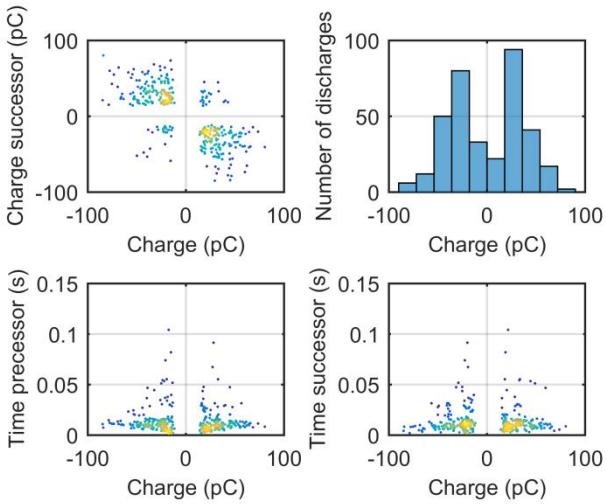

Figure 300: Free-Moving Particle TRPD cluster 7; 0-5 seconds; 357 discharges.

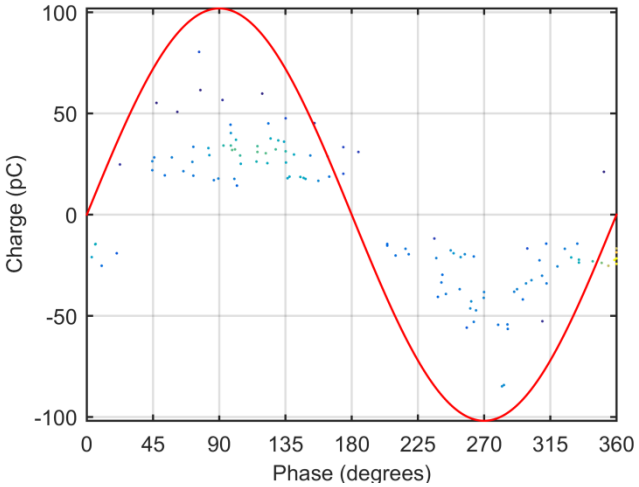

Figure 301: Free-Moving Particle PRPD cluster 8; 0-2 seconds; 118 discharges.

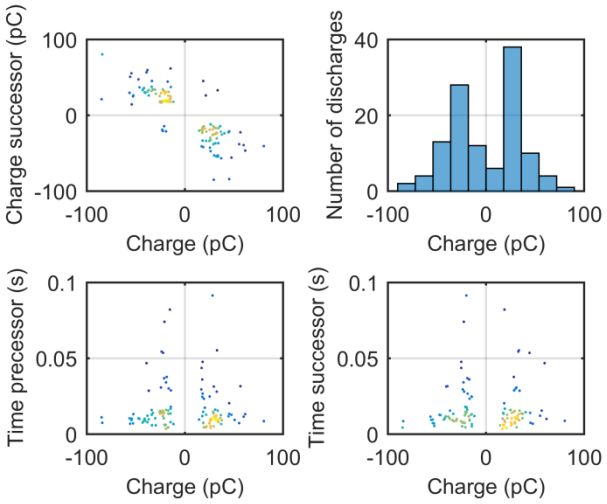

Figure 302: Free-Moving Particle PRPD cluster 8; 0-2 seconds; 118 discharges.

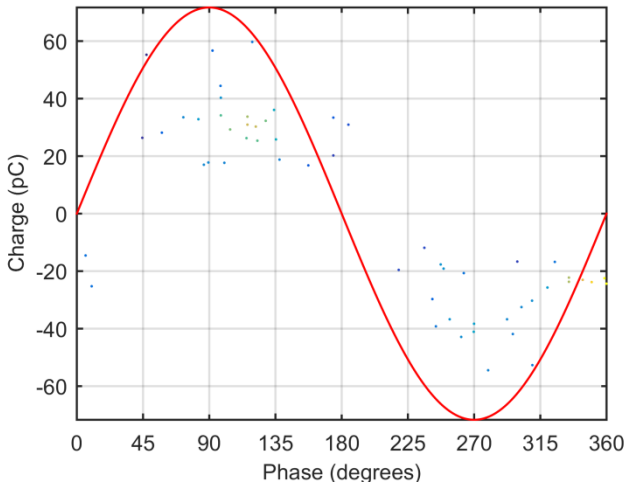

Figure 303: Free-Moving Particle PRPD cluster 9; 0-1 seconds; 55 discharges.

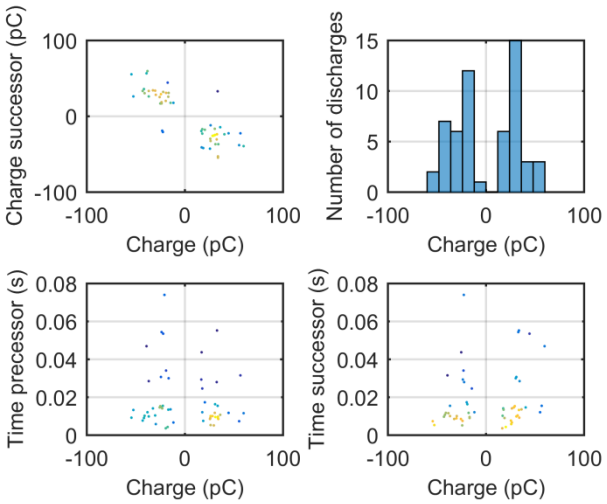

Figure 304: Free-Moving Particle TRPD cluster 9; 0-1 seconds; 55 discharges.

D4. Internal Discharge

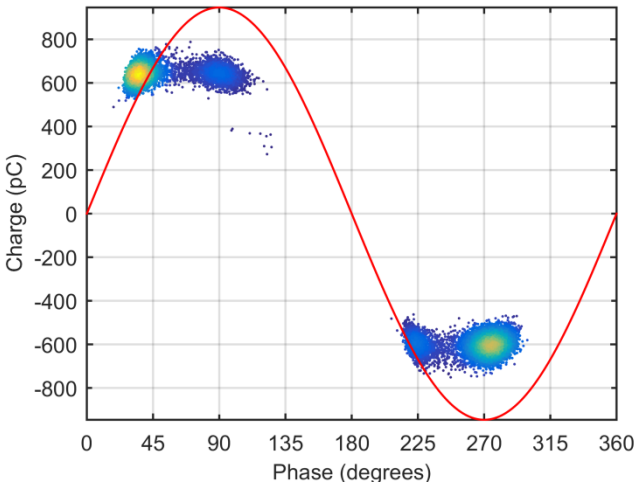

Figure 305: Internal Discharge PRPD cluster 1; 0-250 seconds; 25005 discharges.

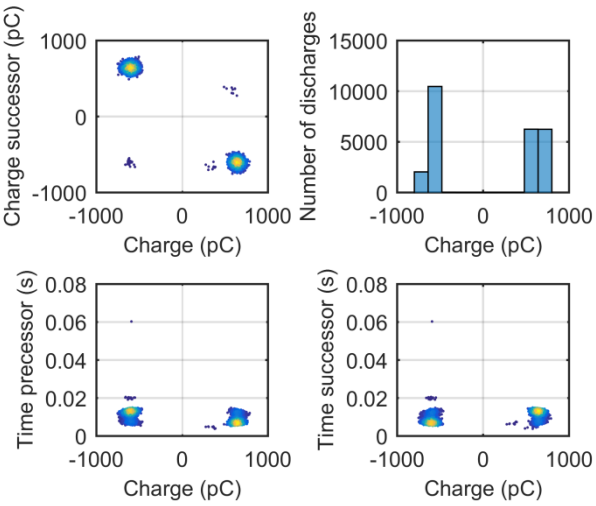

Figure 306: Internal Discharge TRPD cluster 1; 0-250 seconds; 25005 discharges.

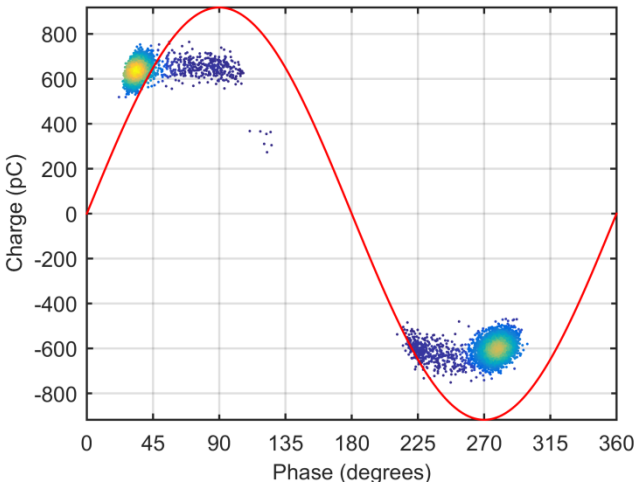

Figure 307: Internal Discharge PRPD cluster 2; 0-100 seconds; 10098 discharges.

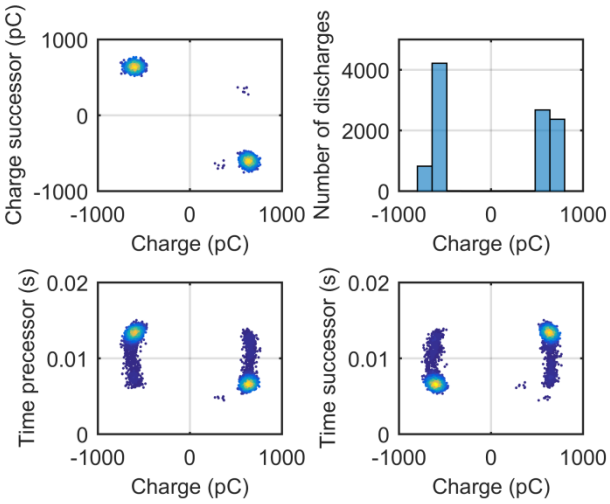

Figure 308: Internal Discharge TRPD cluster 2; 0-100 seconds; 10098 discharges.

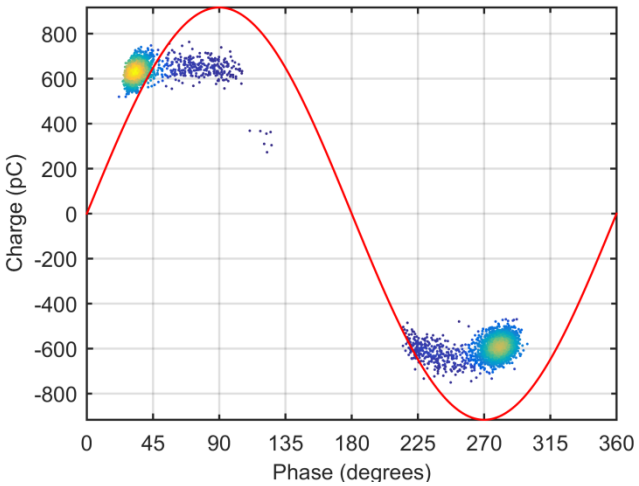

Figure 309: Internal Discharge PRPD cluster 3; 0-50 seconds; 5016 discharges.

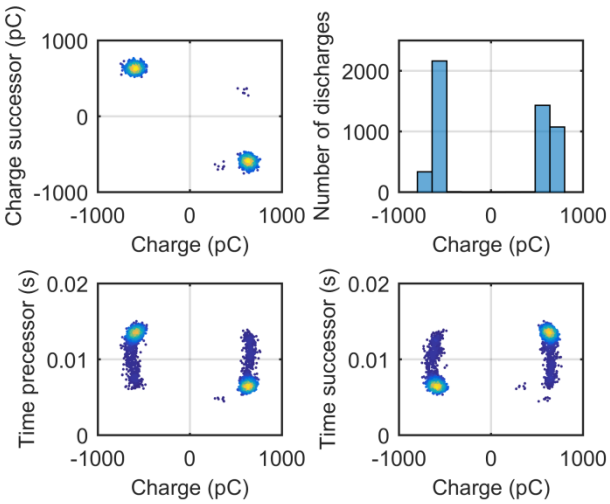

Figure 310: Internal Discharge TRPD cluster 3; 0-50 seconds; 5016 discharges.

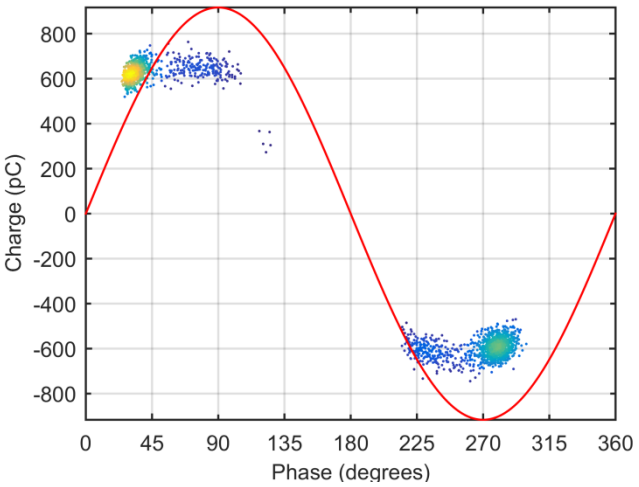

Figure 311: Internal Discharge PRPD cluster 4; 0-20 seconds; 2011 discharges.

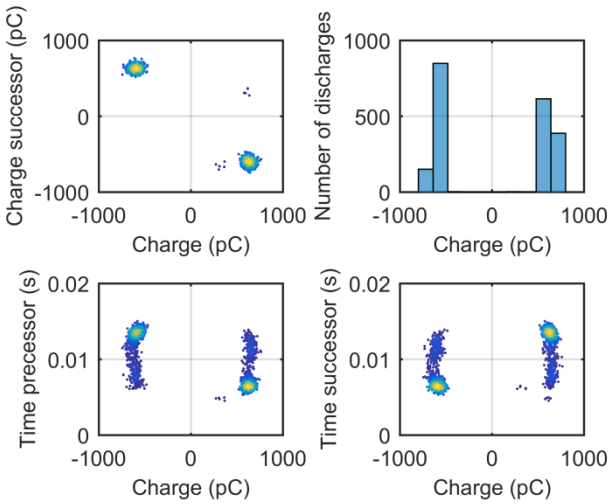

Figure 312: Internal Discharge TRPD cluster 4; 0-20 seconds; 2011 discharges.

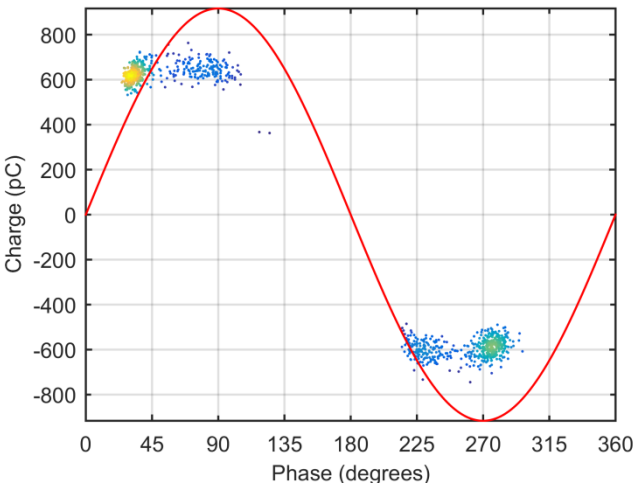

Figure 313: Internal Discharge PRPD cluster 5; 0-10 seconds; 1003 discharges.

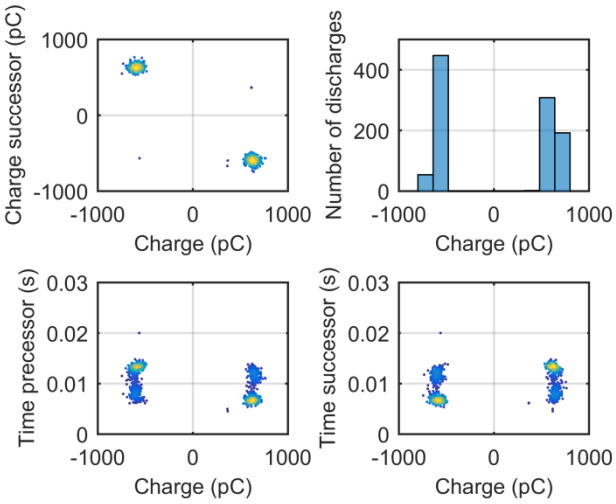

Figure 314: Internal Discharge TRPD cluster 6; 0-10 seconds; 1003 discharges.

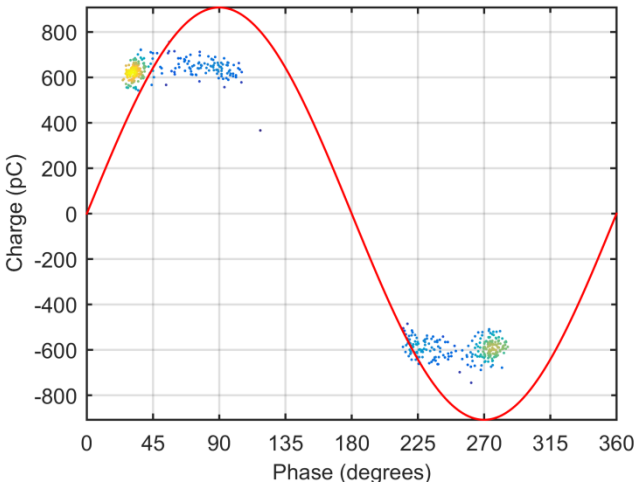

Figure 315: Internal Discharge PRPD cluster 6; 0-5 seconds; 502 discharges.

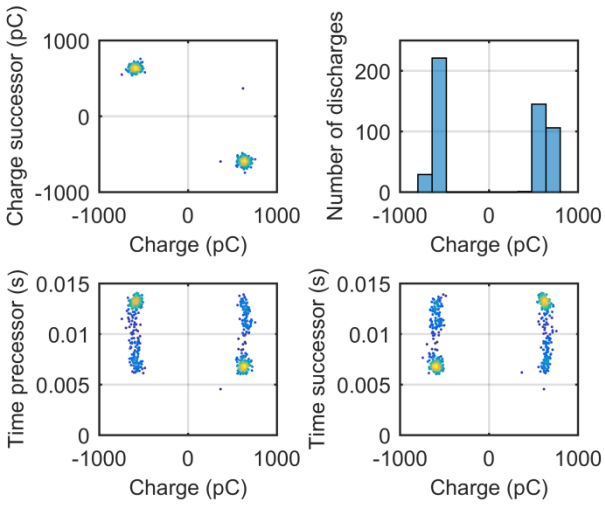

Figure 316: Internal Discharge TRPD cluster 6; 0-5 seconds; 502 discharges.

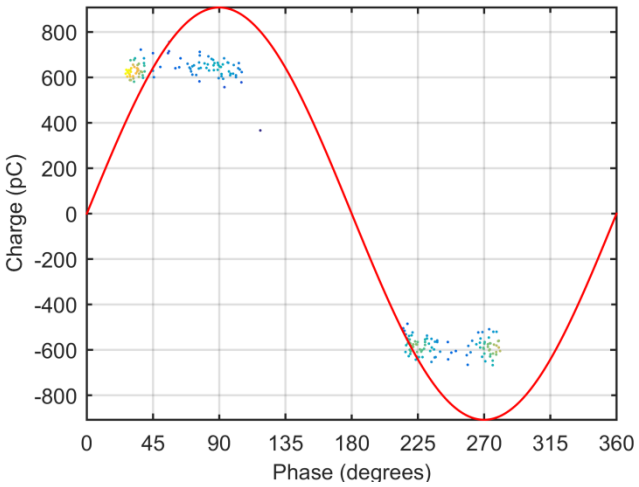

Figure 317: Internal Discharge PRPD cluster 7; 0-2 seconds; 202 discharges.

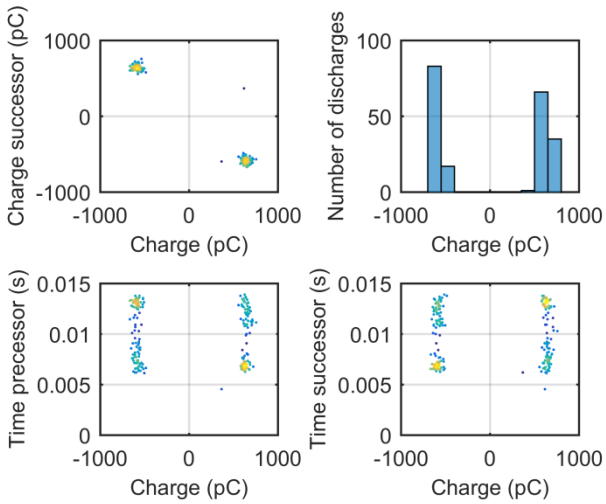

Figure 318: Internal Discharge TRPD cluster 7; 0-2 seconds; 202 discharges.

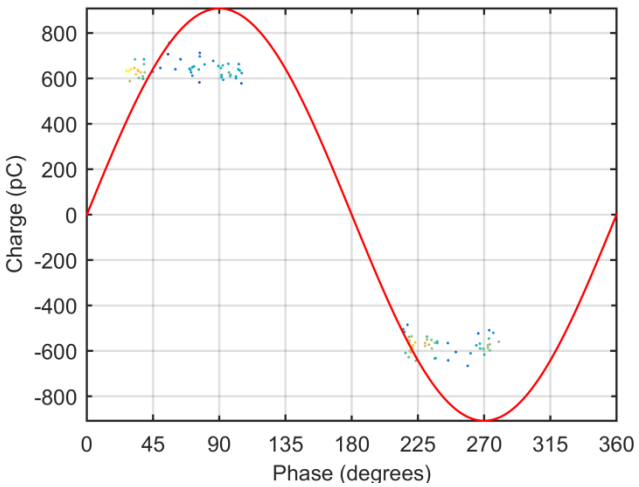

Figure 319: Internal Discharge PRPD cluster 8; 0-1 seconds; 101 discharges.

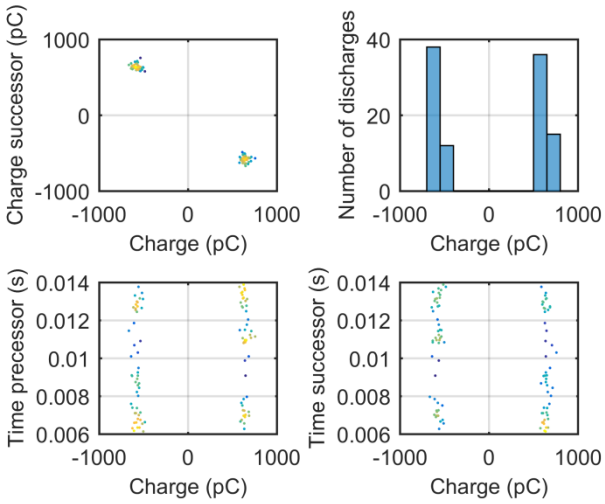

Figure 320: Internal Discharge TRPD cluster 8; 0-1 seconds; 101 discharges.

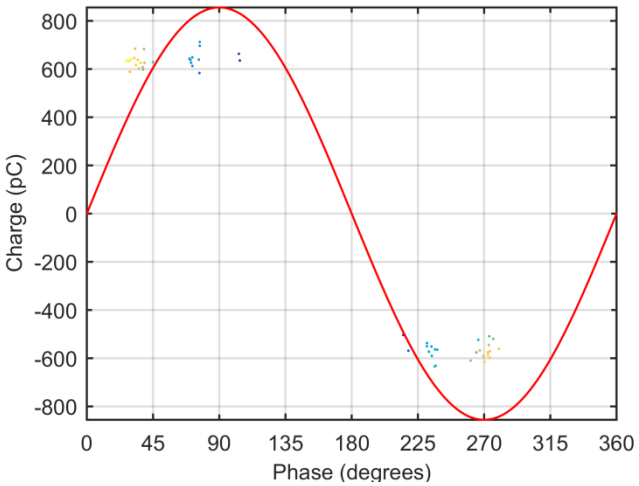

Figure 321: Internal Discharge PRPD cluster 9; 0-0.5 seconds; 51 discharges.

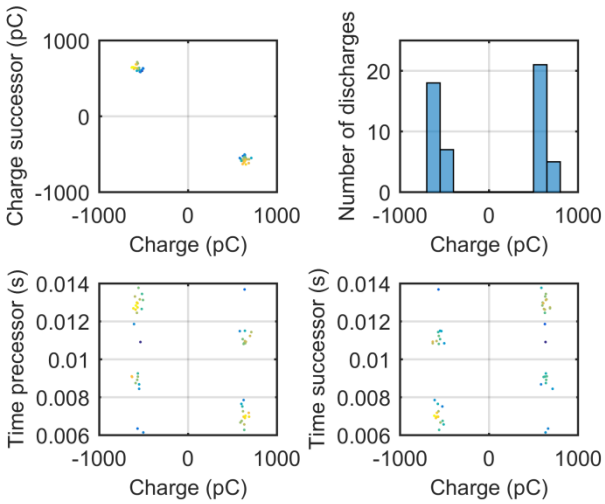

Figure 322: Internal Discharge TRPD cluster 9; 0-0.5 seconds; 51 discharges.

D5. Floating electrode

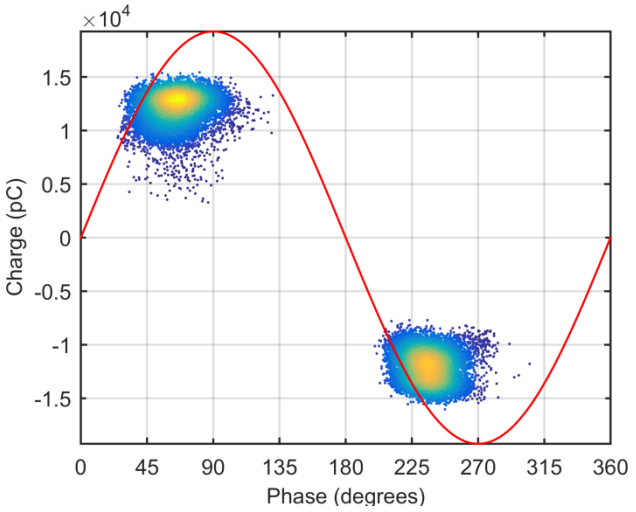

Figure 323: Floating electrode PRPD cluster 1; 0-300 seconds; 27016 discharges.

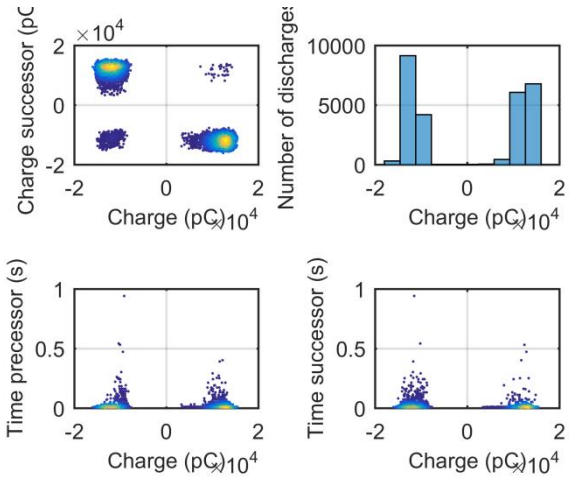

Figure 324: Floating electrode TRPD cluster 1; 0-300 seconds; 27016 discharges.

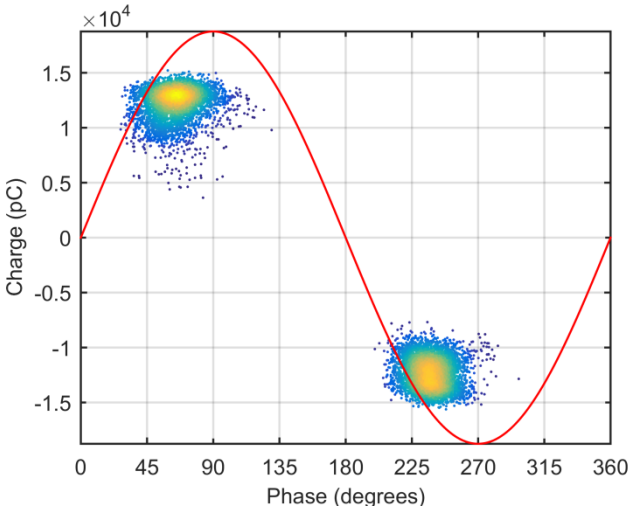

Figure 325: Floating electrode PRPD cluster 2; 0-100 seconds; 9195 discharges.

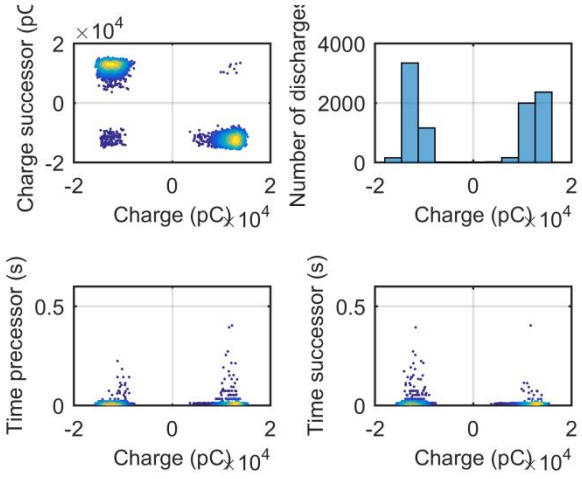

Figure 326: Floating electrode TRPD cluster 2; 0-100 seconds; 9195 discharges.

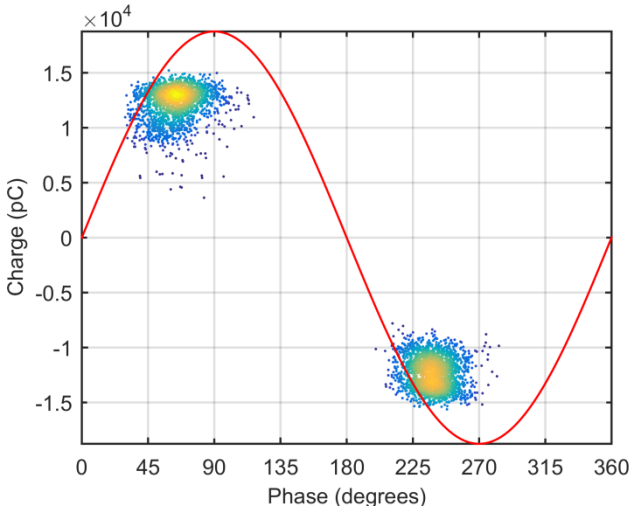

Figure 327: Floating electrode PRPD cluster 3; 0-50 seconds; 4588 discharges.

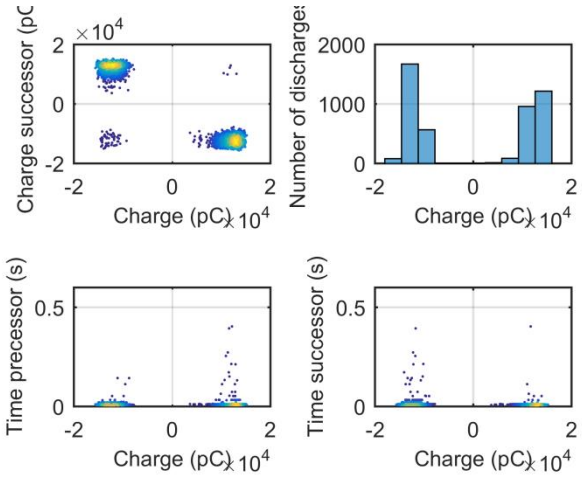

Figure 328: Floating electrode TRPD cluster 3; 0-50 seconds; 4588 discharges.

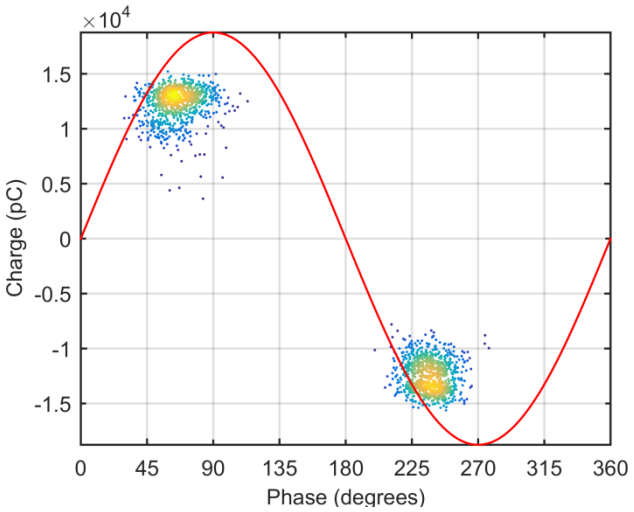

Figure 329: Floating electrode PRPD cluster 4; 0-20 seconds; 1835 discharges.

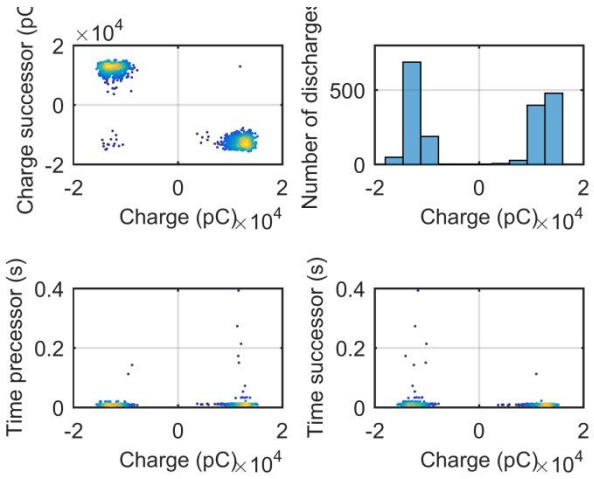

Figure 330: Floating electrode TRPD cluster 4; 0-20 seconds; 1835 discharges.

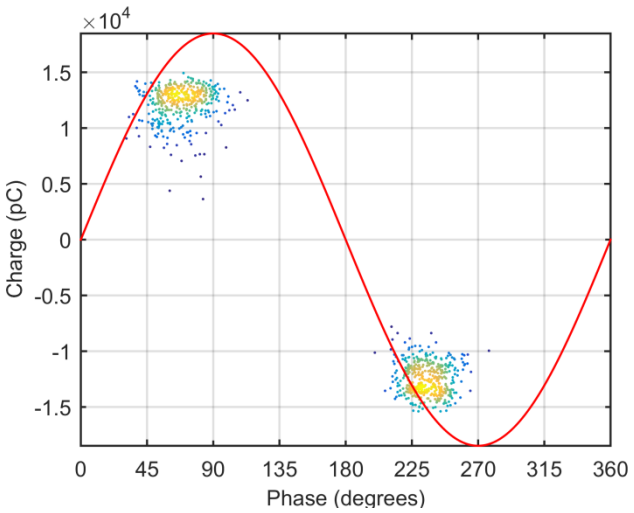

Figure 331: Floating electrode PRPD cluster 5; 0-10 seconds; 863 discharges.

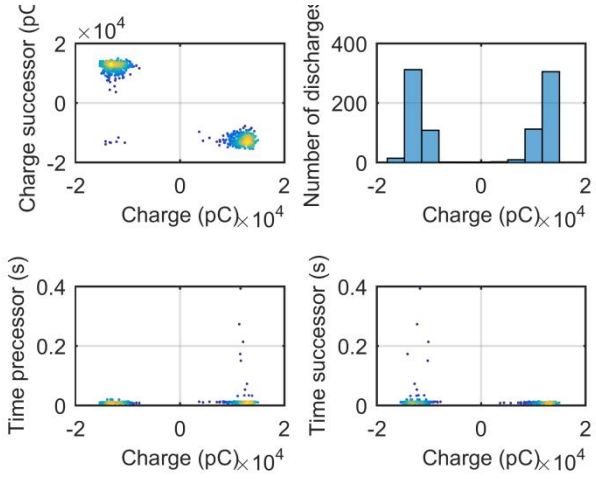

Figure 332: Floating electrode TRPD cluster 5; 0-10 seconds; 863 discharges.

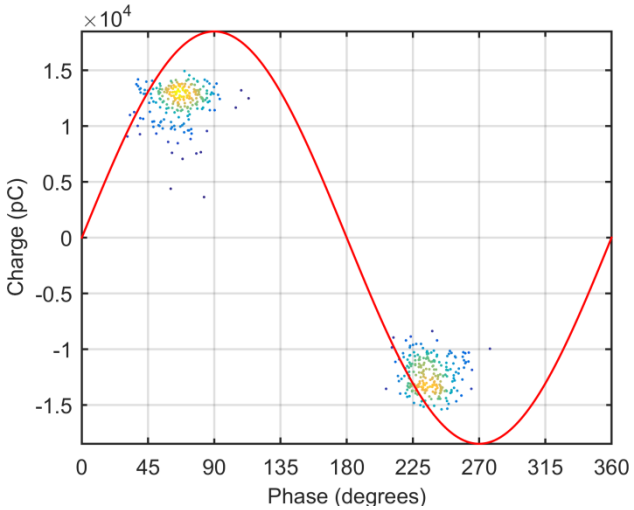

Figure 333: Floating electrode PRPD cluster 6; 0-5 seconds; 474 discharges.

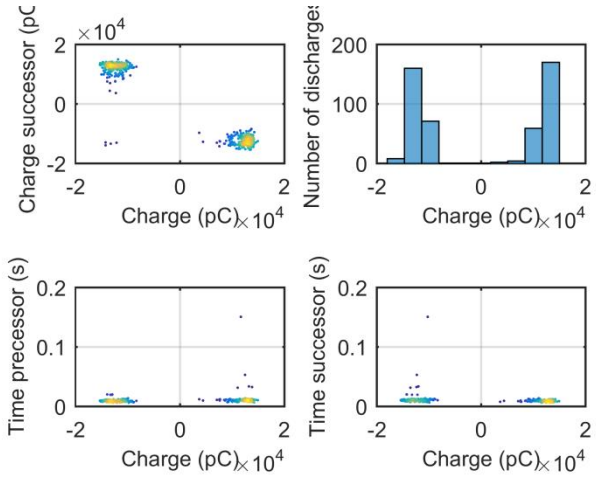

Figure 334: Floating electrode TRPD cluster 6; 0-5 seconds; 474 discharges.

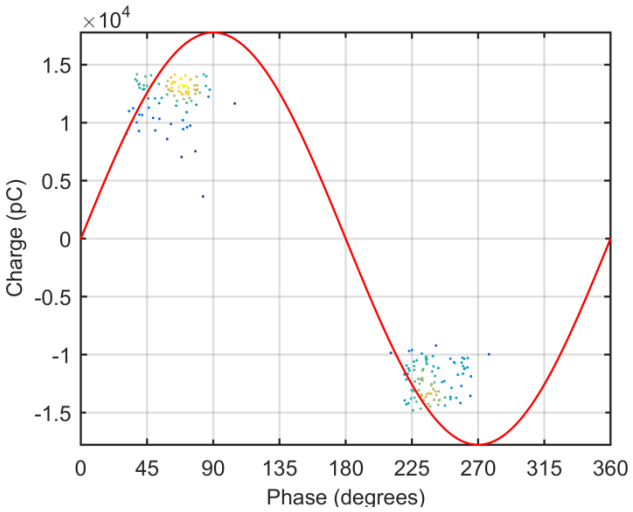

Figure 335: Floating electrode PRPD cluster 7; 0-2 seconds; 185 discharges.

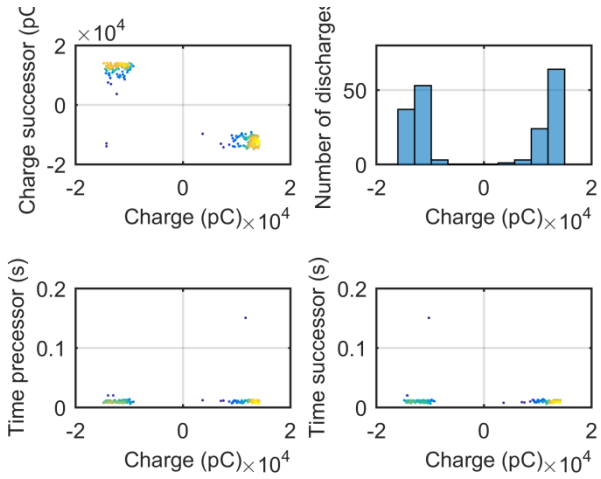

Figure 336: Floating electrode TRPD cluster 7; 0-2 seconds; 185 discharges.

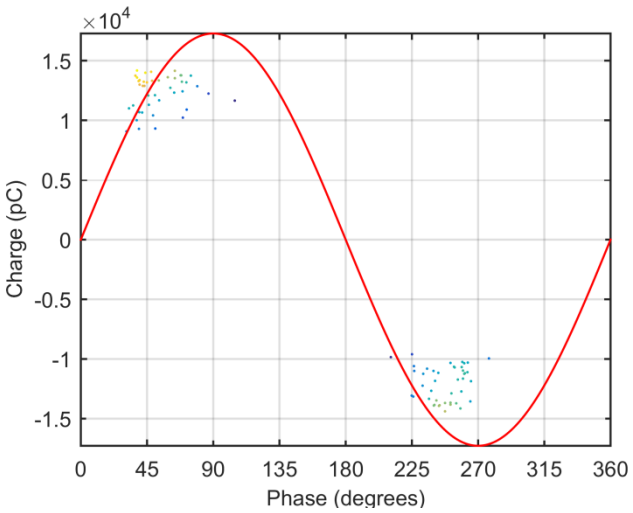

Figure 337: Floating electrode PRPD cluster 8; 0-1 seconds; 86 discharges.

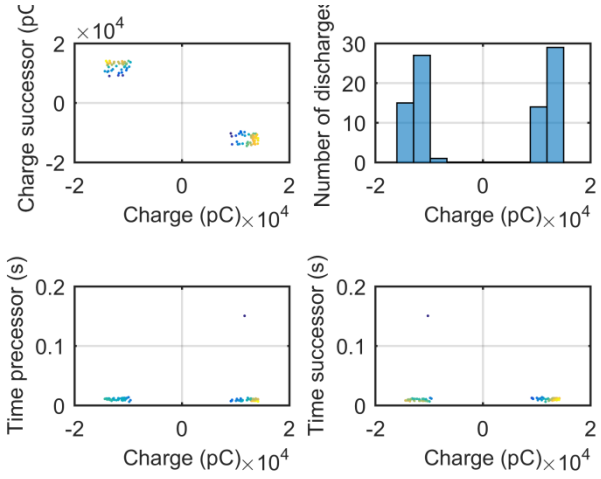

Figure 338: Floating electrode TRPD cluster 8; 0-1 seconds; 86 discharges.

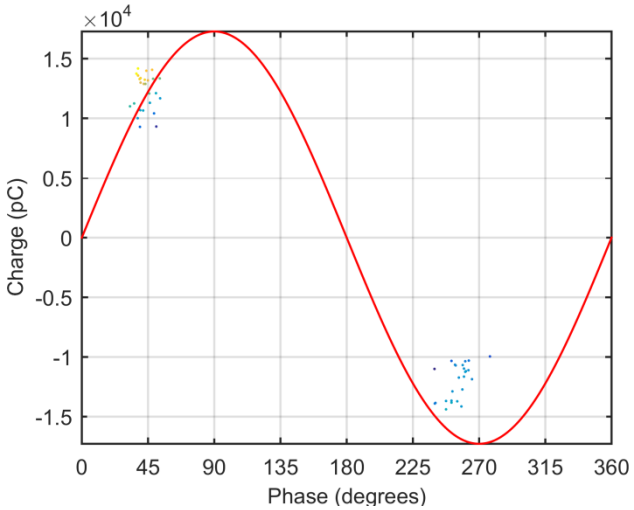

Figure 339: Floating electrode PRPD cluster 9; 0-0.5 seconds; 51 discharges.

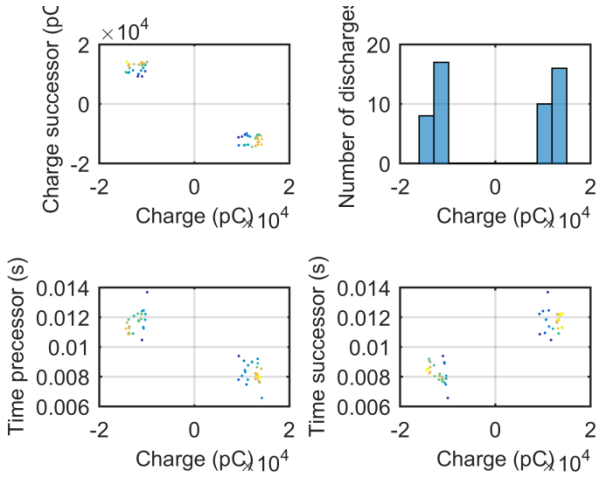

Figure 340: Floating electrode TRPD cluster 9; 0-0.5 seconds; 51 discharges.

D6. Surface Discharge

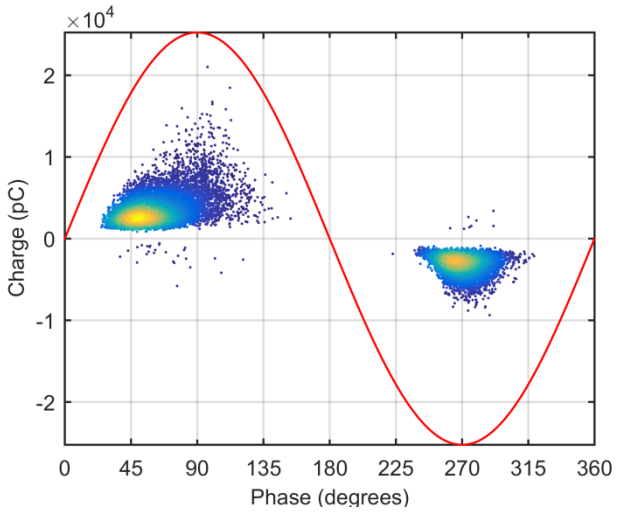

Figure 341: Surface Discharge PRPD cluster 1; 0-500 seconds; 24036 discharges.

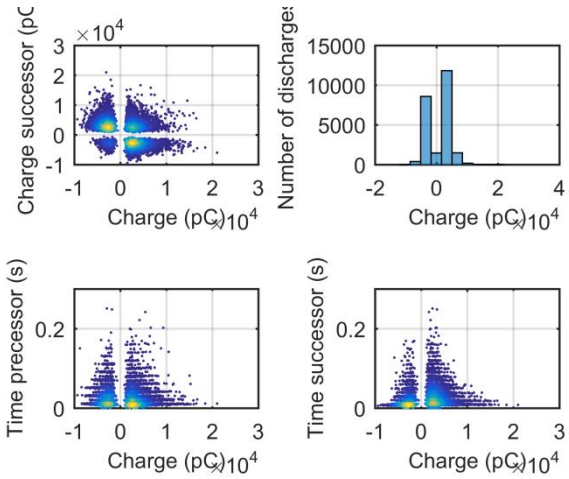

Figure 342: Surface Discharge TRPD cluster 1; 0-500 seconds; 24036 discharges.

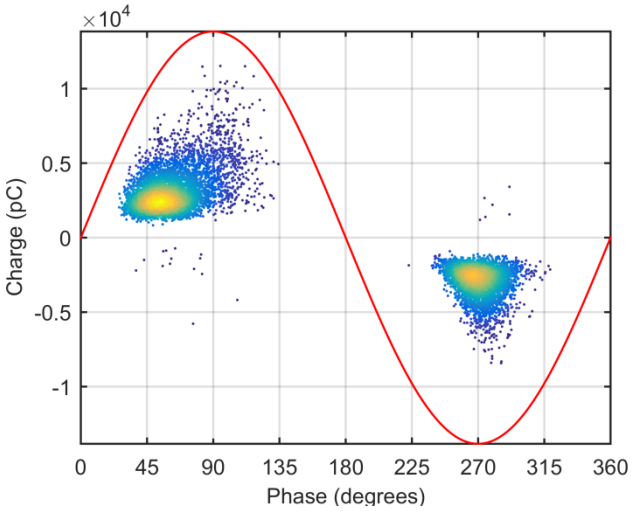

Figure 343: Surface Discharge PRPD cluster 2; 0-250 seconds; 10590 discharges.

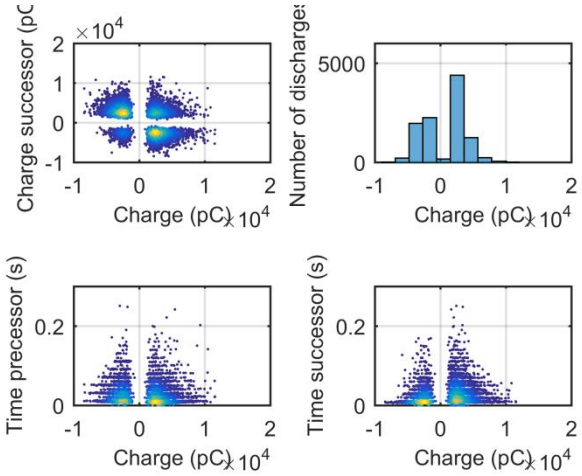

Figure 344: Surface Discharge TRPD cluster 2; 0-250 seconds; 10590 discharges.

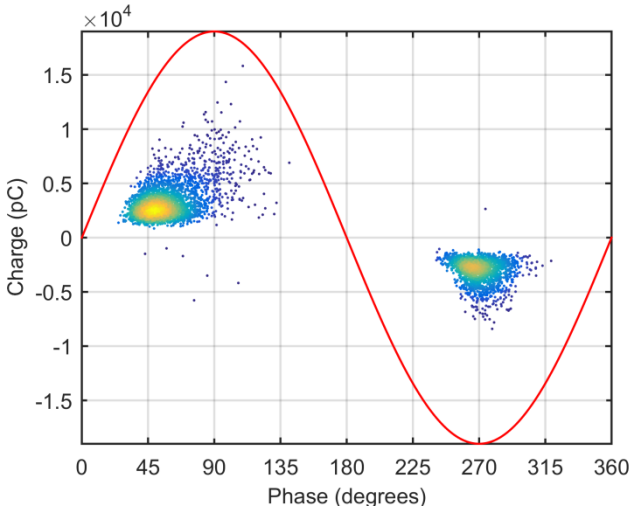

Figure 345: Surface Discharge PRPD cluster 3; 0-100 seconds; 5043 discharges.

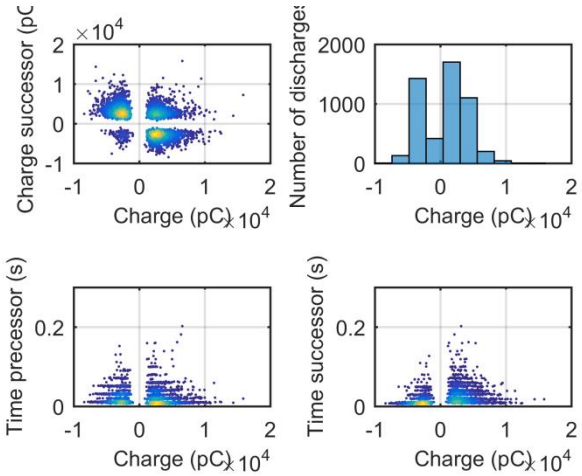

Figure 346: Surface Discharge TRPD cluster 3; 0-100 seconds; 5043 discharges.

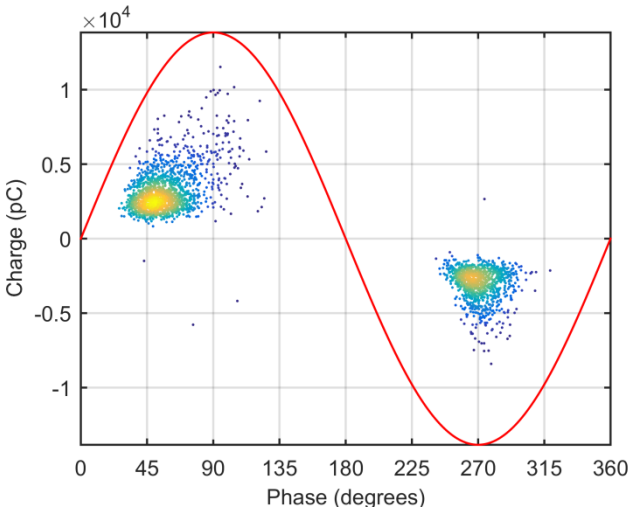

Figure 347: Surface Discharge PRPD cluster 4; 0-50 seconds; 2532 discharges.

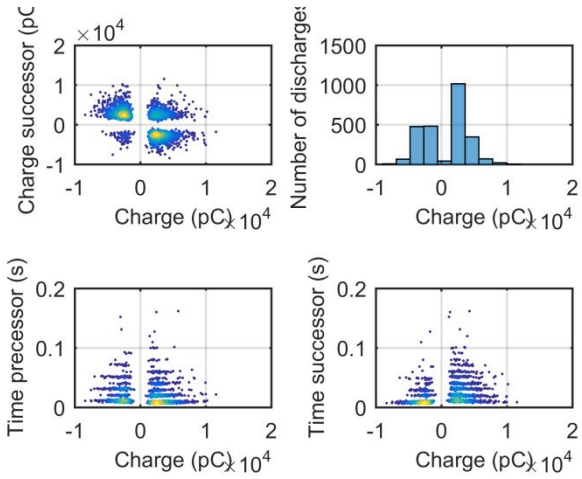

Figure 348: Surface Discharge TRPD cluster 4; 0-50 seconds; 2532 discharges.

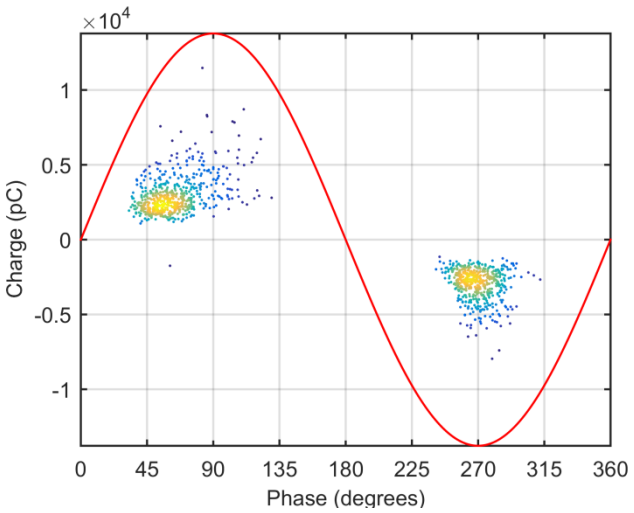

Figure 349: Surface Discharge PRPD cluster 5; 0-25 seconds; 1069 discharges.

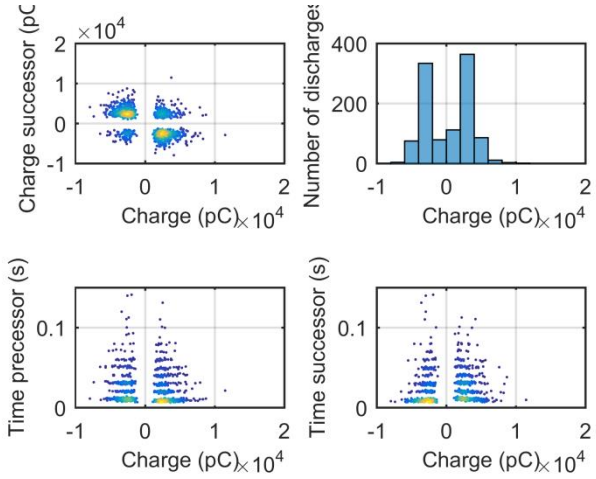

Figure 350: Surface Discharge TRPD cluster 5; 0-25 seconds; 1069 discharges.

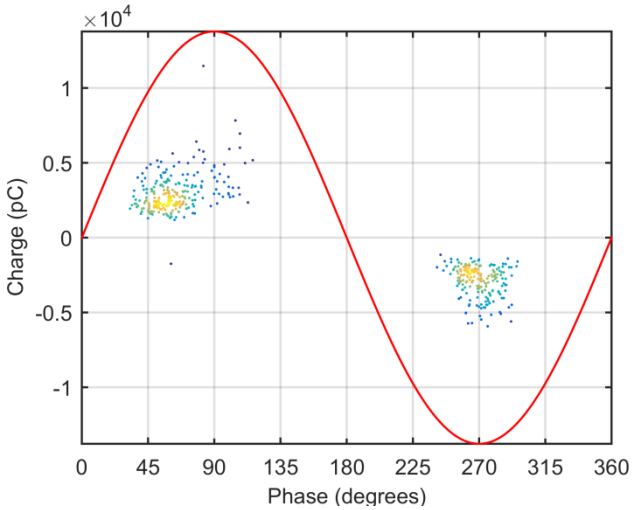

Figure 351: Surface Discharge PRPD cluster 6; 0-10 seconds; 427 discharges.

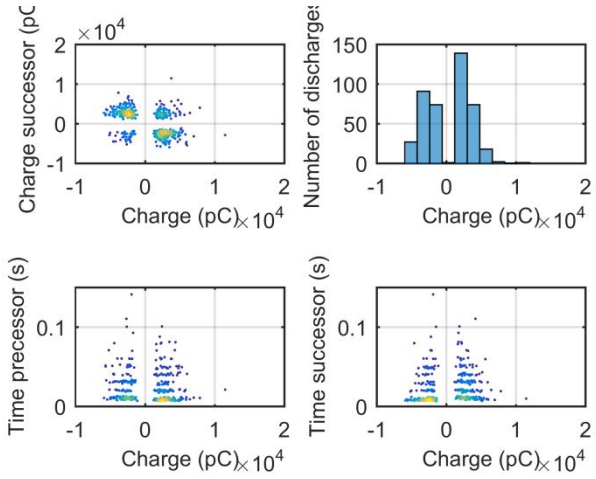

Figure 352: Surface Discharge TRPD cluster 6; 0-10 seconds; 427 discharges.

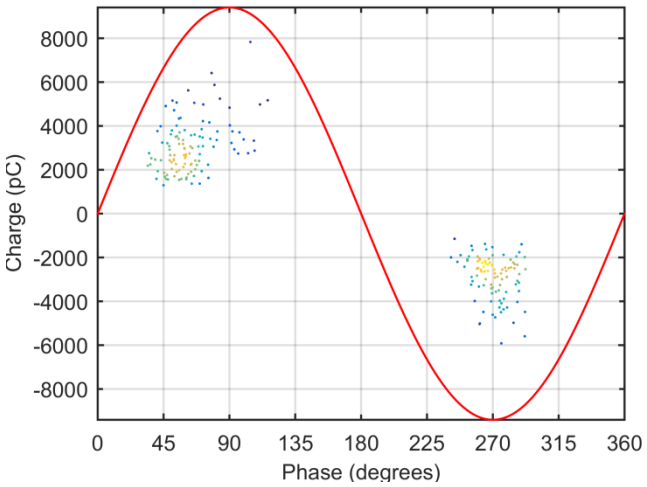

Figure 353: Surface Discharge PRPD cluster 7; 0-5 seconds; 207 discharges.

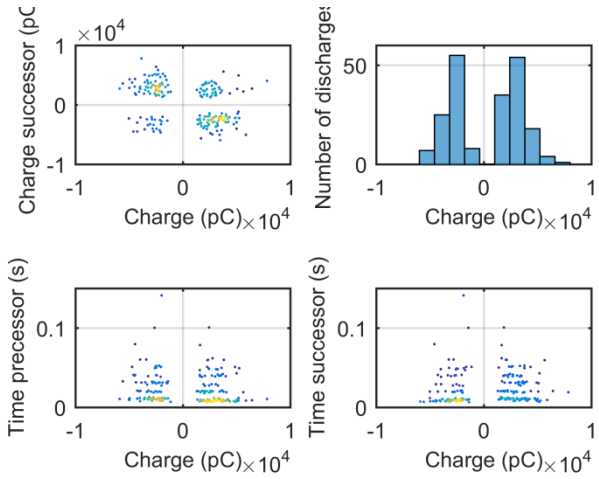

Figure 354: Surface Discharge TRPD cluster 7; 0-5 seconds; 207 discharges.

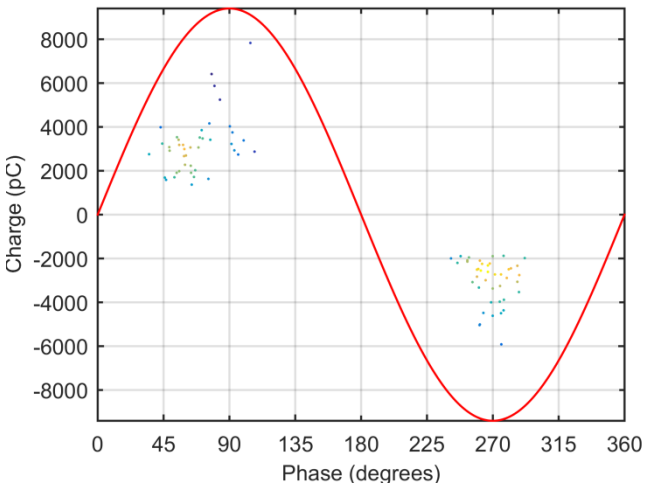

Figure 355: Surface Discharge PRPD cluster 8; 0-2 seconds; 84 discharges.

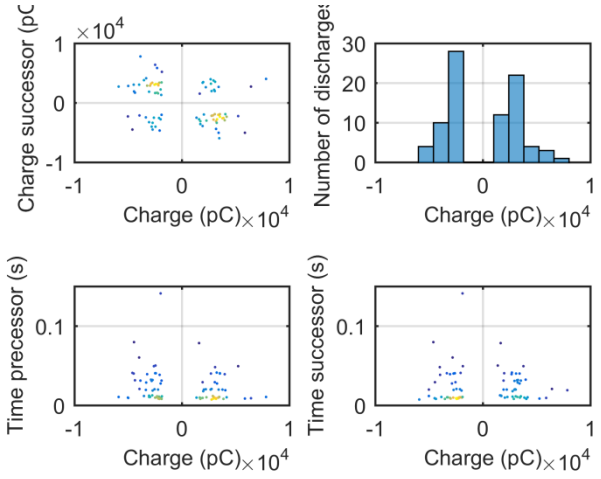

Figure 356: Surface Discharge TRPD cluster 8; 0-2 seconds; 84 discharges.

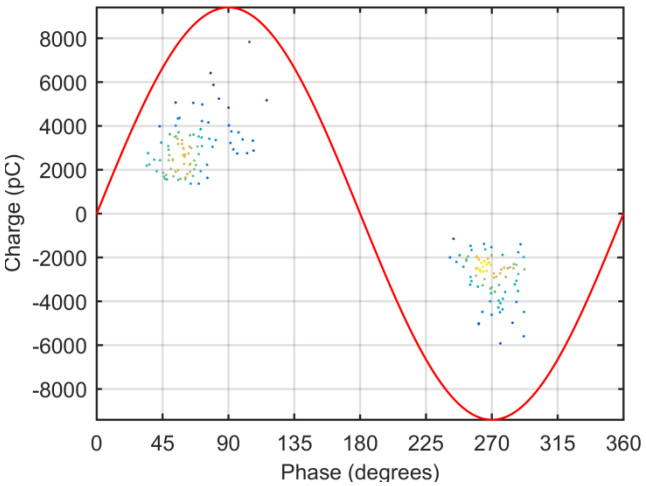

Figure 357: Surface Discharge PRPD cluster 9; 0-4 seconds; 173 discharges.

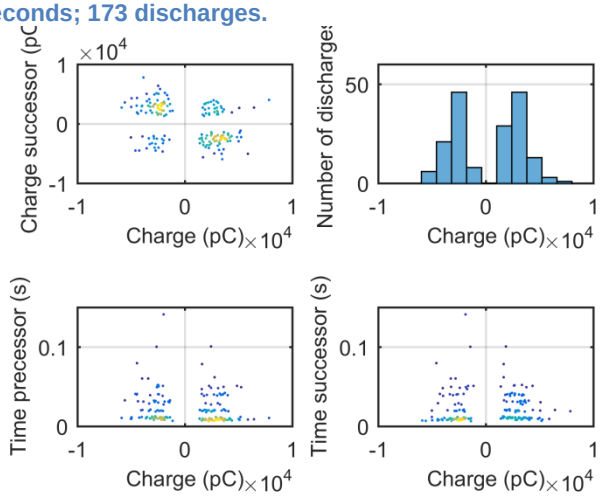

Figure 358: Surface Discharge TRPD cluster 9; 0-4 seconds; 173 discharges.

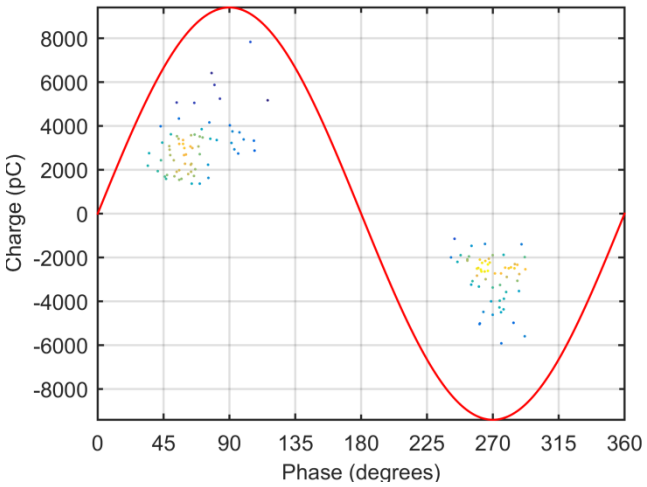

Figure 359: Surface Discharge PRPD cluster 10; 0-3 seconds; 126 discharges.

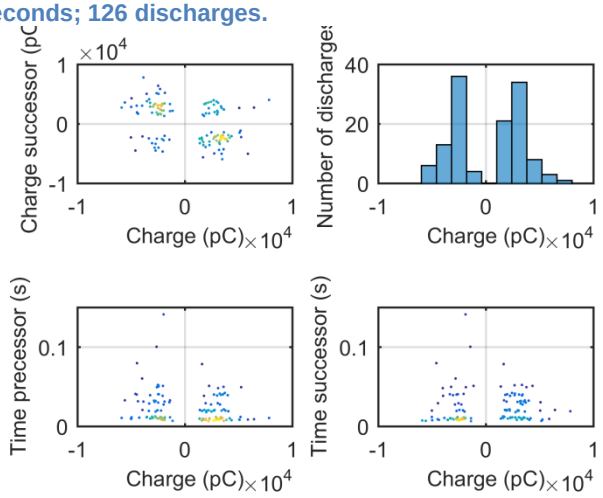

Figure 360: Surface Discharge TRPD cluster 10; 0-3 seconds; 126 discharges.

E. Experimental Setup Schematic

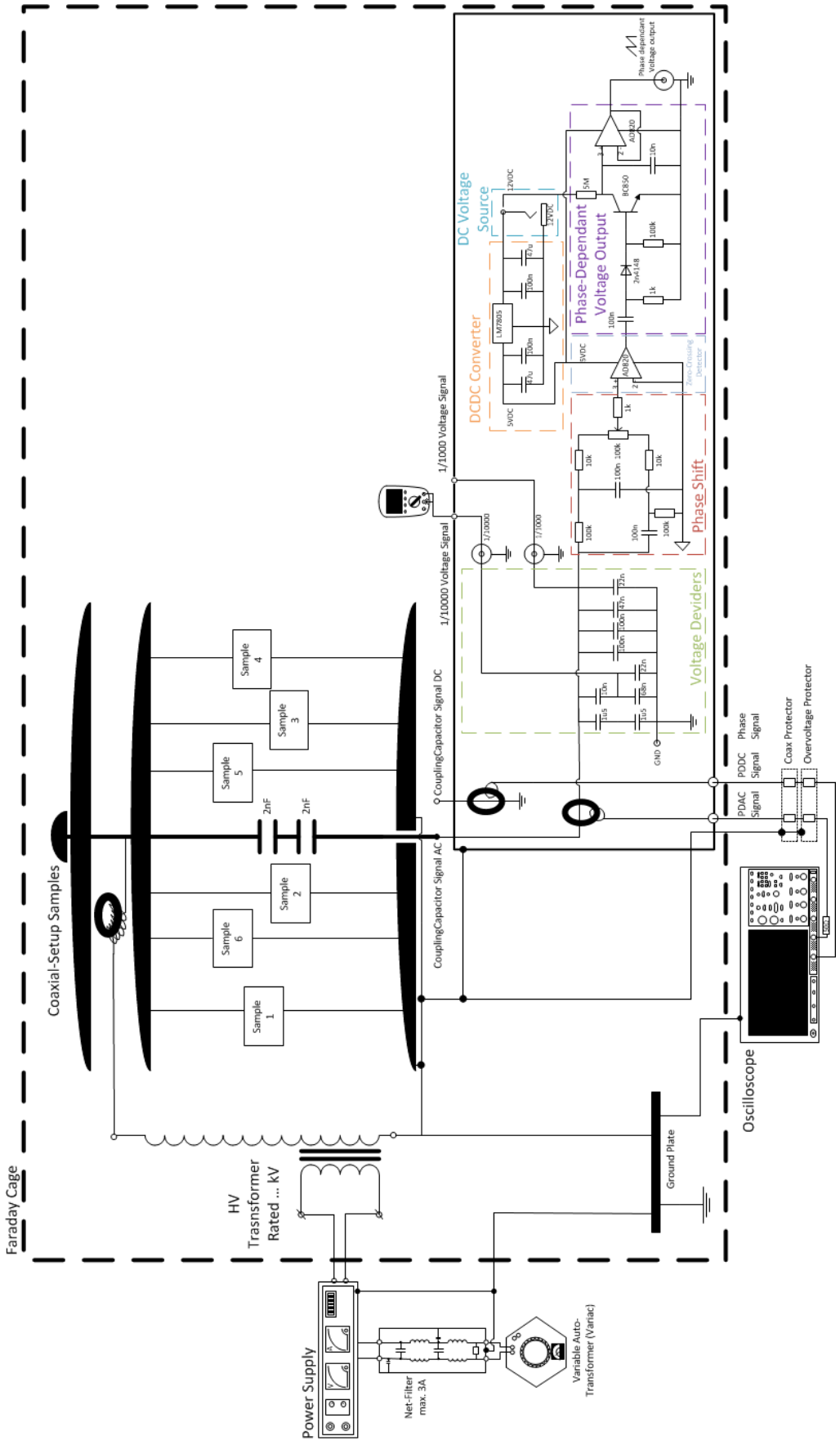

Figure 361: Complete Schematic Experimental Setup

F. Multiple Defect combinations Figures

In Table 57 you can see all possible combinations with the samples.

	Internal Discharge (A)	Positive Corona (B)	Negative Corona (C)	Floating electrode (D)	Surface Discharge (E)	Free-Moving Particle (F)
Internal Discharge (A)						
Positive Corona (B)	AB					
Negative Corona (C)	AC	BC				
Floating electrode (D)	AD	BD	CD			
Surface Discharge (E)	AE	BE	CE	DE		
Free-Moving Particle (F)	AF	BF	CF	DF	EF	

Table 57: All paring sample combinations

F1. Time evolution and Clusters: Defect Combination 1-12

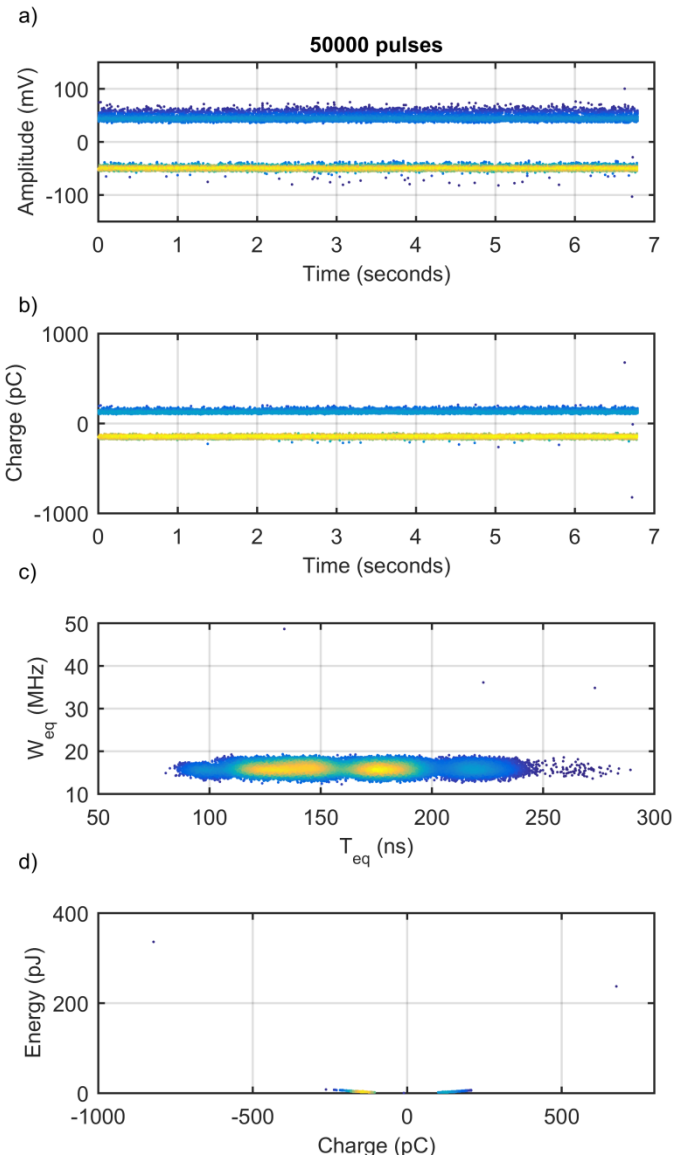

Figure 362: Defect Combination 1: Positive and Negative corona; Time evolution and clusters

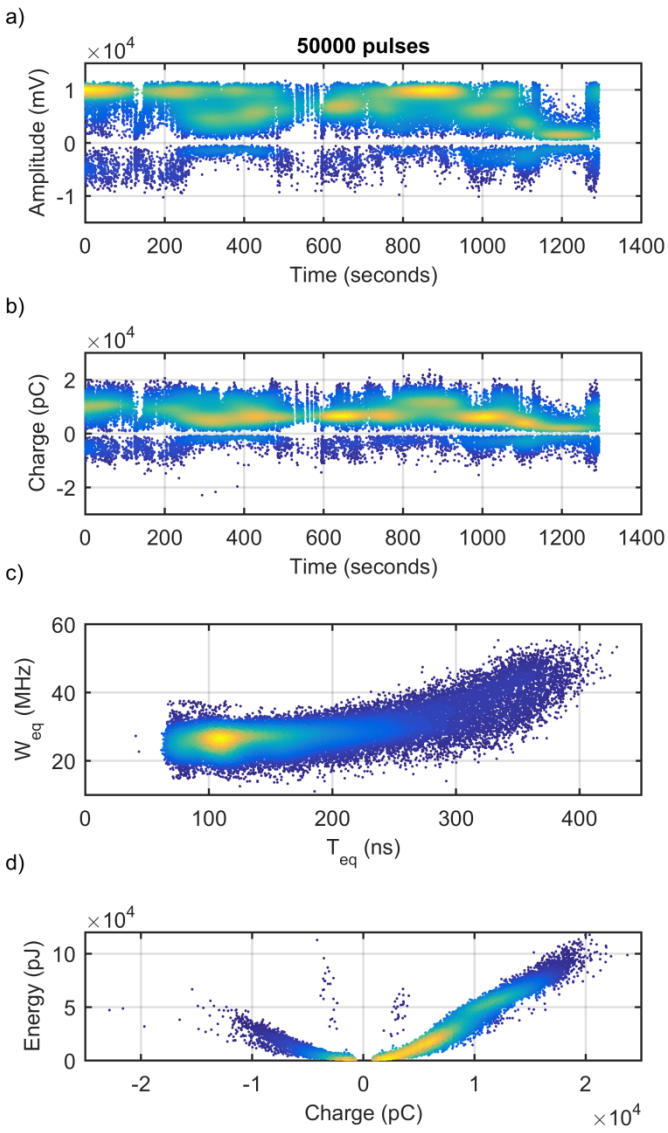

Figure 363: Defect Combination 2: Corona and Internal Discharge; Time evolution and clusters

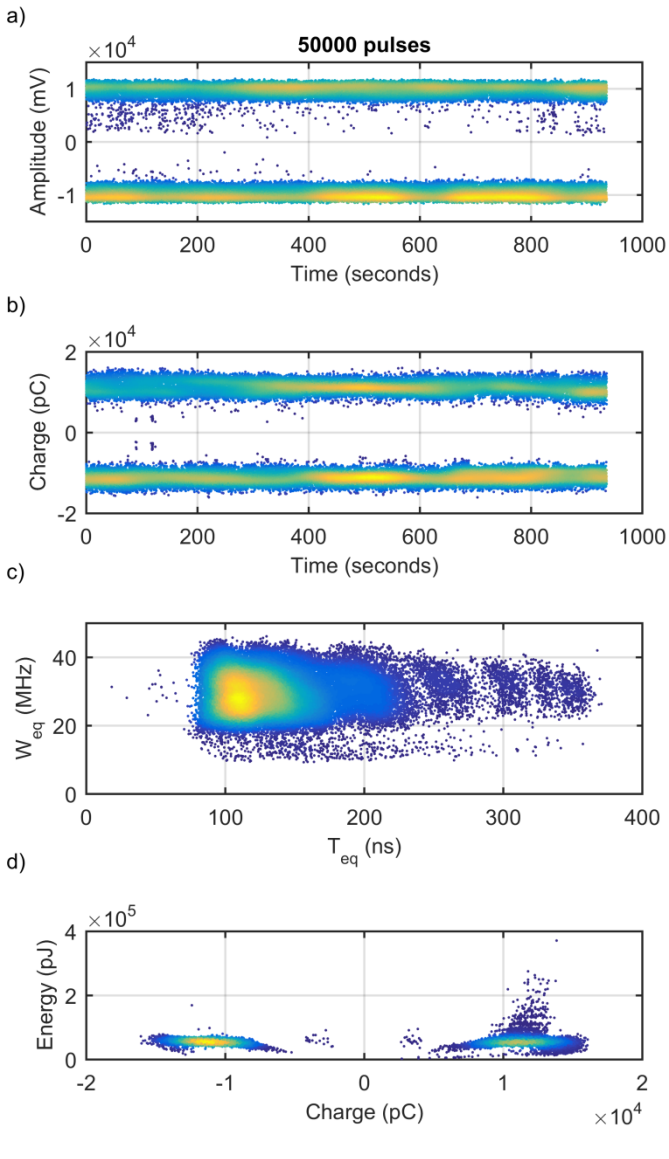

Figure 364: Defect Combination 3: Corona and Floating electrode; Time evolution and clusters

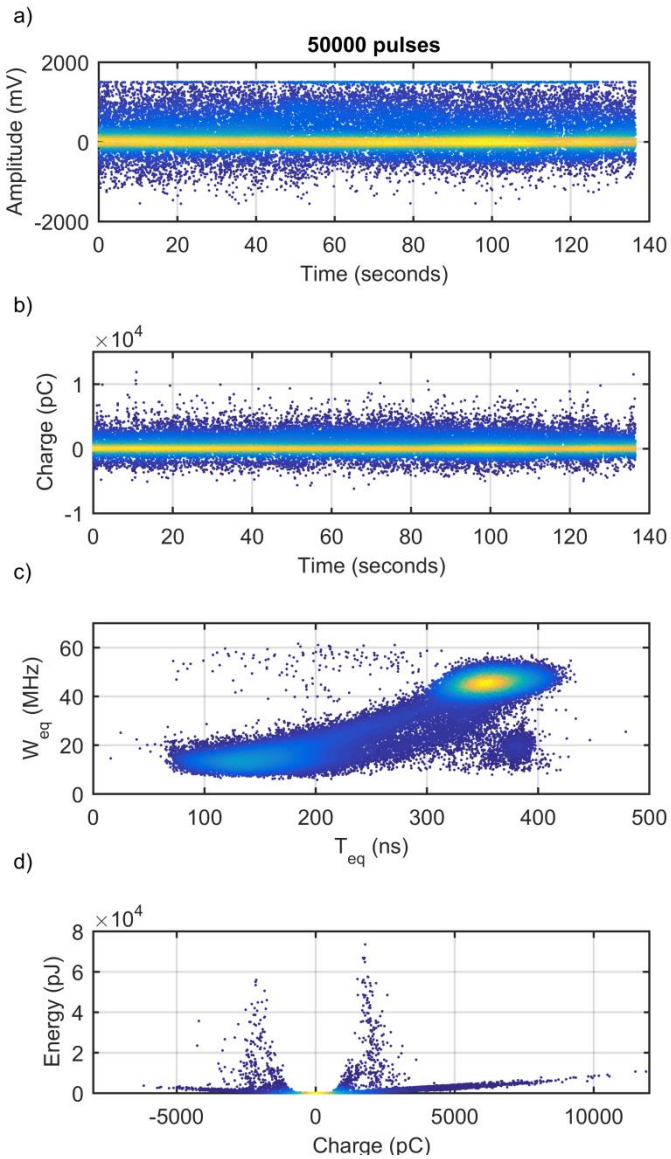

Figure 365: Defect Combination 4: Corona and Surface Discharge; Time evolution and clusters

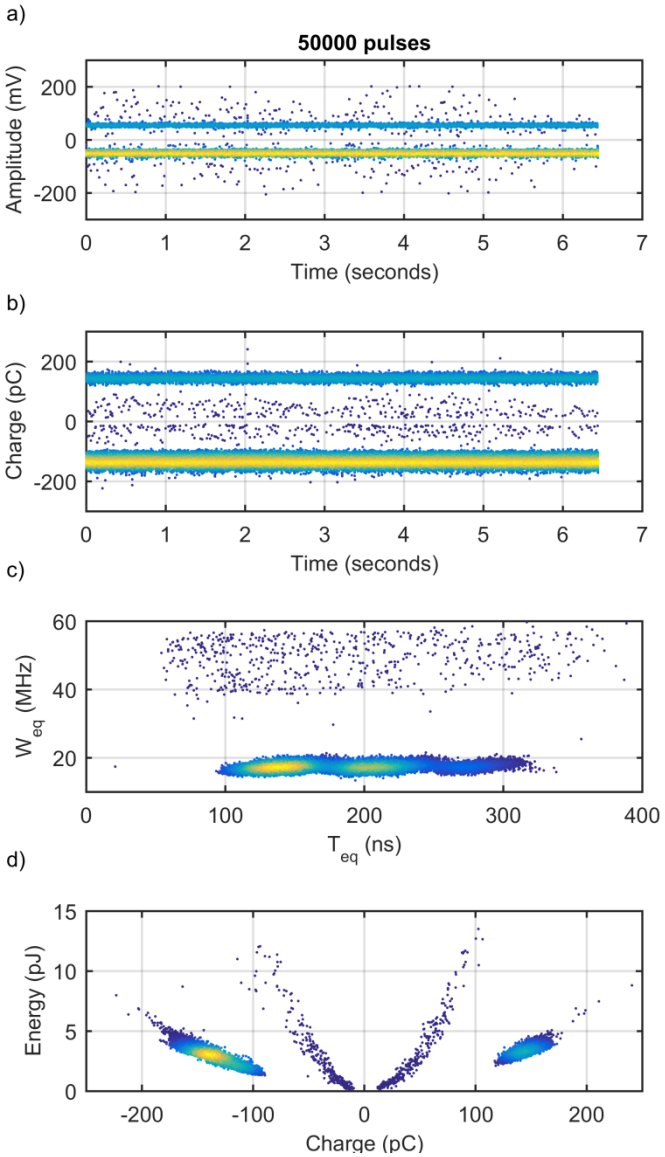

Figure 366: Defect Combination 5: Corona and Free-Moving Particle; Time evolution and clusters

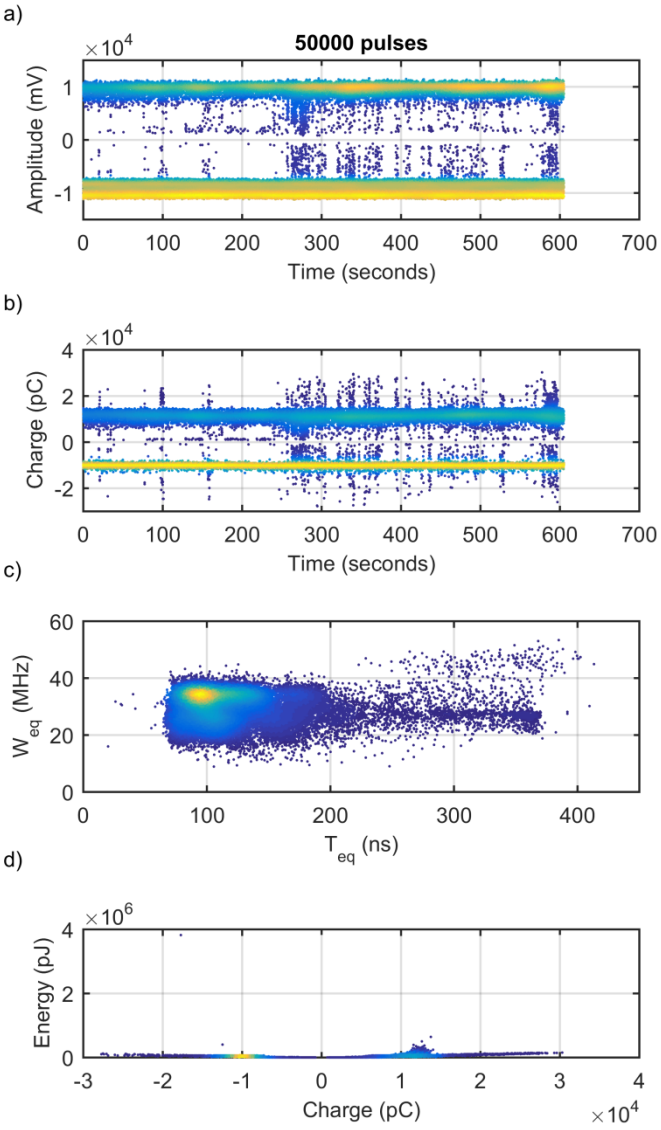

Figure 367: Defect Combination 6: Internal Discharge and Floating electrode; Time evolution and clusters

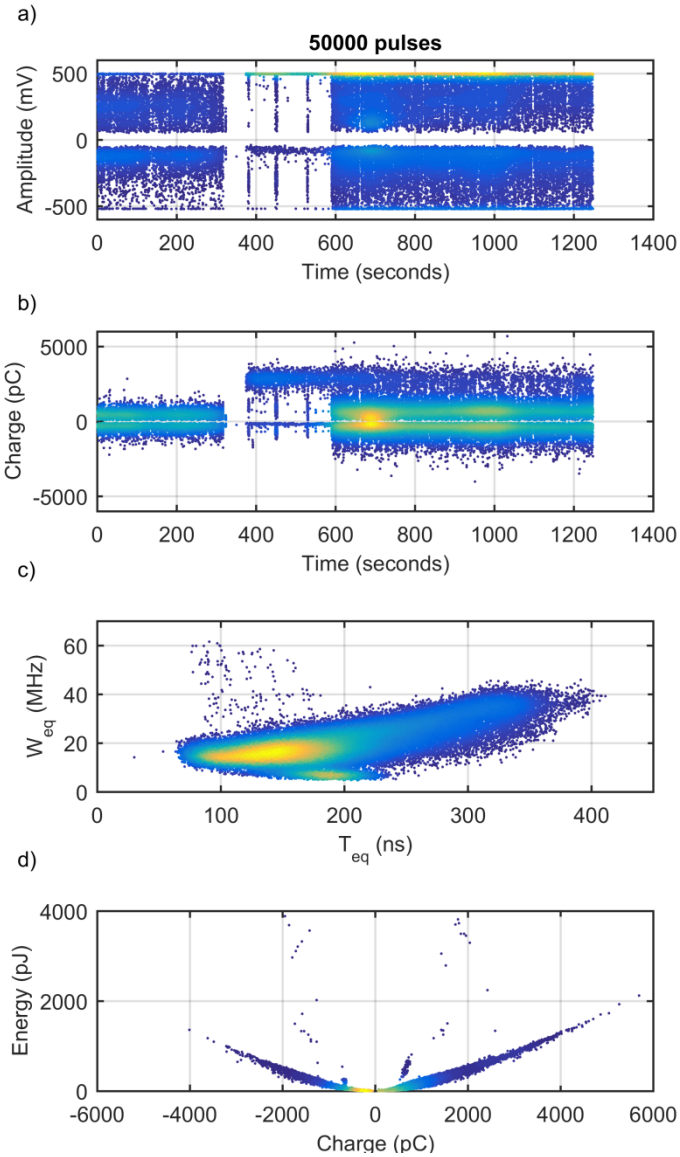

Figure 368: Defect Combination 7: Internal Discharge and Surface Discharge; Time evolution and clusters

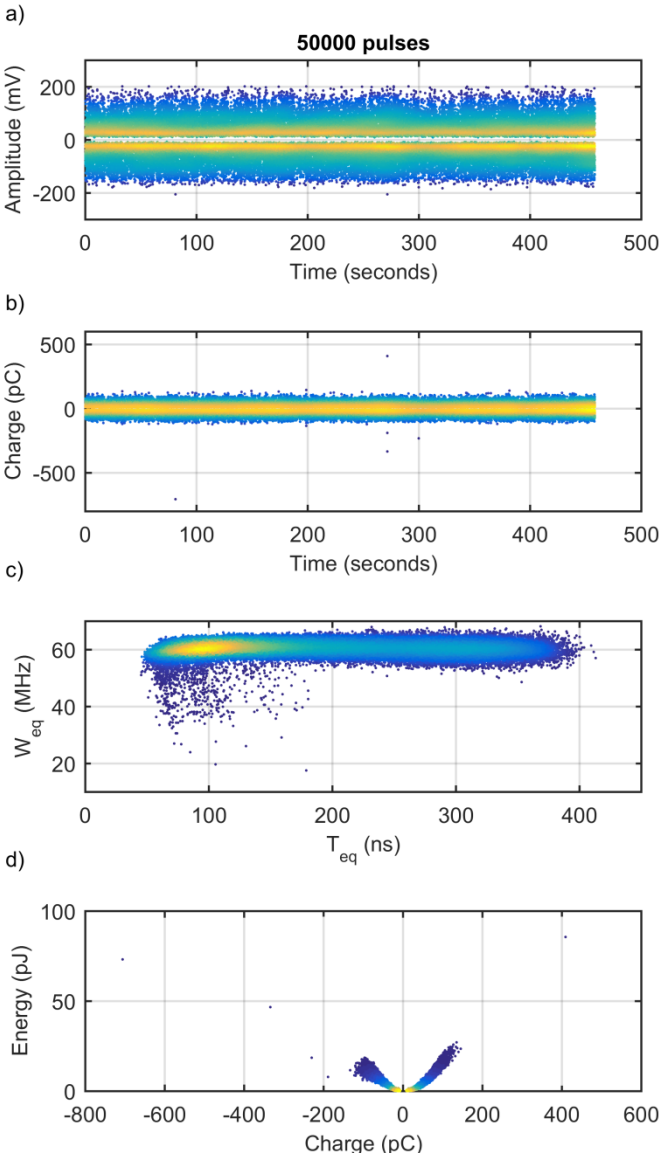

Figure 369: Defect Combination 8: Internal Discharge and Free-Moving Particle; Time evolution and clusters

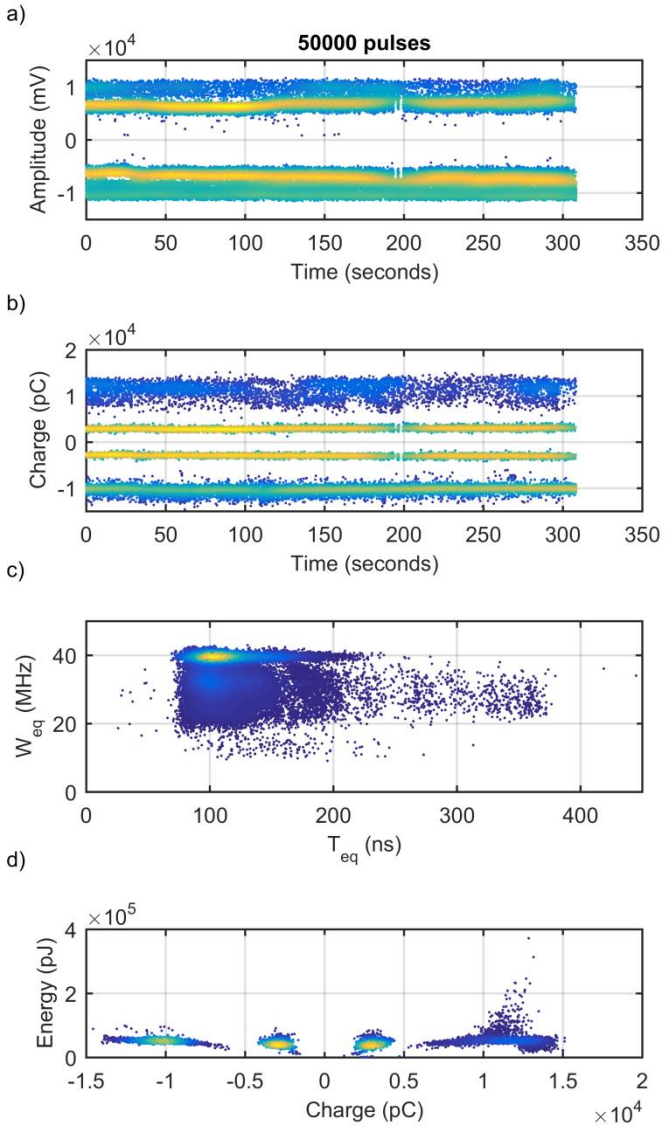

Figure 370: Defect Combination 9: Floating electrode and Surface Discharge; Time evolution and clusters

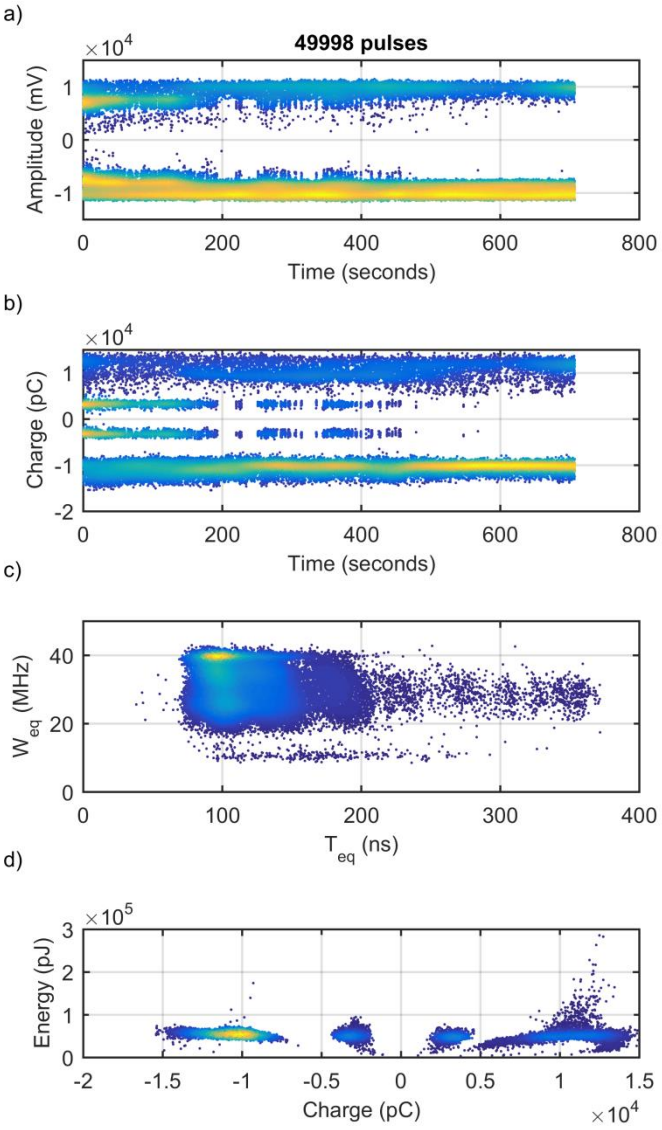

Figure 371: Defect Combination 10: Floating electrode and Free-Moving Particle; Time evolution and clusters

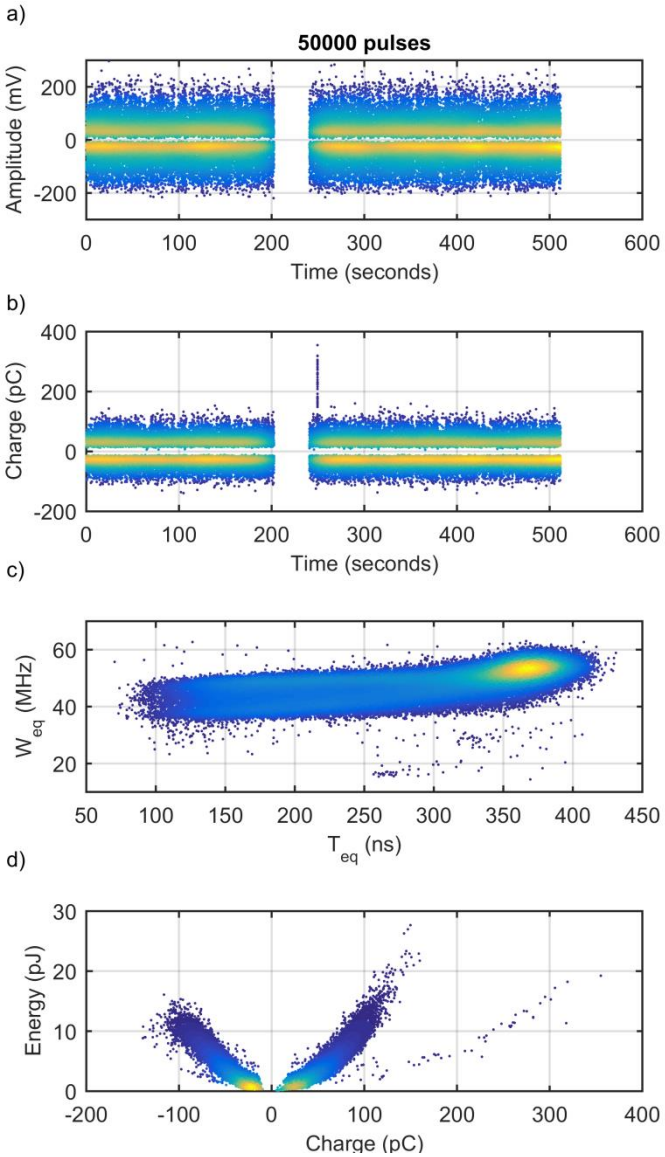

Figure 372: Defect Combination 11: Surface Discharge and Free-Moving Particle; Time evolution and clusters

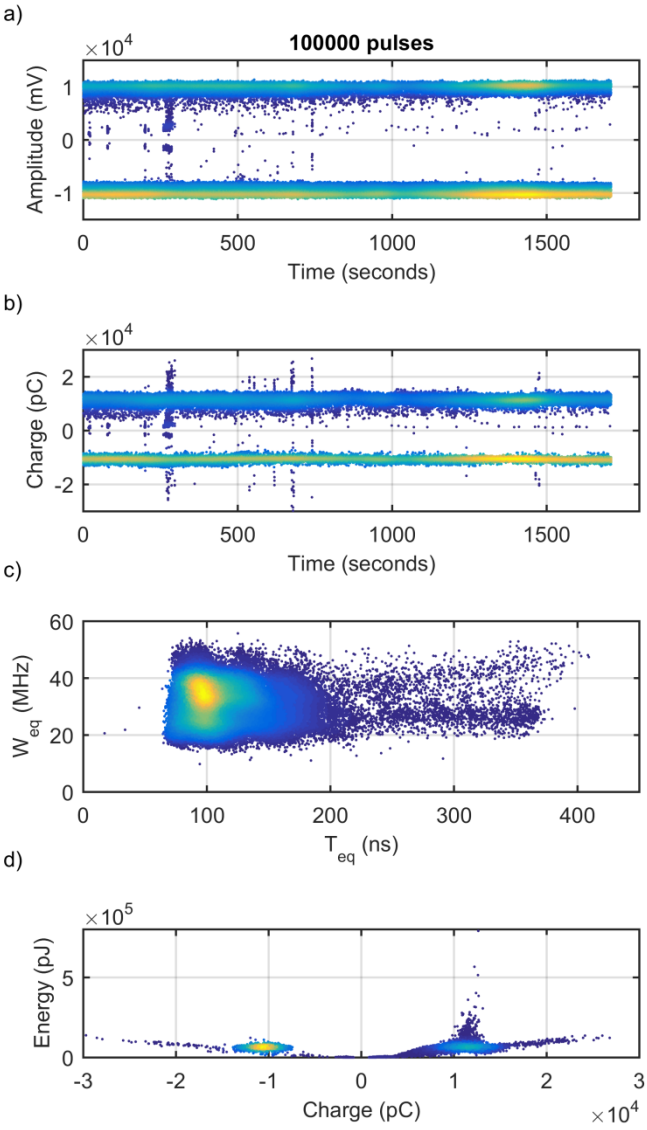

Figure 373: Defect Combination 12: All 6 Defects; Time evolution and clusters

F2. Number of discharges per cycle: Defect Combination 1-12

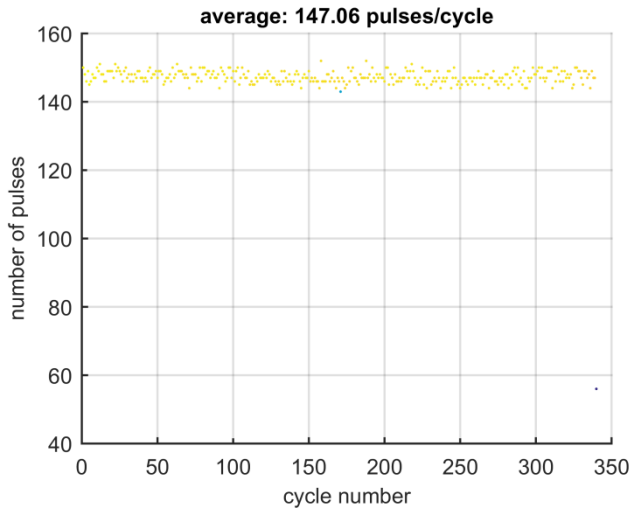

Figure 374: Defect Combination 1: Positive and Negative corona; Number of discharges per cycle

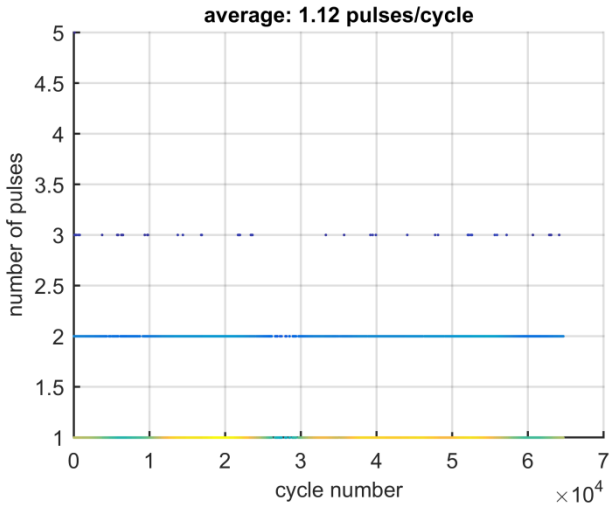

Figure 375: Defect Combination 2: Corona and Internal Discharge; Number of pulses per cycle

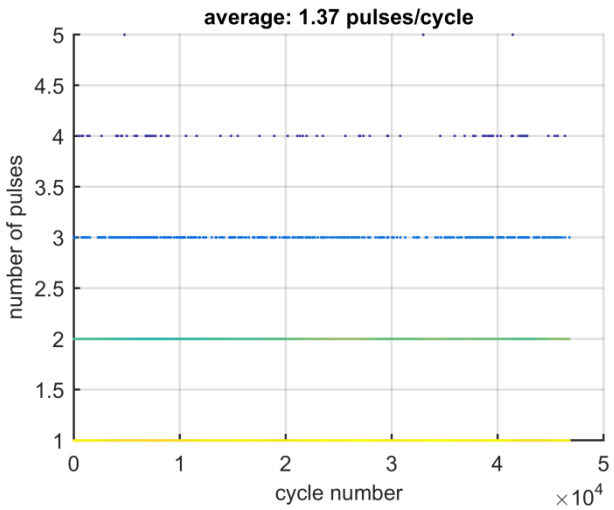

Figure 376: Defect Combination 3: Corona and Floating electrode; Number of pulses per cycle

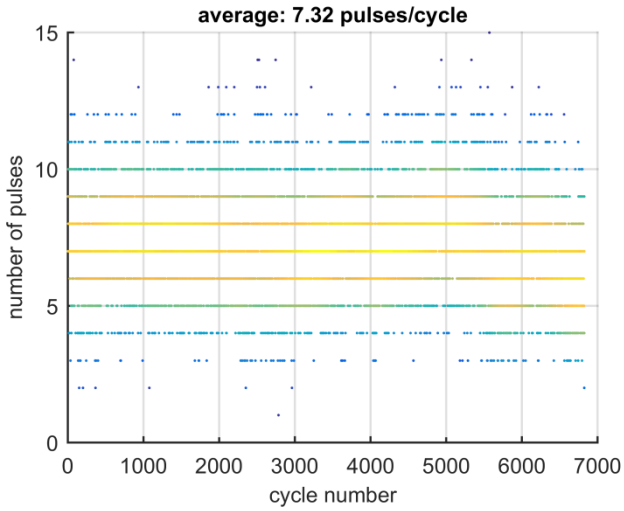

Figure 377: Defect Combination 4: Corona and Surface Discharge; Number of pulses per cycle

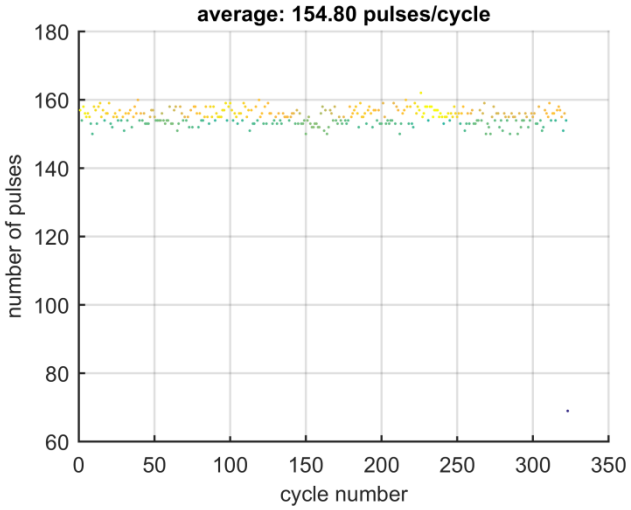

Figure 378: Defect Combination 5: Corona and Free-Moving Particle; Number of pulses per cycle

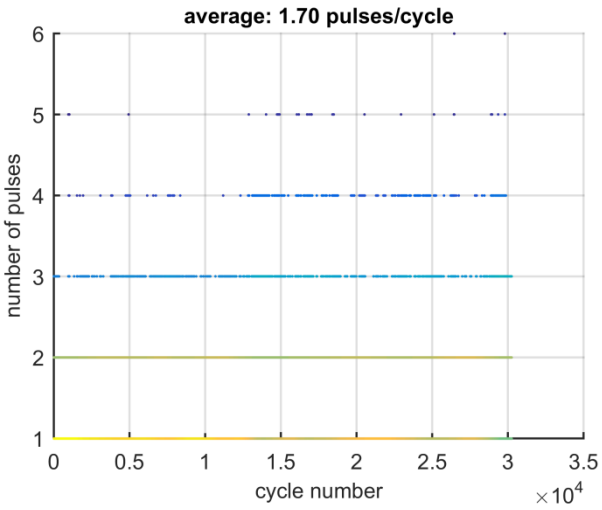

Figure 379: Defect Combination 6: Internal Discharge and Floating electrode; Number of pulses per cycle

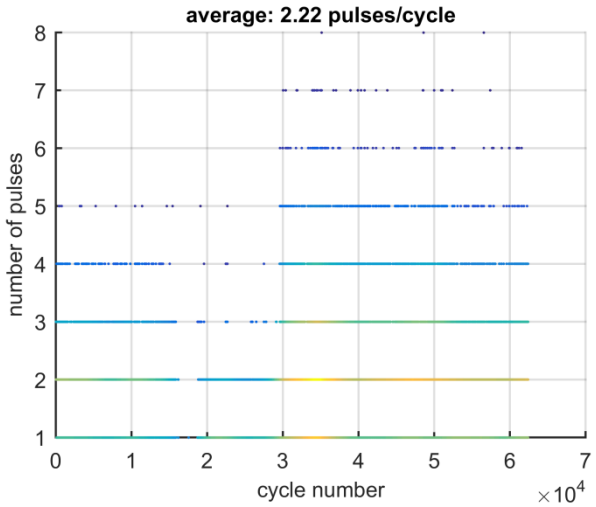

Figure 380: Defect Combination 7: Internal Discharge and Surface Discharge; Number of pulses per cycle

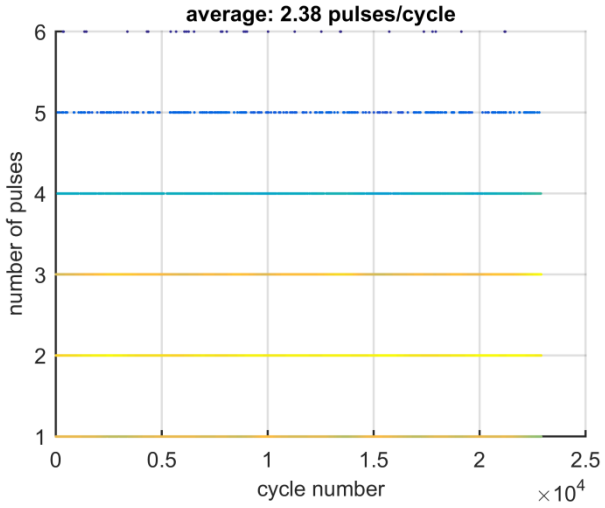

Figure 381: Defect Combination 8: Internal Discharge and Free-Moving Particle; Number of pulses per cycle

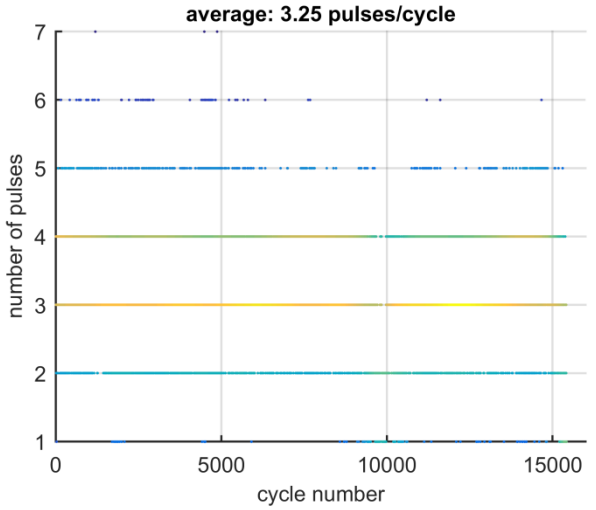

Figure 382: Defect Combination 9: Floating electrode and Surface Discharge; Number of pulses per cycle

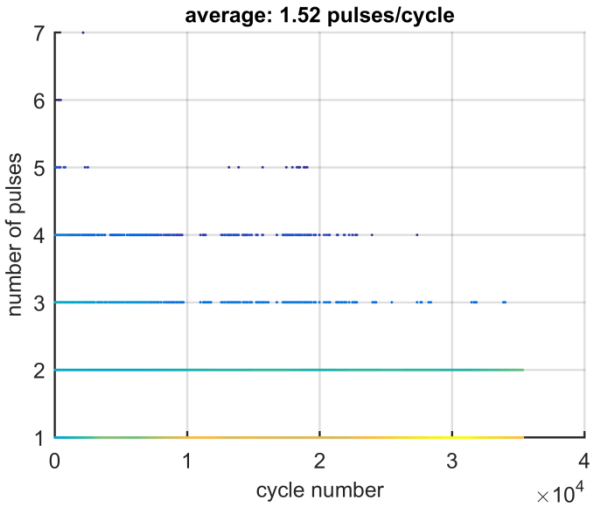

Figure 383: Defect Combination 10: Floating electrode and Free-Moving Particle; Number of pulses per cycle

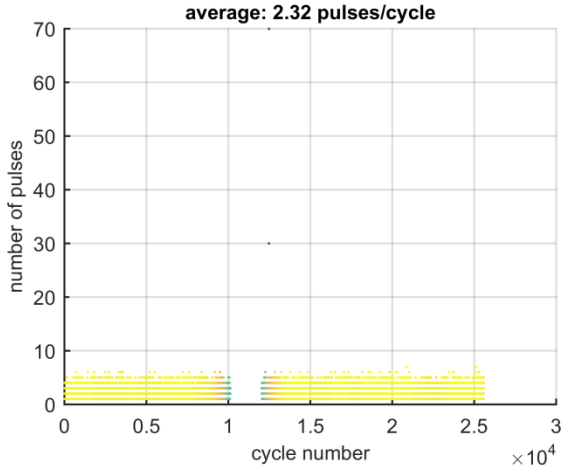

Figure 384: Defect Combination 11: Surface Discharge & Free-Moving Particle; Number of pulses per cycle

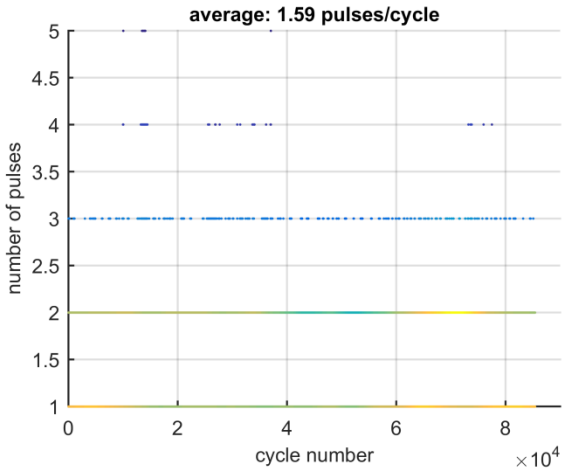

Figure 385: Defect Combination 12: All 6 Defects; Number of pulses per cycle

F3. PRPD: Defect Combination 1-12

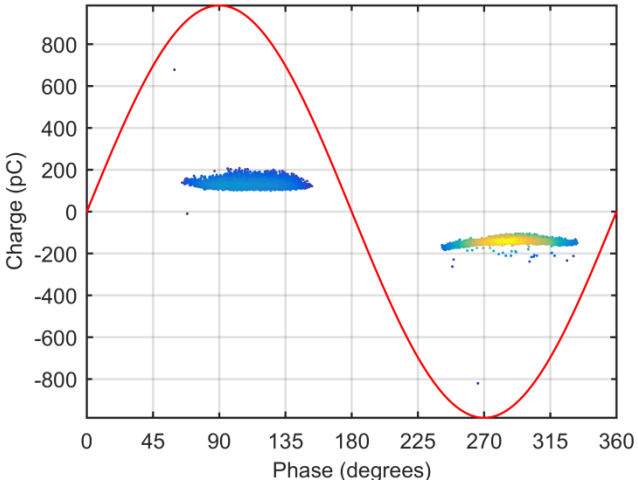

Figure 386: Defect Combination 1: Positive and Negative corona; PRPD

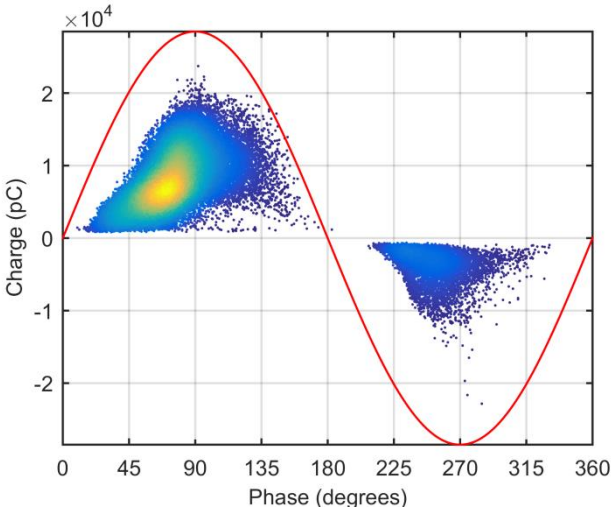

Figure 387: Defect Combination 2: Corona and Internal Discharge; PRPD

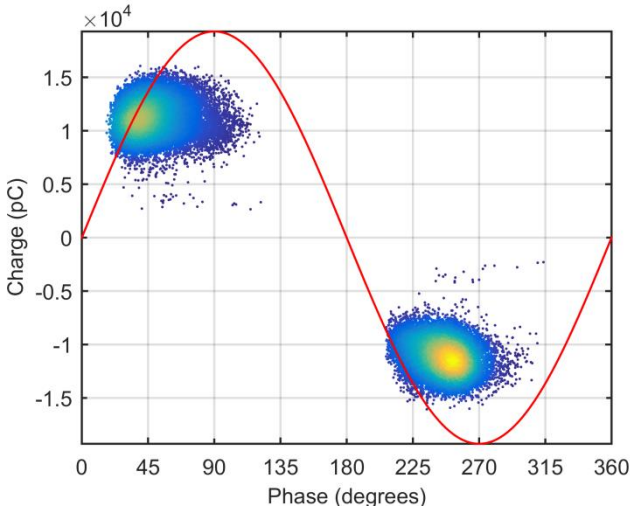

Figure 388: Defect Combination 3: Corona and Floating electrode; PRPD

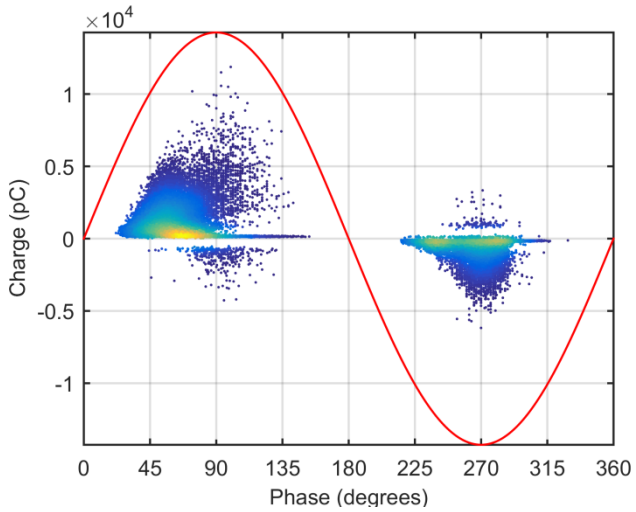

Figure 389: Defect Combination 4: Corona and Surface Discharge; PRPD

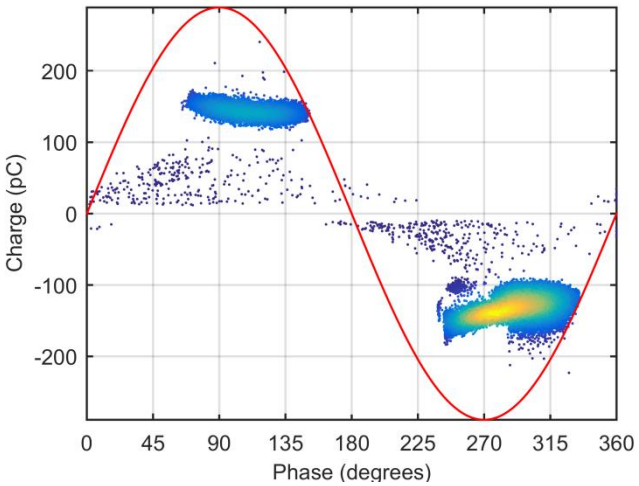

Figure 390: Defect Combination 5: Corona and Free-Moving Particle; PRPD

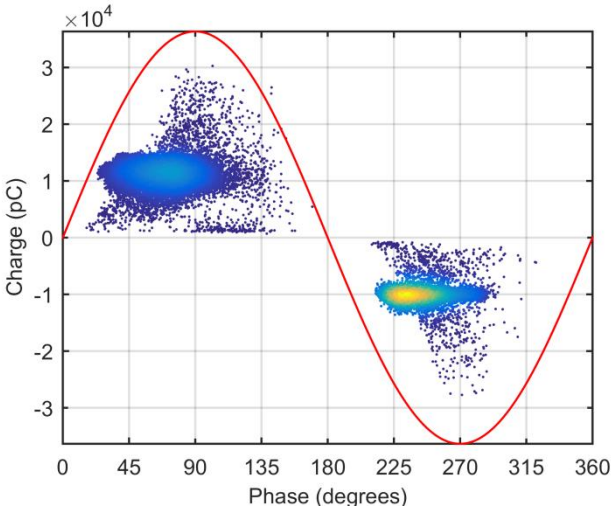

Figure 391: Defect Combination 6: Internal Discharge and Floating electrode; PRPD

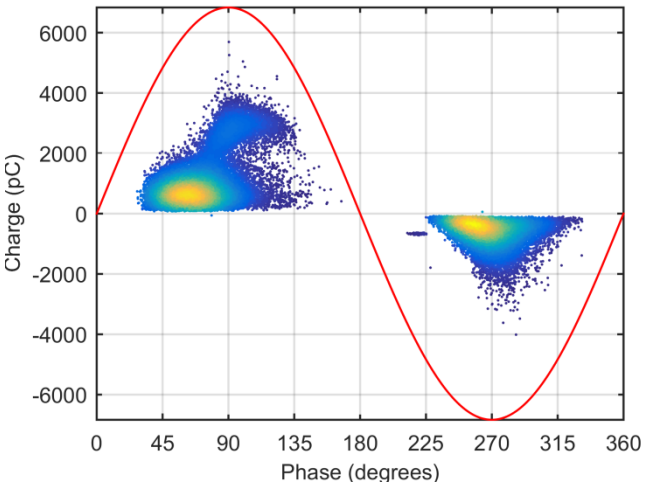

Figure 392: Defect Combination 7: Internal Discharge and Surface Discharge; PRPD

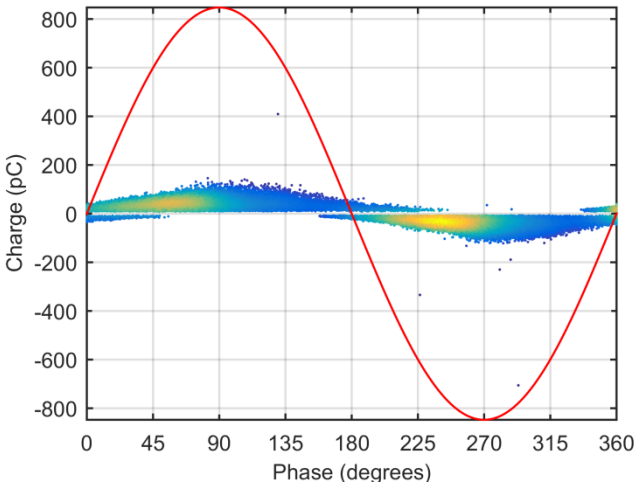

Figure 393: Defect Combination 8: Internal Discharge and Free-Moving Particle; PRPD

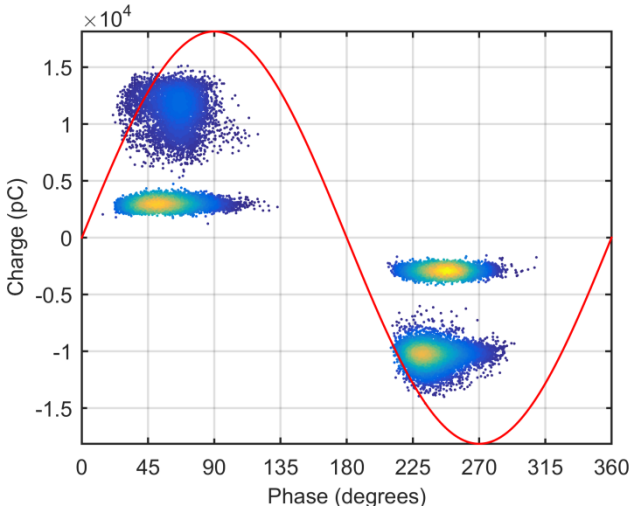

Figure 394: Defect Combination 9: Floating electrode and Surface Discharge; PRPD

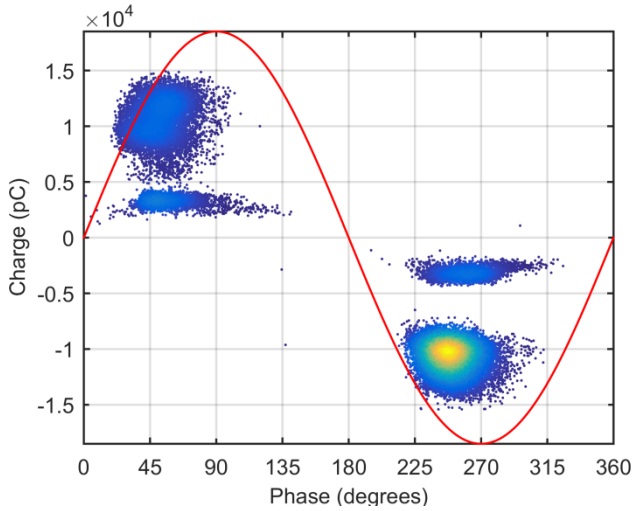

Figure 395: Defect Combination 10: Floating electrode and Free-Moving Particle; PRPD

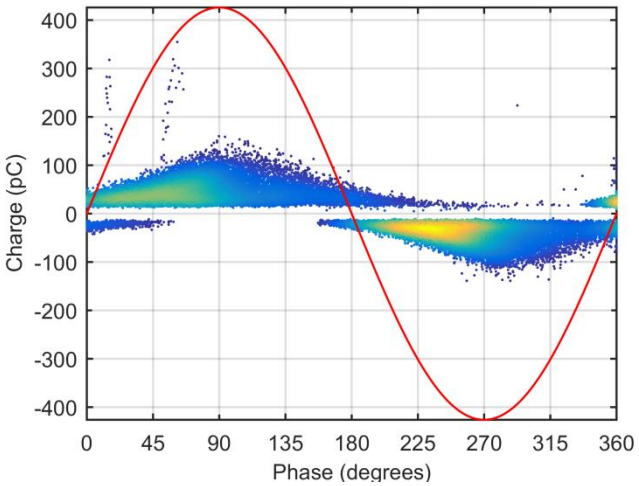

Figure 396: Defect Combination 11: Surface Discharge and Free-Moving Particle; PRPD

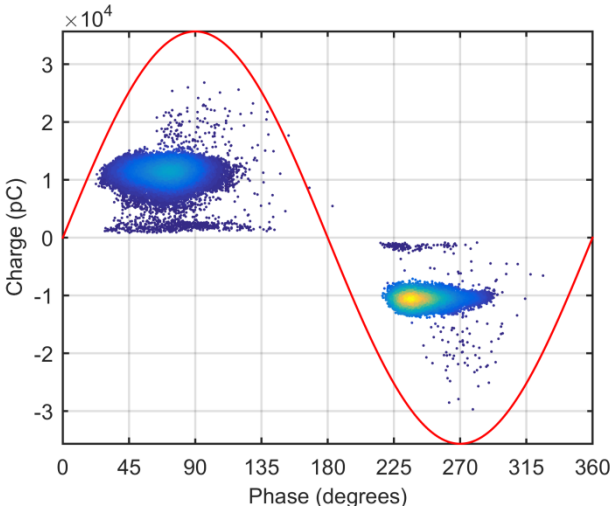

Figure 397: Defect Combination 12: All 6 Defects; PRPD

F4. TRPD: Defect Combination 1-12

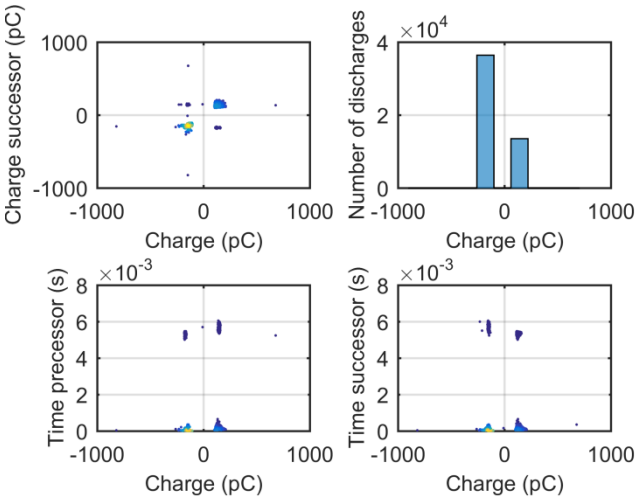

Figure 398: Defect Combination 1: Positive and Negative corona; TRPD

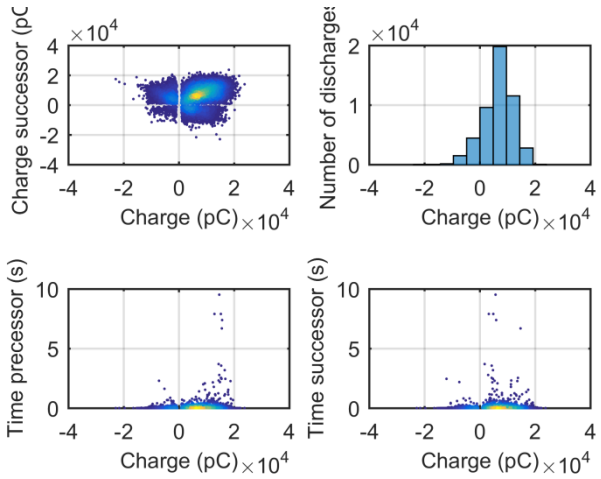

Figure 399: Defect Combination 2: Corona and Internal Discharge; TRPD

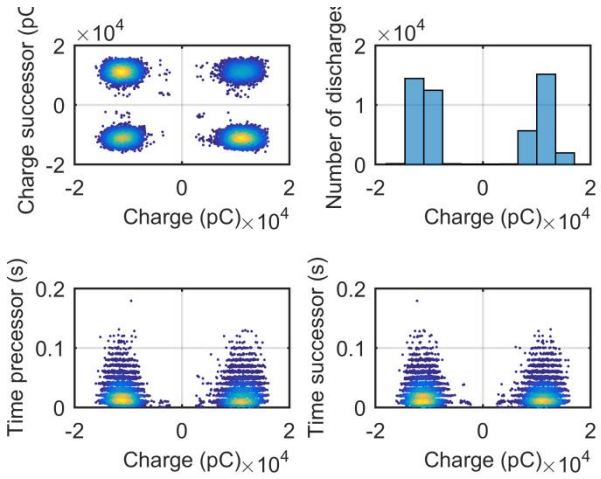

Figure 400: Defect Combination 3: Corona and Floating electrode; TRPD

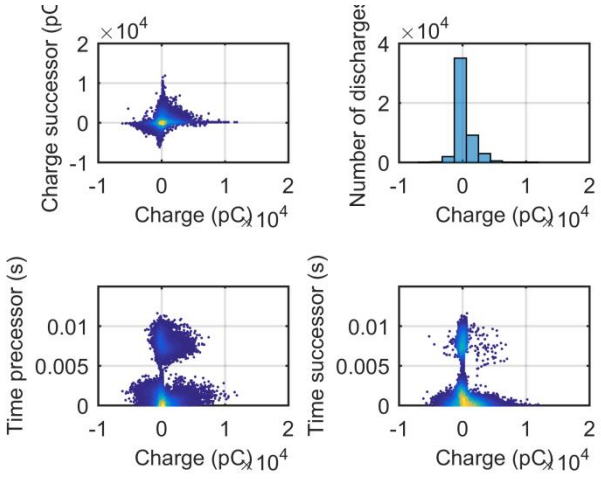

Figure 401: Defect Combination 4: Corona and Surface Discharge; TRPD

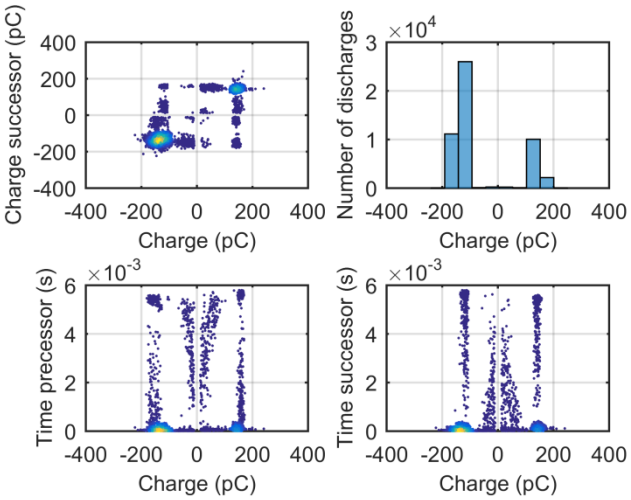

Figure 402: Defect Combination 5: Corona and Free-Moving Particle; TRPD

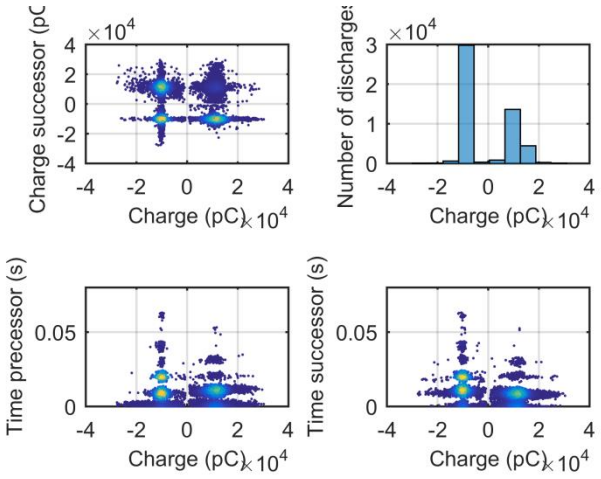

Figure 403: Defect Combination 6: Internal Discharge and Floating electrode; TRPD

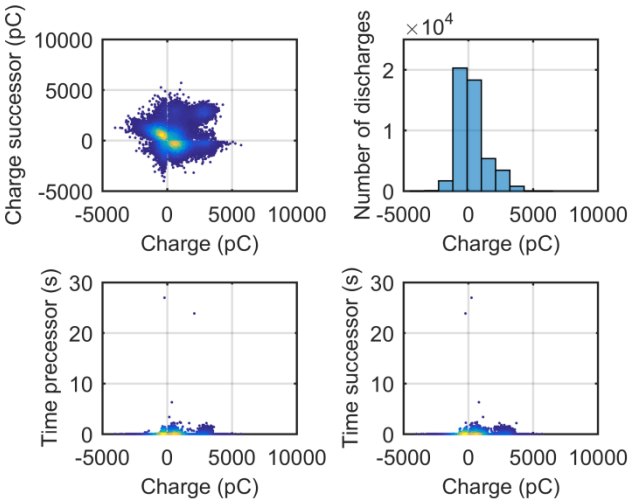

Figure 404: Defect Combination 7: Internal Discharge and Surface Discharge; TRPD

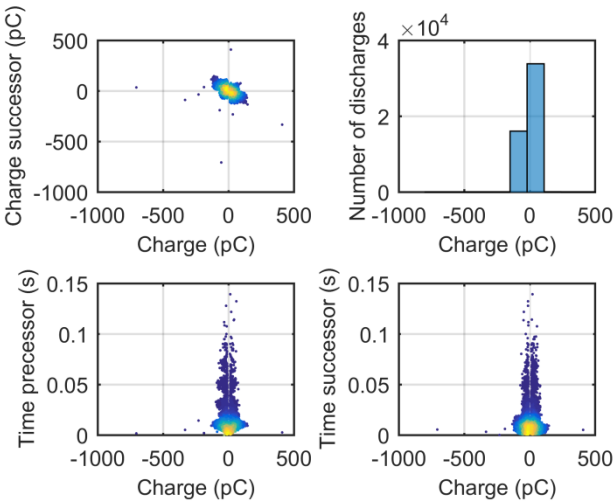

Figure 405: Defect Combination 8: Internal Discharge and Free-Moving Particle; TRPD

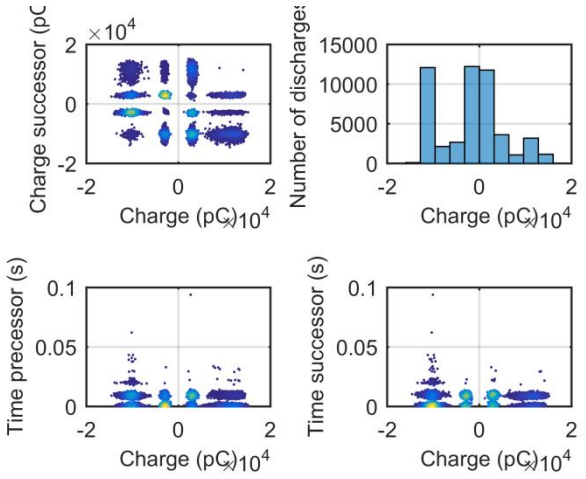

Figure 406: Defect Combination 9: Floating electrode and Surface Discharge; TRPD

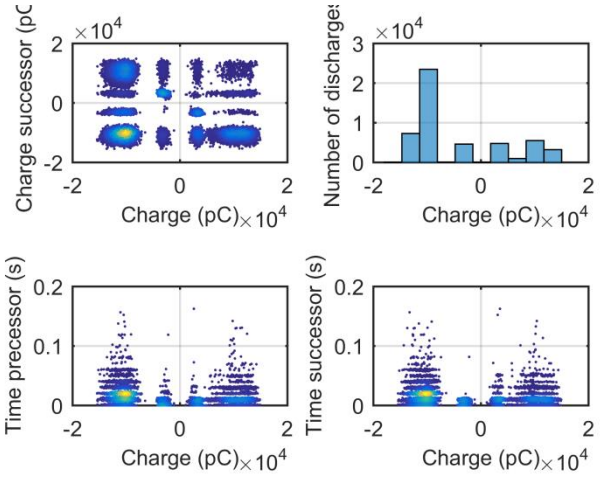

Figure 407: Defect Combination 10: Floating electrode and Free-Moving Particle; TRPD

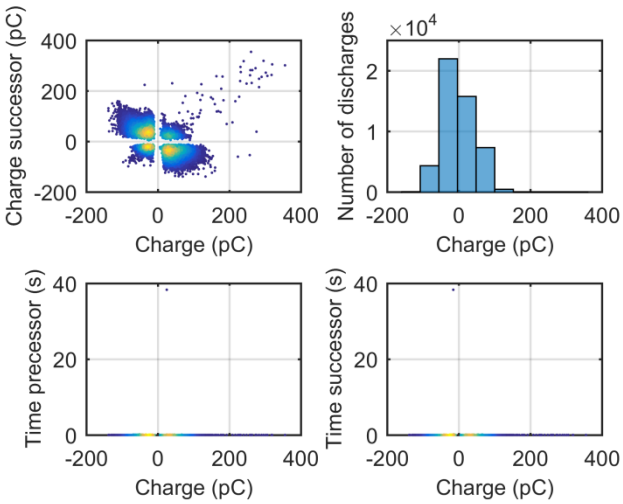

Figure 408: Defect Combination 11: Surface Discharge and Free-Moving Particle; TRPD

Figure 409: Defect Combination 12: All 6 Defects; TRPD

F5. Energy Per Charge versus Charge Analysis: Defect Combination 1-12

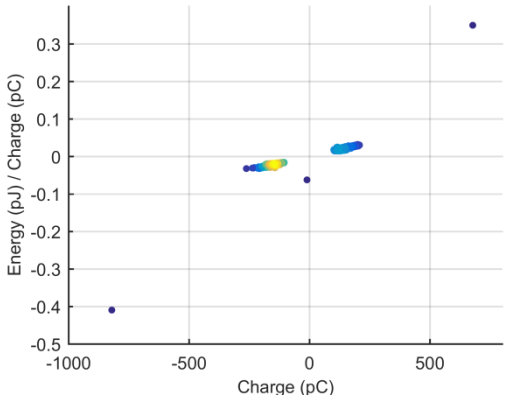

Figure 410: Defect Combination 1: Energy per charge versus charge; Positive & Negative Corona

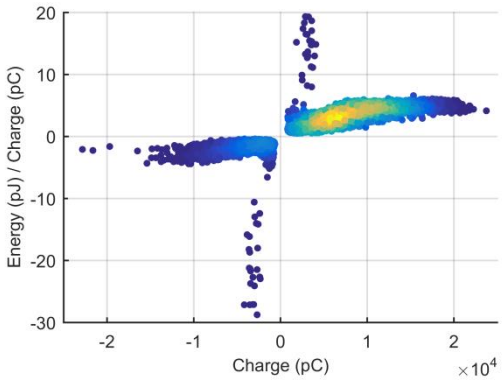

Figure 411: Defect Combination 2: Energy per charge versus charge; Corona & Internal Discharge

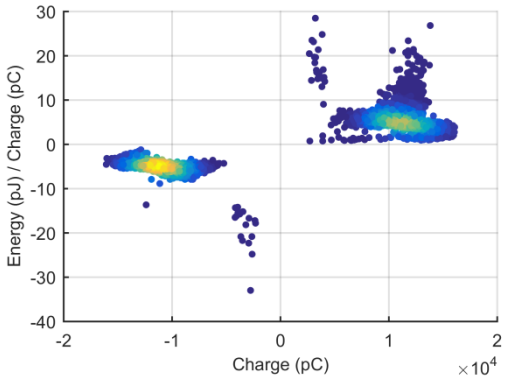

Figure 412: Defect Combination 3: Energy per charge versus charge; Corona & Floating electrode

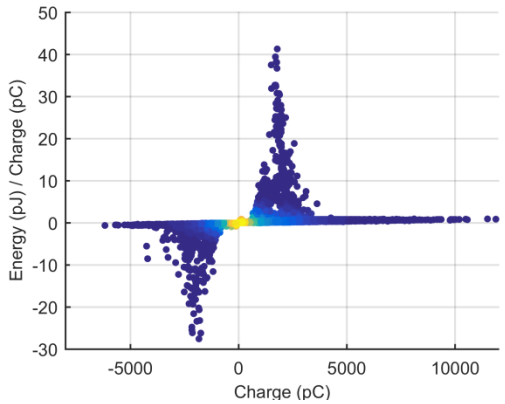

Figure 413: Defect Combination 4: Energy per charge versus charge; Corona & Surface Discharge

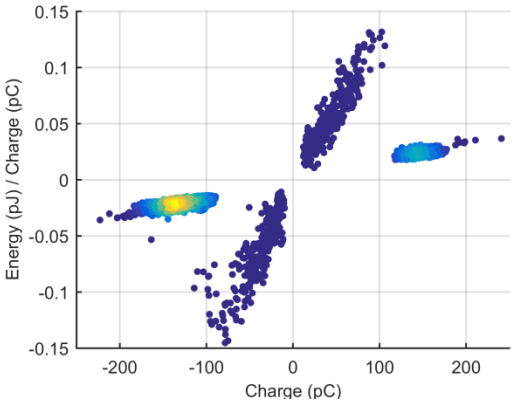

Figure 414: Defect Combination 5: Energy per charge versus charge; Corona & Free-Moving Particle

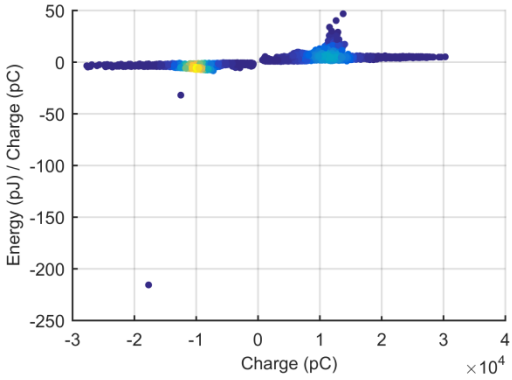

Figure 415: Defect Combination 6: Energy per charge versus charge; Internal Discharge & Floating electrode

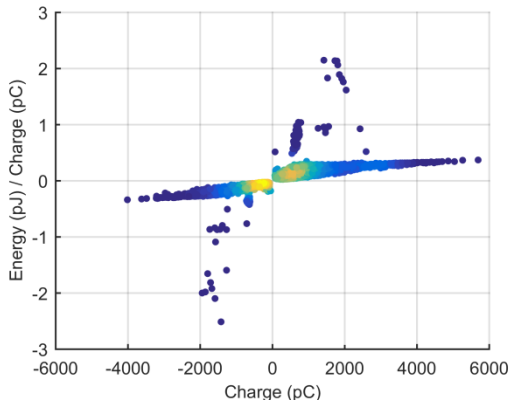

Figure 416: Defect Combination 7: Energy per charge versus charge; Internal Discharge & Surface Discharge

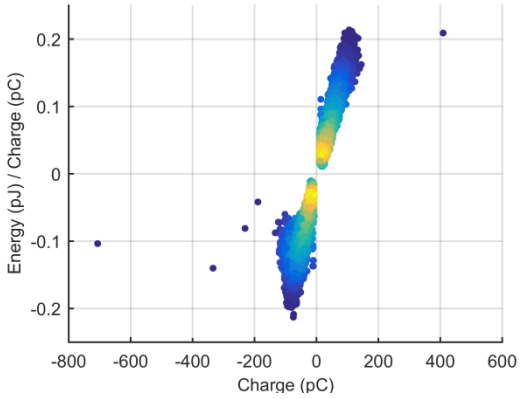

Figure 417: Defect Combination 8: Energy per charge versus charge; Internal Discharge & Free-Moving Particle

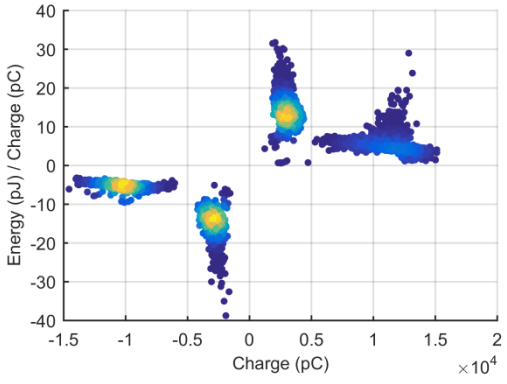

Figure 418: Defect Combination 9: Energy per charge versus charge; Floating electrode & Surface Discharge

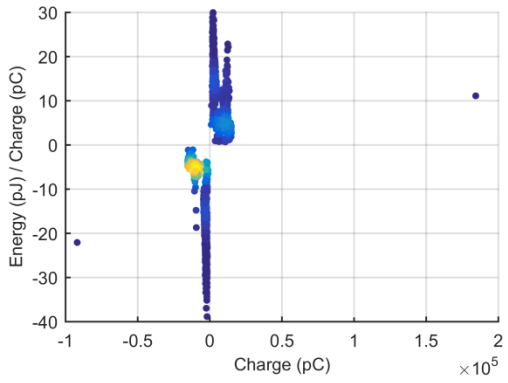

Figure 419: Defect Combination 10: Energy per charge versus charge; Floating electrode & Free-Moving Particle

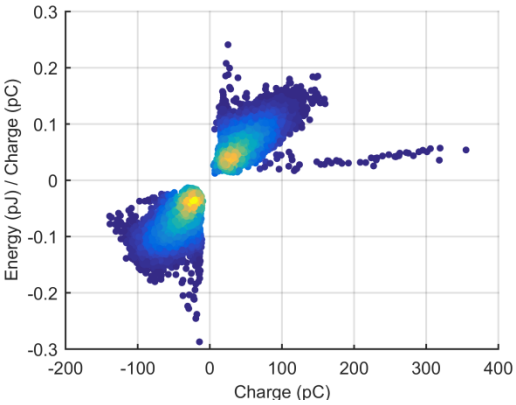

Figure 420: Defect Combination 11: Energy per charge versus charge; Surface Discharge & Free-Moving Particle

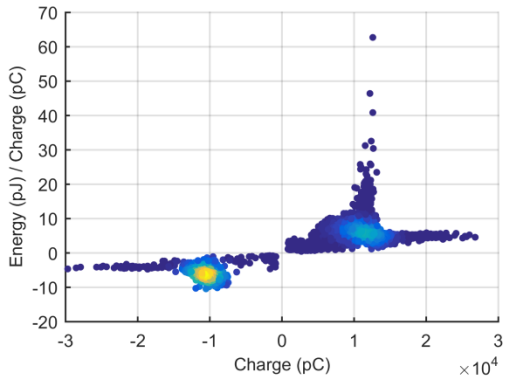

Figure 421: Defect Combination 12: Energy per charge versus charge; All 6 Defects

F6. Rise-time versus Fall-time Cluster: Defect Combination 1-12

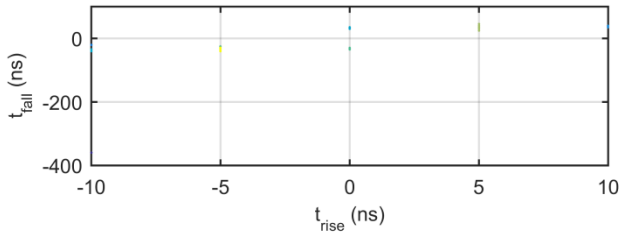

Figure 422: Defect Combination 1: Rise-time versus Fall-time Cluster; Positive & Negative Corona

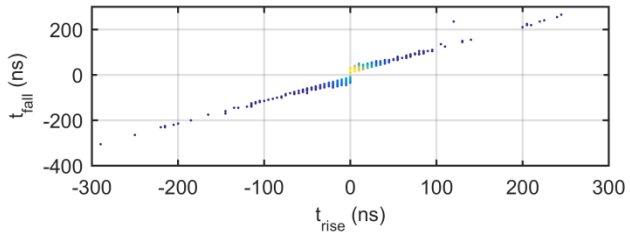

Figure 423: Defect Combination 2: Rise-time versus Fall-time Cluster; Corona & Internal discharge

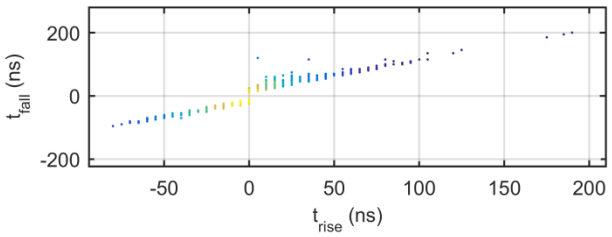

Figure 424: Defect Combination 3: Rise-time versus Fall-time Cluster; Corona & Floating electrode

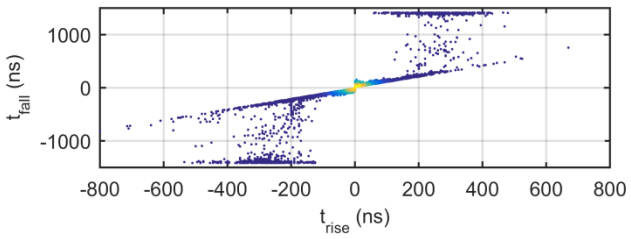

Figure 425: Defect Combination 4: Rise-time versus Fall-time Cluster; Corona & Surface Discharge

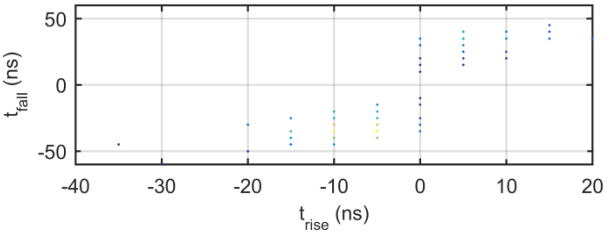

Figure 426: Defect Combination 5: Rise-time versus Fall-time Cluster; Corona & Free-Moving Particle

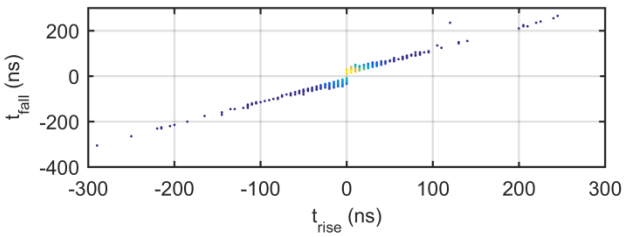

Figure 427: Defect Combination 6: Rise-time versus Fall-time Cluster; Internal Discharge & Floating electrode

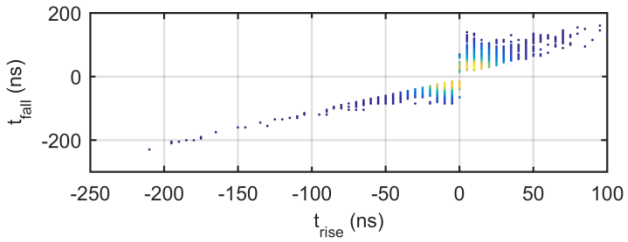

Figure 428: Defect Combination 7: Rise-time versus Fall-time Cluster; Internal Discharge & Surface Discharge

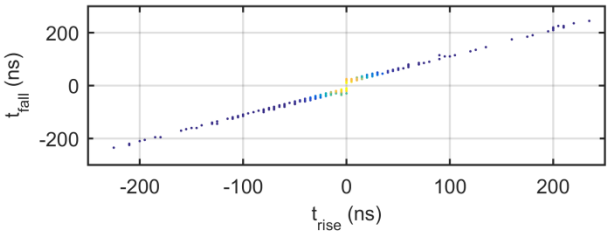

Figure 429: Defect Combination 8: Rise-time versus Fall-time Cluster; Internal Discharge & Free-Moving Particle

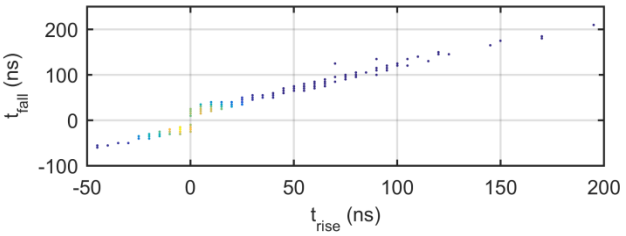

Figure 430: Defect Combination 9: Rise-time versus Fall-time Cluster; Floating electrode & Surface Discharge

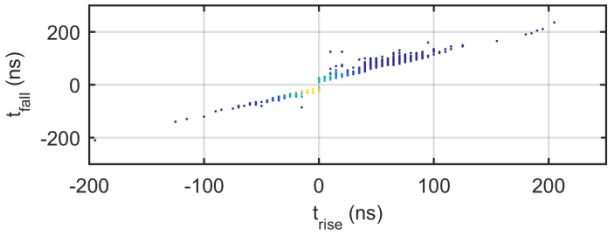

Figure 431: Defect Combination 10: Rise-time versus Fall-time Cluster; Floating electrode & Free-Moving Particle

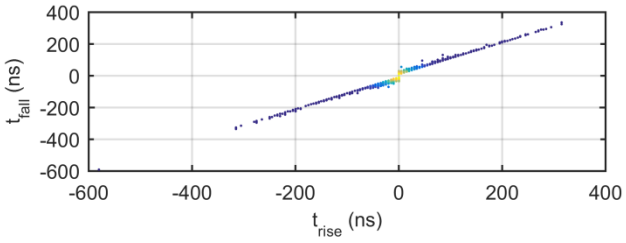

Figure 432: Defect Combination 11: Rise-time versus Fall-time Cluster; Surface Discharge & Free-Moving Particle

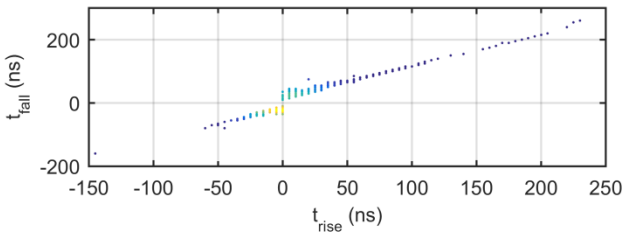

Figure 433: Defect Combination 12: Rise-time versus Fall-time Cluster; All 6 defects

G. Multiple defect combinations figures of renewed internal discharge

G1. Time evolution and Clusters: Defect Combination 2, 6, 7 and 8

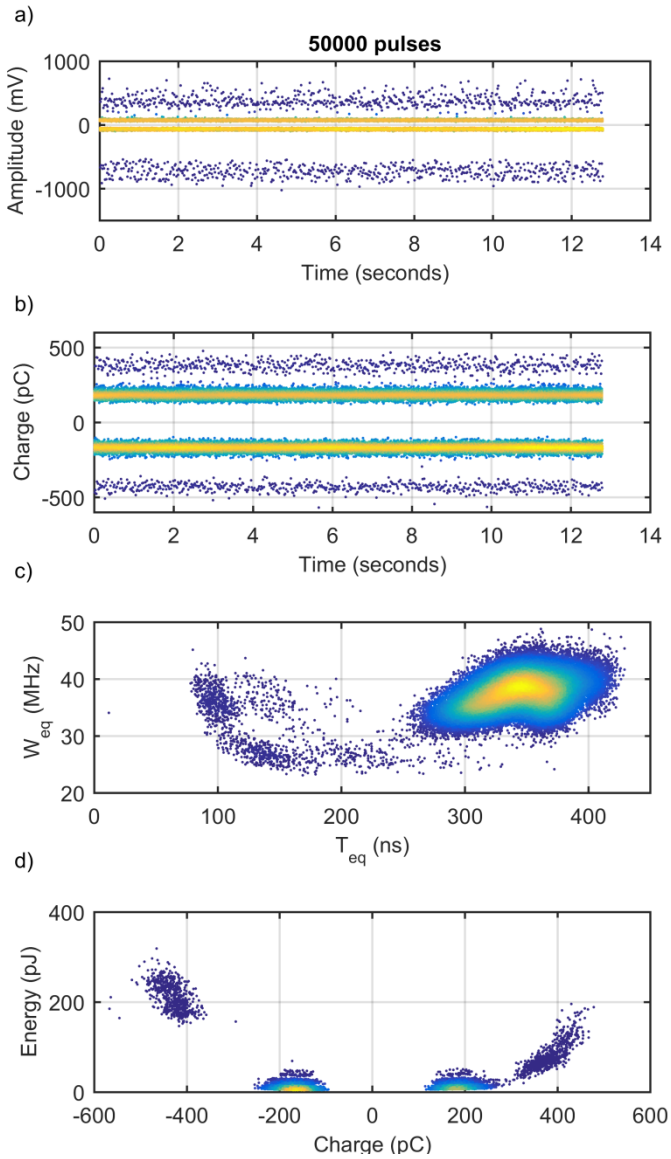

Figure 434: Defect Combination 2 (Internal Discharge & Corona)

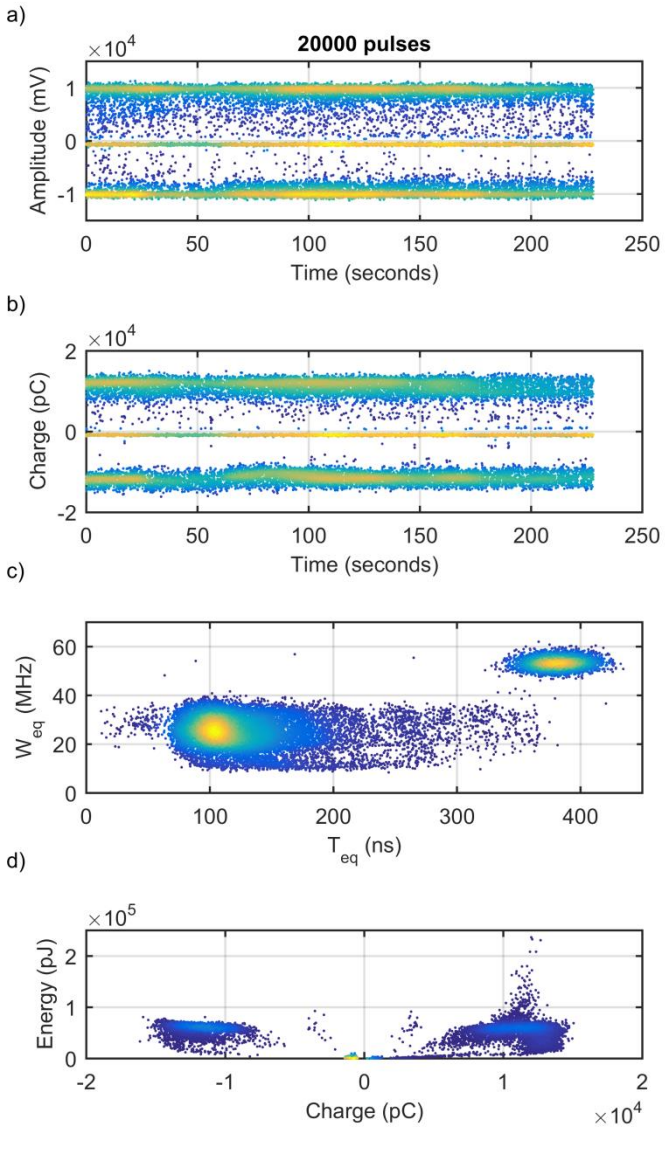

Figure 435: Defect Combination 6 (Internal Discharge & Floating electrode)

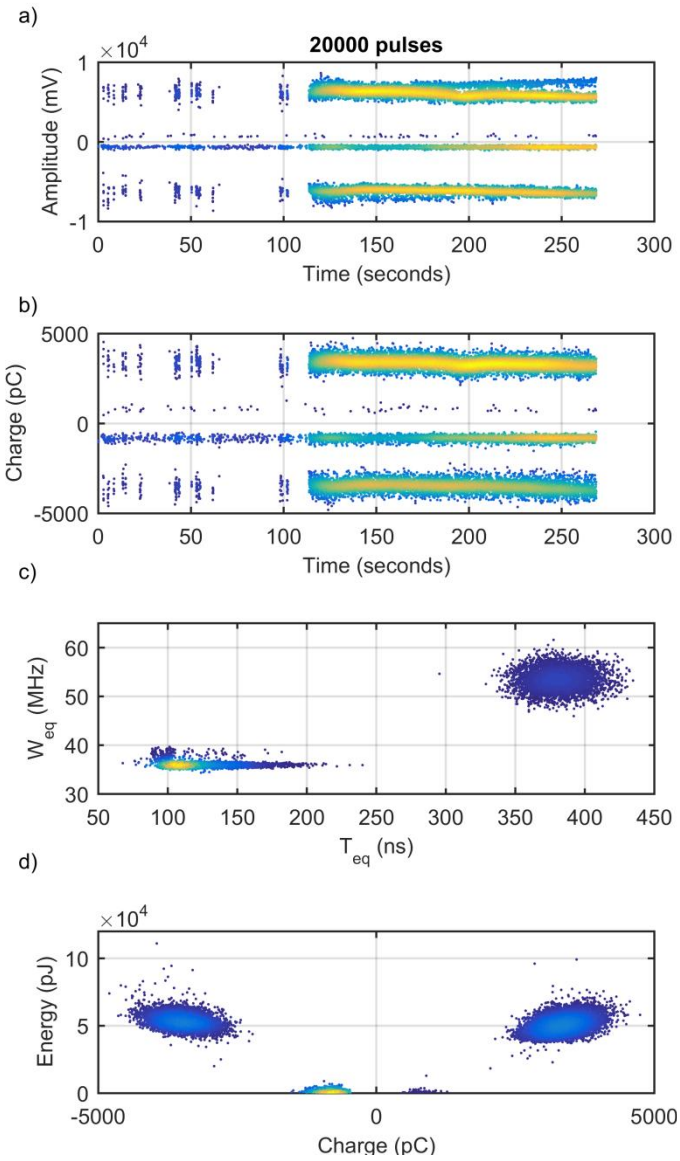

Figure 436: Defect Combination 7 (Internal Discharge & Surface Discharge)

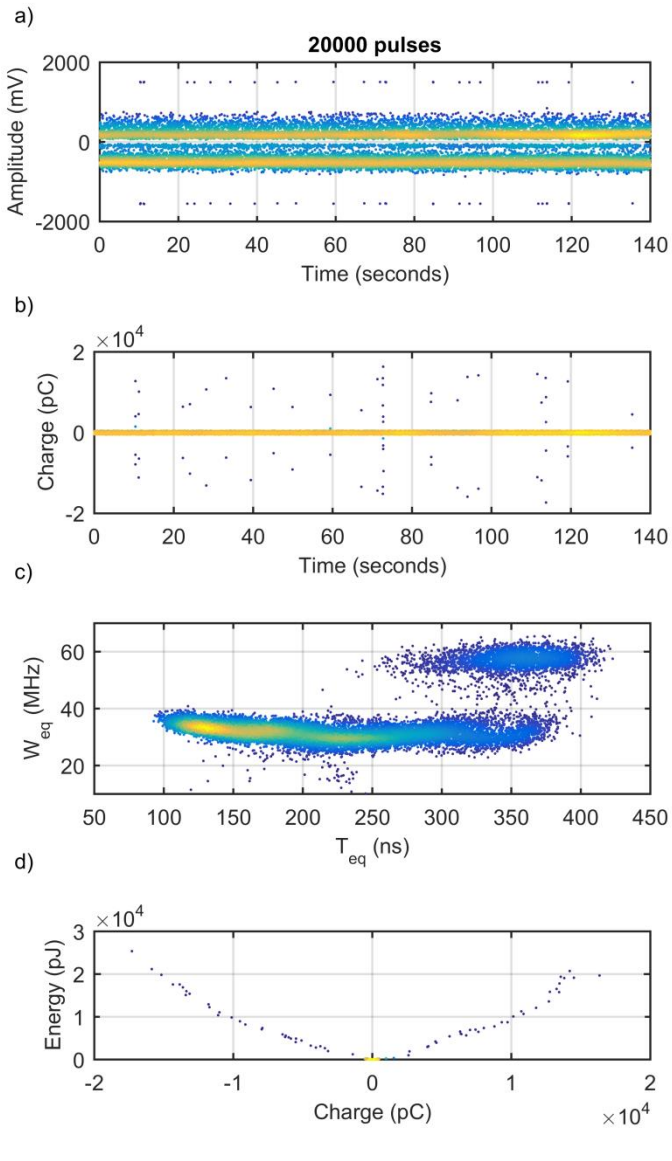

Figure 437: Defect Combination 8 (Internal Discharge & Free-Moving Particle)

G2. Number of discharges per cycle: Defect Combination 2, 6, 7 and 8

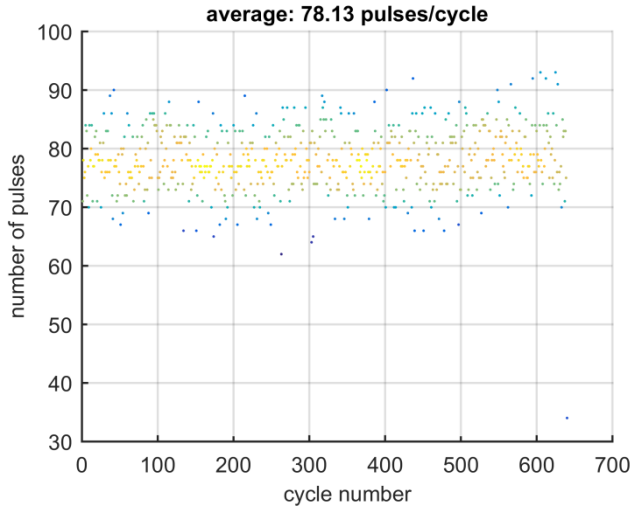

Figure 438: Defect Combination 2 (Internal Discharge & Corona)

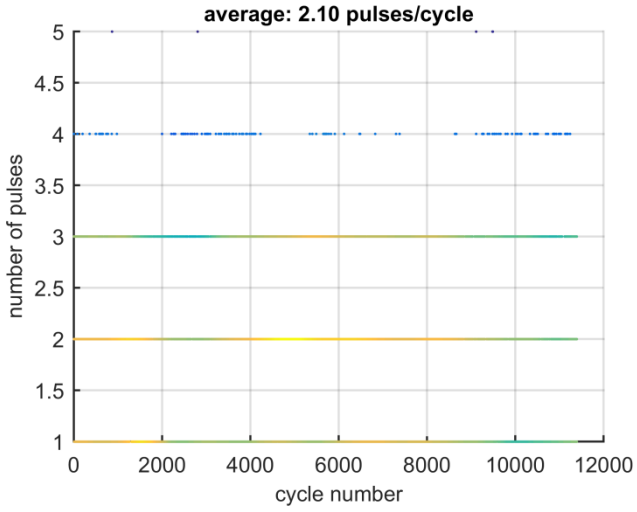

Figure 439: Defect Combination 6 (Internal Discharge & Floating electrode)

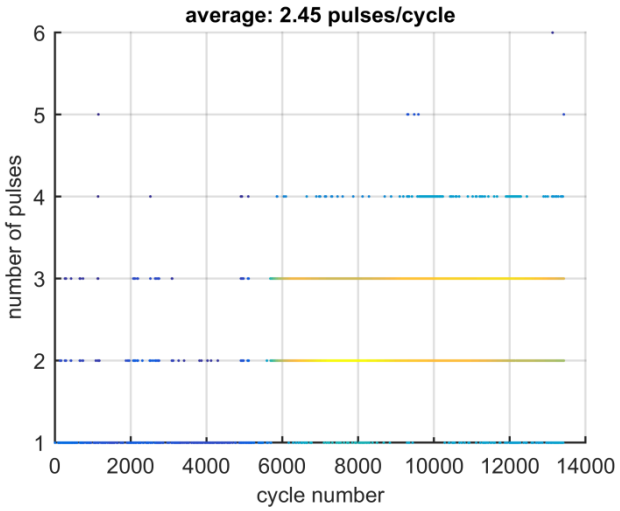

Figure 440: Defect Combination 7 (Internal Discharge & Surface Discharge)

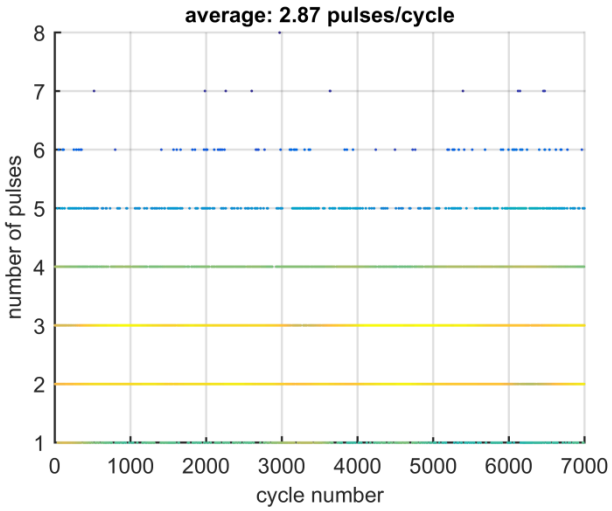

Figure 441: Defect Combination 8 (Internal Discharge & Free-Moving Particle)

G3. PRPD: Defect Combination 2, 6, 7 and 8

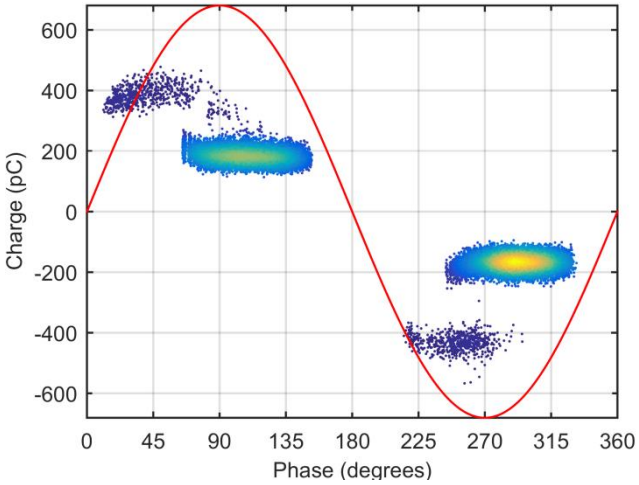

Figure 442: Defect Combination 2 (Internal Discharge & Corona)

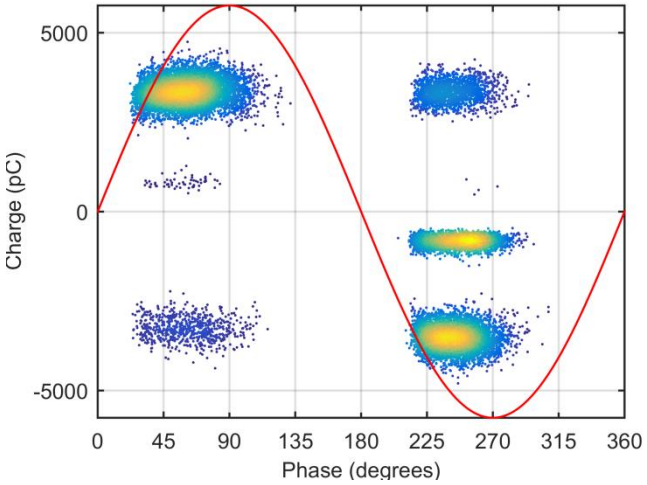

Figure 444: Defect Combination 7 (Internal Discharge & Surface Discharge)

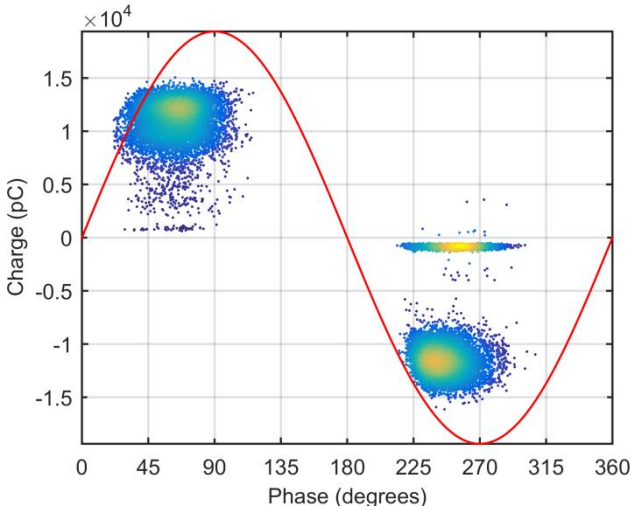

Figure 443: Defect Combination 6 (Internal Discharge & Floating electrode)

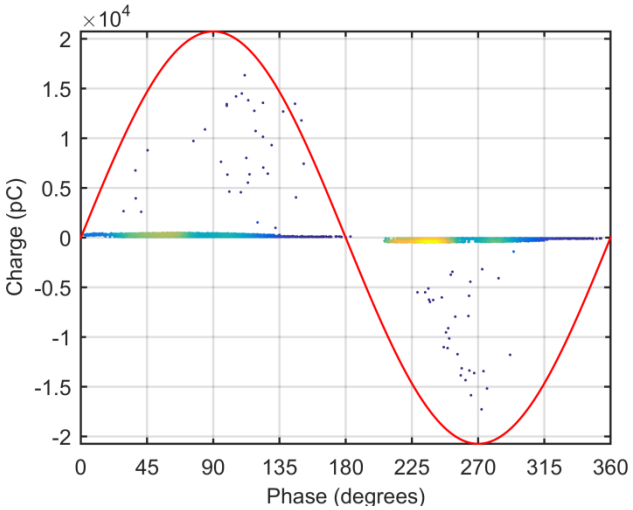

Figure 445: Defect Combination 8 (Internal Discharge & Free-Moving Particle)

G4. TRPD: Defect Combination 2, 6, 7 and 8

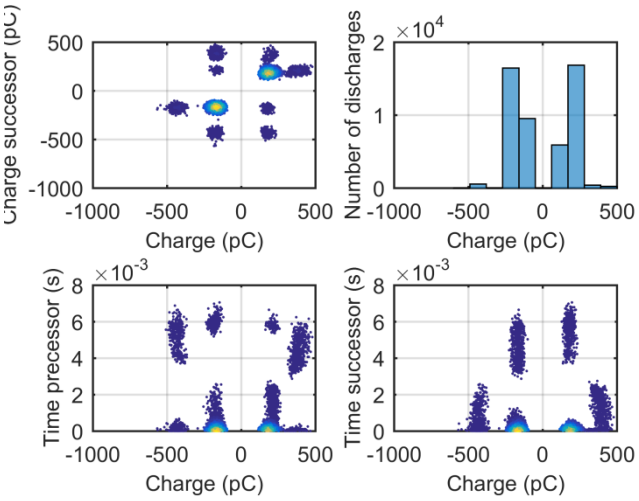

Figure 446: Defect Combination 2 (Internal Discharge & Corona)

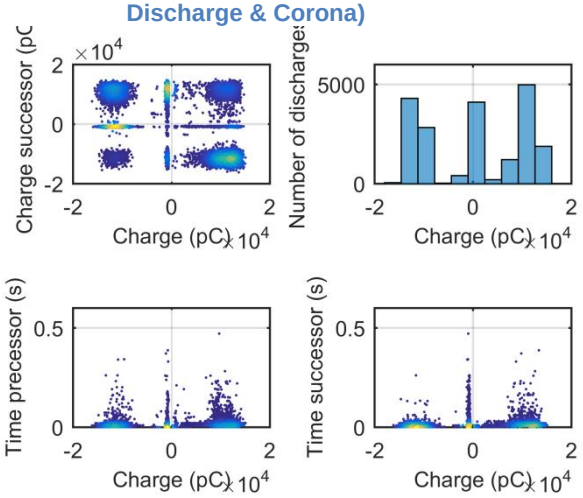

Figure 447: Defect Combination 6 (Internal Discharge & Floating electrode)

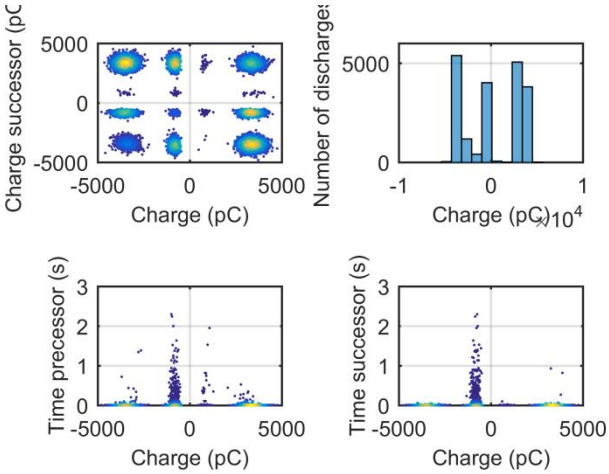

Figure 448: Defect Combination 7 (Internal Discharge & Surface Discharge)

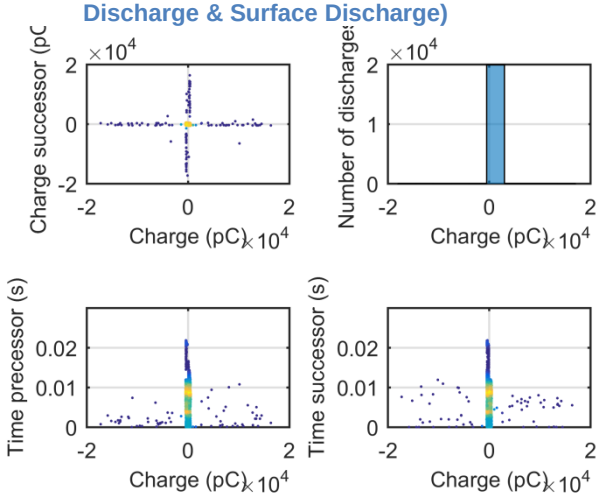

Figure 449: Defect Combination 8 (Internal Discharge & Free-Moving Particle

G5. Cluster in logarithmic scale: Defect Combination 2, 6, 7 and 8

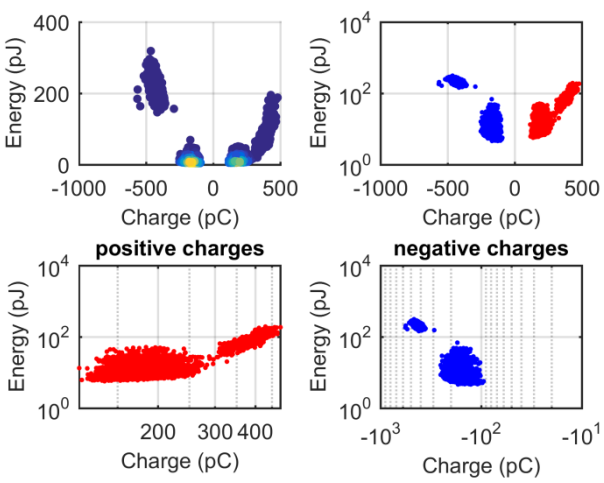

Figure 450: Defect Combination 2 (Internal Discharge & Corona)

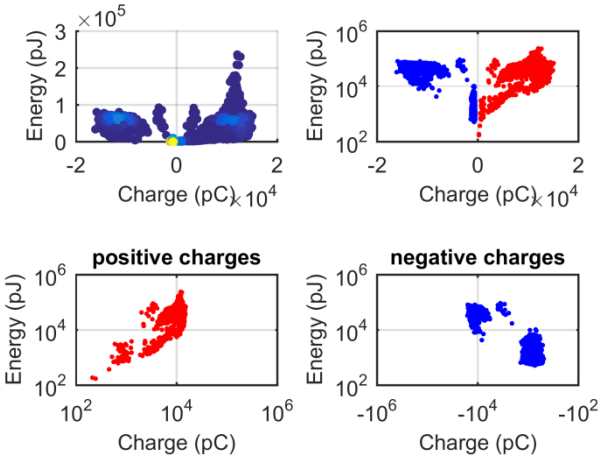

Figure 451: Defect Combination 6 (Internal Discharge & Floating electrode)

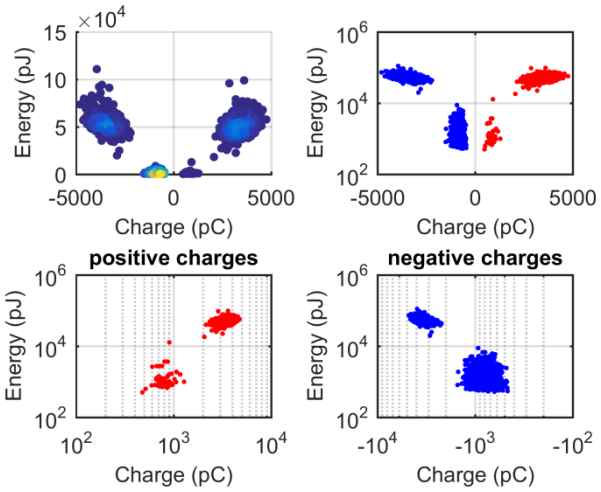

Figure 452: Defect Combination 7 (Internal Discharge & Surface Discharge)

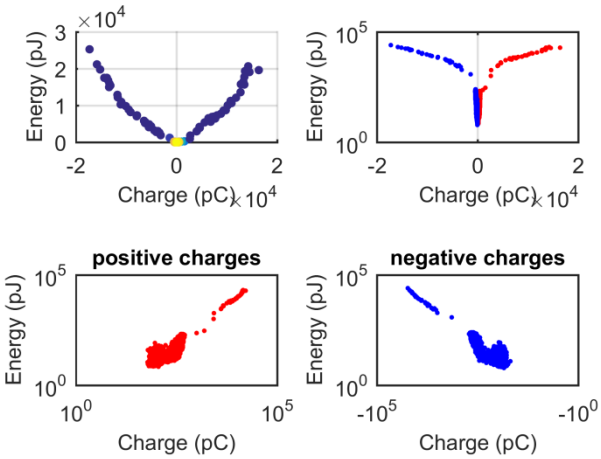

Figure 453: Defect Combination 8 (Internal Discharge & Free-Moving Particle)

G6. Energy per Charge versus charge: Defect Combination 2, 6, 7 and 8

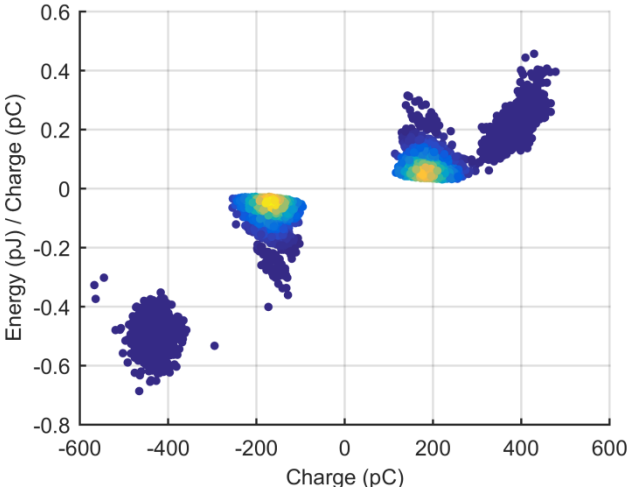

Figure 454: Defect Combination 2 (Internal Discharge & Corona)

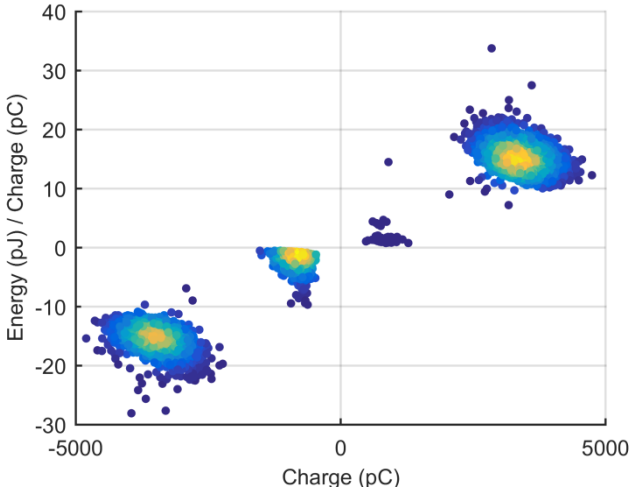

Figure 456: Defect Combination 7 (Internal Discharge & Surface Discharge)

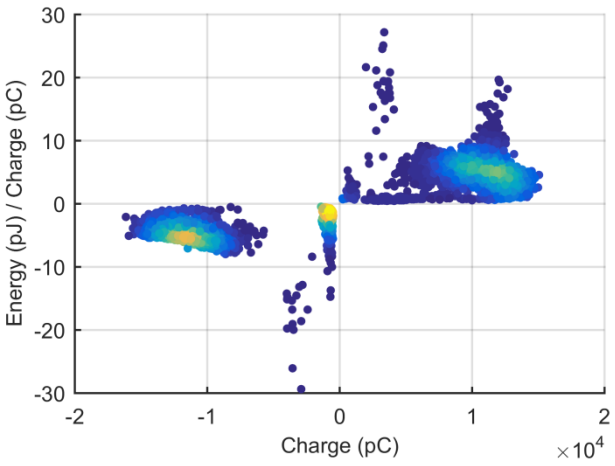

Figure 455: Defect Combination 6 (Internal Discharge & Floating electrode)

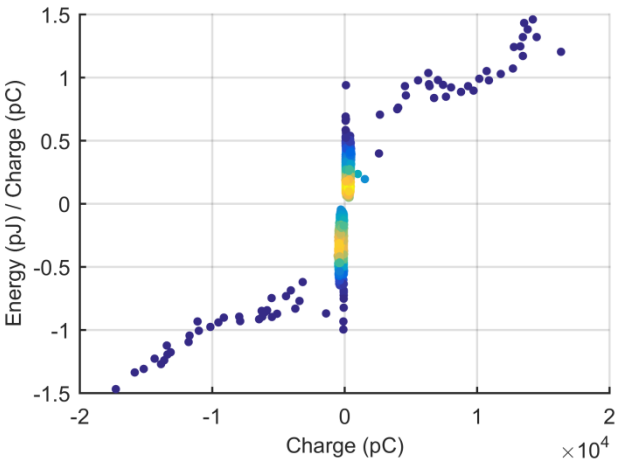

Figure 457: Defect Combination 8 (Internal Discharge & Free-Moving Particle)

H. Shapes for PD Recognition

•	Charge Polarity	Qsuc VS Q	Tpre VS Q
Negative Corona	-Q	-	-
	+Q		
Positive Corona	-Q		
	+Q	-	-
Surface Discharge	-Q	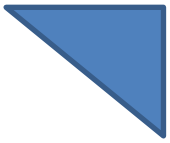	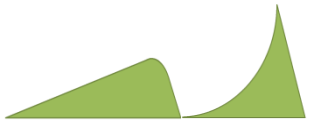
	+Q	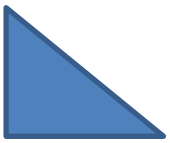	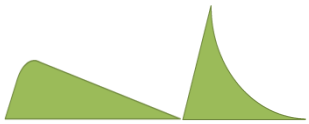
Free-Moving Particle	-Q		
	+Q		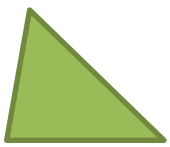
Floating Electrode	-Q		
	+Q	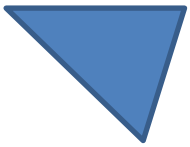	
Internal Discharge	-Q		
	+Q		

Table 58: Summary shapes for recognition artificially created defects

J. Graphs 2nd Internal Discharge & Floating Electrode Samples

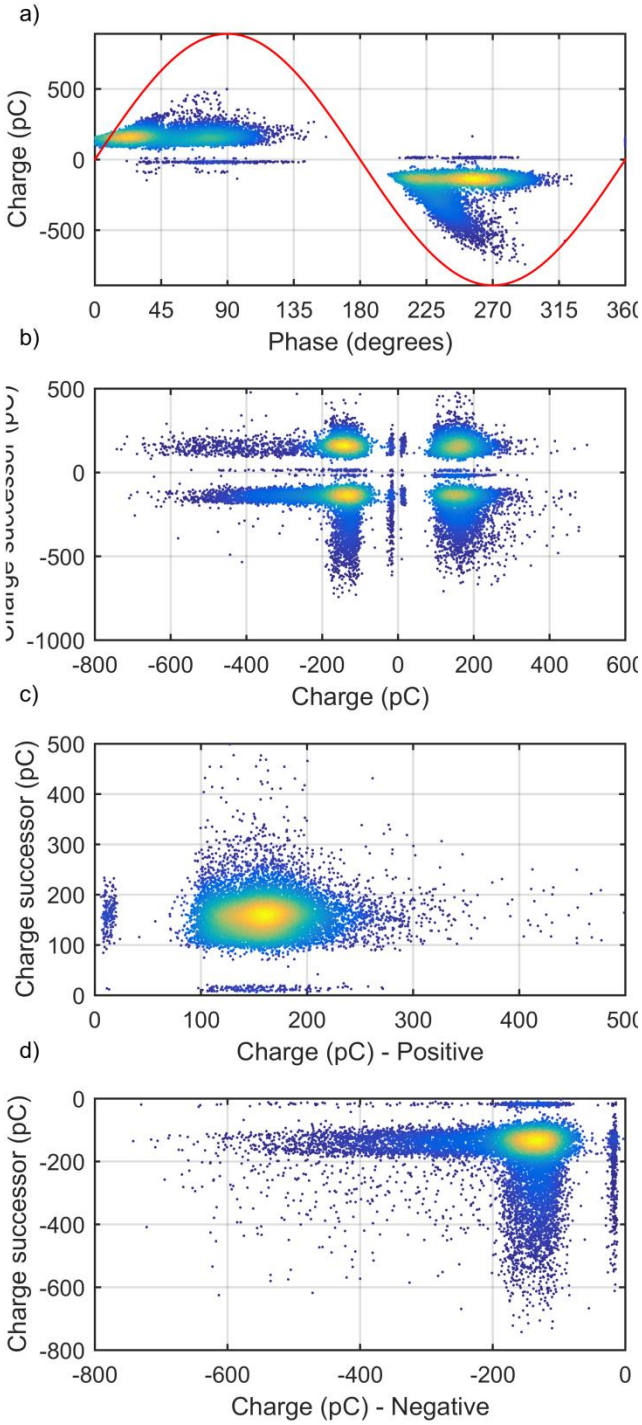

Figure 458: 1st measurement: PRPD, positive and negative PD's in TRPD of the 2nd Internal Discharge Sample.

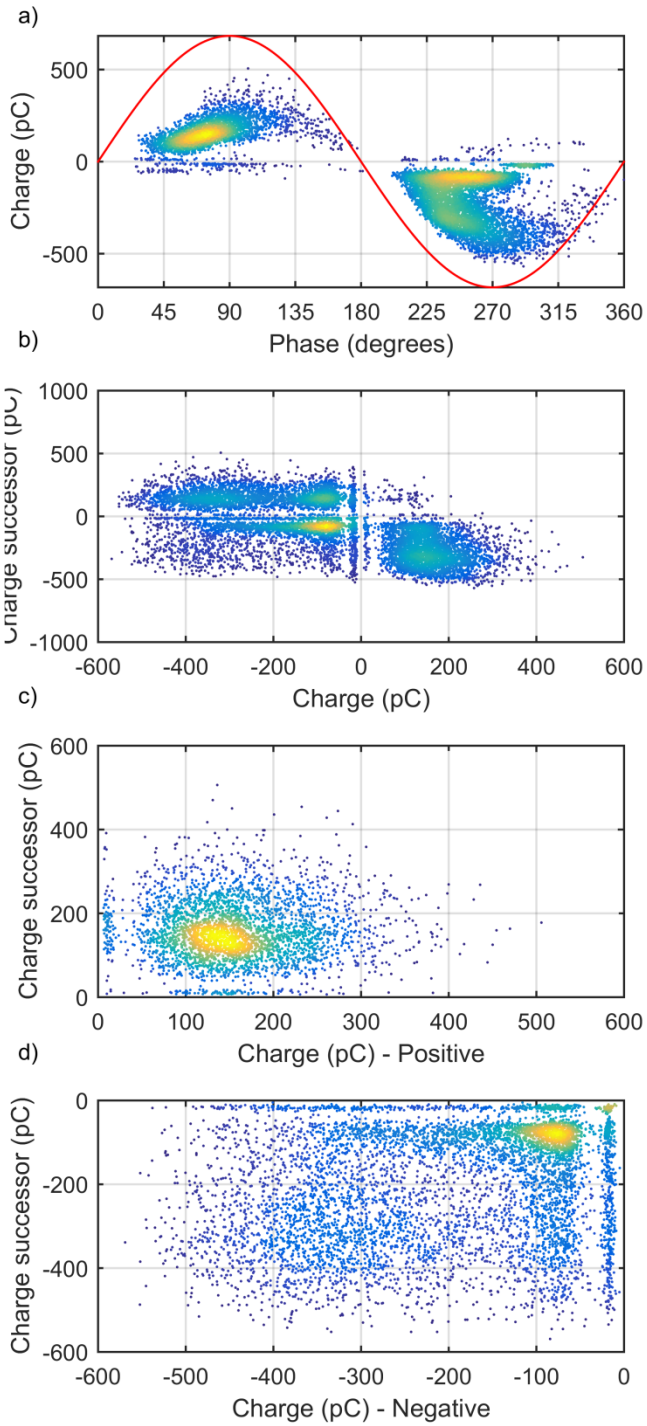

Figure 459: 2st measurement: PRPD, positive and negative PD's in TRPD of the 2nd Internal Discharge Sample.

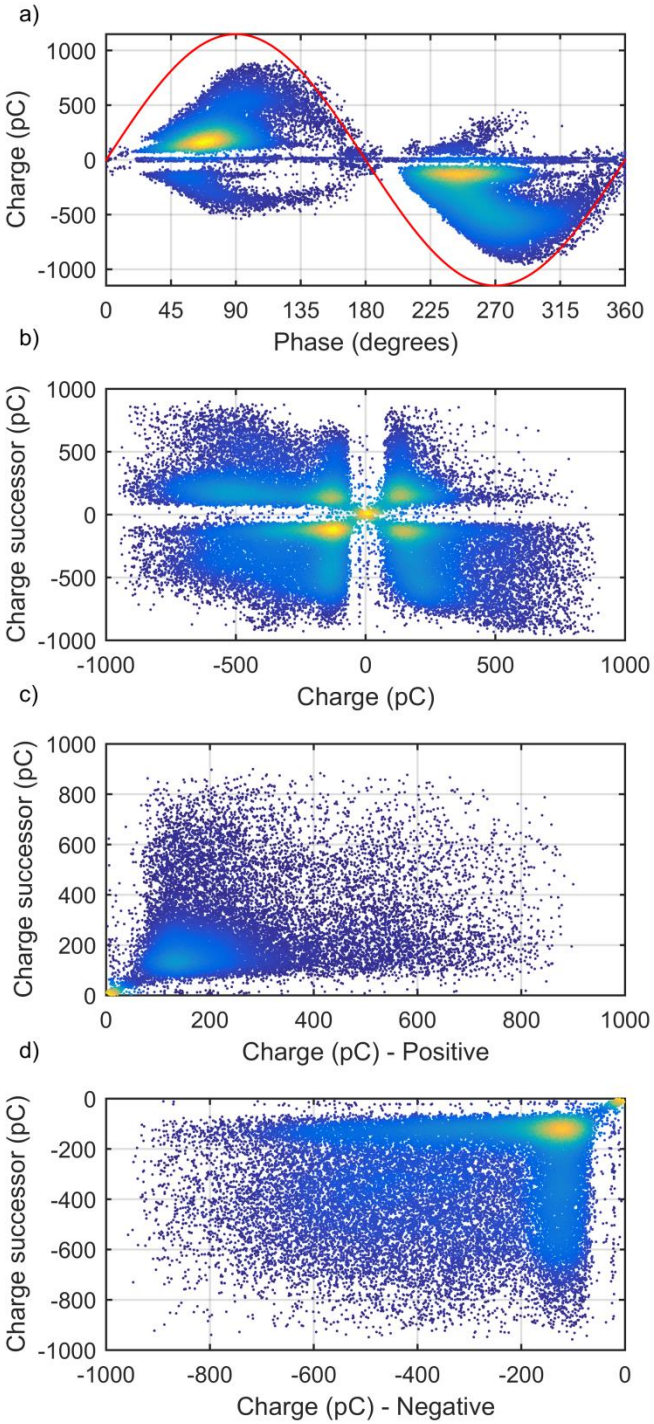

Figure 460: 3st measurement: PRPD, positive and negative PD's in TRPD of the 2nd Internal Discharge Sample.

Bibliography / References

[1] *International Standard IEC 60270 (International Electrotechnical Commission), Third edition*., Nederlands Normalisatie-instituut, Delft, ZH, 2001, *sec. 3.1.*

[2] M. Goldman, A. Goldman and R.S. Sigmond, "*The corona discharge, its properties and specific uses", Vol. 57, No. 9,* GB: Pure & Appl. Chem., 1985, pp. 1353-1362.

[3] *International Standard IEC 60270 (International Electrotechnical Commission), Third edition*., Nederlands Normalisatie-instituut, Delft, ZH, 2001, *sec. 5.1.*

[4] *International Standard IEC 60270 (International Electrotechnical Commission), Third edition*., Nederlands Normalisatie-instituut, Delft, ZH, 2001, *sec. 4.2.*

[5] *International Standard IEC 60270 (International Electrotechnical Commission), Third edition*., Nederlands Normalisatie-instituut, Delft, ZH, 2001, *sec. 10.*

[6] W. Hauschild and E. Lemke, *High-Voltage Test and Measuring Techniques,* DOI: 10.1007/978-3-642-45352-6_4, © Springer-Verlag Berlin Heidelberg 2014

[7] *International Standard IEC 60270 (International Electrotechnical Commission), Third edition*., Nederlands Normalisatie-instituut, Delft, ZH, 2001, *Annex F.*

[8] Z.W. Zhong at al., *Characterization of partial discharge signals,* in 2010 IEEE/ASME International Conference, © July 2010 IEEE, DOI: 10.1109/MESA.2010.5552024.

[9] Birsen Yazici, "*Statistical Pattern Analysis of Partial Discharge Measurements for Quality Assessment of Insulation Systems in High-Voltage Electrical Machinery", Vol. 40, No. 6,* IEEE Transactions on Industry Applications., November/December 2004, pp. 1579-1594.

[10] G.C. Montanari, *"On line partial discharge diagnosis of power cables"*, IEEE EIC, pp. 210-215, Montreal, Canada, giugno 2009.

[11] F.H. Kreuger, *"1.Electric Fields 2.Dielectrics 3.Constructions," in Industrial High Voltage,* Delft, The Netherlands: Delft Univ. Press, 1991.

[12] F.H. Kreuger, *"4.CO-Ordinating 5.Measuring 6.Testing," in Industrial High Voltage,* Delft, The Netherlands: Delft Univ. Press, 1992.

[13] Hubbell Power Systems, Inc., "What is Corona?", Bulletin EU1234-H, Centralia, Missouri, 2004.

[14] *HV Cables Testing & Monitoring*, Techimp Systems S.r.l., Bologna, Italy, 01-12-09.

[15] *Techimp PDBasell OPERATOR's MANUAL*, Techimp Systems S.r.l., Bologna, Italy, 01-01-09, pp. *01-56.*

[16] Priyanka M. Kothoke at al., "Analysis of Partial Discharge using Phase-Resolved (n-q) Statistical Techniques," *International Journal of Engineering Research and Applications (IJERA)*, vol. *3,* no. *3,* pp*. 1317-1323,* May-Jun, 2013.

[17] C. Chang and Q. Su, "Statistical Characteristics of Partial Discharges from a Rod-Plane Arrangement," Center for Electrical Power Engineering, Clayton, Australia.

[18] N.C. Sahoo at al., "Trends in Partial Discharge Pattern Classification: A Survey," *IEEE Transactions on Dielectrics and Electrical Insulation*, vol. *12,* no. *2,* pp*. 248-264,* April, 2005.

[19] J.M. Martínez-Tarifa et al.,“Partial Discharge Pulse Shape Recognition Using an Inductive Loop Sensor,” in IOP Publishing Measurement Sience and Technology, 2010 © IOP Publishing Ltd. doi: 10.1088/0957-0233/21/10/105706

[20] J.H. Mason, “The Deterioration and Breakdown of Dielectrics Resulting From Internal Discharges,” in *Britisch Electrical and Allied Indstries Research Association.*, vol. *2,* no. 1053*,* pp*. 44-59,* 3 July 1950, year.

[21] M.U. Zuberi et al., “Estimation of Partial Discharge Inception Voltages Due to Voids in Solid Sheet Insulation,” in *Electrical Insulation Conference*, Ottawa, Ontario, 2 to 5 June 2013, pp. *124-128.*

[22] Yeqin Huang et al., “Integral Equation Method for the Computation of PD Inception Voltage in Voids,” Annual Report Conference on Electrical Insulation and Dielectric Phenomena, Cullowhee, Carolina, 2009, pp. 565-568.

[23] N. Malik et al., “Discharge inception voltages Due to Voids In Power Cables,” IEEE Trans. Electr. Insul, vol. EI-22, no. 6, pp. 787-793,Dezember, 1987.

[24] R. Piccin et al., “Partial Discharge Analysis of Gas Insulated Systems at High Voltage AC and DC,” in SuperGrid Institute, 2014©. doi: 10.1109/TDEI.2014.004711

[25] H.-D. Schelemper and K. Feser, “Estimation of Mass and Length of Moving Particles in GIS by Combined Acoustical and Electrical PD Detection,” IEEE Conf. Electr. Insul. Dielectr. Phenomena (CEIDP), pp. 90-93, 1995.

[26] American Heritage® Dictionary of the English Language, 5th Edition. Copyright © 2011 by Houghton Mifflin Harcourt Publishing Company, Published by Houghton Mifflin Harcourt Publishing Company, Boston: Houghton.

[27] Wikimedia Foundation Inc., (2015, October 4). Magnetostriction [The Free Encyclopedia]. Available: http://www.wikipedia.org

[28] *Techimp PDBaseII Operator’s Manyal*, *for software release 1.01.08*, TECHIMP Systems S.r.l., pp. *00-56.*

[29] Jiyu Wang et al., “Experimental Investigations on Surface Discharge Characteristics over Oil/Pressboard Interface Based on a Rod-to-Plane Electrode,” in *IEEE*, State Key Laboratory of Power Transmission Equipment & System Security and New Technology, Chongqing University, Chongqing, P.R. China.

[30] H. Anis and K.D.Srivastava, “Free Conducting Particles in Compressed Gas Insulation,” *IEEE Transactions on Electrical Insulation*, vol. *EI-16,* no. *4,* pp*. 327-338,* Aug., 1981.

[31] J. Lesurf (University of St. Andrews, St Andrews, Fife KY169SS, Scotland). *Cables: Transmission & Loss* [Online]. Available: https://www.st-andrews.ac.uk/~www_pa/Scots_Guide/audio/part7/page1.html

[32] G. Robinson, “Discharges in asymmetric cavities under AC stresses,” *IEE Proceedings-A*, vol. 138*,* no. 2*,* pp*. 119-126, March*, 1991.

[33] L.A. Dissado and J.C. Forthergill, “Electrical degradation and breakdown in polymers,” *Peter Peregrinus Ltd.*, London, 1992.

[34] T. Tanaka, “Internal Partial Discharge and Material Degradation,” IEEE Transactions on Electrical Insulation, Vol. EI-21, No. 6, December 1986, pp. 899-905.

[35] P.H.F. Morshuis, “Time-Resolved Discharge Measurements,” *Proc. Int. Conf. on Partial Discharge*, No 378, Canterbury, 1993, pp. 43-46.

[36] P.H.F. Morshuis, “Partial Discharge Meachanisms,” Ph.D. dissertation, T.U. Delft, Delft, Z.H., 1993.

[37] S. Blufpand, “Partial Discharge Recognition of Defects in Gas Insulated Systems under DC Voltage,” M.S. thesis, E.S.E., T.U. Delft., Delft, Z.H., 2014.

[38] S. Meijer, “Influence of Power Frequency on Partial Discharge Phenomena,” T.U. Delft., Delft, Z.H., Rep. *002*, January 2003.

[39] E. Kuffel, W. Zaengl, and J. Kuffel. High Voltage Engineering: Fundamentals. Newness, 2000.

[40] W. Hauschild and E. Lemke, *High-Voltage Test and Measuring Techniques,* DOI: 10.1007/978-3-642-45352-6_10, © Springer-Verlag Berlin Heidelberg 2014

[41] M. Bao et al., “The initiation Phenomena of Electrical Treeing in XLPE Cable Insulation,” in *Internaltional Conference on High Voltage Engineering and Application, Shanghai, China, September 2012*, pp. *431-434.*

[42] O. Bergius, “Implementation of On-Line Partial Discharge Measurements In Medium Voltage Cable Network,” M.S. thesis, Faculty of Computing and Electrical, Tampere University of Technology, Tampere, Finland, April 2011.

[43] C. Lee et al., “Characteristics analysis of sensors for on-line partial discharge measurement,” *Condition Monitoring and Diagnosis*, pp. 1275-1278, April 2008

[44] V. Latva-Pukkila and P. Pakonen, “Disturbances occurring in on-site partial discharge measurements,” Nordic Insulation Symposium, Tampere, June 2003

[45] ABB (2007). *Condensor Bushings* [Online]. Available: http://www.trafomaterials.com.sg/pages/bushings.html

[46] S. Meijer, “Partial Discharge Diagnosis of High-Voltage Gas-Insulated Systems,” Ph.D. thesis, Delft University of Technology, Optima Grafische Communicatie, Z.H., Delft, 2001.

[47] G. Simson. (2016). *Silicones Offers Better Solutions for Cable Accessories* [Online]. Available: http://www.inmr.com/silicones-offers-better-solutions-cable-accessories-2/#!prettyPhoto

[48] Encyclopaedia Britannica Inc. (2016). *Ionization Chemistry and physics* [Online]. Available: http://www.britannica.com/science/ionization

[49] G Hartmann and I Gallimberti, “The influence of metastable molecules on the streamer progression,” Journal of Physics D: Applied Physics, vol. 8, July 1975.

[50] R. Piccin, “Partial Discharge Analysis in HVDC Gas Insulated Substations,” Delft University of Technology, Department Of Intelligent Electrical Power Grids, July 2013.

[51] E. Kuffel et al., “Electrical breakdown in gases,” in *High Voltage Engineering: Fundamentals,* 2nd ed. Great Britain, Newnes, 2000.

[52] Siemens AG, “Partial Discharge Measurement Increases Availability of Electrical Machinery,” Siemens Industrial Turbomachinery, Inc. 10730 Telge Road Houston, Texas 77095, USA, 2007.

[53] Zettlex UK Ltd. (2015). *How Inductive Sensors Work* (ZET32) [Online]. Available: http://www.zettlex.com/articles/inductive-sensors-work/

[54] Gill Sensors & Controls Limited. (2016). *How does capacitive level sensing work?* [Online]. Available: http://www.gillsc.com/blog/2014/02/how-does-capacitive-level-sensing-work/

[55] A. Hong and G. Elert. (2000). *Dielectric Strength of Air* [Online]. Available: http://hypertextbook.com/facts/2000/AliceHong.shtml

[56] E. Kuffel et al., “Non-destructive insulation test techniques,” in *High Voltage Engineering: Fundamentals,* 2nd ed. Great Britain, Newnes, 2000.

[57] J. Kim et al., “Characteristics of partial discharge by AC and DC,” in *IEEE International Conference on Condition Monitoring and Diagnosis.*, Bali, Indonesia, September 2012, pp. *489-492.*

[58] Z. Sun et al., “Comparing Investigation of Partial Discharge Under AC, DC, and Impulse Voltage,” in 16th International Symposium on High Voltage Engineering, 2009 © SAIEE, Innes House, Johannesburg. doi: 978-0-620-44584-9

[59] Wikipedia the free encyclopaedia. (2016, February 16). *Corona Discharges* [Online]. Available: https://en.wikipedia.org/wiki/Corona_discharge

[60] Webcraft GmbH. *DIALEV* (DLD-01) [Online]. Available: http://www.supermagnete.de/eng/physics-magnets/dialev-levitating-graphite-disc-diamagnetic_DLD-01?img=1

[61] A. Rodrigo et al., “Influence of high frequency current transformers bandwidth on charge evaluationin partial discharge measurements, ”IEEE Trans. Dielectric. Electr. Insul., vol. 18, no. 5, pp. 1798-1802, 2011

[62] A. Rodrigo Mor et al., “Comparison of charge estimation methods in partial discharge cable measurements”, IEEE Trans. Dielectr. Electr. Insul., vol. 22, no. 2, pp. 657-664, April 2015.

[63] A. Rodrigo Mor et al., “Charge Estimation Methods in Partial Discharge Cable Tests,” Electrical Insulation Conference (EIC)., Seattle., Washington, USA, June 2015, pp. *463-466.*

[64] A. Contin et al., “Digital Detection and Fuzzy Classification of Partial Discharge Signals,” IEEE Transactions on Dielectrics and Electrical Insulation., Vol. 9, No. 3, June 2002, pp. *335-348.*

Partial discharge (PD) measurements are an effective tool used for insulation diagnostics and assessment, therefore a good understanding of these PD measurements are essential for an electrical engineer's background knowledge. During this research project a PD test platform was designed and made for electrical PD detection. The setup includes artificially created defects for 6 different types of PD's, with origins in positive and negative corona, internal discharge, floating electrode, free-moving particle, and surface discharge. These defects are designed to have a partial discharge inception voltage (PDIV) of around 10kV, and can easily be connected or disconnected from the set-up, therefore it is possible to measure individual defects or a combination of them. This PD test platform was used during this research project for characterizing the different PD types (single and multiple), and as a check for testing new clustering and pattern recognition techniques. Besides, it can also be used as a test platform for educational purposes and to train people and test equipment.

Daniel Antonio Harmsen

Was born in Willemstad, Curaçao, in 1990. He received the B.S. degree in electrical engineering from the University of the Netherlands Antilles, Willemstad Curaçao. This thesis was written as the final step in completing the Master of Science degree in Electrical Engineering at Delft University of Technology.

TU Delft